Lehrstuhl für Umformtechnik und Gießereiwesen
Fakultät für Maschinenwesen
Technische Universität München

Residual Stresses Induced by Shear Cutting

Targeted Use For Manufacturing Functional Surfaces With An Improved Fatigue Behavior

Jens-Michael Stahl

Vollständiger Abdruck der von der Fakultät für Maschinenwesen der Technischen Universität München zur Erlangung des akademischen Grades eines Doktor-Ingenieurs (Dr.-Ing.) genehmigten Dissertation.

Vorsitzender:

Prof. Dr. Karsten Stahl

Prüfer der Dissertation:

1. Prof. Dr.-Ing. Wolfram Volk
2. Prof. Dr.-Ing. Dr. h.c. Fritz Klocke

Die Dissertation wurde am 08.02.2021 bei der Technischen Universität München eingereicht und durch die Fakultät für Maschinenwesen am 28.06.2021 angenommen.

Vorwort

"Das Ganze ist mehr als die Summe seiner Teile."- nach Aristoteles

Dieses Zitat trifft aus meiner Sicht sowohl auf diese Dissertation als auch auf das Zusammenleben und -arbeiten in der Wissenschaft zu. Bei den vielen Personen die zum Gelingen dieser Arbeit beigetragen haben, möchte ich mich im Folgenden bedanken.

Diese Dissertation entstand während meiner Tätigkeit als wissenschaftlicher Mitarbeiter am Lehrstuhl für Umformtechnik und Gießereiwesen (*utg*) der Technischen Universität München. Mein besonderer Dank gilt Herrn Prof. Dr.-Ing. Wolfram Volk, meinem Doktorvater. Durch seine stete Unterstützung und viele hilfreiche Diskussionen hat er wesentlich zur erfolgreichen Durchführung beigetragen. Weiterhin möchte ich mich besonders bei Herrn Prof. Dr.-Ing. Hartmut Hoffmann bedanken, sowohl für seine Unterstützung als auch für die unvergesslichen Dienstreisen.

Weiterhin möchte ich mich bei den Kolleginnen und Kollegen am *utg* für die schöne und lehrreiche Zeit bedanken. Herrn Tom Greß und Herrn Philipp Lechner möchte ich für angeregte Diskussionen, viele schöne Stunden und einen umfangreichen Einblick in die Gießerwelt danken. Herrn Hannes Alois Weiss und Herrn Christoph Hartmann danke ich für die wertvollen Denkanstöße zu dieser Arbeit. Weiterhin gilt mein Dank dem nichtwissenschaftlichen Personal. Insbesondere Herr Andreas Fuhrmann und Herr Marco Olbrich-Baier haben durch Ihr Fertigungswissen und Ihre Unterstützung bei zeitkritischen Aufträgen vieles erst möglich gemacht. Ein ganz herzliches Dankeschön gilt auch den Studentinnen und Studenten deren Arbeiten ich betreuen durfte für Ihre Beiträge zu dieser Arbeit. Frau Isabella Pätzold, meiner langjährigen Bürokollegin, danke ich für die schöne Zeit und Ihre fröhliche Art auch in stressigen Zeiten.

Herrn Daniel Müller von der Forschungsstelle für Zahnräder und Getriebebau gilt mein Dank für die gute und unkomplizierte Zusammenarbeit im Rahmen des gemeinsamen Forschungsprojektes. Der Firma Schwaben Präzision Fritz Hopf GmbH danke ich für Ihre Unterstützung durch Rat und Tat. Hier möchte ich Herrn Rainer Hertle, Herrn Johann Niemeier und Herrn Timo Ebert meinen herzlichen Dank aussprechen.

Ganz besonders Danke ich meinem Vater, Wolfram Stahl, der mir als Mensch und Ingenieur stets ein Vorbild ist. Zu Guter letzt gebührt der größte Dank meiner Freundin und meiner Familie für Rückhalt und allzeit gebotene Unterstützung.

Euch widme ich diese Arbeit.

Jens Stahl

München, im Februar 2021

Kurzbeschreibung

Scherschneiden ist ein hochgradig wirtschaftlicher Fertigungsprozess, der zur Herstellung von einer Vielzahl von Alltagsprodukten verwendet wird. Vom Fahrrad bis zum Computer, in so gut wie jedem Gebrauchsgegenstand sind schergeschnittene Teile verbaut. Aus diesem weiten Anwendungsspektrum ergibt sich auch die Vielzahl der Anforderungen, die an eine schergeschnittene Kante gestellt werden. Im einfachsten Fall wird durch Scherschneiden nur die Bauteilgeometrie hergestellt. In den meisten Fällen muss die schergeschnittene Kante jedoch komplexere Funktionen erfüllen, da sie nachfolgende Fertigungsoperationen überstehen oder äußere Lasten übertragen muss. Die Lebensdauer eines Bauteils ist besonders bei Antriebskomponenten oder Zahnrädern ein wichtiges Auslegungskriterium. In der klassischen Zahnradfertigung wird oft eine Vielzahl an Prozessen eingesetzt um die Lebensdauer zu gewährleisten. Mit Scherschneiden ist dies prinzipiell in einem einzigen Fertigungsschritt realisierbar, da Bauteilgeometrie und -eigenschaften vom Schnitt definiert werden.

Der Eigenspannungszustand ist eine solche mechanische Eigenschaft mit einem signifikanten Einfluss auf die Lebensdauer metallischer Bauteile. Eigenspannungen können diese negativ beeinflussen, bei gezielter Nutzung jedoch auch zu einer erhöhten Schwingfestigkeit führen. In dieser Arbeit wird der Einfluss des Scherschneidvorgangs auf den Eigenspannungszustand und der daraus resultierenden Schwingfestigkeit anhand der für die Fertigung von Antriebskomponenten besonders relevanten Near-Net-Shape-Blanking-Verfahren untersucht.

Zunächst wurde identifiziert wie sich über die Wahl des Near-Net-Shape-Blanking-Verfahrens und den zugehörigen Prozessparametern ein gewünschter Eigenspannungszustand einstellen lässt. Dazu wurden fünf verschiedene Prozessvarianten mit drei Schneidspalten und zwei Schneidkantenpräparationen untersucht. Auf Basis dessen wurden grundlegende Zusammenhänge der Eigenspannungsentstehung mithilfe der Finite-Elemente-Methode herausgearbeitet. Zusätzlich wurde eine Korrelation durchgeführt, um zu zeigen, wie die Eigenspannungen mit einfach zu messenden Bauteilmerkmalen verknüpft sind. Anschließend wurde die Schwingfestigkeit der Bauteile untersucht, um die Bedeutung der scherschneidinduzierten Eigenspannungen herauszuarbeiten. Es wurde festgestellt, dass eine Lebensdauersteigerung von 29 % klar auf Eigenspannungen zurückgeführt werden kann. Darauf aufbauend wurde der Eigenspannungszustand für ausgewählte Prozesse weiter verbessert. Um die industrielle Nutzbarkeit der Ergebnisse zu gewährleisten, wurde eine Zykloidkurvenscheibe gefertigt und in einem Getriebe getestet. Zuletzt wurde eine Methode zur Inline-Überwachung des Bauteileigenspannungszustands vorgestellt.

In dieser Arbeit wird somit ein grundlegendes Verständnis der prozessinduzierten Eigenspannungen geschaffen, deren Nutzbarkeit zur Schwingfestigkeitssteigerung gezeigt um anschließend die industrielle Anwendbarkeit zu gewährleisten. Dies ermöglicht es schergeschnittene Teile mit einer verbesserten Schwingfestigkeit, geringer Prozesskettenkomplexität und niedrigem Energieaufwand herzustellen.

Executive Summary

Shear cutting is a highly economic manufacturing process for a variety of products that we use in everyday life. From the bicycle to the computer, almost every commodity shows a shear cut part. This widespread use also demonstrates the multitude of requirements for shear cut edges. In the easiest case, it is only used for defining the part geometry. Typically, the requirements are much more complex as the edge has to endure additional manufacturing steps, must not be harmful during handling and assembly, and has to be able to withstand applied loads during its lifetime. Thus, the shear cut edge is a functional surface in all relevant cases.

The lifetime of a shear cut edge under cyclic loading is especially important in drivetrain or gear applications. For the classical manufacturing of, for example, gear wheels, many energy and time-consuming steps are necessary to define the part's geometry and mechanical properties. Shear cutting on the other hand is able to define these within a single manufacturing step.

One mechanical property that has a significant influence on the lifetime of metallic parts is the residual stress state. The residual stresses can be harmful or can be used to increase the fatigue strength. For shear cutting, and especially for the gear manufacturing relevant Near-Net-Shape-Blanking processes, the influence of the chosen process and its process variables on the residual stress state and the resulting fatigue strength are investigated in this thesis.

To identify process variants with the according process parameters that are able to achieve a desired residual stress state, parts are manufactured by five different Near-Net-Shape-Blanking processes with three different die clearances and two active element edge conditions. On the basis of these parts, a basic understanding on the formation of the residual stress state during the shear cutting process is generated by using Finite-Element-Simulations. Additionally, the residual stress state is linked to easy to measure geometrical part attributes.

Following, the fatigue strength was tested. By identifying the influence of the part's geometry and hardness on its lifetime, the significance of the residual stresses are highlighted. It was found that a lifetime increase of 29 % can be clearly attributed to the process induced residual stresses.

After improving the residual stress state for highly relevant Near-Net-Shape-Blanking processes, the basic results are transferred to industry relevant applications by manufacturing cycloidal disks and testing them in a specially designed gearbox. Finally, a method for a relative in-line measurement of the residual stress of punched holes is presented.

Thus, this thesis spans from the basic understanding on the formation of the process induced residual stresses over the resulting fatigue strength of the manufactured part to industry relevant applications with the corresponding production process monitoring. This allows to reliably manufacture blanked parts with an improved fatigue behavior with a comparably low process chain complexity and energy consumption.

Content

List of Symbols

Symbol	Unit	Meaning
A	mm	Maximum distance from fit
a_i	mm	Distance from measurment point to fit
A_g	%	Uniform elongation
b_E	mm	Die roll width
B_L	MPa	Ludwik model parameter
b_R	mm	Scar height
B_V	-	Voce model parameter
C_1, C_2, C_3	-	Johnson and Cook fracture model parameters
C_{L0}, C_{L1}	MPa	Parameters modelling the Luders behavior
D	mm	Hörmann bending coefficient
$d_{ActiveElement}$	mm	Active element diameter
d_{Part}	mm	Part diameter
E	MPa	Young's modulus
F_{GH}	N	Counter punch force
F_H, F'_H	N	Horizontal force on punch and die
F_{NH}	N	Blank holder force
F_P	N	Punch force
F_Q, F'_Q	N	Lateral cutting force on punch and die
F_{R1}	N	Frictional force before reaching the bottom dead center
F_{R2}	N	Frictional force after reaching the bottom dead center
F_{RZ}	N	V-ring force
F_S, F'_S	N	Cutting force on punch and die
F_{Smax}	N	Maximum cutting force
F_V, F'_V	N	Vertical force on punch and die
h_E	mm	Die roll height
h_G	mm	Burr height
h_R	mm	Fracture zone height
h_{RZ}	mm	V-ring height
h_S	mm	Clean cut height
HV_0	HV	Base hardness
HV_1	HV	Local hardness
I_1	MPa	First invariant of the Cauchy stress tensor
i	-	Index
J_2	MPa	Second invariant of the deviatoric stress
k	-	Slope of the limited lifetime fatigue strength line

k_f	MPa	Yield stress
k_{f0}	MPa	Initial yield stress
$k_{f\infty}$	MPa	Voce's saturated yield stress
K_t	-	Notch factor
l_H	mm	Horizontal lever arm
l_V	mm	Vertical lever arm
l_R	mm	Scar length
l_{RZ}	mm	V-ring length
l_S	mm	Cutting line length
m	-	Number of measurement points
N	-	Number of load cycles
$N_{50\,\%}$	-	Number of load cycles to failure for a 50 % failure probability
n	-	Ludwik strain hardening exponent
R	mm	Bending coefficient
R_S	-	Stress ratio
Ra	mm	Arithmetic average roughness
R_m	MPa	Ultimate tensile strength
r_M	mm	Die cutting edge radius
$R_{p0.2}$	MPa	0.2 % yield strength
r_S	mm	Punch cutting edge radius
Rz	mm	Mean roughness depth
S_m	MPa	Stress amplitude
s	mm	Sheet metal thickness
S_m	MPa	Mean stress
S_o	MPa	Upper stress
S_u	MPa	Lower stress
u_i	mm	Displacement of a material point
u_{rel}	%	Relative die clearance
α	°	Clean cut angle
β	-	Interpolation variable
Δd	mm	Size deviation
δ_{ij}	-	Kronecker delta
ε_{ij}	-	Strain tensor
η	-	Stress triaxiality
λ_L	MPa	Lamé parameter
μ	-	Coefficient of friction
μ_L	MPa	Lamé parameter
ν	-	Poisson's ratio

σ	MPa	Stress
σ^I, σ^{II}, σ^{III}	MPa	Type I, II, and III residual stresses
σ_{ax}	MPa	Axial stress
σ_{ij}	MPa	Cauchy stress tensor
σ_{ij}^D, σ_D	MPa	Deviatoric stress
σ_{ij}^H, σ_H	MPa	Hydrostatic stress
σ_M	MPa	Mises stress
σ_{max}	MPa	Maximum stress
σ_{min}	MPa	Minimum stress
$\sigma_{R,\parallel}$	MPa	Residual stress in load direction
$\sigma_{R,\perp}$	MPa	Residual stress perpendicular to the load direction
σ_{rad}	MPa	Radial stress
σ_{tan}	MPa	Tangential stress
σ_0	MPa	Base stress
φ	-	Logarithmic strain
$\dot{\varphi}$	s^{-1}	Logarithmic strain rate
φ_{frac}	-	Logarithmic strain at fracture

List of Abbreviations

Abbreviation	**Meaning**
B	Blanking
BV	Blanking with v-ring
DIN	Deutsches Institut für Normung
FEM	Finite element method
FB	Fineblanking
FZG	Lehrstuhl für Maschinenelemente - Forschungsstelle für Zahnräder und Getriebebau
NNSB	Near-Net-Shape Blanking
NNSBP	Near-Net-Shape Blanking process
PB	Precision blanking
PBwBH	Precision blanking without blank holder
RD	Rolling direction
RVE	Representative volume element
SR	Stress relief heat treatment
VDI	Verein Deutscher Ingenieure
utg	Lehrstuhl für Umformtechnik und Gießereiwesen

1 Introduction

Shear cutting is such an omnipresent manufacturing process that we usually do not recognize it anymore. The coffee machine I use in the morning shows a blanked stainless steel tray and housing. The bike I use to and from work shows blanked brake disks and a chain made of shear cut links, and the last thing I do before going to bed is switching off the light with a switch containing a frame and contacts manufactured by shear cutting. This widespread use also demonstrates the multitude of requirements for shear cut edges. In the easiest case, it is only used for defining the part geometry. But in most cases the requirements are much more complex as the edge has to endure additional manufacturing steps, must not be harmful during handling and assembly, and has to be able to withstand applied loads during its lifetime. Thus, the shear cut edge is a functional surface in all relevant cases.

One example which demands a complex set of requirements are gear wheels manufactured by (fine)blanking which "have widespread applications including automotive, office equipment, appliances, medical equipment, electronic instruments, etc." (Gupta, Jain, and Laubscher, 2017). When these gears are used to transmit power, they are subjected to cyclic loads consisting of high pressure, friction, bending, and thermal loads, among others. The lifetime of a gear wheel is not only determined by these loads but also by the precision of the cutting line, the geometry of the cut-surface as well as its mechanical properties.

As shown for example by Stenico, 2007, not only the hardness but also the residual stress state can significantly affect the part lifetime. To fulfill the requirements for the manufactured tooth, several manufacturing steps are necessary in the traditional gear manufacturing by machining: Initial cutting of the coarse geometry, hardening, grinding the fine geometry, and for example shot-peening for a desired residual stress state (Linke, 2010; Niemann and Winter, 2003). Since so many manufacturing steps are required, this is time-consuming, costly, and energy consuming, but it also results in a very high gear performance.

Shear cutting on the other hand is a very economic process that has the potential to achieve all these requirements in a single manufacturing step in which the geometry is defined and the surface is strain hardened. However, how the shear cutting process in general and the chosen process parameters in detail influence the resulting residual stress state has not been investigated for gear applications. Also, the influence of the residual stress state on the resulting durability or fatigue strength has not been addressed for the relevant precision shear cutting processes. Thus, the material's load bearing potential is not fully used which results in overdimensioned parts, i.e., wasted material and energy, and a limitation of the field of application of fineblanked gears due to a lower transmissible power density.

This thesis aims to address the formation and use of the shear cutting induced residual stresses. After a thorough state of the art investigation, the relationship between the chosen shear cutting process and its process parameters on the residual stress state is researched. Using finite

element simulations together with a mechanical and geometrical characterization of the manufactured parts, an explanation model for the residual stress state formation is developed and tested. Afterwards, fatigue strength and lifetime of the manufactured parts are investigated. To trace back the residual stress state influence on the part lifetime, the effect of geometry, hardness, and roughness are discussed as well. Following, the results are transferred from the comparably simple test geometries to an industry relevant gear application with a focus on the cutting line geometry influence and the stability of the residual stress state under typical conditions. To achieve this, a cycloidal drive is used that incorporates the idea that part design should consider both the manufacturing and the final application. Finally, a model is given that allows to calculate the residual stresses with a finite element model which allows designers to consider the residual stress state for their specific application.

By also considering the residual stress state, this thesis tries to question the way shear cut parts are designed and their requirements are specified. In the classical approach, only the part dimensions and the shear cut edge geometry are of interest. When the application case is known, these properties are not enough as a high amount of load bearing surface, i.e., clean cut height, is not useful when a low hardness and an unsuitable residual stress state cause a low fatigue strength. Additionally, a perfect geometry might be unsuitable when it causes increased wear during manufacturing. Thus, the final application case has to be considered in the shear cutting process while the shear cutting process has to be considered in the part design. Only if all factors influencing the performance regarding the final purpose are considered, parts can be produced economically while also achieving a minimal energy consumption from production to the end of their life cycle.

2 State of the Art

2.1 Shear Cutting

2.1.1 Classification and Basic Principle

According to DIN 8580, 2016 shear cutting is part of the separation or severing manufacturing processes. Here, severing or separation is classified as the manufacturing of a work-piece by removing the cohesion of a solid body. This process is further characterized in DIN 8588, 2013 as the mechanical separation of work pieces without the formation of shapeless matter, where two blades or active elements move relative to each other which results in separated work pieces.

The whole length of the blade can be in contact with the work piece from the beginning of the shear cutting process, i.e., a full-edged cut[1], or the blades may show an angle to each other which results in a gradual cut (DIN 8588, 2013; Volk and Stahl, 2015). A cut can be carried out in a single stroke, in multiple strokes or continuously (DIN 8588, 2013). If the cutting process is interrupted before the material separation, it is termed as embossing (Schmidt et al., 2007) or sheet metal extrusion (Zheng, Chan, and Lee, 2005) depending on the process parameters (Feistle and Volk, 2015; Volk and Stahl, 2020).

Another criterion for the classification of shear cutting processes, as illustrated in figure 2.1, is the shape of the cutting line: If the cutting line crosses the rim of the work-piece it is considered as an open cut and otherwise as a closed cut (DIN 8588, 2013). The classification of the open cut especially considers applications where the work piece is cut off the strip, i.e., cutting-off[2], where no scrap is produced (Klocke, 2013; Kopp, 2017). Another variant is trimming, where parts, like the rim of the final work piece, are cut apart (Kopp, 2017). While shear cutting describes the mechanical separation process in general, a distinction can be made regarding which part is of interest, i.e., which part of the sheet metal is used and which is scrap. Piercing (Black and Kohser, 2011) or punching[3] (Cubberly and Bakerjian, 1989) describe processes where the cut out part is scrap, i.e., a hole is cut in the desired part. Here, the scrap is called slug. Blanking[4] on the other hand is used for operations where the cut out part is used. In this case, the cut out part is called blank and the rest of the sheet metal is scrap. As both parts are of interest in this work, the cut out part is referred to as blank and the remains as sheet metal strip in the following. (Black and Kohser, 2011; Cubberly and Bakerjian, 1989)

Typical tool setups for a full-edged closed cut are displayed in figure 2.2. Here, the mechanical separation of the sheet metal is carried out by the active elements punch and die. Their relative movement is commonly carried out either by a moving punch or a moving die. In the following, only the configuration with a moving punch subjected to the punch force F_P is considered. The distance between punch and die perpendicular to the movement direction is called die clearance.

[1] translated from German “vollkantiger Schnitt”
[2] translated from German “Abschneiden”
[3] corresponding to the German “Lochen”
[4] corresponding to the German “Ausschneiden”

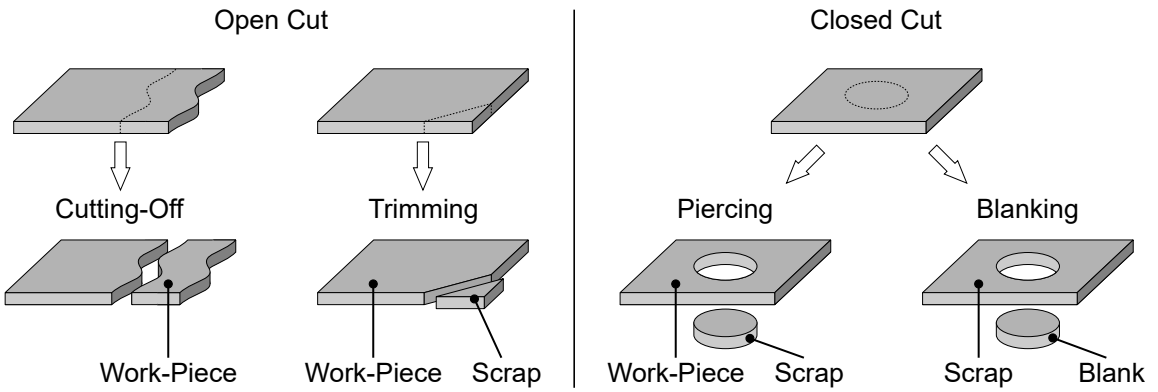

Figure 2.1: Comparison of an open (a) and a closed cutting line (b) with a further sub-categorization in blanking and piercing according to DIN 8588, 2013; Black and Kohser, 2011.

It is often given in percent of the sheet metal thickness and is consequently called relative die clearance u_{rel}. The cutting edges of both, punch and die, can be prepared to show a radius r_S on the punch and r_M on the die, although other edge geometries are possible as well.

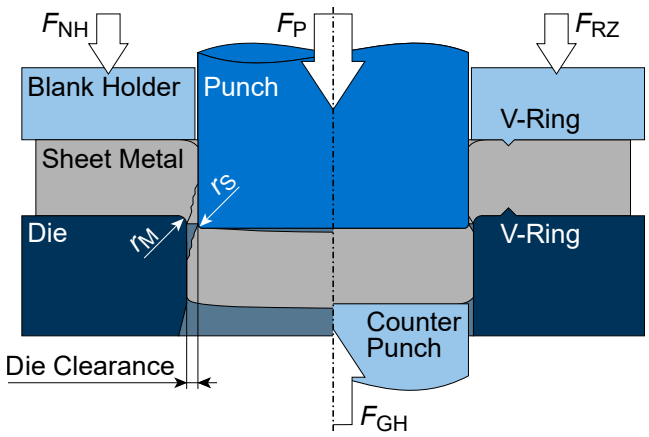

Figure 2.2: Basic tool setup of blanking (left) and fineblanking (right) according to Schmidt et al., 2007.

To prevent the sheet metal from lifting off the die, it can be subjected to a blank holder force F_{NH} by an additional blank holder. A counter punch with a corresponding counter punch force F_{GH} can be used to prevent the cut out part from lifting off the punch. Thus, the additional tool elements reduce the bending of the respective part of the sheet metal which can result in an improved work-piece flatness. Additionally, the blank holder can be used to guide the punch and to slip the sheet metal strip off the punch. A counter punch on the other hand is also used to eject the cut out part from the die. (Schmidt et al., 2007; Hörmann, 2008)

These different tool setups lead to a further sub-categorization in standard shear cutting and precision shear cutting[5], as proposed by Hoffmann, Neugebauer, and Spur, 2012. The precision shear cutting processes are defined as processes which are able to produce parts with a high geometrical cut-surface quality for applications where the manufactured surface is used to, for

[5] translated from German “Normalschneiden” and “Präzisionsschneiden”

example, transmit forces or movements. A typical precision shear cutting process is fineblanking, consisting of a tool setup with a small die clearance, a counter punch, a blank holder, and a v-ring on blank holder and/or die plate as illustrated in figure 2.2. Fineblanking is presented in detail together with other precision shear cutting processes in chapter 2.1.5. (Hoffmann, Neugebauer, and Spur, 2012)

2.1.2 Course and Mechanics of the Shear Cutting Process

Due to the multitude of process variants the basics of the shear cutting process are explained on the example of standard shear cutting. Additionally, a full-edged closed cut with a punch diameter bigger than the sheet metal thickness is considered. Only a brief overview is given here. A more detailed consideration can be found for example in Kopp, 2017 or Demmel, 2014.

According to Cammann, 1986 and Doege and Behrens, 2010, the blanking process can be divided in five phases. The last phase has been split, as published in Kopp, 2017 or Hörmann, 2008, to consider the separate removal of blank and sheet metal strip. The resulting six phases are displayed in figure 2.3. These phases are also visible in the cutting force curve, which is displayed in figure 2.4. Both the phases and the force curve will be explained in the following.

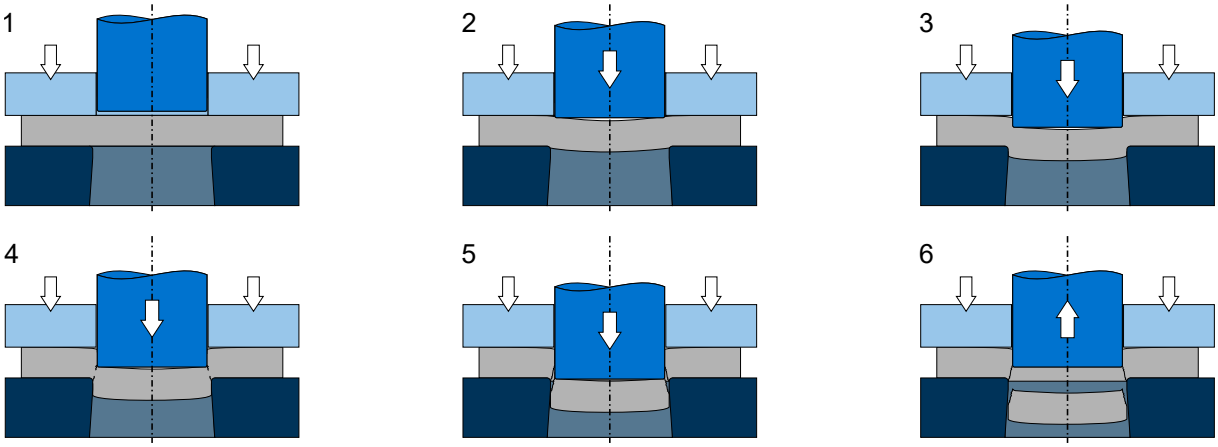

Figure 2.3: Phases of the shear cutting process according to Kopp, 2017 and Hörmann, 2008.

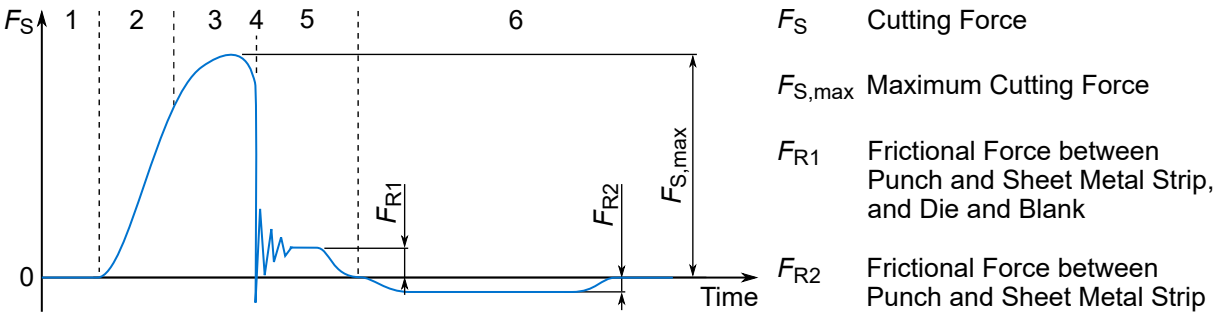

Figure 2.4: Cutting force curve according to Kopp, 2017.

Phase 1: Clamping by the Blank Holder

At the beginning, the sheet metal is placed between punch and die. The blank holder moves towards the sheet metal and clamps it against the die with the blank holder force F_{NH}. Meanwhile, the punch also moves towards the sheet metal. (Kopp, 2017)

Phase 2: Elastic Deformation of the Work-Piece

As soon as the punch gets in contact with the sheet metal, elastic deformation can be observed. A bending torque is induced by the resulting contact forces of punch and die with the sheet metal, which are separated by a lever arm (see figure 2.5). This torque causes the sheet metal to lift off punch and die which results in a comparably small contact zone close to the cutting edges (Kopp, 2017; Timmerbeil, 1957). A blank holder counteracts this bending which results in a reduced lifting off the die. Beside the elastic deformation of the sheet metal, tool and press are elastically deformed. (Schmidt et al., 2007; Hoffmann, Neugebauer, and Spur, 2012)

Phase 3: Plastic Deformation of the Work-Piece

Once the flow stress is reached in the sheet metal, plastic deformation occurs. The plastic flow follows the punch movement and forms the cut-surface geometry[6]. This deformation is influenced by the roughness of the sheet metal, the lubrication, the geometry of the cutting edges (Kienzle, 1956) and the used material. Plastic deformation mainly occurs in proximity of the cutting edges, the so called shear affected zone. The mechanic situation during Phase 3 is schematically illustrated in figure 2.5. (Kopp, 2017; Demmel, 2014)

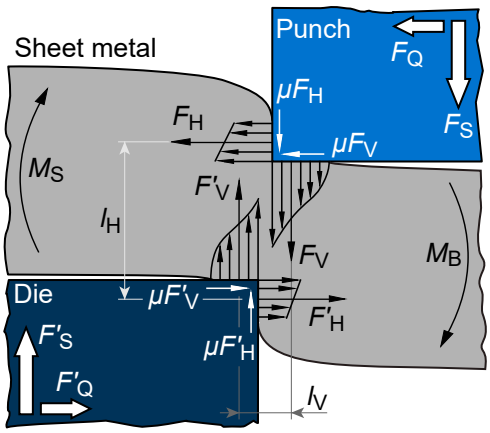

Cutting force on punch and die	F_S, F'_S
Lateral force on punch and die	F_Q, F'_Q
Vertical force on punch and die	F_V, F'_V
Horizontal force on punch and die	F_H, F'_H
Vertical frictional force on punch and die	μF_V, $\mu F'_V$
Horizontal frictional force on punch and die	μF_H, $\mu F'_H$
Vertical and horizontal lever arm	l_V, l_H
Torque on blank and sheet metal strip	M_B, M_S

Figure 2.5: Stresses, forces and torques acting on sheet metal and active elements during the shear cutting process according to Romanowski, 1959; Krämer, 1975.

Due to friction, elastic and plastic deformation stresses are acting on both punch and die. These stresses can be summed up in their resultants. In vertical direction F_V is acting on the punch close to the cutting edge. Its counterpart F'_V is acting on the die. These vertical forces cause frictional forces μF_V and $\mu F'_V$. In horizontal direction, the active elements are subjected to the

[6] Particularly die roll and clean cut, as defined in chapter 2.1.3, are formed.

forces F_H and F'_H which cause the frictional forces μF_H and $\mu F'_H$. Together, these forces are in dynamic equilibrium. (Romanowski, 1959; Doege and Behrens, 2010)

The cutting force F_S is the combination of all components[7] acting on the punch in its movement direction. These are the vertical components in the case displayed in figure 2.5. Its opposing force F'_S acts on the die. The maximum cutting force is influenced by the length of the cutting line, the sheet metal thickness, the material specific cutting resistance, the condition of the cutting edges, the surface of the active elements, the size of the die clearance, and the lubrication (Schmidt et al., 2007; Kolbe and Hellwig, 2015). The lateral forces can reach significant levels of more than 50 % of F_S (Mackensen et al., 2010) and are, among other factors, affected by the die clearance, the cutting edge conditions, the active element surface, and the tool's stiffness (Kopp, 2017). It should be noted that the lateral force components cancel each other for an ideal axial symmetric closed cut. (Doege and Behrens, 2010; Kopp et al., 2016)

The distances l_V and l_H between the resulting forces in vertical and horizontal direction result in the bending torques M_B and M_S in the sheet metal. The bending torque M_S causes the sheet metal to lift off the die if it is not counteracted by a blank holder. A counter punch may be used to prevent the sheet metal strip from lifting off the punch by counteracting M_B. (Doege and Behrens, 2010)

During this phase, a significant temperature rise can be observed at the cutting edges, caused by friction between sheet metal and tool and by the conversion of plastic work to heat. This temperature can reach more than 260 °C for small die clearances, big sheet metal thicknesses and high punch velocities. (Rosakis, Mason, and Ravichandran, 1993; Demmel, 2014)

Phase 4: Crack Initiation and Separation of the Work-Piece

With ongoing plastic deformation the sheet metal material is strain hardened, which leads to micropores due to a stress concentration on coarser and harder particles, for example non-metallic inclusions, which lead to the fracture of particles or their separation from the metallic matrix (Bergmann, 2013). With ongoing deformation these voids grow and coalesce while their behavior is significantly influenced by the subjected hydrostatic stress (see chapter 2.1.7) (Murakami, 2012). Finally, macrocracks are formed. Depending on the process parameters, a crack initiation is possible from the punch edge, the die edge or both. If both punch and die show the same cutting edge radius, the crack initiates at the die edge due to the overlayed stress caused by the sheet metal bending (Timmerbeil, 1957). Cracks are typically formed at the lateral surfaces of the active elements close to the cutting edges which results in a burr on the manufactured parts (Demmel, 2014; Kienzle, 1956). Finally, the cracks lead to the separation of the sheet metal in two parts. It is also possible that a crack propagates in the sheet metal and stops there which results in a scar on the surface (Timmerbeil, 1957).

[7] This does not include the counter punch force when a counter punch is used.

Phase 5: Removal of the Blank

After the separation the blank is still located in the die channel while the sheet metal strip surrounds the punch. Depending on the process parameters, the blank may be stuck in the die channel by the remaining elastic stresses and is pushed further by the punch until the bottom dead center is reached. This causes the frictional force F_{R1} which consists of the frictional force between sheet metal strip and punch, and the one between the blank and the die channel. (Volk, Kindsmüller, et al., 2018; Stahl, D. Müller, Tobie, et al., 2019) It is also possible that additional blanks from previous cutting operations are still located in the die channel. This increases the frictional force as multiple blanks have to be pushed through. As soon as the blank is removed from the die channel, the released elastic stresses cause a springback which changes the part geometry. (Buchmann, 1962; Hoogen, 1999; Hoffmann, Neugebauer, and Spur, 2012)

Phase 6: Return of the Punch and Stripping Off the Sheet Metal Strip

The same effect of the remaining elastic stresses causes the sheet metal strip to clutch the punch (Volk, Kindsmüller, et al., 2018). After reaching the bottom dead center, the punch moves upward again and lifts the sheet metal strip. Due to the tight fit between punch and sheet metal strip, a stripper plate has to be used to remove the strip from the punch[8]. This means that the stripper plate has to overcome the frictional force F_{R2}. For the tool setup displayed in figure 2.3, the blank holder serves that purpose. Finally, the blank is removed and a new sheet metal is inserted. As soon as the punch reaches the top dead center, a new cutting operation can be carried out. (Hörmann, 2008)

2.1.3 Cut-Surface Characteristics and Part Quality Measures

Depending on the field of application, different geometrical and mechanical requirements are placed on shear cut components. The geometrical characteristics regard size and flatness of the whole part, the dimensions of the shear-cut edge and its roughness. Mechanical properties of a shear-cut part are its hardness and its stress and damage state. As the question of how to quantify damage is still being actively discussed in the research community, this topic is not addressed in the following (Tekkaya et al., 2020).

Geometrical Properties

Geometrical tolerances of shear cut parts made of steel are standardized in DIN 6930-2, 2011. Shear cutting forms a characteristic surface of the cut edge. Depending on the chosen cutting process, these cut-surface characteristics are standardized in VDI 2906-1, 1994 to VDI 2906-6, 1994. According to VDI 2906-1, 1994, a cut-surface can be divided in die roll, clean cut, fracture zone, and burr. For fineblanking the cut-surface characteristics are illustrated in figure 2.6.

[8] During this stripping off operation, a second temperature rise can be observed which can reach more than 100 °C (Demmel, 2014).

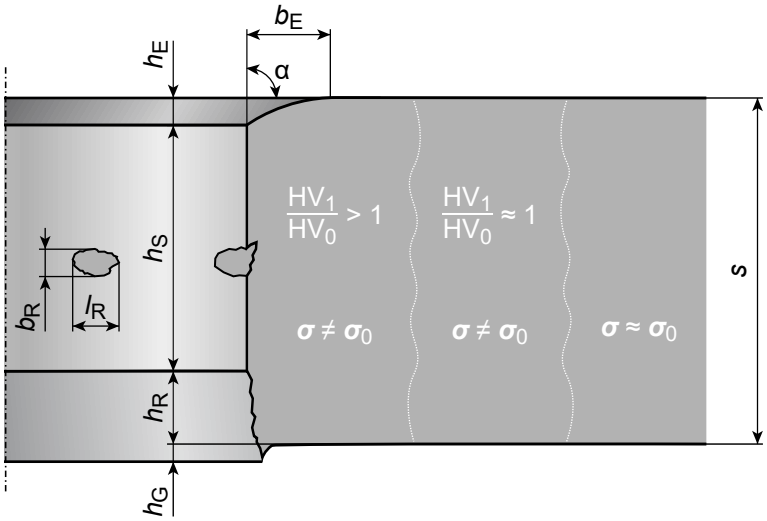

Die Roll Height	h_E
Die Roll Width	b_E
Clean Cut Height	h_S
Clean Cut Angle	α
Scar Height	b_R
Scar Length	l_R
Fracture Zone Height	h_R
Burr Height	h_G
Base Hardness	HV_0
Local Hardness	HV_1
Base Stress	$\boldsymbol{\sigma}_0$
Local Stress	$\boldsymbol{\sigma}$
Sheet Metal Thickness	s

Figure 2.6: Cut-surface characteristics of a fine-blanked part with the shear affected zone regarding hardness and stresses according to VDI 2906-5, 1994; Manopulo, 2011 extended by the considerations presented in Weiss, 2019.

Die Roll The die roll, a curved region of the sheet metal surface close to the tools, is formed as punch and die pull material from the respective sheet metal surface. It is characterized by the die roll height and the die roll width. A small die roll height is desired for parts with functional surfaces, as the die roll height reduces the surface available for a force transmission. Thus, material can be saved by reducing the die roll height. (Manopulo, 2011)

Clean cut The die roll is followed by a smooth area, the clean cut. Here, a surface roughness $Rz < 8\,\mu m$ is achievable by fineblanking (Hoffmann, Neugebauer, and Spur, 2012). The clean cut is characterized by the clean cut height and the clean cut angle. As this area can be used for transmitting forces and torques, a large amount of clean cut is desirable in many applications. Nevertheless, there are also cases where an as small as possible clean cut height is favored, for example to reduce the formation of sliver (Krinninger, 2019). While it is often desirable that the clean cut shows an angle of 90 ° to the sheet metal plane, a deviation from that is often observed. According to Manopulo, 2011, this effect can be attributed to the tension caused by the cutting edge as the material flows over it, which causes the formed surface to separate from the tool. Additionally, it is stated that the springback caused by the non-uniform strain hardening of the clean cut causes an angle deviation. (Manopulo, 2011)

Fracture The clean cut zone is followed by a fracture zone. This comparably rough surface is usually created when the material's formability is exhausted and the sheet metal is separated. It can show a roughness Rz of more than 15 µm (Pätzold et al., 2017). The fracture zone can be characterized by the fracture zone height. For blanking processes which show a big amount of fracture zone, the fracture zone angle is used as well. The fracture zone of parts manufactured by precision shear cutting processes is usually very small. In this case, it is also called tear-off zone (Hoffmann, Neugebauer, and Spur, 2012). As the fracture zone directly decreases the

amount of clean cut, a small fracture zone is desirable for many force transmitting applications. (Manopulo, 2011)

Scars Sometimes an additional fracture occurs before the complete separation of the sheet metal. The resulting crack is moving inside the sheet metal and not towards the opposing cutting edge. The remainder of the sheet metal is sheared of again, while a second clean cut zone is formed (Timmerbeil, 1957). These local fracture zones are referred to as surface scars in fineblanking. They are characterized by the scar height[9] and the scar length. (Romanowski, 1959; Manopulo, 2011)

Burr Following the fracture zone, a burr is observed on shear cut parts, which is characterized by the burr height. As a burr increases the injury risk or can cause problems during the painting of the parts, a small burr height is often desired. Furthermore, the burr can break off during operation. This is critical when the shear-cut parts are used, e.g., in gearboxes. (Kopp, 2017)

Flatness Due to the bending torques, a plastic bending of the shear-cut parts may be observed (Hörmann, 2008). It should be noted that bending also causes a springback which affects the clean cut angle (Kienzle, 1963).

Mechanical Properties

Hardness Beside the geometrical characteristics, the mechanical properties of a shear-cut part may be of interest. The plastic deformation which forms die roll and clean cut, causes strain hardening in the shearing zone which results in a higher hardness in this region. More than 2.5 times the sheet metals base hardness was measured by König and Rotter, 1982, for example. This increased hardness can be beneficial for the part's wear in its later application, but can also be negative for following manufacturing steps (Hoffmann, Neugebauer, and Spur, 2012). It should be noted that hardness and cold working are correlated, i.e., that a higher hardness indicates a higher strain (Weißbach and Dahms, 2007).

Stresses As stated by Theimert, 1975, plastic deformation of the shear-cut edge also causes elastic deformations in the part. These deformations cause a stress state σ that is different from the stress state of the base material σ_0. These elastic stresses reach further into the material as the hardness change. The area where the stress state is changed compared to the base stress state is called shear affected zone. The stresses in the shear affected zone do not necessarily have to be greater than zero, as shown by Doege and Kühne, 1990. Thus, the illustration given in Weiss, 2019 was altered to consider this phenomenon. (Weiss, 2019)

2.1.4 Parameters Affecting the Part Quality

The geometrical and mechanical properties of a work piece manufactured by shear cutting processes can be influenced by many different parameters, e.g., by the tool design, the chosen press,

[9] The scar height is referred to as scar width in Manopulo, 2011 and VDI 2906-5, 1994, which was changed to comply with the height/width terminology in this chapter.

the sheet metal material, and the used lubricant. These will be addressed in the following.

Tool and Press

Die Clearance According to C. Fritsch, 2002, the die clearance is the most important parameter regarding the part quality. It affects all the cut-surface characteristics and part quality measures listed in chapter 2.1.3 including the stress state (VDI 2906-2, 1994; Weiss, 2019). As published by Krämer, 1975, the clean cut height is increased when the die clearance is reduced. This is caused by the higher compressive stresses that allow the material to flow longer before fracture occurs (Hörmann, 2008). Still, differences between blank and sheet metal strip were observed by (Kienzle, 1963). Here, a too small die clearance caused scars on the part. According to VDI 2906-2, 1994, a bigger die clearance leads to an increased die roll height. This is caused by the additional volume in the gap between punch and die (Hörmann, 2008). A small burr height can be achieved by small die clearances (Schmidt et al., 2007). A small die clearance also reduces the resulting bending torque and therefore results in a smaller plastic bending of the part (Doege and Kühne, 1990). Still, Hörmann, 2008 found that an increased die clearance can reduce the bending of blanks manufactured by precision shear cutting processes.

Cutting Edge Condition The clean cut height is increased by using a bigger punch and die edge radius (Hoffmann, Neugebauer, and Spur, 2012). The formation of the die roll is primarily governed by the condition of the cutting edges, where a bigger radius or chamfer leads to a bigger die roll (Hoffmann, Neugebauer, and Spur, 2012). Small cutting edge radii result in a small burr height (Schmidt et al., 2007). By using a bigger punch edge radius a smaller part bending of the blanks can be observed (Volk, Kindsmüller, et al., 2018). A rounded die edge can have the opposite effect (Hörmann, 2008).

Blank Holder and Blank Holder Force The use of a blank holder reduces the bending of the sheet metal strip (Demmel et al., 2015) and can slightly increase the clean cut height (Hörmann, 2008). The blank holder force has only a small influence on the manufactured cut-surface (Hörmann, 2008).

V-Ring and V-Ring Force A v-ring leads to an increased hydrostatic pressure and prevents the material from flowing out of the shearing zone. That causes an increased clean cut height and a reduced die roll height. The use of a v-ring leads to a smaller deviation of the clean cut angle from 90 degree, but it can also lead to severe bending of the blank if no counter punch is used. (C. Fritsch, 2002; Hörmann, 2008).

For punching, the v-ring force has only a small influence on the clean cut height and no influence on the die roll height (König and Rotter, 1982). For blanking, a higher v-ring force leads to a smaller die roll height and a bigger clean cut height. Also, a v-ring on blank holder and die leads to a smaller die roll height than just one v-ring on either blank holder or die. (König and Rotter, 1982) It should be noted that also the position (J.D. Kim et al., 2012) and the shape (Su et al., 2014) of the v-ring have an influence on the cut-surface characteristics.

Counter Punch and Counter Punch Force The counter punch significantly reduces bending of the produced blank as it pushes the part against the punch (Kienzle, 1963). The counter punch force has no significant influence on the die roll height and the clean cut height of the blank. Nevertheless, an increased counter punch force may reduce the part bending and occurrence of scars. (Hörmann, 2008) For piercing with die clearances bigger than 0.5 %, an increased counter punch force can lead to an increased clean cut height but it can also lead to an increased deviation of the clean cut angle from 90 ° (König and Rotter, 1982).

Cutting Line Geometry The cutting line geometry has a significant influence on the die roll and clean cut height. Here, an opposing effect is observed on blank and sheet metal strip. A convex radius on the die leads to a smaller die roll height on the blank but it increases it on the sheet metal strip. Smaller radii and narrow geometries increase that effect. Scars or fracture or also more likely on convex parts of the blank with small radii (Wesner, 2017). (Volk and Stahl, 2020; VDI 2906-5, 1994)

Other Factors Other factors influencing the cut-surface characteristics are the active element coating, the stiffness of tool and press and the cutting velocity. The latter affects die roll, clean cut and fracture zone height (Weiss et al., 2017). The guidance of the tool influences the clean cut angle, the burr height and the occurrence of scars (VDI 2906-2, 1994). No significant influence of the tool stiffness on the cut-surface characteristics was observed by Kopp, 2017 for new active elements. The press stiffness on the other hand influences the cut-surface characteristics, especially for eccentric force application (Behrens and Pielka, 2011). The roughness of the clean cut can be decreased by using smoother active element surfaces (Kienzle, 1963). A coated surface can further reduce the part roughness (VDI 2906-5, 1994).

Materials and Lubricants

Sheet Metal Material and Thickness The used sheet metal material especially influences the occurrence of scars and the fracture zone height. Ferritic steels with finely distributed carbide are very well suited for fineblanking (Schmidt et al., 2007). An increasing amount of carbon and alloying elements make blanking more difficult (VDI 3345, 1980). Therefore, a high sheet metal strength achieved by micro-alloying instead of an increased carbon content is more suitable for fineblanking (Kasparbauer, 1999). An increased material thickness and tensile strength increase the die roll height (VDI 2906-5, 1994). Additionally, high strain hardening results in a bigger die roll height. Thicker sheets are more susceptible to scars. (Hörmann, 2008)

Lubricant The use of a lubricant has a significant effect on the cut-surface characteristics. Its most important effect is the reduction of tool wear, which affects all cut-surface characteristics as it may change the die clearance and the cutting edge radii over time. Apart from that, the clean cut height may increase (Kienzle, 1963) and the temperature during the process may decrease (Tröber, Golle, and Volk, 2015) when a lubricant is used.

2.1.5 Precision Shear Cutting Processes

According to Hoffmann, Neugebauer, and Spur, 2012, precision shear cutting processes are processes which are able to produce parts which can be used with minimal post-processing. To achieve this goal, several factors that influence the parts quality are used in different combinations. Among the precision shear cutting processes are the Near-Net-Shape-Blanking (NNSB) processes. As the word blanking indicates, the blank and not the sheet metal strip is usually of interest. A detailed summary of Near-Net-Shape-Blanking Processes is given in Hörmann, 2008 and Hoffmann, Neugebauer, and Spur, 2012, for example. An overview over the precision shear cutting processes based on these works, extended by recent findings, is shown in table 2.1.

Table 2.1: Extended overview of the precision shear cutting processes according to Hörmann, 2008; Hoffmann, Neugebauer, and Spur, 2012.

	Unique Punch or Die Design	Blank Holder	V-Ring	Counter Punch	Additional Scrap
One-Stage Precision Shear Cutting Processes					
Fineblanking		×	×	×	
Standard Blanking with Small Positive Die Clearance		(×)			
Standard Blanking with Negative Die Clearance		(×)			
Standard Blanking with Small Die Clearance and V-Ring		×	×		
Precision Blanking		×		×	
Precision Blanking without Blank Holder				×	
Opposing Dies Shearing Process		×		×	
Concave Nosed Punching	×	×			
Flow Blanking	×	(×)			×
Multi-Stage Precision Shear Cutting Processes					
Shaving and Two-Stage Shear Cutting		(×)			×
Counter Cutting		×			
Two-Stage Counter Cutting		×			×

× Necessary
(×) Optional

The focus in table 2.1 is on the used active elements, as proposed by Hörmann, 2008. Another categorization was proposed in this work regarding the possible tool technologies. The definition by Hörmann, 2008 is only used regarding the number of shear cutting steps that are necessary for manufacturing the part.

A further categorization is given in Hoffmann, Neugebauer, and Spur, 2012. Here, precision shear cutting processes are divided in those without the formation of shapeless matter and those

with the formation of shapeless matter. This questions the initial definition of shear cutting or the definition of shapeless. As the formed matter is well-defined for example in two-stage shear cutting (see Stahl, Pätzold, et al., 2020), it is referred to as additional scrap in table 2.1.

The use for piercing and blanking of some of these processes is addressed in Hoffmann, Neugebauer, and Spur, 2012. In the following, a short overview including piercing and blanking is given which extends the former works where recent research is available. Here, the nomenclature for blanking is used where possible.

Fineblanking

Fineblanking, with the typical tool setup displayed in figure 2.7, was patented in 1923 by Fritz Schiess as a blanking process with a v-ring, a counter punch and a small die clearance to achieve a smooth part surface without fracture. Usually a triple action press is necessary to control the ram force, the blank holder force and the counter punch force independently. (Hörmann, 2008)

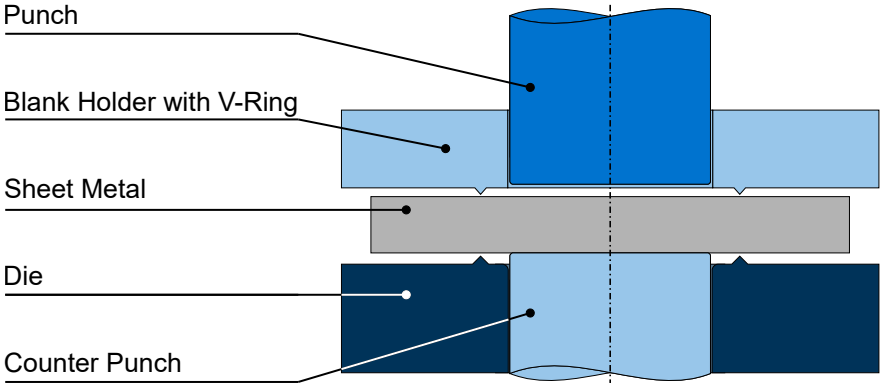

Figure 2.7: Tool setup of fineblanking with a v-ring on both blank holder and die.

The shape of the v-ring was standardized in VDI 3345, 1980. For sheet metal thicknesses up to 0.8 mm usually no v-ring is used, while a v-ring on the blank holder plate is recommended for thicknesses up to 5 mm. Beginning from a sheet thickness of 4 mm, v-rings on the blank holder plate and on the die plate are used together. As a v-ring on the die plate prevents grinding this plate after it is worn, a v-ring on the blank holder plate only is preferred if possible. The force for the v-ring to penetrate the sheet metal can be calculated according to Schmidt et al., 2007, although higher forces may be necessary, e.g., for cutting thick sheets (C. Fritsch, 2002). The counter punch force is given in Schmidt et al., 2007 and VDI 3345, 1980 with 20 to 70 MPa. Here, formulas for the ejector of stripping force are given as well.

As fineblanking is the most common NNSBP (Hörmann, 2008), many works deal with different aspects of this manufacturing technique. While it can be used for piercing and blanking, it is commonly used for blanking. For piercing, the imprint of the v-ring would be visible on the final part, which is often undesirable. Also, a variant with a v-ring on punch and blank holder can be imagined. When fineblanking is used for piercing it is also referred to as finepiercing (Aravind, Chakkingal, and Venugopal, 2019).

Standard Blanking with Small Positive Die-Clearance

Standard blanking, often just referred to as blanking, is a non-standardized term common in research and industry for blanking with a v-ring-less blank holder and without a counter punch. It is typically used for manufacturing cut-surfaces which show a significant fracture zone, i.e., which are used rather for separation than for the formation of a functional surface which is able to transmit forces and movements. Commonly, a die clearance between 8 and 12 % of the sheet metal thickness is used. The term standard blanking with a small positive die clearance[10] was coined by Hörmann, 2008 for this tool setup with a die clearance of 1 % or less. This process can be used for piercing and blanking. A rounded cutting edge is used to aid the material flow of the desired part, i.e., a rounded die edge for blanking or a rounded punch edge for piercing. As the blank holder is usually subjected to the blank holder force by springs, a single action press can be used for this process. (Hörmann, 2008; Hoffmann, Neugebauer, and Spur, 2012)

Standard Blanking with Negative Die Clearance

Blanking with a negative die clearance is closely related to blanking with a small die clearance, only that the die clearance is negative, i.e., the punch is bigger than the die. Depending on the cutting line geometry, the punch diameter is chosen 5 to 40 % of the sheet metal thickness bigger than the die. Again, rounded cutting edges are used. This process can be carried out on a single action press and can be used for piercing and blanking. Its main disadvantage is that the penetration of the punch has to be controlled precisely in order to fully separate the sheet metal without destroying the tool. (Hörmann, 2008; Kienzle, 1963)

Blanking with Small Die Clearance and V-Ring

The process blanking with a small die clearance and v-ring has also been coined by Hörmann, 2008. The tool setup consists of a punch, a die, a blank holder and v-rings on blank holder and/or die as illustrated in figure 2.8. Therefore, it is basically standard blanking with a small die clearance and a v-ring or fineblanking without a counter punch. Due to the missing counter punch it can be carried out on a single action press. It can be used in principle for piercing and blanking. As for fineblanking, piercing with a v-ring is uncommon due to the imprint left by the v-ring on the final part. (Hörmann, 2008)

[10] translated from German “Normalschneiden mit kleinem positivem Schneidspalt”

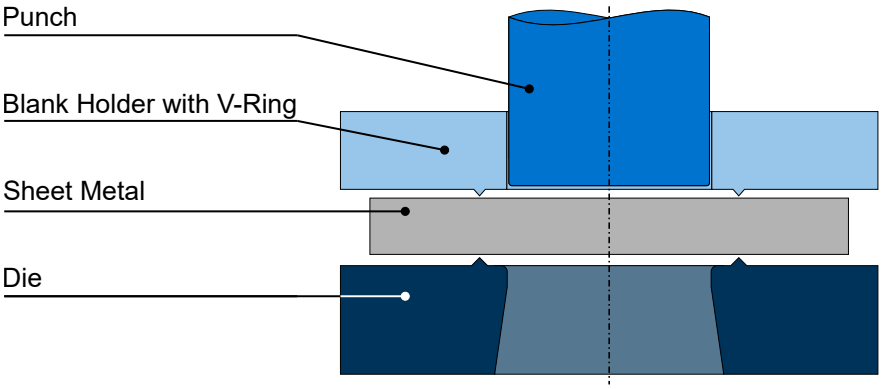

Figure 2.8: Tool setup of blanking with small die clearance and v-ring after Hörmann, 2008.

Precision Blanking

Precision blanking or precise blanking[11] (Manopulo, 2011) is a Near-Net-Shape Blanking process with a tool setup consisting of a punch, a die, a blank holder without a v-ring, and a counter punch, as illustrated in figure 2.9. It can be used for piercing and blanking. Again, a rounded die edge is used when the blank is of interest and a rounded punch edge when the sheet metal strip is used. The die clearance should not be bigger than 2 %. Due to the missing v-ring, the die roll is usually bigger than for NNSBPs with a v-ring. As three independent forces are necessary to control blank holder, ram, and counter punch, this process is carried out on triple action presses. (Hörmann, 2008; Hoffmann, Neugebauer, and Spur, 2012)

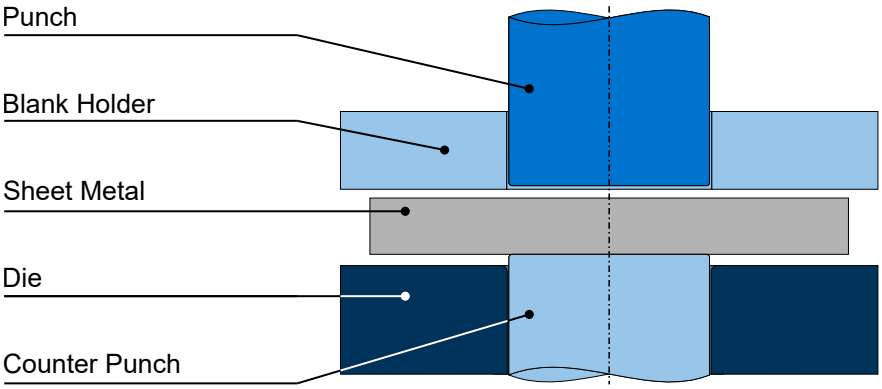

Figure 2.9: Tool setup of precision blanking according to Neugebauer et al., 2004.

Precision Blanking without Blank Holder

Precision blanking without blank holder, also known under the name grip blanking, was invented in 1971 by E. D. Bennett (Walker, 1997). This process shows the same tool setup as precision blanking, i.e., a punch, a die, and a counter punch, but no blank holder, as illustrated in figure 2.10. Nevertheless, a stripper plate is used to strip the sheet metal strip off the punch after the cutting operation. To prevent the counter punch from pushing the blank back into the strip, distance blocks are used. These allow the counter punch to remove the blank from the die

[11] translated from German “Genauschneiden”

channel before the sheet metal strip is stripped of the punch. By applying the counter punch force by springs or hydraulic cylinders, this process can be carried out on a single action press. While this process can be used in principle for piercing and blanking, it is not used for piercing due to the unrestricted bending of the sheet metal strip. (Bates, 2001; Hörmann, 2008)

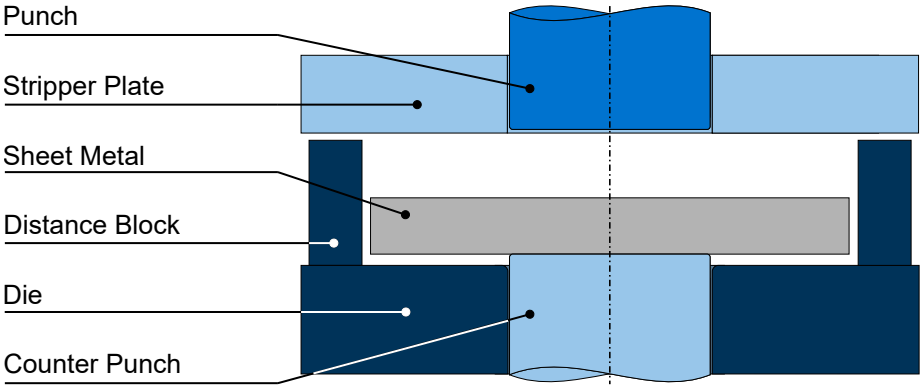

Figure 2.10: A typical tool setup for precision blanking without blank holder according to Hörmann, 2008; Bates, 2001.

Opposing Dies Shearing Process

The opposing dies shearing process was published by Kondo and Maeda, 1972. It consists of a punch, a die, a counter punch and an opposing die, the so called protruding die. This protruding die not only induces compressive stresses, but also penetrates into the sheet metal and causes the material to flow from the blank in the direction of the sheet metal strip. After the protruding die has penetrated the sheet metal material up to 80 % of its thickness, the punch is used to shear away the remains. Unlike the v-ring in fineblanking, the protruding die takes an active part in the material separation. This active use for guiding the material flow makes it possible to produce parts without a burr.

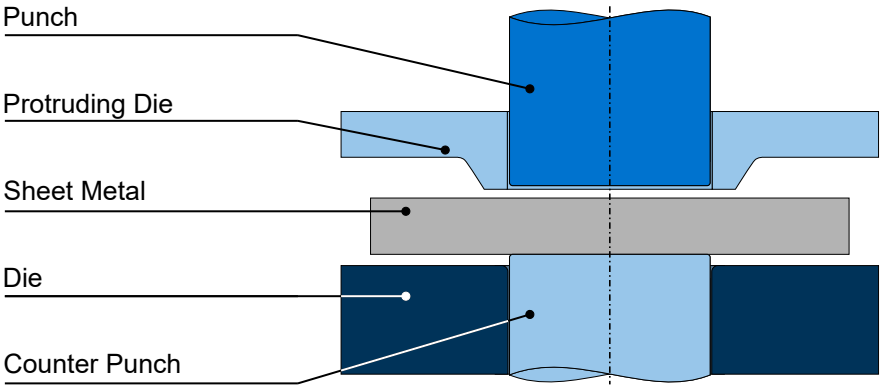

Figure 2.11: A typical tool setup for the opposing dies shearing process according to Kondo and Maeda, 1972.

The opposing dies shearing process can be used for piercing and blanking. In the case of piercing, the counter punch is designed to act as the protruding die by locally inducing material flow. To allow the material to flow from the final part, an initial hole is necessary, which makes

this case a multistage precision shear cutting process. Because of the protruding die and the counter punch, a triple action press is necessary. (Kondo and Maeda, 1972; Hörmann, 2008; Hoffmann, Neugebauer, and Spur, 2012)

Concave Nose Punching

Concave nose punching, as proposed by Senn and Liewald, 2018, is a process with the same tool setting as standard blanking or piercing, but with a punch that shows a concave nose close to the cutting edge as displayed in figure 2.12. This nose locally induces compressive stresses which delay the formation of cracks. With this punch design it is possible to cut holes without a fracture zone for comparably big die clearances of 5 % on a single action press. This process was proposed for piercing, but it could be used for blanking as well. (Senn and Liewald, 2018; Senn and Liewald, 2019)

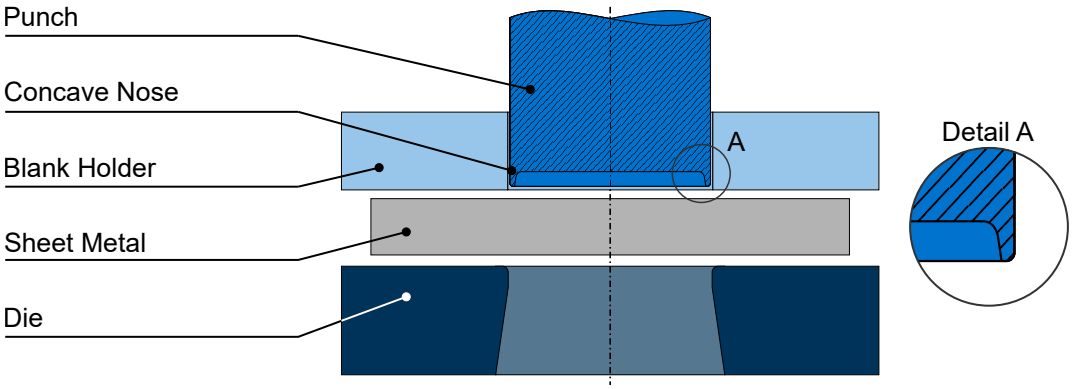

Figure 2.12: Tool setup for concave nose punching according to Senn and Liewald, 2018.

Flow Blanking

Flow blanking[12], as illustrated in figure 2.13, consists of a punch and a specifically designed die with a conical die channel. At first, a blank with an oversize is produced. In a second step, similar to a two-stage shear cutting process, the final contour is manufactured by extruding the part through a smaller hole in the die. The conical die channel assists the material flow in the second shear cutting step. Although the two steps are incorporated in a single punch stroke, additional scrap is formed. This scrap has to be removed before the next cut can be performed. There is also a process variant used for piercing, i.e., flow piercing[13]. For the piercing variant a punch that shows a conical region is used. Both process variants can be used on a single action press. Parts produced by this process shows a comparably small die roll, a high dimensional accuracy and also a small burr. As the removal of the extra scrap is challenging when this process is used for blanking, flow blanking is rarely used. (Hörmann, 2008; Hoffmann, Neugebauer, and Spur, 2012)

[12] translated from German “Fließausschneiden”
[13] translated from German “Fließlochen”

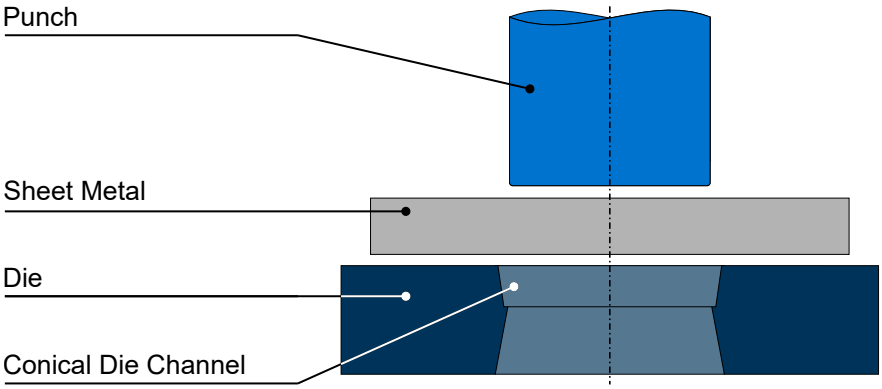

Figure 2.13: The tool setup for flow blanking as published in Hoffmann, Neugebauer, and Spur, 2012.

Multiple-Stage Precision Shear Cutting Processes

All the above mentioned precision shear cutting processes are able to produce parts in a single manufacturing step[14], but parts with functional surfaces can also be manufactured by using multiple manufacturing steps. Two-stage shear cutting is one example of such a process variant. Here, a slightly bigger contour is manufactured in a first shear cutting operation. The final contour is manufactured in a second shear cutting operation where only a small amount of the sheet metal is cut off. This means that an additional scrap is produced. Depending on the process parameters this process is also referred to as shaving (Schmidt et al., 2007). Sometimes more than two cutting operations are used (Kienzle and Timmerbeil, 1955). As for example illustrated in Hoffmann, Neugebauer, and Spur, 2012, this process can be used for piercing and blanking. The tool setup of two-stage shear cutting is similar to that of standard blanking for each cutting operation. Still, small die clearances have to be used to achieve a high amount of clean cut. A die clearance of 2-4 % for both cutting operations was suggested in Kienzle and Timmerbeil, 1955, although much bigger die clearances of up to 12.5 % are possible for some sheet metal materials (Kühlewein, 2003). As for example illustrated in Hoffmann, Neugebauer, and Spur, 2012, this process can be used for piercing and blanking. This process can be carried out on a single action press. Due to the high amount of clean cut together with a small die roll that can be produced with a comparably easy tool and press, this process is widely used. (Kienzle and Timmerbeil, 1955; Hoffmann, Neugebauer, and Spur, 2012)

As suggested in Kienzle and Timmerbeil, 1955, the second cut can be carried out in the opposite direction. With this counter shaving process it is possible to manufacture cut surfaces without a burr and with a die roll on both sides of the part (Hoffmann and Hörmann, 2007).

Counter cutting follows a similar idea regarding the opposite cutting directions. Here, the sheet metal is extruded in a first manufacturing step in one direction and afterwards cut in the opposite direction, i.e., the first operation is no cutting operation. Therefore, no additional scrap as in two-stage shear cutting is produced. In principle, this process can be used for piercing and

[14] except the opposing dies shearing process for piercing

blanking. This process can be carried out in a tool with a controlled counter punch which acts as the punch in the second manufacturing step. Another possibility is to use two stages in a tool. In this case, it can be carried out on a single action press. Parts produced by this process show no burr and a die roll on both sides if the process parameters are correctly chosen. It is also possible to use more than two steps. This means that the part is extruded in, for example, two opposite directions before the part is finally cut. (Stromberger and Thomsen, 1965; Liebing, 1979; Hörmann, 2008)

2.1.6 Blanking of Drive Parts

According to Gupta, Jain, and Laubscher, 2017 “fine-blanked gears have widespread applications including automotive, office equipment, appliances, medical equipment, electronic instruments, etc.”. For manufacturing spur gears, fineblanking is one of the most economic processes (Hydrel AG, 2020). As shown in Schuler GmbH, 1996, this can be attributed to the few necessary manufacturing steps of fineblanking compared to conventional machining processes. But fineblanking does not only offer economic benefits, but improves other qualities like the quietness during the operation compared to milled gears (Hydrel AG, 2020). Not only spur gears but also helical gears can be manufactured (Zimmermann et al., 2011).

Beside these advantages, blanked gear wheels also show several disadvantages. The available press force and the active element material strength limit the sheet metal thickness and strength. Additionally, shear-cut edges show a die roll and a fracture zone which reduce the load bearing surface. Especially the tips of the teeth show a distinct die roll, as shown in figure 2.14. (Klocke and Brecher, 2016)

Figure 2.14: Fineblanked gear wheel with a distinct die roll.

Not only involute gears can be manufactured by fineblanking. In Moench and Cettier, 2006, it was proposed to manufacture parts of a cycloidal drive by shear cutting. A cycloidal drive, when it is designed with a shortened cycloid (see Lehmann, 1976 and Lehmann, 1981), usually doesn’t show sharp edges or small radii that would cause a big die roll.

2.1.7 Simulation of the Shear Cutting Process

Elasticity and Plasticity

As presented above, many process variants are available for achieving functional surfaces with a high amount of clean cut. Furthermore, each variant requires adjusted process parameters for different materials to achieve the desired cut-surface characteristics. To reduce the experimental effort by part quality prediction and to gain additional insight, many researchers have investigated the simulation of the shear cutting process. In the following, the basics of elastic and plastic material behavior modeling are presented together with fracture modeling.

The Cauchy stress tensor σ_{ij} is the basis for the following considerations:

$$\sigma_{ij} = \begin{bmatrix} \sigma_{11} & \tau_{12} & \tau_{13} \\ \tau_{21} & \sigma_{22} & \tau_{23} \\ \tau_{31} & \tau_{32} & \sigma_{33} \end{bmatrix} \tag{2.1}$$

Strain ε_{ij} is defined, for example in a linearized form, by the infinitesimal displacements u_i of a material point as follows:

$$\varepsilon_{ij} = \frac{1}{2}\left(u_{i,j} + u_{j,i}\right) \tag{2.2}$$

Elasticity is commonly modeled using the Hook's law of elasticity with the Lamé parameters μ_L and λ_L. For an isotropic material undergoing small deviations it can be written:

$$\sigma_{ij} = 2\mu_L\varepsilon_{ij} + \lambda_L\varepsilon_{kk}\delta_{ij} \tag{2.3}$$

Instead of the Lamé parameters μ_L and λ_L, the form with Young's modulus E and Poisson's ratio ν is often used:

$$E = \frac{\mu_L(3\lambda_L + 2\mu_L)}{\lambda_L + \mu_L} \tag{2.4}$$

$$\nu = \frac{\lambda_L}{2(\lambda_L + \mu_L)} \tag{2.5}$$

The hydrostatic stress σ_H can be calculated from the first invariant I_1 of σ_{ij}:

$$\sigma_H = \frac{1}{3}I_1 = \frac{1}{3}(\sigma_{11} + \sigma_{22} + \sigma_{33}) \tag{2.6}$$

Or in Einstein notation:

$$\sigma_{ij}^H = \frac{1}{3}\sigma_{kk}\delta_{ij} = \sigma_H\delta_{ij} \tag{2.7}$$

As the hydrostatic stress does not lead to plastic deformation, the Cauchy stress tensor is split up in a hydrostatic and a deviatoric part:

$$\sigma_{ij} = \sigma_{ij}^H + \sigma_{ij}^D \tag{2.8}$$

Mises plasticity assumes that the second invariant J_2 of the deviatoric stress tensor is responsible for plastic deformation:

$$J_2 = \frac{1}{2}\sigma_{ij}^D \sigma_{ij}^D \tag{2.9}$$

The material starts to flow if the local von Mises stress σ_M is equal to a material, state variable, and forming history specific value k_f. Thus, the plastic flow is independent of the hydrostatic stress:

$$\sigma_M = \sqrt{3J_2} \tag{2.10}$$

Most metallic materials show a strain hardening behavior, i.e., the value k_f increases with increasing strain. This behavior can be described by many different models. One of these was proposed by Ludwik using the logarithmic strain φ (Ludwik, 1909):

$$k_f(\varphi) = k_{f0} + B_L \varphi^n \tag{2.11}$$

Here, k_{f0} is the initial yield stress while B_L and n are additional material parameters.

Many other authors proposed different models. The Voce model for example, saturates for high strains towards $k_{f\infty}$ (Voce, 1948):

$$k_f(\varphi) = k_{f\infty} - (k_{f\infty} - k_{f0}) \exp(-B_V \varphi) \tag{2.12}$$

Again, this model has three parameters k_{f0}, $k_{f\infty}$, and B_V which have to be identified.

Fracture

Most metals used in forming show a large plastic deformation which leads to micropores in the material which grow and coalesce with ongoing deformation. This finally causes ductile fracture. There is a variety of models to describe damage and fracture where the most prominent ones are micromechnical and phenomenological approaches (Volk, Groche, et al., 2019). In the following, measures and a phenomenological model for the prediction of ductile fracture are presented. (Bergmann, 2013)

In contrast to von Mises plasticity, the hydrostatic stress significantly effects the fracture behavior (Kahlow and Avitzur, 1974; Rice and Tracey, 1969). The stress triaxiality η can be used to consider the stress state during plastic deformation:

$$\eta = \frac{\sigma_H}{\sigma_M} \tag{2.13}$$

Beside the stress state, the magnitude of the plastic deformation has to be considered. A model proposed by Johnson and Cook, 1985 that considers both, plastic deformation and the stress triaxiality, allows to calculate the fracture strain φ_{frac} as follows:

$$\varphi_{frac} = C_1 + C_2 \exp(C_3 \eta) \tag{2.14}$$

According to this criterion, fracture occurs as soon as the fracture strain φ_{frac} is reached for the current triaxiality. C_1 and C_2 are experimentally determined calibration factors. Sometimes this model can also be found in an integral form.

Precision Shear Cutting Simulation Using the Finite Element Method

Blanking processes induce high plastic strains up to 7 (Zhao, Chen, and Dong, 2016), can cause a high temperature of over 250 °C (Demmel, 2014), and show strain rates over $10^3\,s^{-1}$ (Subramonian et al., 2013). Even a comparably low punch velocity of $10\,mm\,s^{-1}$ can cause a significant strain rate of up to $50\,s^{-1}$ (Hartmann et al., 2021). Describing this big range of state variables is challenging for material modeling, material model parameter identification, and for the finite element program.

Especially the fineblanking process is challenging to simulate. An excellent overview of the state of the art of fineblanking simulation with the finite element method was published by Manopulo, 2011 and Wesner, 2017. Therefore, this topic is not addressed in detail but only extended by recent publications.

Both Manopulo and Wesner predicted fracture by using damage criteria. Nevertheless, they did not simulate actual fracture, i.e., the complete separation of blank and sheet metal strip, which means that springback after the removal of sheet metal strip and blank from the tool can not be calculated by these methods. This topic has been dealt with for standard blanking by many authors, as published for example by Weiss, 2019.

Investigations considering the opening of the tool after separation of the sheet metal have been carried out by Baer et al., 2019 and Aravind, Chakkingal, and Venugopal, 2019. Both of these publications use rigid tools to reduce the calculation time. In Baer et al., 2019, the forces on the tools after the springback of the blanked part were of interest. Aravind, Chakkingal, and Venugopal, 2019 consider the stress state after fracture and the complete removal from the tools, i.e., the stresses in the manufactured parts without an external load acting on them.

2.2 Residual Stresses

2.2.1 Classification

Residual stresses are stresses in a body on which no external loads or torques are acting (Macherauch, Wohlfahrt, and Wolfstieg, 1973). This also includes that the body has to be in equilibrium of temperature and force (Withers and Bhadeshia, 2001b; Heyn, 1913). Every polycrystalline material is subjected to residual stresses (Macherauch, Wohlfahrt, and Wolfstieg, 1973). They can be useful to improve the fatigue behavior of a part, for example by inducing compressive residual stresses by shot-peening, or can lead to an unexpected failure of the part, for example by stress corrosion cracking (Häfele, Issler, and Ruoß, 2003b; Häfele, Issler, and Ruoß, 2003a). As residual stresses can be undesired, they can be reduced by a stress relief heat treatment. But

even at room temperature, residual stresses slowly relax over time (Heyn, 1921). Depending on the scale, residual stresses can be divided into three groups, as displayed in figure 2.15.

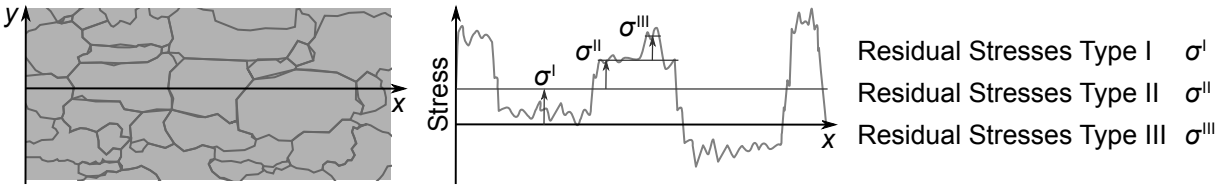

Figure 2.15: Classification of residual stresses according to Macherauch, Wohlfahrt, and Wolfstieg, 1973; Reihle, 2015.

Macrostresses or type I residual stresses vary over a large distance, i.e., on the scale of the whole part and over several grains. This is expressed in equation 2.15 by the mean over a representative volume element (RVE)[15]. When the equilibrium of type I residual stresses is disturbed, macroscopic changes of the part's dimension occur. Intergranular stresses or type II residual stresses are homogeneous over a single grain, which is given in equation 2.16. As they are in equilibrium with several grains, they can also cause macroscopic changes. Type III residual stresses vary on the atomic scale, i.e., within a single grain as given in equation 2.17. Therefore, they do not cause macroscopic changes of the part's dimension when the equilibrium is disturbed. In all typically used materials these stresses are superposed. (Withers and Bhadeshia, 2001a; Macherauch, Wohlfahrt, and Wolfstieg, 1973)

$$\sigma^I = \underset{\text{RVE}}{\text{mean}}(\sigma) \tag{2.15}$$

$$\sigma^{II} = \underset{\text{grain}}{\text{mean}}(\sigma) - \sigma^I \tag{2.16}$$

$$\sigma^{III} = \sigma - (\sigma^I + \sigma^{II}) \tag{2.17}$$

Residual stresses in a material can have different causes. Kloos, 1979 separates those caused by material effects, those caused by loads and those caused by the manufacturing process. The material related residual stresses are for example caused by non-metallic inclusions or lattice defects. Loads leading to residual stresses can be thermal, chemical, or mechanical. Thermal residual stresses can be caused by temperature fields during operations, chemical ones by hydrogen diffusion, and mechanical ones by local plastic deformation. Residual stresses induced by manufacturing processes are subcategorized according to DIN 8580, 2016, which includes forming and separating. Here, inhomogeneous or anisotropic plastic deformations are listed as reasons for forming induced residual stresses. (Reihle, 2015; Heyn, 1921)

[15] A RVE as discussed by Kanit et al., 2003 is considered, i.e., a RVE in which inhomogenities between single grains are averaged.

2.2.2 Residual Stresses induced by Shear Cutting and Related Processes

Both forming and blanking cause inhomogeneous plastic deformations which cause residual stresses. These have been analyzed and subsequently used by many authors. As residual stresses induced by shear cutting influence the efficiency and the size accuracy of electrical sheets, most research was carried out in this field. Therefore, this topic will be addressed separately followed by standard shear cutting and fineblanking of sheet metal materials used for typical parts manufactured by forming.

Standard Shear Cutting of Electrical Sheets

In a study using neutron radiation conducted by Zaizen et al., 2016 on an electrical sheet with a thickness of 0.30 mm, it was found that the blanking process changes the residual stress state almost a millimeter away from the sheared edge. A significant hardness change caused by plastic deformation was only measured up to a distance of 0.2 mm. Dehmani et al., 2016 measured the residual stresses of ten stacked shear-cut electrical sheets by X-ray diffraction, where a tensile stress state was identified.

The influence of the cutting process on the size accuracy and the residual stress state of electrical stators and rotors was investigated by Doege and Kühne, 1990. The stress state was measured by X-ray diffraction and strain gauges. It was found that piercing reduced the initial compressive stress state close to the holes independent of the die clearance. The produced blanks on the other hand showed that the blanking process induced tensile residual stresses on the die roll side while it caused no change or slight compressive stresses on the burr side. Here, a bigger die clearance led to a more compressive stress state on the burr side while it caused bigger tensile stresses on the die roll side. This was attributed to the springback of the bend blanks. A changed blank holder force showed no clear effect on the residual stress state of blank and sheet metal strip. (Doege and Kühne, 1990)

A recent publication by Weiss, 2019 investigates the effect of the shear cutting induced residual stresses on the efficiency of electrical sheets. Here, Finite-Element simulations were carried out for different process parameters. It was found that blanking causes a locally high residual field on the sheared edge. For small die clearances, the field decreases rapidly with increasing distance from the shear-cut edge while bigger die clearances cause a slower decrease. Additionally, worn cutting edges were found to generate higher and more extended residual stresses compared to sharp edges. (Weiss, 2019)

Standard Shear Cutting

The residual stress of an edge manufactured by guillotining, a shear cutting process used for cutting-off where the blades usually show an angle to each other, was measured by Martins et al., 2006. Here, significant tensile stresses over 2500 MPa were measured close to the edge. (Martins et al., 2006)

Yasutomi et al., 2017 measured the residual stresses on the shear-cut edge of pierced parts by X-ray diffraction for three die clearances of 5, 10 and 20 %. Significant tensile stresses in tangential and in thickness direction were measured close to the die roll, in the middle of the sheet, and close to the burr. Here, the burr side showed the highest tensile stresses. It was not addressed how the die clearance affects the residual stress state. (Yasutomi et al., 2017)

An early investigation of the residual stresses induced by blanking was published by Doege and Fugger, 1983. It was postulated that the residual stresses lead to a changed contour of the part after fracture. This changed geometry was connected to friction between the punch and the sheet metal strip or between the die and the blank. Additionally, X-ray diffraction measurements were carried out to identify the residual stress state in the radial center of circular blanks manufactured with a die clearance of 8 %. It was found that a compressive residual stress state can be observed on both sides of the blank when new active elements are used. Here, the burr side showed smaller compressive stresses than the die roll side. Nevertheless, only a small portion of bending stresses was calculated. Worn cutting edges further increase these compressive stresses. Close to the shear-cut edge, tensile residual stresses were measured in tangential and radial direction on the burr side of the sheet metal while compressive residual stresses dominate the die roll side. An increased die clearance of 12 and 20 % resulted in compressive stresses on both sides. (Doege and Fugger, 1983)

The influence of die clearance and the punch edge radius on the residual stresses of pierced high strength steels was investigated by Purwo, 2014. Residual stresses in thickness direction were measured in the middle of the sheared edge by X-ray diffraction. Here, a rounded punch led to higher compressive stresses compared to a sharp punch edge. While mostly tensile residual stresses were measured for a die clearance of 10 %, a compressive residual stress state was present for a die clearance of 0.8 %.

A method that allows to calculate the part deflection caused by shear cutting induced residual stresses using the Finite-Element method was proposed by Moesdijk et al., 1998. It was found that these residual stresses cause a severe bending of the parts. Not only the finite element method can be used to calculate the blanking induced residual stresses. For example the Smoothed Particle Hydrodynamics method can be used, as published by Bohdal et al., 2016.

Fineblanking

Česnik et al., 2012 found that the distortion of fineblanked rings is related to residual stresses by carrying out Finite-Element simulations. They calculated differences between the die roll side and the burr side of the part where the die roll side showed significant tensile stresses. On both sides higher compressive stresses were identified close to the blanked surface. They state that the residual stresses are influenced by the shape of the part, the condition of the active elements, and the chosen sheet metal material. (Česnik et al., 2012)

Another study where residual stresses induced by fineblanking were investigated by Finite-Element simulations was published by Aravind, Chakkingal, and Venugopal, 2019. Here, compressive residual stresses were calculated in the tangential direction of a hole on the die roll side that change to tensile stresses close to the burr. (Aravind, Chakkingal, and Venugopal, 2019)

2.3 Fatigue Strength

2.3.1 Basics

Fatigue describes the phenomenon that a part or a structure fails under a repeated load, although the part does not show any damage when it is subjected to the same load once. This means that the material is weakened by cyclic loading even though the stress is below its yield strength. (Milella, 2012)

As many parts are subjected to cyclic loading, like gears for example, it is of interest to characterize a material's strength under such loads in order to calculate the part's lifetime. A characterization can be carried out by subjecting specimens to a defined cyclic stress while counting the number of cycles to failure. This is performed for a batch of specimens for different stress levels. Subsequently, the stress amplitude S of each batch is plotted against the mean of the number of cycles to failure N in an S-N-diagram. The connecting line between the data points in this diagram is called a Wöhler-Curve. A schematic Wöhler-Curve with a double-logarithmic scale according to Basquin is displayed in figure 2.16 for a typical steel. (Haibach, 2006)

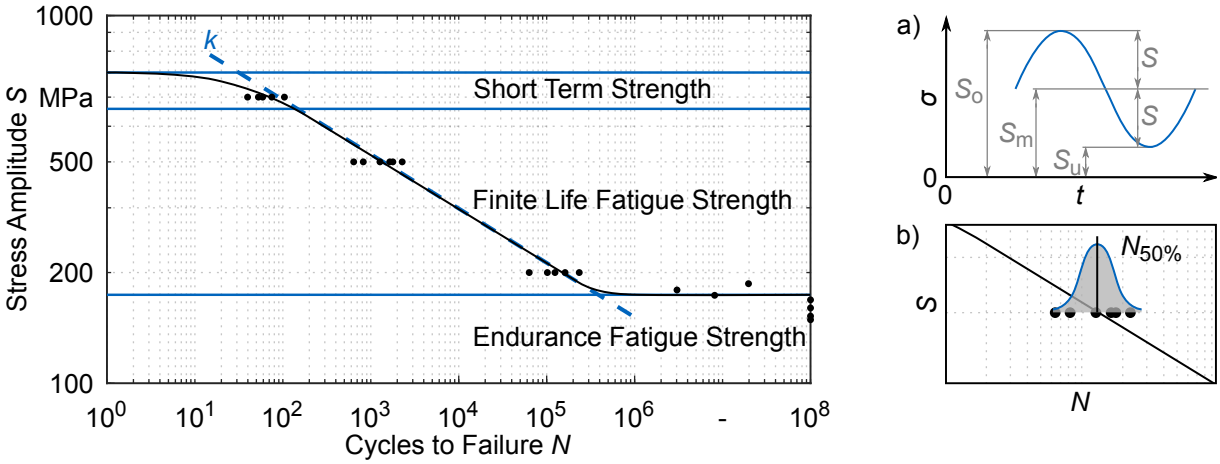

Figure 2.16: A schematic Wöhler-Curve with a double-logarithmic scale according to Basquin (left) together with the load on a specimen (a) and a probability distribution of the specimens (b) according to Haibach, 2006.

For a typical Wöhler test, a sinusoidal load is chosen. As illustrated in figure 2.16 a), this load can be characterized by the mean stress S_m, the upper stress S_o, and the lower stress S_u where the stress amplitude S can be calculated by $\frac{1}{2}(S_o - S_u)$. The stress ratio $R_S = S_u/S_o$ is often used to characterize the load case. A different shape of the subjected load may lead to a different part lifetime (Gassner and Lowak, 1978). (Haibach, 2006)

Within each batch a single fractured specimen shows N_i cycles to failure, as indicated by black dots in figure 2.16. The underlying statistical distribution has to be considered to be able to calculate a mean and a failure probability as illustrated in figure 2.16 b). A logarithmic normal distribution can be assumed, for example, where the 50 % failure probability $N_{50\,\%}$ can be calculated with the following equation: (C. Müller et al., 2017)

$$\lg\left(N_{50\,\%}\right) = \frac{1}{n}\sum_{i=1}^{n}\lg(N_i) \tag{2.18}$$

The Wöhler-Curve can be divided in three different regions. In the German-speaking research community, a division regarding the stresses is common, as in Haibach, 2006, while the English-speaking community favors a division regarding the number of cycles to failure, as for example in Kobelev, 2018.

For a stress amplitude close to the yield strength, very low cycles to failure are observed. Therefore, this region is called short term strength (J. Kim and Weidlich, 2017) or low cycle fatigue. Fracture in this region is dominated by plastic deformation (see chapter 2.1.7). (Bolotin, 1999)

This region is followed by the finite life fatigue strength or high cycle fatigue. As the load decreases, more and more cycles to failure are observed. In this region, the stress is low enough that the specimens mainly show elastic material behavior. Plastic deformation only occurs at the tip of cracks. (Milella, 2012) According to Basquin, the Wöhler-curve in the double-logarithmic *S-N*-diagram can be described by a line. The slope of the line is also called *k*-factor. It can be calculated by using the number of cycles to failure N_1, N_2 and the fatigue strength σ_1, σ_2 of two load levels: (Haibach, 2006; Häfele, Issler, and Ruoß, 2003a)

$$k = -\frac{\lg(N_1/N_2)}{\lg(\sigma_1/\sigma_2)} \tag{2.19}$$

If the load is further reduced, below the fatigue or endurance limit, no fracture occurs for a very high number of load cycles. This region is called endurance fatigue strength. Nevertheless, an infinite number of endurable load cycles has been questioned for example by Sonsino, 2005.

The fatigue strength of a part is influenced by many different factors. The used material and its hardness significantly influence the fatigue strength, where, in the case of steels, a higher tensile strength or hardness are beneficial for the fatigue behavior. Regarding the Vickers hardness this effect has been published by Casagrande, Cammarota, and Micele, 2011. An increased hardness achieved by cold working can also result in a more brittle behavior as ductility is lost.

Corrosion and high operation temperatures can lead to a lower fatigue strength. A higher mean stress results in a lower fatigue strength. Multiaxial loading has to be considered. Notches in the part lead to a stress concentration, i.e., high local stresses. These can be considered by notch factors K_t. The same effect causes parts with a rougher surface to show a lower number of

cycles to failure. Bigger specimens tend to have a lower fatigue strength because the probability of a weak point in the material is bigger. (Radaj, 2003)

As mentioned in chapter 2.2.1, residual stresses significantly influence the fatigue strength. Here, compressive residual stresses lead to a higher fatigue strength whereas tensile residual stresses may lead to an early failure (Häfele, Issler, and Ruoß, 2003a). This effect can be explained by the capability of a crack to grow under a cyclic load. Compressive residual stresses can close a crack on the specimen surface. Thus, crack growth can be inhibited or completely stopped. (Habschied et al., 2015)

The effect of residual stresses on the fatigue behavior can be calculated by several models. The Mertens model assumes a linear influence of the residual stress in loading direction on the endurable stress (Kleemann and Zenner, 2006). According to Radaj, 2003, the Sines approach can be used. Here, non-uniform residual stresses are considered by their mean hydrostatic stress. A linear dependency on the endurable stress is assumed. (Radaj, 2003) These approaches have been questioned by Kleemann and Zenner, 2006 regarding their consideration of residual stresses perpendicular to the loading direction.

The fatigue strength is significantly influenced by how the specimen is manufactured (Radaj, 2003). This can be attributed to the fact that the manufacturing technique and its process parameters affect, for example, the surface hardness and the residual stress state among others. A method to consider the influence of the manufacturing techniques shear cutting and laser cutting on the resulting fatigue strength was proposed by Dittmann and Pätzold, 2018. Here, a factor is used that considers the decreased ductility of the shear-cut and laser-cut specimens compared to a polished reference. However, no clear correlation between this factor and the measured hardness and cut-surface condition could be made. Thus, the experimentally determined factors should be used. (Dittmann and Pätzold, 2018)

2.3.2 Fatigue Strength of Shear-Cut Edges

As it is challenging to calculate the fatigue strength of shear-cut edges, it is usually determined experimentally. However, the fatigue strength of shear-cut edges has been investigated by few authors compared to other edge properties like the cut-surface characteristics (Dittmann and Pätzold, 2018). Most authors focus on standard blanking compared to machining or laser cutting, while only few publications address NNSB- or other blanking processes. Thus, standard shear cutting is addressed at first.

Standard Shear Cutting

Meurling et al., 2001 found that the fatigue strength of edges manufactured by shear cutting with a die clearance of 6 % is usually lower than that of edges manufactured by laser cutting for the investigated deep drawing and stainless steels. This was attributed to the presence of larger surface defects of the shear-cut specimens. No information is given on the active element edge

preparation and whether a closed or open cut was used. (Meurling et al., 2001).

In the work published by Lara, Picas, and Casellas, 2013 specimens made of 22MnB5 (thickness 1.8 mm) and DP1000 (thickness 2.0 mm) were manufactured with an open cut. One group of specimens was manufactured with a die clearance of 6 % and a punch edge radius of 30 µm whereas the second group was produced with a die clearance of 10 % and a punch edge radius of 100 µm. For both materials the first group showed a higher endurance fatigue strength. Due to the simultaneous change of the die clearance and the punch edge, no statement was given regarding the influence of a single process parameter on the fatigue strength. For the specimens made of 22MnB5 it was found that the cracks initiate either between clean cut and fracture zone, in the fracture zone or close to the burr. (Lara, Picas, and Casellas, 2013)

Maronne et al., 2003 investigated the die clearance influence on the fatigue strength reduction of shear cutting compared to polishing. Specimens with a notch factor of $K_t = 1.03$ were manufactured from steel sheets with a thickness of 1.50 to 2.55 mm and tested under a tensile stress with a ratio of $R_S = 0.1$. By continuously reducing the die clearance from 30 % up to 5 % they found that if the die clearance is too big, a significant reduction of the fatigue strength can be observed. For the nine steel grades it was found that steels with a high tensile strength are more sensitive to the shear cutting process. No information is given on the preparation of the cutting edges and whether an open or closed cut was used. (Maronne et al., 2003)

Thomas et al., 2011 investigated the influence of the die clearance on the fatigue strength for $R_S = -1$ for specimen made of S355MC and DP600 (thickness 3 mm) manufactured with a die clearance of 6.6 %, 9.9 %, and 13.2 %. The specimen showed parallel edges in the smallest cross section. It was found that the big die clearance is beneficial when cutting S355MC and the small die clearance delivers the best fatigue strength for DP600. This effect was attributed to compressive residual stresses, which were not measured. Furthermore, a tilting of the finite lifetime fatigue line of the shear cut specimens compared to polished specimens was observed. The cutting edge preparation and the nature of the cut were not addressed. (Thomas et al., 2011)

A detailed investigation on the effect of blanking process parameter on the resulting fatigue strength has been published by Pätzold et al., 2017 and Dittmann and Pätzold, 2018. Specimens made of DP800 with a thickness of 1.5 mm were manufactured with $K_t = 2.5$ by cutting a hole in the middle of the sheet and tested with $R_S = -1$. While a standard shear cutting strategy with sharp active element edges ($r_S < 10\,\mu m$; $r_M < 10\,\mu m$) and a die clearance of 15 % led to a significant decrease of the fatigue strength compared to polished specimens. Specimens manufactured with the same die clearance and a bigger punch edge radius of $r_S = 300\,\mu m$ resulted in a fatigue strength as high as that of the polished specimens. An almost identical finite life fatigue strength and slightly lower endurance fatigue strength was achieved by cutting with a punch edge radius $r_S = 200\,\mu m$ and a die clearance of 2 %, although the specimen cut with the small die clearance showed no fracture zone. For all other investigated variants, a correlation between the amount of clean cut and the resulting fatigue strength was identified,

which was explained by the lower probability of a point of origin for a fatigue crack. Another strategy aimed to decrease the specimen roughness by polishing and coating the punch. This configuration with a $r_S = 50\,\mu m$ and a die clearance of 15 % showed no improvement compared to the initial strategy with $r_S < 10\,\mu m$ and $u_{rel} = 15\,\%$. It was stated that the roughness has no influence on the fatigue strength for specimen manufactured with a closed cut. These results were extended by additional specimens made of DC04 (thickness 1.5 mm), CP800 (thickness 1.5 mm), DP1000 (thickness 1.4 mm), CP1000 (thickness 1.4 mm), and 22MnB5 (thickness 1.5 mm), by specimens manufactured with different notch factors and with an open cutting line. Those investigations showed that the observations made for the reference material and notch factor are not necessarily transferable to other materials and geometries. (Pätzold et al., 2017; Dittmann and Pätzold, 2018)

Precision Shear Cutting Processes

Piercing of high-strength steels with a small die clearance of 0.8 % and different punch edge radii was investigated by Purwo, 2014. Here, the rounded punch edge radii with $r_S = 0.13\,mm$ and $r_S = 0.33\,mm$ led to a higher strength in a plane bending fatigue test compared to a sharp punch edge. This was attributed to the higher compressive residual stresses of the parts manufactured with rounded cutting edges. No significantly different fatigue strength was observed between two round punch edge configurations. (Purwo, 2014)

The fatigue strength of flat bars with a hole manufactured by blanking, fineblanking and precision blanking with different process parameters compared to machined holes was published in König and Rotter, 1982, R. Fritsch, 1983 and Klocke, 2013. Here, sheets with a thickness of 14 mm made of S235JRG2 and S355J2+N were used and tested with $R_S = -1$. The fatigue strength of the holes manufactured by all blanking processes was found to be higher than that of holes manufactured by drilling and drilling with reaming. This effect was attributed to the strain hardening of the edge caused by the shearing processes (Klocke, 2013). Die clearances of 0.25 %, 0.5%, and 1 % were investigated for precision blanking, although no significant effect on the fatigue strength was observed (König and Rotter, 1982). Still, a die clearance of 0.25 % compared to 0.5 % led to a slightly higher fatigue strength, as mentioned in (Klocke, 2013). Additionally, the effect of the v-ring[16] was investigated. A significantly higher fatigue strength was observed for the variant with a v-ring compared to the variant without a v-ring while using the same die clearance. No information was given on the preparation of the active element edges. (König and Rotter, 1982; R. Fritsch, 1983; Klocke, 2013)

Multistage Shear Cutting Processes and Post-Treatment Processes

A strategy to minimize residual stresses by two-stage shear cutting was proposed in Dittmann and Pätzold, 2018. Here, specimens made of DP800 (thickness 1.5 mm) were manufactured

[16] Termed as “knife-edged ring” in Klocke, 2013.

with a cutting edge radius of 10 µm and a die clearance of 15 % in the first and the second shear cutting operation. A cutting offset of 2 mm was used. This strategy resulted in a lower fatigue strength compared to the one-stage reference strategy where the specimens were manufactured with an open cutting line, the same cutting edge preparation and die clearance. Nevertheless, no residual stress measurements were carried out. (Dittmann and Pätzold, 2018)

A study considering the influence of residual stresses on the fatigue strength of electrical sheets was carried out by Dehmani et al., 2016. A tensile residual stress state was measured on the sheared edge of ten specimens simultaneously using X-ray diffractometry. Additionally, shear-cut and subsequently polished specimens were analyzed, which showed a compressive residual stress state. A reduced fatigue strength of the shear-cut specimen compared to the shear-cut and polished specimen was observed for $R_S = 0.1$. However, no information was given regarding the die clearance and the active element edge condition. (Dehmani et al., 2016)

Shirasawa, 1994 found a much lower fatigue strength of specimen made of B60 and C80 (thickness 2.3 mm) with holes manufactured by shear cutting compared to ones manufactured by drilling and subsequent reaming. He was able to improve this low fatigue strength by coining the burr side of the shear-cut parts, which he attributed to the smoother surface, a higher hardness and possibly a changed residual stress state. (Shirasawa, 1994)

Yasutomi et al., 2017 followed that idea by using the scrap and a counter punch to coin the fracture surface of the manufactured specimen (material JSC980Y, thickness 1.6 mm). As mentioned in chapter 2.2.2, the initial tensile stress state of shear cut holes was changed to a compressive stress state by this method, which resulted in a significantly higher fatigue strength. (Yasutomi et al., 2017)

The works of Yasutomi et al., Purwo and Dehmani et al. are the only publications known to the author that consider the influence of residual stresses on the fatigue strength of parts manufactured by shear cutting or related processes.

2.4 Need for Research

Parts manufactured by precision shear cutting processes like fineblanking are used in many industrial applications where the cut edge has to transmit forces or movement. As an as high as possible clean cut height is desirable, a lot of effort has been put into the investigation of the cut-surface characteristics.

Nevertheless, functional surfaces do not only have to withstand local pressure but are also subjected to cyclic loads, for example in automobile drivetrains. This means that the fatigue strength has to be considered as well. While many works deal with the influence of the process parameters on the fatigue strength for standard piercing, only few works deal with this topic for surfaces manufactured by precision shear cutting processes. While the listed publications show tendencies, a clear statement regarding suitable process parameters often can not be made as a

precise and complete overview of process parameters used, like the cutting edge preparation, are not mentioned.

To complicate matters, the residual stress state of the shear-cut edge is usually not considered although the significance of residual stresses on the fatigue strength have been shown by many. Again, only few authors deal with residual stresses induced by precision shear cutting processes. Mostly, either the stress state of the produced sheet metal strip or the blank are investigated. An overview of the influence of the process parameter on the residual stress state has not been published for these processes, even though a significant influence of, for example die clearance or cutting edge preparation, have been shown for standard blanking. Additionally, only fineblanking and standard blanking have been investigated regarding the residual stresses while there is a variety of other one-stage precision shear cutting processes. Since it has been shown that the selection of the blanking process significantly affects the cut-surface characteristics, its effect on the residual stress state has not been shown yet. Furthermore, only circular or linear geometries have been investigated. As most relevant parts show complex geometries, this influence has to be addressed. In typical applications, the part is subjected to many load cycles under increased temperatures. To be able to use to positive effect of residual stresses, their stability under typical operation conditions should be investigated.

For the targeted use of these process induced residual stresses for an improved fatigue strength, a basic understanding of the relationship between the chosen precision shear cutting process, the process parameters and the residual stress state is necessary.

3 Problem Definition, Objectives, and Solution Approach

3.1 Problem Definition

A general objective in industry is the reduction of production costs while maintaining or improving component quality. For high volume applications, shear cutting is much more cost-efficient than machining, especially when additional post processing steps are necessary (Schuler GmbH, 1996). Therefore, two challenges can be identified for these applications:

- How can the properties of shear-cut functional surfaces be improved?
- How can machining processes be substituted by shear cutting processes for edges subjected to cyclic loads?

Regarding the second challenge, precision shear cutting has been shown to be applicable by König and Rotter, 1982, where fineblanked holes were able to endure a higher number of cycles to failure as machined holes. As stated for example in Schuler GmbH, 1996, fineblanking can be used with minimal post processing compared to machining.

The improvement of shear-cut edges regarding their fatigue behavior has been investigated by many authors, especially for standard shear cutting. For precision shear cutting processes only few results have been published. Furthermore, these lack important process parameters like the cutting edge preparation. This also means that a clear recommendation regarding a suitable precision shear cutting process and suitable process parameters can not be made.

Most of the factors influencing the fatigue strength of shear-cut parts have been investigated. Among these are the clean cut height, the roughness, and the hardness of the shear-cut edge. But an important factor influencing the fatigue strength is missing in most publications: the residual stress state of the investigated part. While it has been shown for machined gears that shot-peening induced compressive residual stresses can increase the fatigue strength of gear wheels up to 66 % (Stenico, 2007), the shear cutting induced residual stresses are rarely investigated. Not only are these residual stresses not used but minimized, for example in Dittmann and Pätzold, 2018.

When residual stresses were used for the improvement of a part's fatigue strength, it was mostly carried out by additional post processes, like the coining operation published by Yasutomi et al., 2017. As these additional steps result in increased manufacturing costs, one-stage processes without post processing are favourable.

That shear cutting induced residual stresses are not used directly is not surprising given the few works who deal with the relationship between residual stress state and the used process variant or the process parameters. Here, the main problem is the missing basic understanding how residual stresses are developed in the shear cutting process.

3.2 Objectives

On the basis of the aforementioned problems, the objective of this thesis is to create a basic understanding of the development and control of residual stresses in parts manufactured by precision shear cutting processes without any post processing steps. Furthermore, their targeted use for an improved fatigue strength of shear-cut edges regarding industrial applications will be addressed. The objective of this thesis is to answer the questions that arise from these considerations:

- How do different precision shear cutting processes and their respective process parameters influence the residual stress state of the shear-cut part?
- Which mechanisms lead to the development of residual stresses?
- How does the residual stress state influence the fatigue strength of parts manufactured by precision shear cutting processes? Can these process induced residual stresses be used for the improvement of the fatigue strength without any post processing?
- How can the understanding of the relationship between residual stresses, fatigue strength and the process parameters be used in industrial applications?

3.3 Solution Approach

To solve the above defined objectives, the mechanical properties and the chemical composition of a steel typically used in precision shear cutting applications will be investigated at first. Furthermore, a defined initial residual stress state is achieved by a stress relief heat treatment with a subsequent residual stress measurement.

Afterwards, one-stage precision shear cutting processes, i.e., processes that require minimal post processing, are investigated regarding their effect on the induced residual stress state. Here, one-stage precision shear cutting processes are chosen that can be out in a single tool by simply changing active elements and press settings. Thus, errors by using different tools are eliminated while many influence factors can be analyzed. The investigated shear cutting processes are fineblanking, precision blanking with blank holder, precision blanking without blank holder, blanking with a small die clearance and a v-ring, and standard blanking with a small die clearance. Additionally, the process parameters die clearance and active element edge radii are varied. Both sheet metal strip and blank are measured regarding their cut-surface characteristics, dimensional accuracy, hardness, roughness, and bending. Finite element models of the investigated process variants are build up and validated using a material model derived from the initially determined material properties.

Following, the process induced residual stresses are measured. An explanation model for the formation of the residual stresses during the shear cutting processes is derived from the experimental observations. Afterwards, the measurements are discussed regarding the different

influence factors by using the finite element models. In this discussion the explanation model is tested using a wide range of state variables.

The fatigue behavior of the manufactured sheet metal strips is identified in the following. The results are discussed regarding the influence of the residual stress state on the fatigue strength. To accomplish this, the effect of part geometry, roughness, and hardness are investigated and singled out. Furthermore, error sources are identified by a finite element model of the fatigue test setup. By using these results, guidelines can be developed for designing shear-cut edges with an improved fatigue behavior.

These guidelines will be used to identify suitable precision shear cutting processes for further investigation. At first the residual stress state is improved for these processes. Additionally, the results are tested regarding their suitability for industrial applications by investigating the influence of the active element surface preparation, i.e., by polishing and coating. By cutting a complex shape, the influence of the cutting line geometry is discussed.

Following, the applicability of the results will be investigated with a shear-cut gear. Here, the focus lies on the stability of the residual stresses under typical operation conditions. This aims to show that shear-cut gears with an improved residual stress state are able to be used in gear drives to transmit high torques. The work is concluded by giving an outlook highlighting the process monitoring of residual stresses without expensive equipment and by showing that the residual stresses can be calculated with sufficient accuracy by using the Finite-Element method. Thus, designers can use the results of this thesis in the early development stage to improve their products regarding an increased fatigue strength.

A complete overview of the procedure for accomplishing the objectives is given in figure 3.1

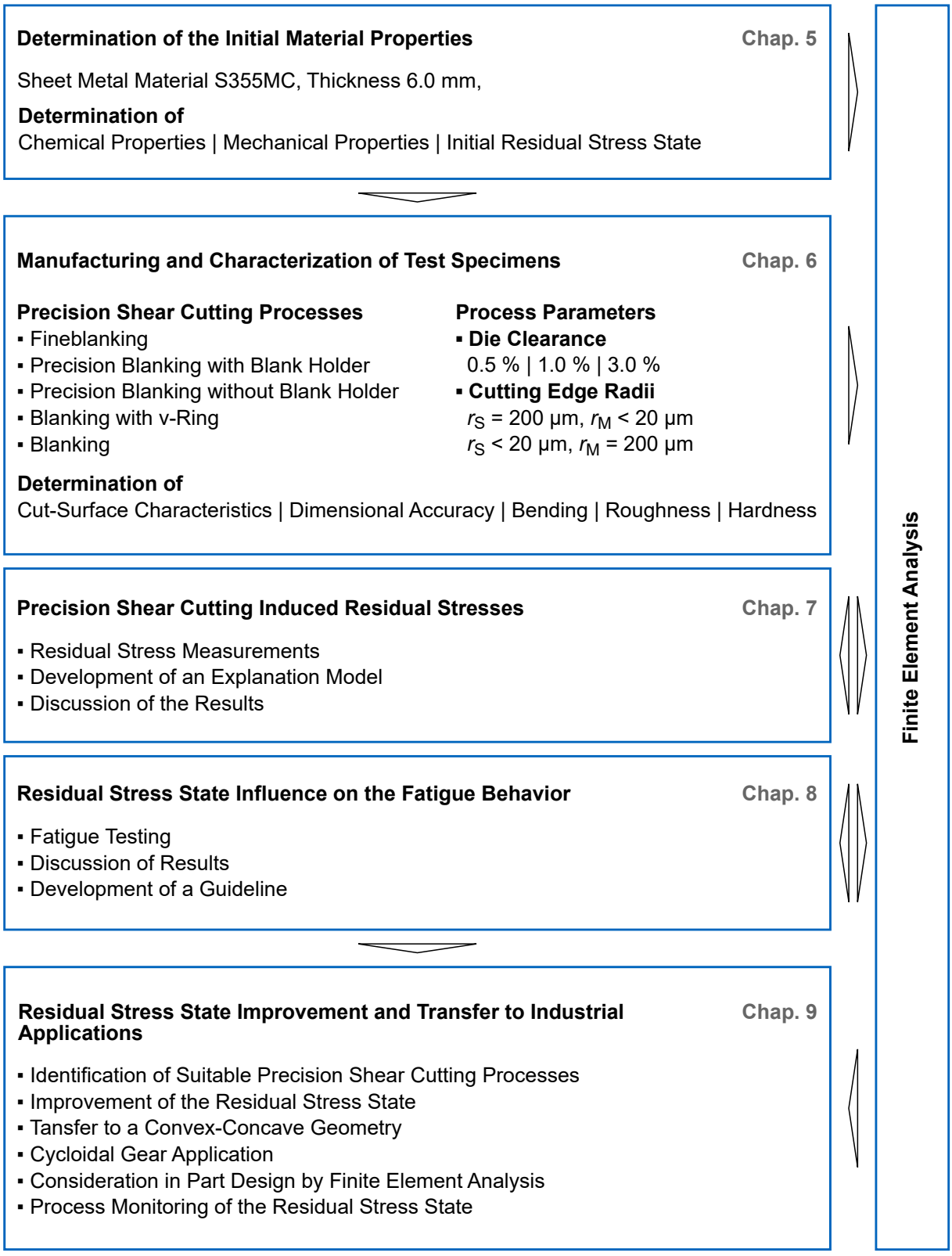

Figure 3.1: Design of experiments of this thesis.

4 Experimental Equipment, Measurement Devices and Software

4.1 Fineblanking Press

All shear cutting experiments are carried out on the triple action fineblanking press Feintool HFA 3200 plus made by Schuler AG, Göppingen (Germany). This kind of machinery is characterized by a high guiding accuracy, a good parallelism of the tool mounting surfaces, and a high press frame stiffness. The nominal pressing force of 3200 kN can be split up in cutting force, blank holder force (140 kN up to 1400 kN) and counter punch force (70 kN up to 700 kN). The punch speed can vary between 5 and 70 mm/s. (Feintool International Holding AG, 2002)

4.2 Experimental Tool

For the shear cutting experiments, an experimental tool was used which is capable of performing five different precision shear cutting processes with small modifications. This tool is displayed in figure 4.1.

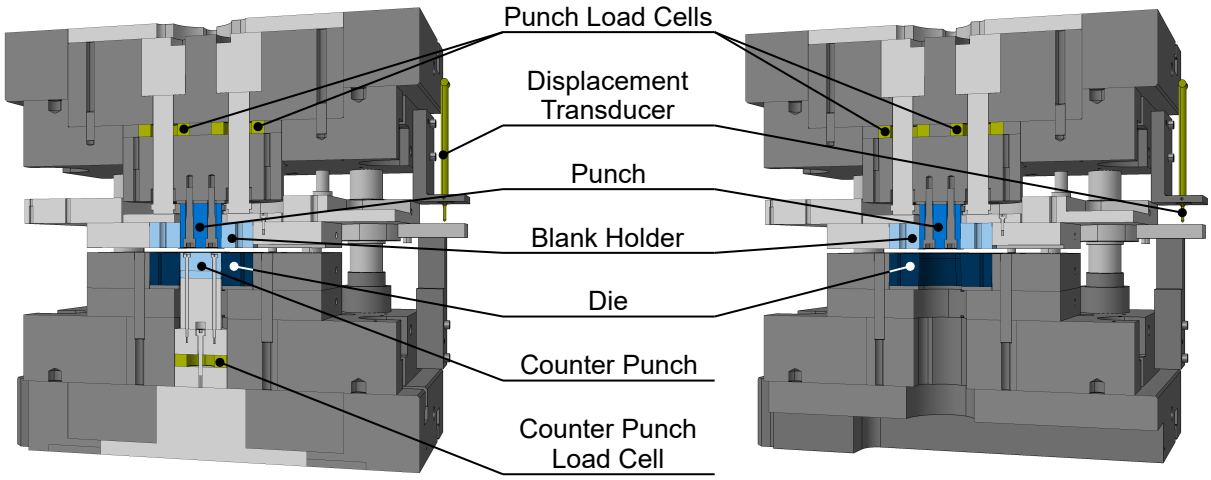

Figure 4.1: Precision shear cutting tool in the configuration with counter punch (left) and with an open passage (right).

The tool is build in a stiff four pillar construction. These pillars are fixed to the upper assembly and guide the blank holder assembly and the lower assembly by high precision roller cages. The upper assembly consists of an exchangeable punch, punch load cells and a displacement transducer, which are all fixed to massive steel plates. These plates show four holes in which pressure pins are located. The pins are used to submit the blank holder or v-ring force to the blank holder assembly. The latter consists of several steel plates and an exchangeable blank holder or v-ring plate, which is also used to guide the punch. The lower assembly shows an exchangeable die inserted in a steel plate and, depending on the configuration, a counter punch. This counter punch submits the counter punch force on the sheet metal and is therefore movable in the lower assembly. A load cell allows to measure this force. For the configuration without a counter punch, the base plate has to be changed. Here, an open passage below the die allows

the parts to fall down on a foam cushion, where they can be removed from the tool. With the exchangeable blank holder insert, die and base plate, the manufacturing of parts by several one-stage precision shear cutting processes is possible in a single tool.

The punch force is measured by four 9071 A load cells by the company Kistler Instrumente AG, Winterthur (Switzerland) with a measuring range of up to 400 kN for each sensor. To reduce the load on each cell and, therefore, increase the measuring range, steel plates surround the sensors. An additional 9071 A load cell is integrated in the tool to measure the counter punch force. Here, no additional steel plate is used. The signal was conditioned by a multichannel laboratory charge amplifier 5017 also manufactured by the Kistler Instrumente AG. The punch travel was measured by the inductive displacement transducer WA-T 20 manufactured by Hottinger Baldwin Messtechnik GmbH, Darmstadt (Germany). Additional information on the tool can be found in Hörmann, 2008.

4.3 Tactile Surface Measurement Device

Both the cut surface characteristics and the active element radii are measured on a measuring station MarSurf XCR 20 by the company Mahr GmbH, Göttingen (Germany). The surface is measured with the profile method by moving a needle with a small radius at its tip over a specimen. The thus generated two-dimensional result is evaluated in the respective software MarWin XCR20. (Mahr GmbH, 2005; Kopp, 2017; DIN EN ISO 4287, 2010)

Punch and die radii were measured with an arm with a length of 350 mm and a needle with a length of 59 mm and a single tip with a radius of 25 µm at its end (Mahr GmbH, 2007a). This needle allows for a longer measurement length as the collision between the arm and the specimen is later due to the long needle. The cut-surface characteristics were measured with an arm with a length of 350 mm and a needle with a length of 18 mm. This needle has two tips, each with a radius of 25 µm. (Mahr GmbH, 2007b) This allows to measure the upper and lower surface of the specimen without having to change its position.

4.4 Coordinate Measuring Machine

To measure the dimensional accuracy of the active elements and the manufactured parts, a 3D coordinate measuring machine by the company Wenzel Präzision GmbH, Wiesthal (Germany), is used. This tactile measurement machine shows an accuracy of 1.5 + L/450 µm (L in mm). The software Metrosoft Quartic R9 was used for defining the measurements and to evaluate the results. (Wenzel Präzision GmbH, 2012; Benkert, 2019)

4.5 Laser Scanning Microscope

The surface roughness is measured by a VHK-150 laser scanning confocal microscope manufactured by the company Keyence Corporation, Osaka (Japan). This microscope offers an

accuracy of 0.2 + L/100 µm or better for the highest magnification which makes it suitable for precise surface measurements. (Keyence Corporation, 2015)

4.6 Optical Surface Measurement Device

Bending of the shear-cut specimen surface is measured with the optical surface scanning device ATOS II 400 manufactured by the company GOM GmbH, Braunschweig (Germany). Here, stripes are projected on the specimen surface which are detected by two cameras and later used to reconstruct the height information. A lens with a focal length of 17 mm was used on the cameras. The surface fittings necessary for the determination of the height deviation were carried out in GOM Inspect V8 by using a Gauss algorithm. (Gesellschaft für Optische Messtechnik, 2008)

4.7 Universal Testing Machine

The mechanical material properties are determined on a universal tension/compression testing machine 1484/DUPS-M by the company ZwickRoell GmbH & Co. KG, Ulm (Germany). This machine has two testing chambers which allow tests up to 200 kN. The elongation of the specimen is measured by a tactile extensometer. (ZwickRoell GmbH, 1998)

4.8 Micro Hardness Testing Device

The Vickers hardness is measured according to DIN 6507, 2018 by a micro/macro-indentation hardness testing device AMH43 manufactured by LECO Instrumente GmbH, Saint Joseph (United States). This measurement system allows testing from a load of 10 g up to 1000 g with an automatic determination of the indent size. (Leco Corporation, 2005)

4.9 Optical Emission Spectrometer

The chemical compositions of sheet metal and active element material are identified using the optical emission spectrometer Foundry Master manufactured by Oxford Instruments plc, Abingdon (United Kingdom). This machine creates a plasma vaporizing the specimen material by an electrical spark. The thus excited atoms emit a radiation with a spectrum characteristic for the contained elements. This spectrum and can be used for determining the chemical composition. (Gey, 2008)

4.10 Heat Treatment Furnace

The stress relief heat treatment is carried out in a furnace N 250/A manufactured by Nabertherm GmbH, Lilienthal (Germany). By the integrated controller C40, it allows to program temperature curves with a maximum temperature of up to 750 °C. Additional thermocouples can be inserted by two small holes in the door of the furnace. Here, type K class 1 thermocouples were

used together with a NI cDAQ-9174 chassis with NI 9213 data acquisition module manufactured by National Instruments Corporation, Austin (United States). (Nabertherm GmbH, 1988)

4.11 Residual Stress Measurement by the Hole Drilling Method

The residual stresses in the sheet metal before blanking are determined by the hole drilling method. Here, the residual stresses are relieved by drilling a small hole in the specimen while detecting the resulting deformation on the specimens surface. This information can be used to calculate the stress state before the hole was drilled. (Schajer, 1988)

Here, the high speed drilling device MTS3000 manufactured by SINT Technology s.r.l., Calenzano (Italy) together with a drill showing a diameter of 1.6 mm is used. The hole with a depth of 1 mm was drilled in steps of 0.05 mm while measuring the specimen deformation with a strain gage rosette 1.5/120K CRY61 and the amplifier Spider 8-30, both manufactured by Hottinger Baldwin Messtechnik, Darmstadt (Germany). The Schwarz and Kockelmann method is used for the calculation of the residual stress state. (SINT Technology s.r.l., 2015)

4.12 Residual Stress Measurement by X-Ray Diffraction

X-ray diffraction is a phenomenon were X-ray radiation is scattered on the surface layers of a polycristalline material. Constructive interference causes peaks under specific angles between the incoming ray and the surface normal following Bragg's law. By using these peaks, the spacing between the atomic planes can be calculated. Stresses on the specimen cause elastic strains in the material which change the spacing between the atomic planes. Thus, the angles under which constructive interference is observed is changed as well and can be used to calculate the specimens elastic strain. Finally, Hook's law is used for determining the elastic stresses from these strains. If no external loads or torques are acting on the specimen, this method can be used for measuring residual stresses by X-ray diffraction. Residual stresses of type I and II combined are determined. By removing layers of the specimen surface by electrochemical erosion, depth profiles can be obtained. (Hauk and Nikolin, 1988; Totten, Howes, and Inoue, 2002; Spieß et al., 2009)

The X-ray diffraction residual stress measurements were carried out by the Gear Research Centre (FZG) on a Seifert RD 3003 PTS System manufactured by the company XRD Eigenmann GmbH, Schnaittach-Hormersdorf (Germany). Where the parts were to big and were not allowed to be cut, a μ-X360s X-ray stress analyzer by sentenso GmbH, Datteln (Germany), was used.

4.13 Fatigue Testing System

Fatigue tests are carried out by the FZG on a servo-hydraulic fatigue testing system Instron® 8872, Norwood (United States). The test load can be set between ± 25 kN and is measured with an integrated load cell during the tests. (Instron, 2020)

4.14 Gear Lifetime Test Bench

The gear lifetime test are performed on a test bench as illustrated in figure 4.2. A servo actuator generates the input torque that is transmitted via two flexible jaw couplings and a torque measuring shaft in between those couplings to the test drive's input shaft. The drive's output shaft is connected to another servo actuator by two additional flexible jaw couplings and a second torque measuring shaft. A planetary drive with a transmission of 4 before the output servo actuator adjusts the rotational speed.

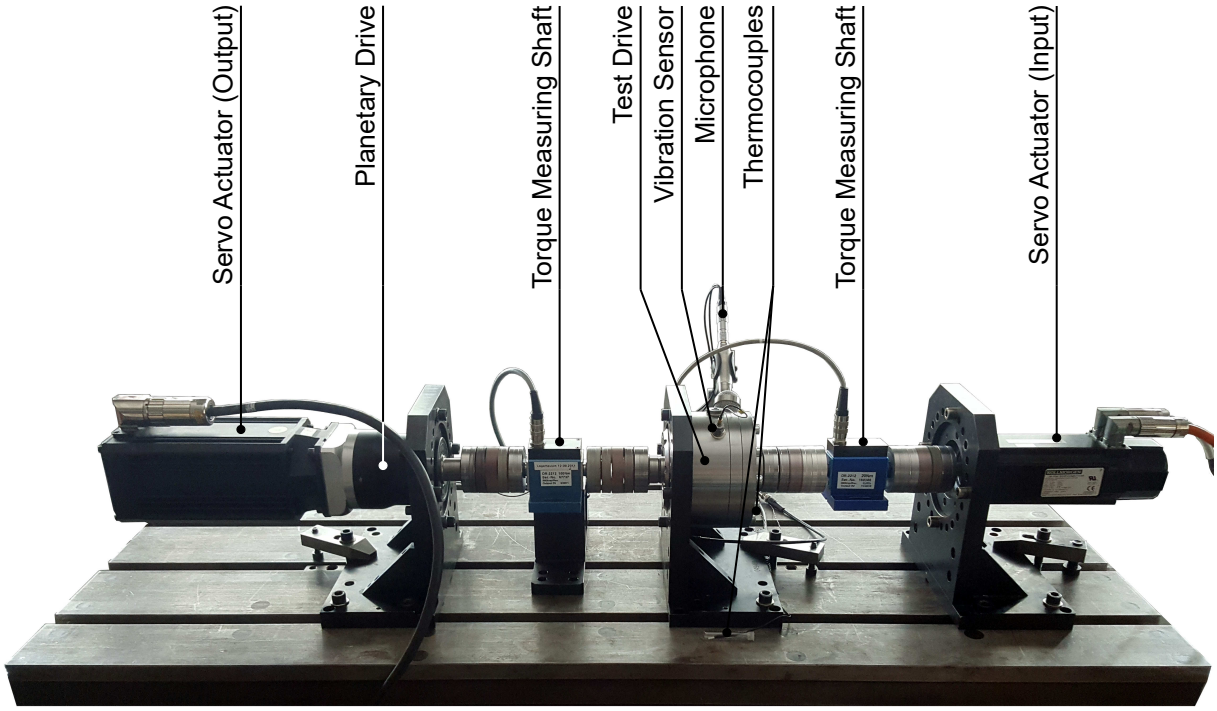

Figure 4.2: Gear lifetime test bench.

The input servo actuator, an AKM 44J-ANC2S-02 by Kollmorgen Europe GmbH, Ratingen (Germany), shows a standstill torque of 6 Nm (Kollmorgen Europe GmbH, 2005). The output servo, a DSG 56-L by Baumüller with a standstill torque of 10 Nm is used as a generator to apply the countering torque (Baumüller Nürnberg GmbH, 2005). Both torque measurement shafts DR-2212 are manufactured by Lorenz Messtechnik GmbH, Alfdorf (Germany). The one on the input side is calibrated up to 20 Nm with an accuracy of 0.05 % while the other is calibrated to 100 Nm with 0.1 %.

To monitor the test drive condition, a vibration sensor 3056D1 manufactured by Dytran Instruments Incorporated, Chatsworth (USA), and a microphone are installed. Additionally, two PT1000 thermocouples are used to measure the room temperature and the temperature of the gear housing. A type K thermocouple is available to measure the temperature inside the test drive. Thus, this gear test bench can measure the rotational speed by the servo actuators' position encoders, the drive efficiency by the input and output torque measurement shafts, the temperature inside and outside of the gear housing, and the test drives noise and vibrations.

This allows detecting gear failure at an early stage.

4.15 Finite Element Analysis Environment

The numerical analyses are carried out in the Finite Element environment Abaqus 2018 by Dassault Systèmes SE, Vélizy-Villacoublay (France). This program allows solving large problems both by an explicit and an implicit solver. Additionally, pre- and postprocessing can be carried out with a graphical user interface. (Dassault Systemes SE, 2020[b])

5 Materials and Lubricant

5.1 Sheet Metal Material

All experiments are carried out with the thermomechanically-rolled fine grain structural steel S355MC with a thickness of 6 mm. This micro-alloyed cold forming steel with the material number 1.0976, as standardized in DIN EN 10149-2, 2013, was chosen due to its good formability, its ability to withstand stress relief heat treatments without a significant alteration of the mechanical behavior (Salzgitter Flachstahl GmbH, 2011).

Additionally, it does not show austenite, which may transform to martensite by sudden cooling or plastic deformation. This phase transformation alters the residual stress state of the material (Schumann, 1975; Müller-Bollenhagen, 2011). These phase transformation induced residual stresses are challenging to separate from the residual stresses caused by plastic deformation and are therefore undesired in basic investigations. The chemical composition of the sheet metal material measured by the optical emission spectrometer is listed in table 5.1.

Table 5.1: Alloying elements of the sheet metal material S355MC in percentage by mass.

Alloying element	**C**	**Mn**	**Si**	**P**	**S**	**Al_{Ges}**	**Nb**	**V**	**Ti**
m%	0.06	0.503	<0.01	0.014	0.007	0.019	0.023	<0.002	<0.001

The sheet metal material was subjected to a stress relief heat treatment according to Salzgitter Flachstahl GmbH, 2011 and Kohtz, 2013 to reduce residual stresses left from the material's production and the specimen manufacturing. This stress relief heat treatment was carried out in the furnace described in chapter 4.10. To ensure stable results, the specimen surface temperature was measured with a type K thermocouple. Exemplary results are displayed in figure 5.1.

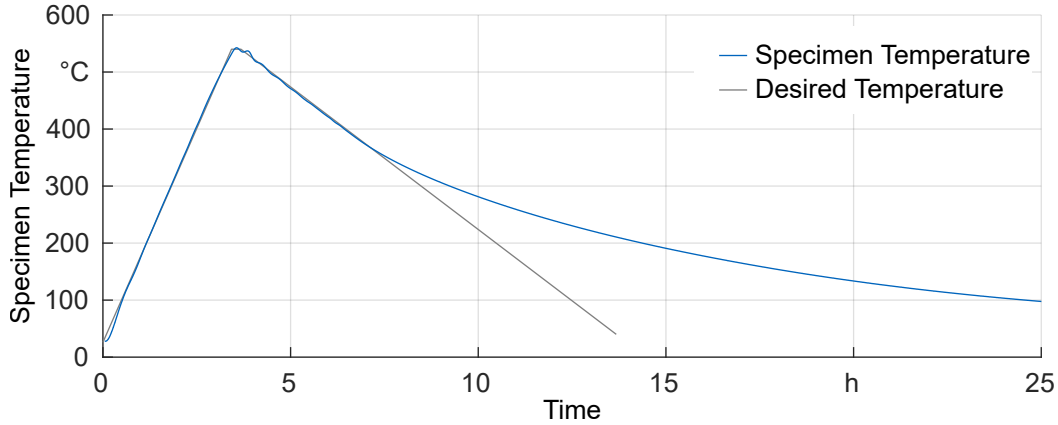

Figure 5.1: Temperature of the specimen during the stress relief heat treatment.

It can be observed that the specimen temperature follows the desired temperature well for the heating phase. After this phase with a slope of 150 K h^{-1}, the temperature was set constant at 540 °C for 15 min followed by a slope of less than -50 K h^{-1}. Both slopes are chosen much smaller than the ones proposed in Kohtz, 2013 as especially a slow cooling phase is desirable

to ensure a low stress level. After the temperature dropped below 100 °C, the specimens were taken out of the furnace.

The initial residual stress state of the specimens before and after the stress relief heat treatment were measured by the hole drilling method in the center of quadratic specimens with an edge length of 88×88 mm. The results are displayed in figure 5.2. A significant reduction of the initial residual stress range from [-70 MPa; 31 MPa] to [-18 MPa; 9 MPa] was achieved by the stress relief heat treatment. The standard deviation of the mean stress dropped from ± 14.3 MPa to ± 5.8 MPa.

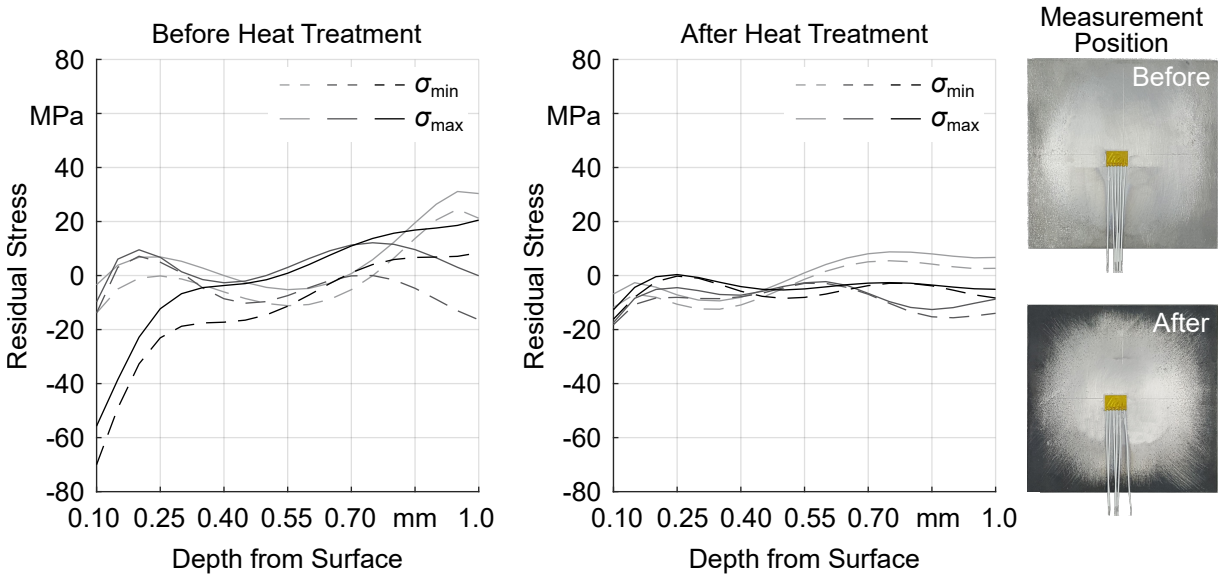

Figure 5.2: Initial residual stress state of three specimens measured by the hole drilling method before and after the stress relief heat treatment with a picture of a specimen before (top) and after heat treatment (bottom).

The micro structure longitudinal and perpendicular to the rolling direction before and after heat treatment is illustrated in figure 5.3. It is dominated by ferrite with fine perlite. Due to the thermomechanical rolling, the grains are only slightly elongated. The heat treatment does not significantly alter the micro structure.

The material's mean base hardness after the stress relief heat treatment was measured on 11 indents over the sheet metal thickness longitudinal and perpendicular to the rolling direction. A hardness of 155 ± 3.5 HV 0.2 in rolling direction and 152 ± 2.6 HV 0.2 in perpendicular direction were measured, resulting in a mean base hardness of 153 HV 0.2.

The mechanical properties were measured with tensile test specimen E6×20×60 according to DIN 50125, 2016 and DIN EN ISO 6892-1, 2009. The results for six specimens, each taken out of the sheet metal longitudinal and perpendicular to the rolling direction, before and after the heat treatment are listed in table 5.2 together with the standard deviation. A slight increase of the yield strength and the uniform elongation caused by the stress relief heat treatment, i.e., by the reduction of residual stresses and slight alterations of the micro structure, is visible.

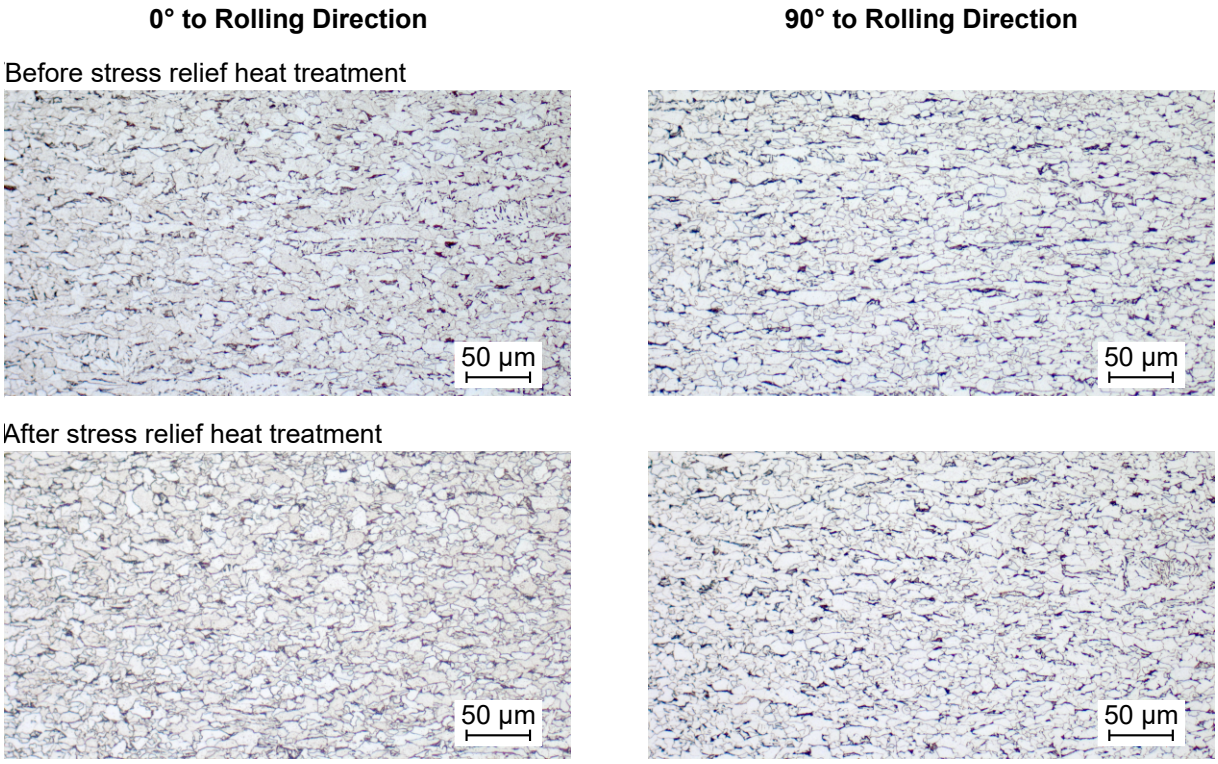

Figure 5.3: Micro structure of the sheet metal material before and after the stress relief heat treatment longitudinal and perpendicular to the rolling direction.

The Young's modulus was measured by tensile tests and evaluated with the approach proposed in Vitzthum et al., 2018, as it is stricter than the standardized method given in DIN EN ISO 6892-1, 2009. The results are listed in table 5.2. As the Poisson's ratio is challenging to measure by tensile tests, the acoustic response of the specimen was considered with the setup published in Lechner et al., 2020. Here, a Young's modulus of 212 ± 0.05 GPa and Poisson's ratio of 0.27 ± 0.003 were measured for specimens subjected to the stress relief heat treatment.

Table 5.2: Mechanical properties of the sheet metal material determined by tensile tests.

	E [GPa]	$R_{p0.2}$ [MPa]	R_m [MPa]	A_g [%]
Before heat treatment				
0° to rolling direction	210 ± 16	387 ± 2	488 ± 3	16.3 ± 0.1
90° to rolling direction	207 ± 10	418 ± 1	499 ± 2	15.2 ± 0.2
After heat treatment				
0° to rolling direction	219 ± 14	418 ± 3	485 ± 2	16.8 ± 0.1
90° to rolling direction	211 ± 11	438 ± 3	496 ± 1	16.0 ± 0.1

5.2 Active Element Material

Punch, die, blanker holder with and without v-ring and the counter punch were made out of X153CrMoV12 (material number 1.2379), an alloy cold-work tool steel standardized in DIN EN ISO 4957, 2018. This ledeburitic chromium steel shows a high wear resistance and toughness (Abrams Premium Steel, 2019). Its chemical composition, measured with the optical emis-

sion spectrometer, is listed in table 5.3. All alloying elements are within the ranges standardized in DIN EN ISO 4957, 2018.

Table 5.3: Alloying elements of the tool steel X153CrMoV12 in percentage by mass.

Alloying element	C	Mn	Si	Cr	Mo	V
wt%	>0.12	0.356	0.264	11	0.809	0.803

5.3 Active Element Coating

To investigate the influence of the surface roughness on the resulting part properties, the active element coating Balinit Alcrona Pro Advanced by the company Oerlikon Balzers Coating Germany GmbH, Bingen (Germany), was used. This AlCrN-based coating with a very high wear resistance reduces scratches on the active element surface. It can be expected that this results in a reduced surface roughness of the manufactured parts. (Oerlikon Balzers Coating Germany GmbH, 2019)

5.4 Lubricant

All experiments were carried out with the fineblanking and deep drawing lubricant Wisura FMO 5001 (ZO 3180) by Fuchs Wisura GmbH, Bremen (Germany). This chlorine and heavy metal free oil is optimized for blanking ferritic sheet metal materials, like S355MC, with a thickness of 6 mm to 8 mm. (Fuchs Wisura GmbH, 2018)

6 Preparation, Manufacturing, and Characterization of Test Specimens

To investigate the residual stress state and the fatigue strength of shear cut edges, specimens have to be manufactured and characterized regarding their mechanical and geometrical properties. The preparation and characterization is explained in this chapter. Starting from the preparation of the delivered sheet metal, the manufacturing of the specimens by the different precision shear cutting processes is explained. Following, the cut-surface characteristics, the dimensional accuracy, the part bending, the roughness, and the hardness of the specimens are presented. On this basis, Finite-Element models are built, which allow to take a detailed look at the stress and strain situation during the shear cutting processes.

6.1 Specimen Geometries and Preparation

To investigate the residual stress state, the fatigue strength, and the geometrical and mechanical properties of the shear cut parts, different specimen geometries were used. Both geometries should show an identical distance from the cutting line to the specimen's outer contour at the measurement position to allow for comparable results. This distance should not be too small, e.g., for fineblanking where a distance of more than the sheet thickness is considered safe (Schmidt et al., 2007). One geometry should show many measurable positions to increase the statistical reliability, e.g., for the geometry measurements. The other should be testable in the fatigue testing rig with a defined stress condition. This requires big clamping surfaces to avoid that the specimens slips inside the gripping jaw when the allowable surface stress is exceeded. To ensure a defined stress situation for a defined force in the fatigue testing rig, the area in the smallest cross section has to be as exact as possible. This requires an exact positioning of these specimens in the shear cutting tool as a cut away from the axis of symmetry would reduce the area on one side while increasing it on the other. Additionally, the influence of the preprocessing should be minimized to ensure that only the alteration by shear cutting is investigated. Geometries that allow testing under these requirements are illustrated together with the necessary preparation steps in figure 6.1.

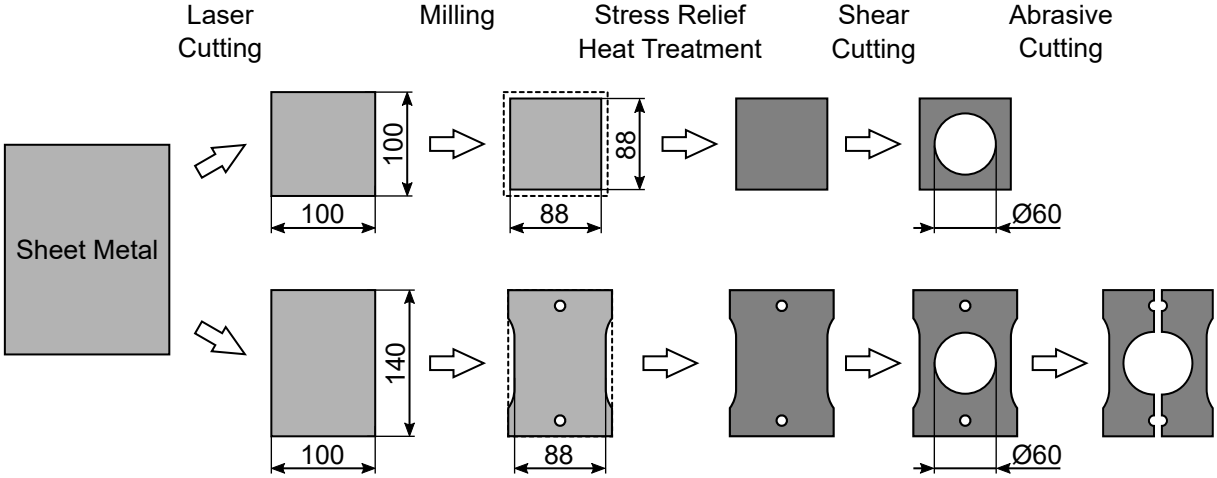

Figure 6.1: Specimen preparation from the sheet metal to the final geometries.

The basic investigations regarding the factors influencing the residual stress state were carried out using quadratic parts, as these are comparably easy to manufacture and interpret due to their two axes of symmetry. To investigate the fatigue strength, C-profiles were manufactured with large clamping surfaces. These surfaces are necessary to ensure that the specimens can be firmly gripped in the fatigue testing rig. Except for the last manufacturing step, a similar specimen preparation was used for these two variants.

At first, small strips of 100×100 mm and 140×100 mm were cut out of the sheet metal by laser cutting. To remove the zone influenced by the laser heat, the specimens were milled to 88×88 mm for the quadratic specimens and 140×88 mm in the smallest cross section for the rectangular specimens. Additional positioning holes were milled in the rectangular specimens for a defined positioning in the shear cutting experiments. Afterwards, the test pieces were subjected to the stress relief heat treatment described in chapter 5.1 to achieve a low initial residual stress state. This is followed by shear cutting a hole with a diameter of 60 mm in the center of the quadratic and C-shaped specimens, which results in a minimal cross section from the hole to the outer edge of 14 mm for both geometries. To be able to test the rectangular specimens under a bending load, they were cut in half by abrasive cutting resulting in C-shaped profiles. To minimize the temperature rise in the specimens, they were water cooled during this abrasive cutting process.

6.2 Precision Shear Cutting Processes and Process Parameters

To single out the influence of different tool elements on the part's residual stress state, tool setups were chosen that differ only by one element to the others. As researched in the state of the art, the setups investigated by Hörmann, 2008 fulfill this requirement. Here, the most commonly used tool elements are combined with punch and die: a blank holder, a counter punch, and v-rings. Additionally, the standard fineblanking setup according to VDI 3345, 1980 with a v-ring on both blank holder and die is considered. This means that a setup that does not show a blank holder cannot include the use of a v-ring to ensure comparability. Thus, five one-stage precision shear cutting processes were investigated: fineblanking (FB), standard blanking with a small die clearance and v-ring (BV), precision blanking without blank holder (PBwBH), precision blanking (PB), and standard blanking with small die clearance (B). In the following shorter names for the processes are used. Standard blanking with small die clearance and v-ring is referred to as blanking with v-ring, and standard blanking with small positive die clearance as blanking. Also, the blanking and not the piercing nomenclature is used. An overview over all five processes is given in figure 6.2.

Each precision shear cutting process shows a different tool setup as listed in table 6.1. As these processes differ from each other by at least one feature, the influence of this feature can be singled out.

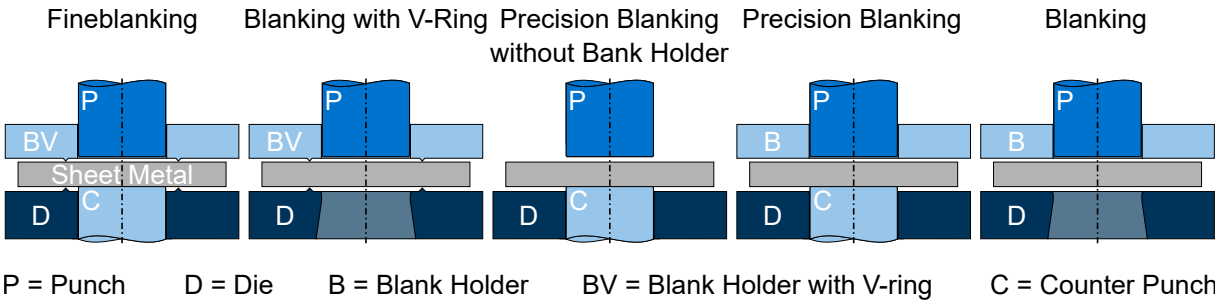

Figure 6.2: The investigated one-stage precision shear cutting processes.

Table 6.1: Tool features of the investigated one-stage precision shear cutting processes.

Precision Shear Cutting Process	**Punch and Die**	**Blank Holder**	**V-Ring**	**Counter Punch**
Fineblanking	×	×	×	×
Blanking with V-Ring	×	×	×	
Precision Blanking without Blank Holder	×			×
Precision Blanking	×	×		×
Blanking	×	×		

The v-ring geometry was chosen according to VDI 3345, 1980. It is displayed in figure 6.3. Additionally, the v-ring edges were polished to show a radius of 50 µm to ensure comparable results. The v-ring, and counter punch forces were calculated according to Schmidt et al., 2007. The blank holder force was chosen slightly higher than the 30 % of the maximum cutting force used in Hörmann, 2008 and Loibl, 2003. This takes into account that the sheet metal strip is comparably small, i.e., a bigger force is needed to counteract the torque induced by the cutting operation. Subsequently, all forces were rounded up. The forces set are listed in table 6.2 while the complete force calculation can be found in appendix F.1.

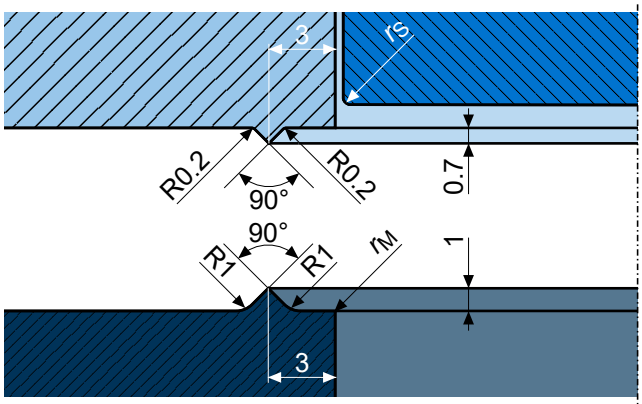

Figure 6.3: The v-ring geometry according to VDI 3345, 1980 used for the experiments.

The die clearances were chosen to 30 µm (0.5 % of the sheet metal thickness), 60 µm (1.0 % of the sheet metal thickness), and 180 µm (3.0 % of the sheet metal thickness). The die clearance was adjusted by using a smaller punch. The punch speed was set to 50 mm/s for all experiments. Both punch and die edge radii were polished by hand to the active elements while continuously measuring the result with the tactile surface measurement station. Here, two main configura-

Table 6.2: Forces set for the different precision shear cutting experiments for the circular cutting line geometry.

Precision Shear Cutting Process	Blank Holder Force	Counter Punch Force
Fineblanking	450 kN	200 kN
Blanking with v-ring	450 kN	-
Precision blanking without blank holder	-	200 kN
Precision blanking	200 kN	200 kN
Blanking	200 kN	-

tions were used: one with a rounded punch edge $r_S = 200\,\mu m$ and a sharp die edge $r_M < 20\,\mu m$, and one with a sharp punch edge $r_S < 20\,\mu m$ and a rounded die edge $r_M = 200\,\mu m$. These configurations were chosen as they are typical for manufacturing a hole or a blank regarding the burr formation. When a sharp die edge radius is used, a small burr height can be expected on the sheet metal strip while a sharp punch edge typically results in a small burr height on the blank. Thus, these configurations represent a typical blanking or piercing operation. Additionally, it can be expected that the material flow is guided towards the sheet metal strip when a round punch edge is used while a round die edge favors material flow towards the blank. This allows to identify how the material flow, caused by the underlying stress situation, influences the induced residual stresses.

A full factorial examination regarding die clearance and active element condition was carried out for fineblanking and blanking, as they are the most commonly used precision shear cutting processes. Blanking with v-ring, precision blanking without blank holder, and precision blanking were investigated for a die clearance of 0.5 % and both cutting edge variants. Before cutting, the sheet metal strips were lubricated with Wisura FMO 5001.

6.3 Characterization of the Manufactured Parts

6.3.1 Cut-Surface Characteristics

Cut-Surface Characteristics Measurement

The tactile surface measurement device presented in chapter 4.3 was used for determining the cut-surface characteristics as defined in VDI 2906-5, 1994. Four measurement positions on the circular geometries were investigated per part. On the sheet metal strips, the smallest cross section was measured. At least four parts were measured which means that 16 cut-surface measurements were carried out for each configuration.

Cut-Surface Characteristics of the Blanks

The cut-surface characteristics of the blanks for both active element radii configurations and three die clearances are displayed in figure 6.4. It should be noted that the cut-surface characteristics do not strictly add up to 100 %, which is possible for example due to the imprint caused by the punch which locally reduces the sheet metal thickness. The standard deviation of the

measurements is not shown in figure 6.4 but can be found in appendix F.2. To get an impression of the precision of the results, the standard deviation is discussed for the fineblanked blanks manufactured with a die clearance of 0.5 %, $r_S = 200\,\mu m$ and $r_M < 20\,\mu m$. This variant shows a die roll share of 5.0 ± 0.2 % , a clean cut share of 95.5 ± 0.3 %, a burr height of $319 \pm 95\,\mu m$, and a clean cut angle of $89.9 \pm 0.1\,°$.

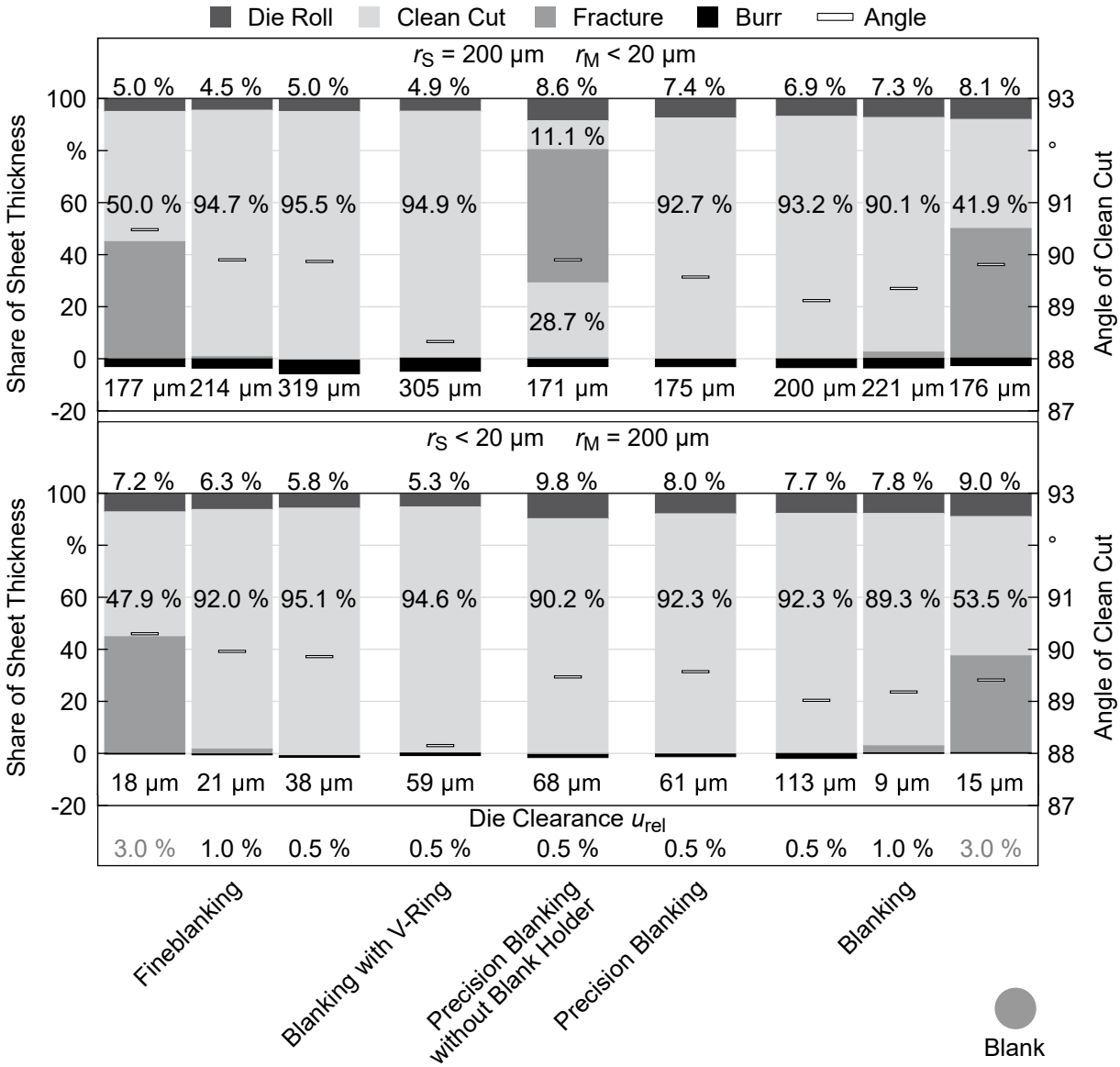

Figure 6.4: Cut-surface characteristics of blanks manufactured by the five precision shear cutting processes as partially published in Stahl, D. Müller, Tobie, et al., 2019.

At first the results for the blanks manufactured with a die clearance of 0.5 % are compared. The cutting edge and die clearance influence are addressed afterwards. It should be noted that a die clearance of 3 % results in a comparably big fracture zone. Thus, the focus is on cut surfaces that are similar and show a high amount of clean cut.

Die Roll Height The precision shear cutting processes with a v-ring, i.e., fineblanking and blanking with v-ring, show the smallest die roll height. These are followed by the blanks manufactured by blanking and precision blanking, i.e., precision shear cutting processes with a blank

holder. Precision blanking without blank holder shows the highest die roll height.

Clean Cut Height The same observations as for the die roll height are also applicable for the clean cut height, i.e., the processes with a small die roll also show a high amount of clean cut. Only precision blanking without blank holder shows a fracture zone for a punch edge radius of 200 µm and a die edge radius smaller 20 µm. This fracture zone is located close to the middle of the sheet metal thickness and followed by secondary clean cut.

Clean Cut Angle The clean cut angle is close to 90 ° for the precision shear cutting processes with a counter punch, i.e., fineblanking and precision blanking. An especially low clean cut angle is observed for the blanks manufactured by blanking with v-ring followed by those manufactured by blanking.

Burr Height The burr height is close to 200 µm, i.e., close to the height of the punch edge radius, for the blanks manufactured with a punch edge radius of 200 µm. Only fineblanking and blanking with v-ring stand out, where more than 300 µm were measured. This means that the fracture did not occur on or close to the punch edge but on the punch's lateral surface. For the blanks manufactured with a punch with an edge radius smaller 20 µm, a burr height between 38 and 113 µm is observed, i.e., it is much bigger than expected from the small punch edge radius.

Cutting Edge Preparation By comparing the cut-surface characteristics of the blanks produced with a punch edge radius of 200 µm and a die edge radius smaller 20 µm with those manufactured with a punch edge radius smaller 20 µm and a die edge radius of 200 µm, a bigger die roll height and a smaller clean cut height can be observed for the configuration with the 200 µm die edge radius. Additionally, the clean cut angle is slightly lower for this configuration. The biggest difference can be observed regarding the burr height, which is much bigger for the configuration with the 200 µm punch edge radius. This configuration shows the only cut-surface with a fracture zone for the small die clearance, i.e., the one produced by precision blanking without blank holder.

Die Clearance An increasing die roll height and a decreasing clean cut height is observed with an increasing die clearance except for fineblanking with a punch edge radius of 200 µm, where the die roll height remains almost constant. Fineblanking shows a slightly higher amount of clean cut than blanking for a die clearance of 1 %. A significant decrease of the clean cut height is observed for a die clearance of 3 % for both fineblanking and blanking. The burr height is decreasing with an increasing die clearance except for blanking with a die clearance of 1 %. Additionally, a higher clean cut angle is observed for an increasing die clearance.

Cut-Surface Characteristics of the Sheet Metal Strips

The cut-surface characteristics of sheet metal strips produced by the five precision shear cutting processes are displayed in figure 6.5. Again, the standard deviation of the measurements can be found in appendix F.2. For the fineblanked strips manufactured with a die clearance of 0.5 %, $r_S = 200\,\mu m$ and $r_M < 20\,\mu m$ the standard deviation is 5.4 ± 0.4 % for the die roll share, 97.6 ± 0.4 % for the clean cut share, $212 \pm 84\,\mu m$ for the burr height, and $90.1 \pm 0.1\,°$ for the clean cut angle. The results for a die clearance of 0.5 % are compared at first followed by the cutting edge preparation and die clearance influence.

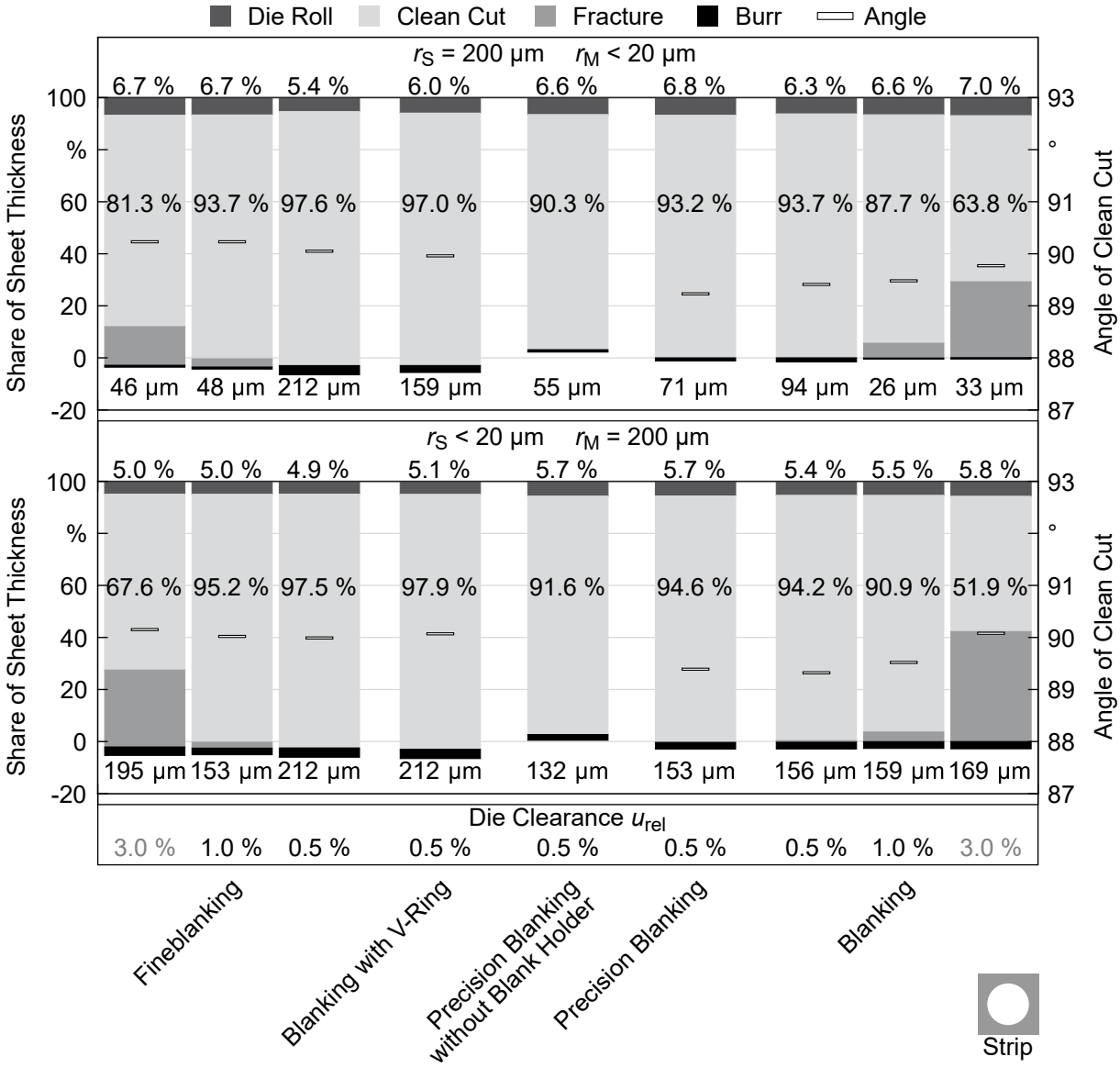

Figure 6.5: Cut-surface characteristics of strips manufactured by the five precision shear cutting processes as partially published in Stahl, D. Müller, Tobie, et al., 2019 and Stahl, D. Müller, Pätzold, et al., 2019.

Die Roll Height The die roll height of the strips shows a similar tendency as those of the blanks. Again, the smallest die roll height is observed for the processes with a v-ring, i.e., fineblanking and blanking with v-ring. The strips produced by blanking show a slightly higher

die roll, followed by precision blanking and precision blanking without blank holder.

Clean Cut Height Fineblanking and blanking with v-ring also show the highest amount of clean cut, followed by the strips manufactured by blanking and precision blanking. As observed for the blanks, precision blanking without blank holder shows the lowest amount of clean cut. Here, a comparably big imprint on the contact zone between sheet metal and the die locally reduced the thickness of the sheet metal, which means that the amount of die roll and clean cut together are significantly smaller than 100 %.

Clean Cut Angle The clean cut angle is closest to 90 ° for the precision shear cutting processes with a v-ring. Both the blanks produced with a regular blank holder, i.e., blanking and precision blanking show an almost 1 ° lower clean cut angle. The clean cut angle of precision blanking without blank holder was 83.05 ° for the configuration with a punch edge radius of 200 µm and 85.35 ° for the configuration with a punch edge radius of 20 µm. Due to this extremely high values these are not displayed in figure 6.5.

Burr Height The burr height is the highest for the strips manufactured by fineblanking and blanking with v-ring. Precision blanking and blanking lead to a smaller burr height while precision blanking without blank holder produces the smallest burrs. For the configuration with the die edge radius of 200 µm the burr is higher than for the sharp die edge, except for fineblanking with where identical burr heights were measured for both die edge variants.

Cutting Edge Preparation Regarding the die roll height and the clean cut height, similar tendencies can be observed for the blanks and the strips. The main difference is that the results for the blanks produced with a punch edge radius of 200 µm and a die edge radius smaller 20 µm correspond to the results of the strips produced with a punch edge radius smaller 20 µm and a die edge radius of 200 µm. A significant influence of the active element radii on the clean cut angle can only be observed for the strips produced by precision blanking without blank holder where the configuration with a punch edge radius of 200 µm shows a significantly lower value.

Die Clearance As for the blanks, the die roll height tends to increase when increasing the die clearance. For fineblanking there is no difference measurable from 1 % die clearance to 3 %. The clean cut height on the other hand is decreasing with an increasing die clearance. For fineblanking only small differences of the clean cut angle can be observed whereas blanking shows an increasing clean cut angle with an increased die clearance. For the configuration with a punch edge radius of 200 µm, the burr height tends to decrease with an increasing die clearance. For a punch edge radius smaller 20 µm no clear tendency is visible.

6.3.2 Dimensional Accuracy

Dimensional Accuracy Measurement

The coordinate measuring machine presented in chapter 4.4 was used with a 6 mm ruby sphere for dimensional accuracy analysis. Two lines were measured with a distance of 3 and 4 mm to

the burr side of the part. These lines were used to calculate the diameters $d_{PartML1}$ and $d_{PartML2}$ and finally the part diameter d_{Part}. This is illustrated in figure 6.6.

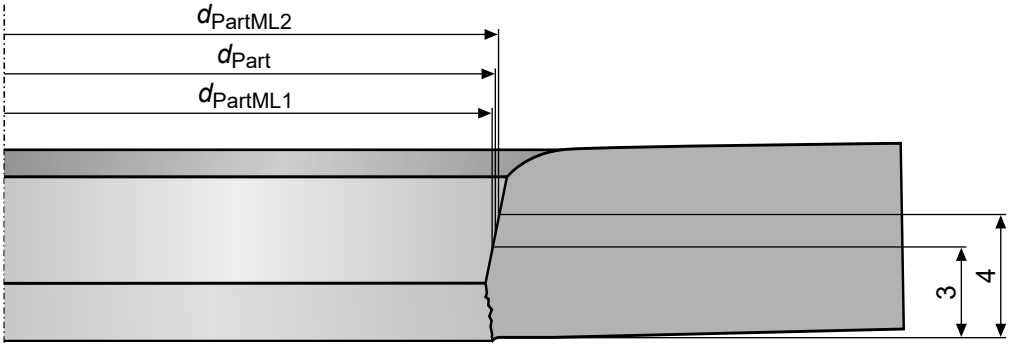

Figure 6.6: Schematic illustration of the size measurement of a specimen with a fracture zone and significant bending.

The distances of 3 and 4 mm to the burr side were chosen to be able to measure parts with a fracture zone of less than 50 % on the clean cut without having to alter the measurement routine, which affects the results for conical holes, for example. It should be noted that the measurement is not independent of part bending, as indicated in figure 6.6.

To consider the different punch diameters used for adjusting the die clearance, the size deviation Δd to the active element diameter is calculated. This is carried out by subtracting the diameter of the respective active element $d_{ActiveElement}$ from the diameter of the part d_{Part}, i.e., the inner diameter of the die is subtracted from the diameter of the blank and the punch diameter from the size of the cut hole:

$$\Delta d = d_{Part} - d_{ActiveElement} \tag{6.1}$$

Dimensional Accuracy of the Blanks

The dimensional accuracy of the blanks is displayed in figure 6.7. It can be observed that all blanks are smaller than 60 mm. The blanks manufactured by precision blanking without blank holder with $r_S = 200\,\mu m$ and $r_M < 20\,\mu m$ show a fracture zone at the measurement position. As this result can not be reasonably compared to the others, it is not displayed in figure 6.7.

Precision Shear Cutting Process Fineblanking with $u_{rel} = 0.5\,\%$, $r_S < 20\,\mu m$ and $r_M = 200\,\mu m$ shows the smallest deviation from the nominal measure while blanking with $u_{rel} = 3\,\%$, $r_S = 200\,\mu m$ and $r_M < 20\,\mu m$ shows the biggest deviation. For a die clearance of 0.5 %, fineblanking shows the smallest deviation while the other precision shear cutting processes show a much higher deviation especially for the variant with the sharp die edge.

Cutting Edge Preparation In all cases, the specimens manufactured with $r_S = 200\,\mu m$ and $r_M < 20\,\mu m$ are smaller than those manufactured with the rounded die edge.

Die Clearance A clear tendency can be observed regarding the die clearance, where an increased die clearance results in smaller blanks.

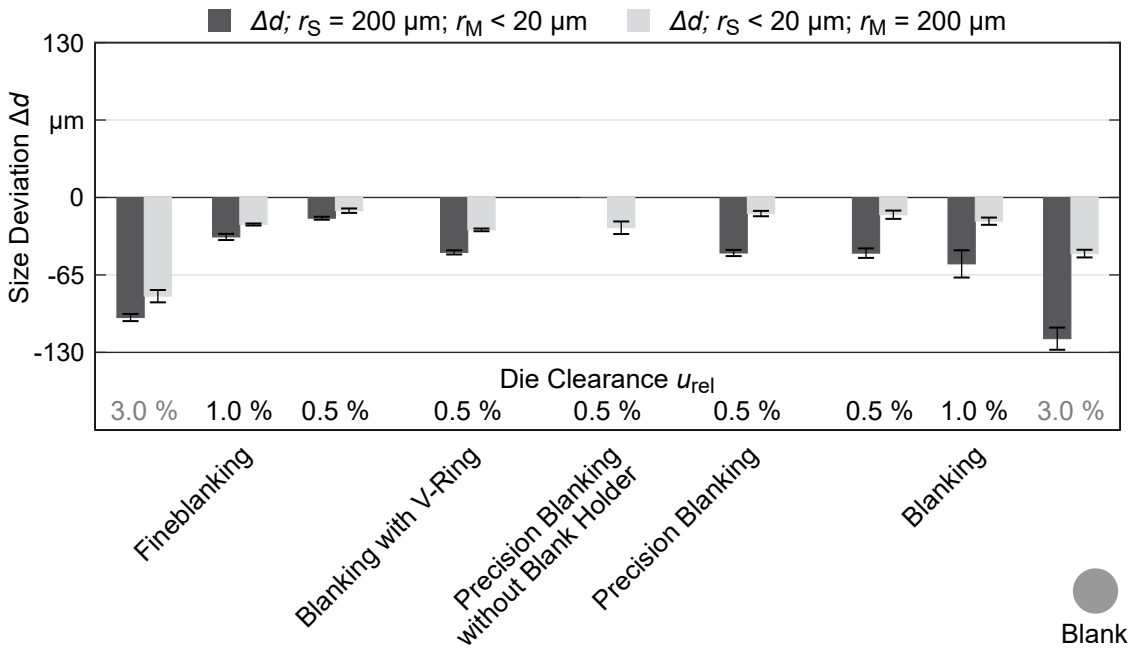

Figure 6.7: Deviation from the nominal measure of the blanks manufactured by the five precision shear cutting processes.

Dimensional Accuracy of the Sheet Metal Strips

The size deviation of the manufactured holes is displayed in figure 6.8. In most cases, the hole is smaller than the nominal diameter. Exceptions are the holes manufactured by precision blanking without blank holder with both active element edge conditions and the one manufactured by blanking with $u_{rel} = 3\,\%$, $r_S < 20\,\mu m$ and $r_M = 20\,\mu m$.

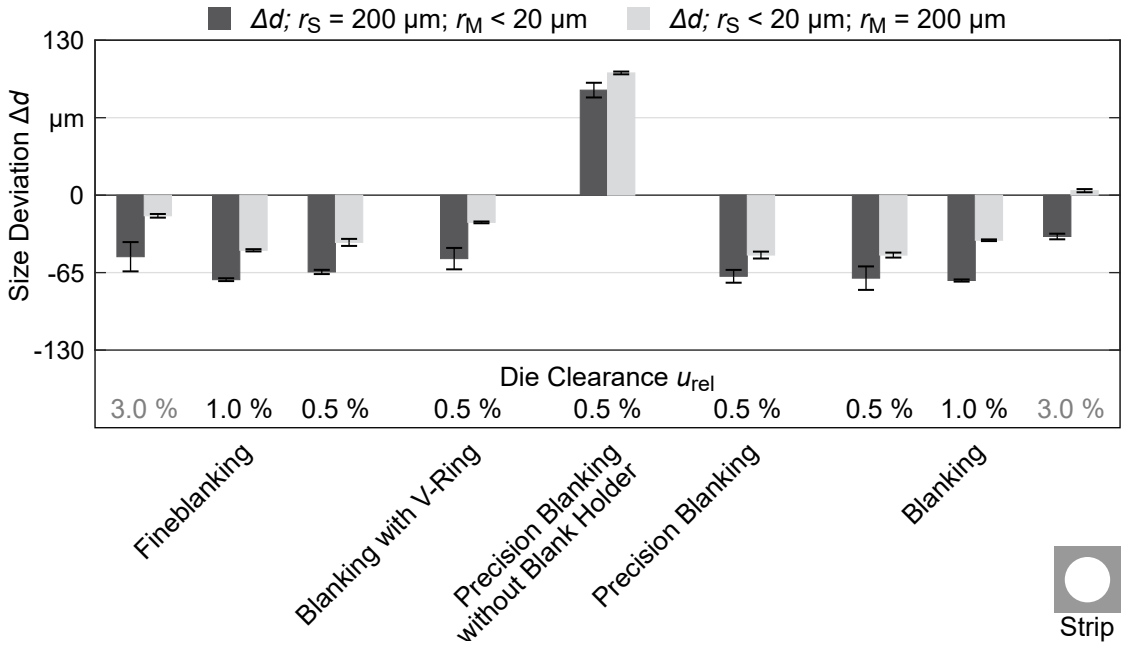

Figure 6.8: Deviation from the nominal measure of the sheet metal strips manufactured by the five precision shear cutting processes.

Precision Shear Cutting Process Only small differences can be observed for the different precision shear cutting processes, especially for the variant with the rounded punch edge. Only precision blanking without blank holder stands out.

Cutting Edge Preparation The holes produced with a round punch edge of 200 µm are smaller than those manufactured with the sharp punch edge in all cases.

Die Clearance A die clearance of 1 % causes only small changes of the dimensional accuracy compared to the small die clearance of 0.5 % while a 3 % die clearance leads to bigger holes.

6.3.3 Bending

Surface Measurement

Part bending was measured with the optical surface measurement device described in chapter 4.6. At first, a chalk spray was used to get an evaluable surface. As the parts show a die roll, the burr side was investigated. Afterwards, the deviation from the mean plane of the measured surfaces was analyzed. This was carried out by calculating the residual R of the fitting. This is inspired by the bending coefficient D proposed in Hörmann, 2008:

$$D = \sqrt{R \times A} \tag{6.2}$$

$$R = \sqrt{\frac{\sum_{i=1}^{m} a_i^2}{m}} \tag{6.3}$$

Here, R is the root-mean-square, A is the maximum deviation from the fitting plane, m is the number of measurement points, and a_i the distance of a measurement point to the fitting plane. In the following, the weighting by the maximum deviation from the fitting plane A is not considered, i.e., the bending coefficient in the following is just the residual of the fit R.

Bending of the Blanks

The bending of the blanks given in height deviation from the mean plane is illustrated in figure 6.9. As only small differences can be observed in the surface measurements, the bending coefficients are given in figure 6.9 as well. Furthermore, the absolute deviation of the clean cut angle from 90 ° is shown[17]. It should be noted that the part bending depends on the part size. Thus, the tendencies are comparable but the absolute values are not transferable to other geometries.

Precision Shear Cutting Process It can be observed that the bending ranges in a comparably small range except for the blanks manufactured by blanking with v-ring. The heavily bend blanks produced by blanking with v-ring also show clean cut angles with the highest deviation from 90 ° measured in chapter 6.3.1.

[17] The absolute clean cut angle deviation is calculated by $|90 - \alpha|$. As the residual can not be negative, the absolute deviation is considered for a comparison.

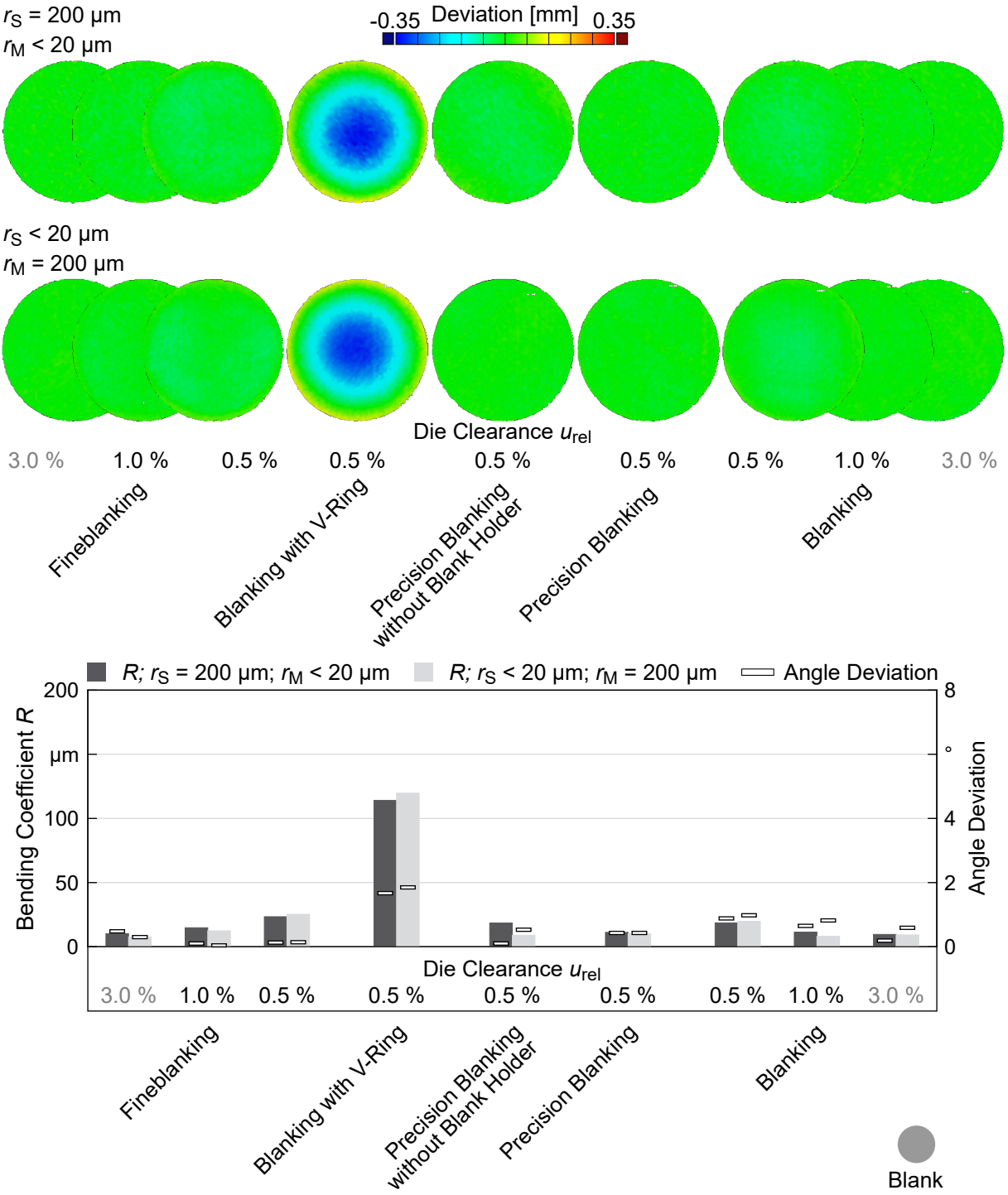

Figure 6.9: Surface measurements (top) and bending coefficients R of the blanks manufactured by the five precision shear cutting processes together with the corresponding clean cut angle deviation (bottom).

Cutting Edge Preparation Regarding the cutting edge preparation influence, no clear tendency can be observed except for the parts manufactured by blanking with v-ring and precision blanking without blank holder. For blanking with v-ring, a slightly higher deviation of the part manufactured with the round die edge is visible while the blanks manufactured by precision blanking without blank holder show an opposing trend.

Die Clearance For both fineblanking and blanking the parts manufactured with a die clearance of 0.5 % show a bigger bending than those manufactured with the bigger die clearances.

Bending of the Sheet Metal Strips

The height deviation from the mean plane of the sheet metal strips manufactured by the five precision shear cutting processes is displayed in figure 6.10. Additionally, the bending coefficients are given. Again, only the tendencies are transferable to other geometries due to the size dependency of the part bending. This effect is even stronger for the comparably big sheet metal strips.

Precision Shear Cutting Process A clear influence of the chosen precision shear cutting process is visible. While the parts manufactured with a v-ring, i.e., by fineblanking and blanking with v-ring, show the smallest bending, the use of only a blank holder, as in precision blanking and blanking, causes a bigger bending. It should be noted that the different blank holder forces might contribute to this effect. Precision blanking without blank holder leads to the biggest bending. This correlates with the measured clean cut angles.

Cutting Edge Preparation The specimen manufactured by precision blanking without blank holder with a punch edge radius of 200 µm and a die edge radius smaller 20 µm bend slightly more than those manufactured with a punch edge radius smaller 20 µm and a die edge radius of 200 µm. A similar observation can be made for the parts manufactured with a die clearance of 0.5 % by fineblanking, precision blanking, and blanking. This corresponds to clean cut angle deviation for all of these processes except blanking.

Die Clearance Both for blanking and fineblanking the strips manufactured with a die clearance of 3 % show a smaller bending than those manufactured with the small die clearance of 0.5 % for the variants produced with the rounded punch edge. Only small differences can be observed for the sharp punch edge.

6.3.4 Roughness

Roughness Measurement

As the roughness is most relevant for the interpretation of the fatigue strength, the C-shaped specimens were measured in their smallest cross section with the laser scanning microscope shown in chapter 4.5. The arithmetical mean roughness *Ra* as standardized in DIN EN ISO 4287, 2010 is given in the following. As the roughness of the blanks is not relevant for this thesis, it is not discussed in this chapter. For completeness, a comparison of the roughness of the sheet metal strips and blanks can be found in the appendix. Eleven lines, parallel to the sheet metal plane, were measured on at least four specimens in the middle of the clean cut. An additional measurement was carried out in the middle of the fracture surface if it was big enough. The procedure is illustrated in figure 6.11.

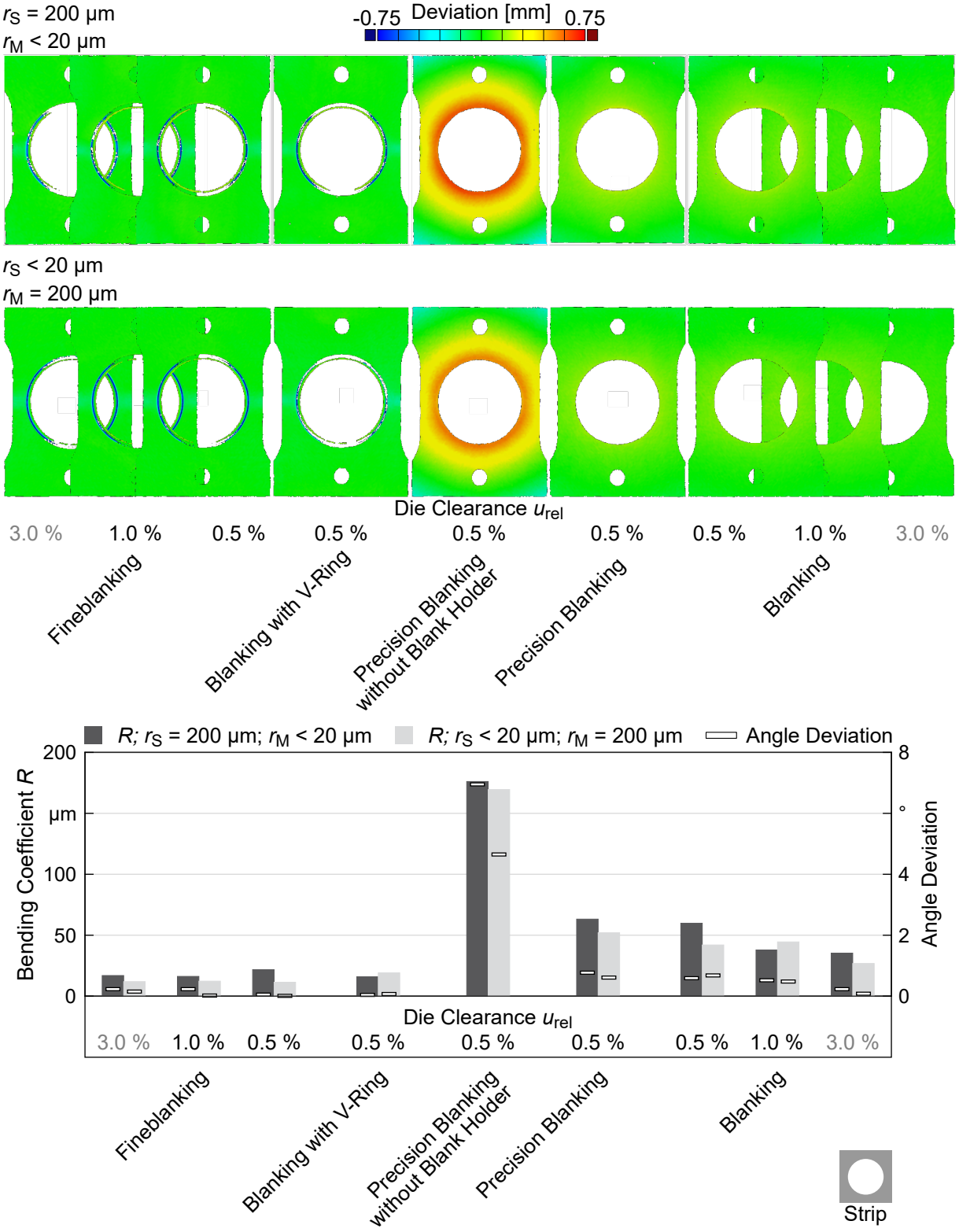

Figure 6.10: Surface measurements of the sheet metal strips (top) and bending coefficients R of the sheet metal strips manufactured by the five precision shear cutting processes together with the corresponding clean cut angles as partially published in Stahl, D. Müller, Pätzold, et al., 2019.

Roughness of the Sheet Metal Strips

The roughness *Ra* of the manufactured sheet metal strips is listed in table 6.3. The clean cut roughness ranges between 0.61 and 2.1 µm. Here, no clear tendency can be observed regarding

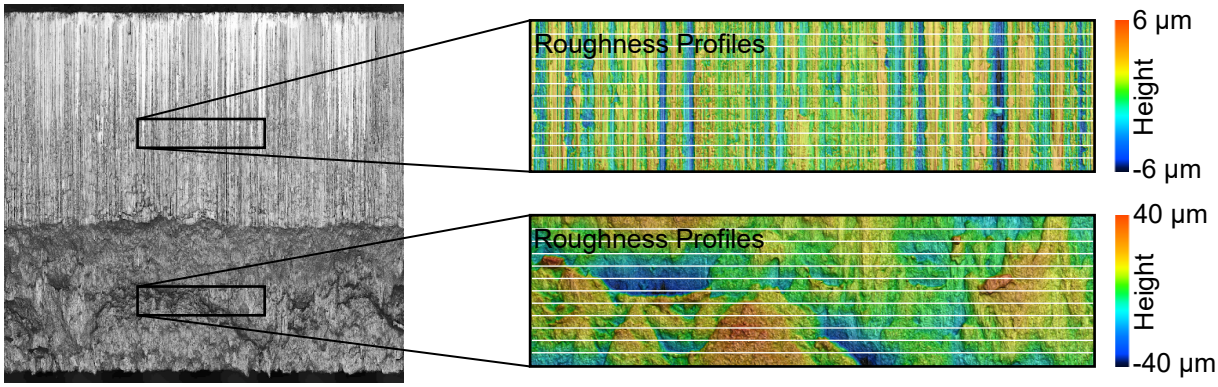

Figure 6.11: Measurement positions for the roughness determination.

the different precision shear cutting processes and the active element edge radii. The roughness of the fracture zone was measured as well where it was big enough to get the same amount of measuring lines on it. This is only the case for a die clearance of 3.0 %. As expected, the roughness is significantly higher and ranges between 6.3 and 8.7 µm.

Table 6.3: Surface roughness Ra of the sheet metal strips manufactured by the five different precision shear cutting processes in the middle of the clean cut with the roughness of the fracture zone in braces.

Precision Shear Cutting Process	u_{rel}	r_S = 200 µm, r_M < 20 µm	r_S < 20 µm, r_M = 200 µm
Sheet Metal Strip			
Fineblanking	0.5 %	1.9 ± 0.21 µm	0.94 ± 0.18 µm
Fineblanking	1.0 %	2.1 ± 0.18 µm	1.8 ± 0.43 µm
Fineblanking	3.0 %	1.5 ± 0.24 µm	1.1 ± 0.14 µm
		(6.3 ± 3.1 µm)	(7.6 ± 3.4 µm)
Blanking with v-ring	0.5 %	1.4 ± 0.29 µm	1.2 ± 0.15 µm
Precision blanking without blank holder	0.5 %	0.84 ± 0.24 µm	1.4 ± 0.19 µm
Precision blanking	0.5 %	0.96 ± 0.17 µm	0.63 ± 0.04 µm
Blanking	0.5 %	1.5 ± 0.26 µm	0.61 ± 0.08 µm
Blanking	1.0 %	1.6 ± 0.10 µm	1.1 ± 0.26 µm
Blanking	3.0 %	1.3 ± 0.19 µm	0.91 ± 0.06 µm
		(6.5 ± 1.5 µm)	(8.7 ± 6.6 µm)

6.3.5 Hardness

Hardness Measurement

The microhardness distribution was measured with the microhardness testing device presented in chapter 4.8. The smallest cross section of the sheet metal strips produced with the circular cutting line was investigated. The blanks were cut in half in the middle. Again, the hardness of the blanks is not relevant for this thesis but is given for completeness in the appendix. A load of 1.961 N, e.g., HV 0.2, was set for all experiments. The positions of the indents are displayed in figure 6.12. For non ideal clean cut angles, the first line was tilted to be aligned with the cut-surface.

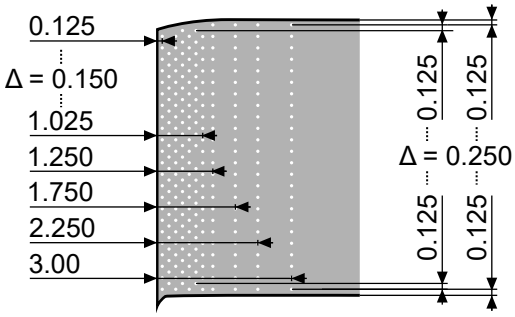

Figure 6.12: Measurement positions for the microhardness measurements.

Hardness of the Sheet Metal Strips

The hardness distribution of the manufactured sheet metal strips is illustrated in figure 6.13.

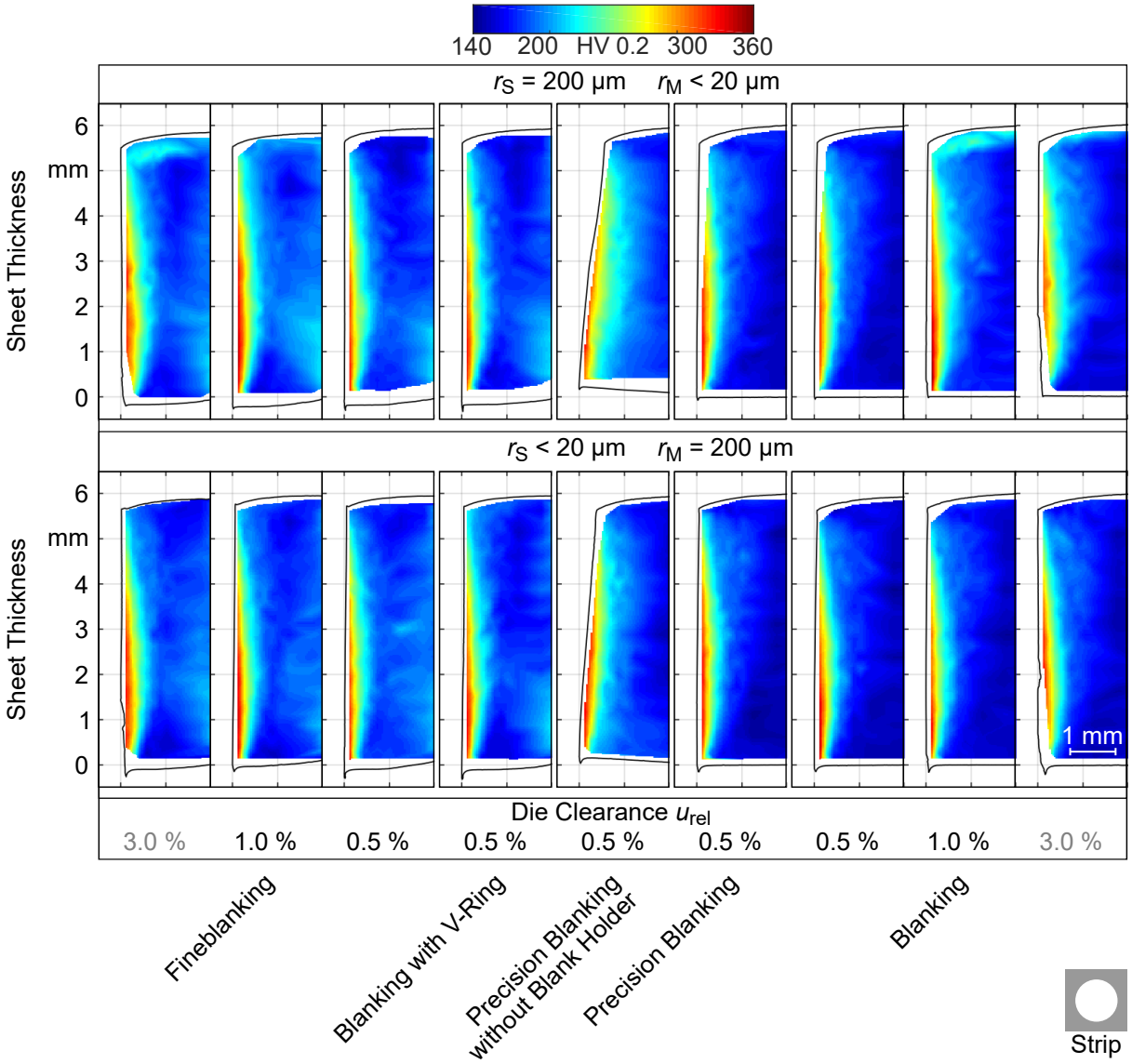

Figure 6.13: HV 0.2 hardness distribution of sheet metal strips manufactured by the five precision shear cutting processes together with exemplary cut-surface profiles as partially published in Stahl, D. Müller, Tobie, et al., 2019.

A similar distribution can be observed for all variants that do not show a fracture zone. Starting from the die roll the hardness is increasing towards the burr side where it reaches its maximum close to the burr. From the cut-surface a steady decrease is visible. This results in a flame shaped hardness distribution.

Precision Shear Cutting Process Similar results were measured close to the clean cut for all variants manufactured with a die clearance of 0.5 %. While the sheet metal strips manufactured without a v-ring show a steady decrease with increasing distance from the clean cut, the parts manufactured with a v-ring show an additional hardness rise at a distance of approximately 1 mm from the clean cut.

Cutting Edge Preparation The cutting edge preparation does not show a clear influence on the hardness distribution. Only where it affects the fracture zone height, significant differences are visible.

Die Clearance For the sheet metal strips that show a fracture zone, the rising hardness towards the clean cut is interrupted by the fracture. This is especially the case for the variants produced with a die clearance of 3 %.

To identify the residual stress state influence independently of the geometry and the hardness, specimens were subjected to a stress relief heat treatment after shear cutting the hole. Their hardness distribution compared to specimens without this heat treatment after shear cutting is displayed in figure 6.14.

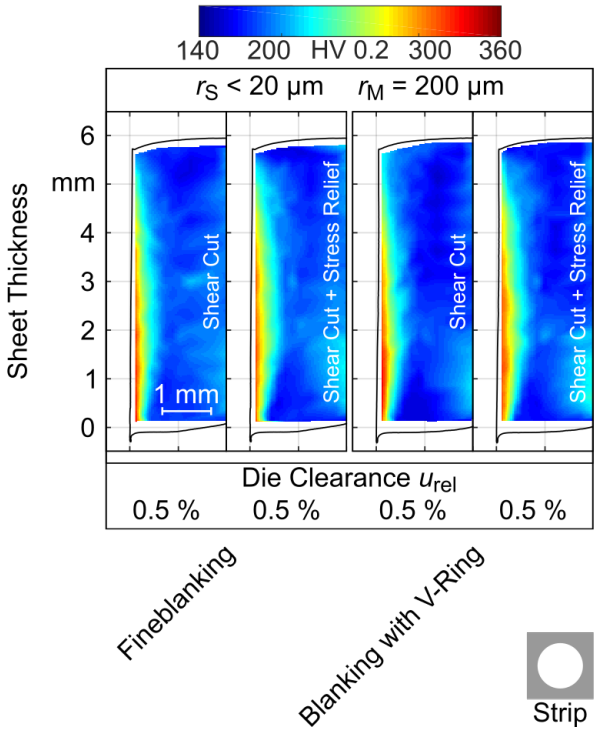

Figure 6.14: HV 0.2 hardness distribution of sheet metal strips manufactured by fineblanking and blanking with v-ring with and without an additional stress relief heat treatment after shear cutting together with exemplary cut-surface profiles.

For both the specimens manufactured by fineblanking and blanking with v-ring, no significant influence of the heat treatment on the hardness distribution can be observed.

6.4 Numerical Analysis

6.4.1 Model Setup of the Precision Shear Cutting Processes

The Finite-Element models were built in Abaqus 2018. The setup is shown exemplary for fineblanking in figure 6.15.

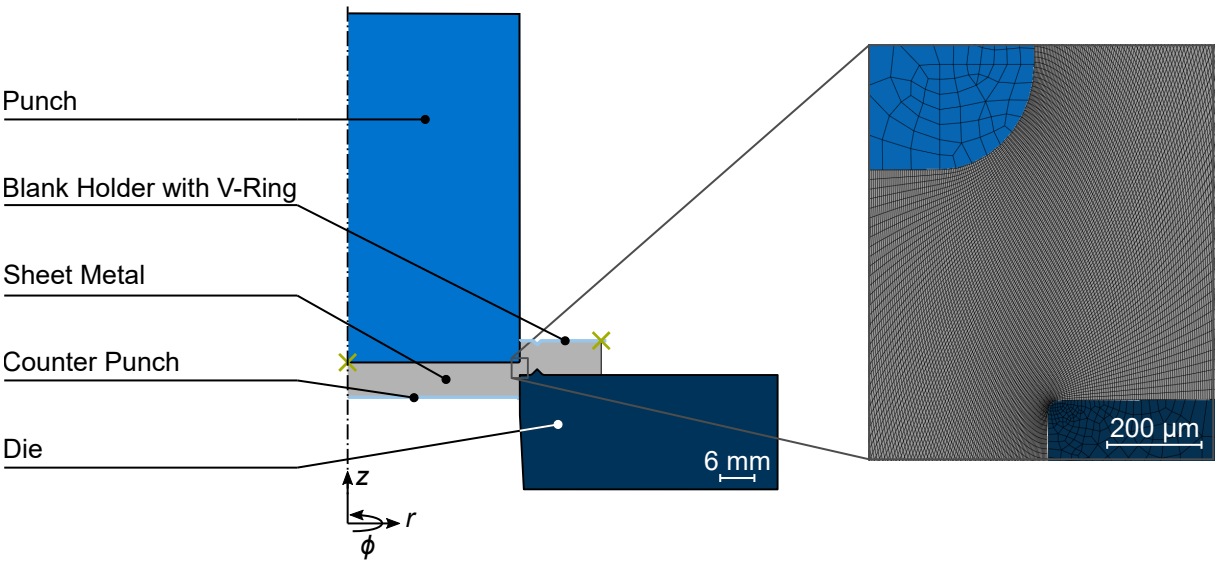

Figure 6.15: Simulation setup for fineblanking (left) with an exemplary result (right).

The process simulation consists of all parts directly involved in the respective blanking process, i.e., punch, die with and without v-ring, blank holder with and without v-ring, counter punch, and sheet metal. To reduce the computational effort, the rotational symmetry of the setup was used. Additionally, mass scaling was used for the whole model in order to decrease the calculation time.

Punch and die are modeled as elastically deformable bodies. The need for computationally expensive deformable active elements will be addressed in chapter 6.4.3. A velocity boundary condition was set for the upper surface of the punch. The lower and the right surface of the die were fixed in space. Both parts were modeled with CAX4R elements, axisymmetric four node elements with reduced integration and hourglass control (Dassault Systemes SE, 2020[a]).

The sheet metal was modeled as an elastically and plastically deformable body using CAX4R elements as well. Due to the extreme deformation in the sheet metal, enhanced hourglass control was set together with ALE adaptive meshing to improve the simulation stability and to reduce excessive element deformation. The movement of the sheet metal is only restricted by the rotational symmetry. The sheet metal's cross section is reduced by punch and die during the blanking process. This means that the initially 6 mm thick sheet metal is compressed to approximately 30 µm for the smallest die clearance before fracture. Therefore, the elements tend

to be extremely elongated if they were quadratic at the beginning. This effect can be reduced if the elements are chosen rectangular, being significantly higher than wide. Here, a height of 55 µm and a width of 5 µm was chosen. As visible in figure 6.15 on the right side, this results in almost quadratic elements shortly before fracture occurs.

The blank holder and the counter punch were modeled as analytical rigids. Their only degree of freedom is the translation in z direction. Both were subjected to the loads set in the shear cutting experiments for the different precision shear cutting processes (see table 6.2).

The sheet metal is in contact with all other parts of the model. Here, the penalty contact method was chosen with a coulomb friction coefficient of 0.05, as published by Lange, 2002 for the contact of steel on steel with a lubricant.

The shear cutting processes were simulated using an explicit solver. The simulation is split in several steps. At first, the blank holder and counter punch force are applied. In the case of fineblanking and blanking with v-ring, the v-ring is embossed in the sheet metal during this step. The blank holder and counter punch force are kept constant during the next step. Here, the punch is moving with a constant velocity and is gradually shearing the sheet metal until fracture occurs. Following, the punch is slowed down and stops in the die channel.

After the explicit simulation of the blanking process, a springback calculation is carried out using an implicit solver. Here, all parts of the tool are removed and only blank and sheet metal strip, i.e., the former sheet metal, are considered. To prevent these from moving, the degree of freedom in z direction was restricted for one node on each part of the sheet metal, as indicated by the green crosses in figure 6.15. Thus, the part geometry after springback can be analyzed.

6.4.2 Elastic and Plastic Material Behavior

Material Modeling

Accurate prediction of stresses during the shear cutting and during fatigue testing demands a very accurate knowledge of the sheet metal and tool material behavior. Thus, a material model is calibrated in the following to describe the materials in the elastic and the plastic region.

For elastically deformable active elements, a Young's modulus of 218 GPa, a Poisson's ratio of 0.29, and a density of 7.68 kg m^{-3} according to Richter, 2020 were chosen.

The elastic behavior of the sheet metal material was modeled by a Young's modulus of 215 GPa, the mean of the measured moduli from the tensile tests for 0 ° and 90 ° to the rolling direction (see table 5.2). A Poisson's ratio of 0.27, as measured by the acoustic response, was used.

For the plastic material model, two representative stress-strain curves of the specimens after the heat treatment, one longitudinal and one perpendicular to the rolling direction, were analyzed. These show a distinct Lüders behavior after reaching the material's yield strength, as illustrated in figure 6.16. This region of the flow curve was modeled by fitting a line with the slope C_{L1} and

a zero crossing C_{L0} to the measured data of the curves for 0 ° and 90 ° to the rolling direction and calculating the mean afterwards. The parameters of this model are listed in table 6.4. It should be noted, that the initial yield stress C_{L0} is also the mean of the measured yield strength in and perpendicular to the rolling direction (see table 5.2).

The strain hardening afterwards was determined by performing a weighted fit of the Ludwik and Voce extrapolation models to the rest of the curves. The resulting parameters are listed in table 6.4. Finally, an interpolation between these curves was performed with equation 6.4. The interpolation factor β was determined inversely by comparing the measured cutting force and cut-surface geometry to those obtained from the simulations. The fitted extrapolation models are displayed together with an interpolated model for $\beta = 0.27$ in figure 6.16 as well.

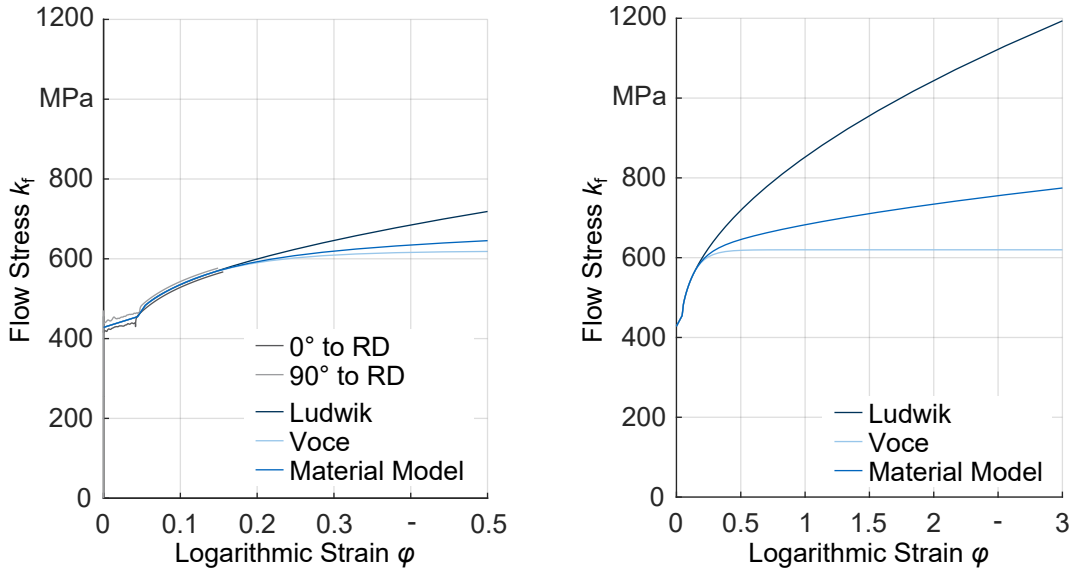

Figure 6.16: Measured stress strain curves in and perpendicular to the rolling direction (RD) together with the material model (left) and comparison of the extrapolations models for high strain (right).

Table 6.4: Parameters of the material model.

Model	**Parameters**		
Lüders	C_{L0} [MPa]	C_{L1} [MPa]	
	428.1	603.3	
Ludwik	k_{f0} [MPa]	B_L [MPa]	n [-]
	448.9	413.5	0.543
Voce	k_{f0} [MPa]	$k_{f\infty}$ [MPa]	B_V [-]
	468.8	619.7	10.51

$$k_f(\varphi) = \beta(k_{f0} + B_L\varphi^n) + (1-\beta)(k_{f\infty} - (k_{f\infty} - k_{f0})\exp(-B_V\varphi)) \tag{6.4}$$

The strain rate hardening was taken from Stahl, 2015 where a power law model was calibrated for the same material grade. Strain rate hardening is mainly used because of its stabilizing

effect. This model is described by the following equation:

$$h(\dot{\varphi}) = \left(\frac{\dot{\varphi}}{0.0005\,s^{-1}}\right)^{0.0028} \tag{6.5}$$

Validation

To check if the chosen material model is able to describe the material behavior during shear cutting accurately, the maximum shear cutting force obtained by simulations and experiments are compared. In both cases, the curves were smoothed before determining the maximum force. This comparison is displayed in figure 6.17.

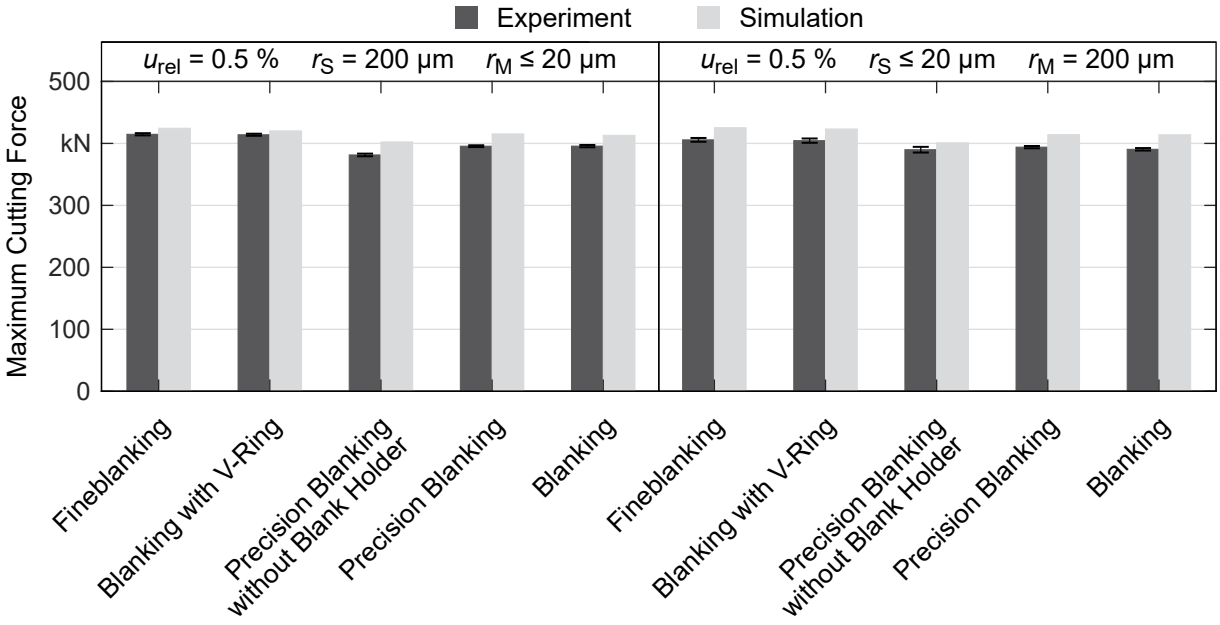

Figure 6.17: Comparison of the maximum shear cutting force obtained from the experiments and simulations.

It can be observed that the material model slightly overestimates the maximum shear cutting force in all cases, which is reasonable as temperature dependency was neglected. Of course, also the strain and strain rate modeling could cause this effect. Still, a good accuracy is achieved which also follows the experimental tendencies even though highly differing processes variants and a comparably big range of active element edge radii is investigated.

6.4.3 Fracture Model

Fracture Modeling

At first, it was checked if the elastic deformation of punch and die has to be considered for fracture modeling. Therefore, simulations were carried out with rigid and with elastically deformable active elements. This is shown in figure 6.18 for fineblanking.

The simulation with rigid active elements shows a triaxiality close to zero, i.e., close to pure shearing, between the cutting edges whereas the elastic deformation of punch and die causes a

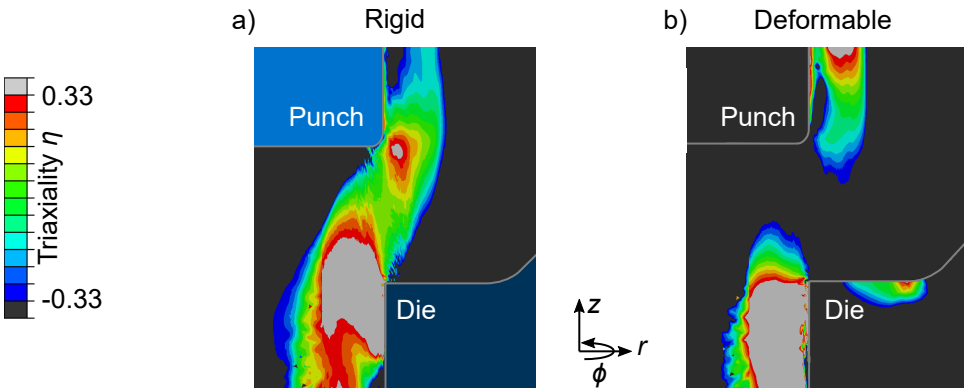

Figure 6.18: Triaxiality field of a fineblanking simulation ($u_{rel} = 0.5\,\%$, $r_S = 200\,\mu m$, $r_M \leq 20\,\mu m$) with rigid punch and die (a), and with elastically deformable punch and die (b) for the triaxility range between uni-axial compression (-0.33) and uni-axial tension (0.33).

significant rise of the hydrostatic stresses which result in a triaxiality below -0.33, i.e., below uni-axial compression. This especially affects the fracture initiation. As the influence of elastic active element deformation can not be neglected, all shear cutting simulations were carried out with an elastically deformable punch and die.

The Johnson Cook fracture model given in equation 2.14 was used for fracture prediction. Again, an inverse approach as presented by Krinninger, 2019 has been used to identify the model parameters. As a starting point, the results presented in Stahl, 2015 were used. The final parameters are listed in table 6.5. The validity of this model will be investigated in the following.

Table 6.5: Parameters of the fracture model.

Model	**Parameters**		
Johnson Cook	C_1 [-]	C_2 [-]	C_3 [-]
	0.777	865.4	13.7

Validation

The cut-surface geometries resulting from the used material and fracture model are displayed in figure 6.19 for fineblanking and blanking with two different active element edge conditions for both blank and sheet metal strip.

Only minor differences can be observed between the calculated and the measured profiles. Thus, it can be assumed that both, the elastic and plastic material behavior as well as fracture, is sufficiently modeled for further analysis.

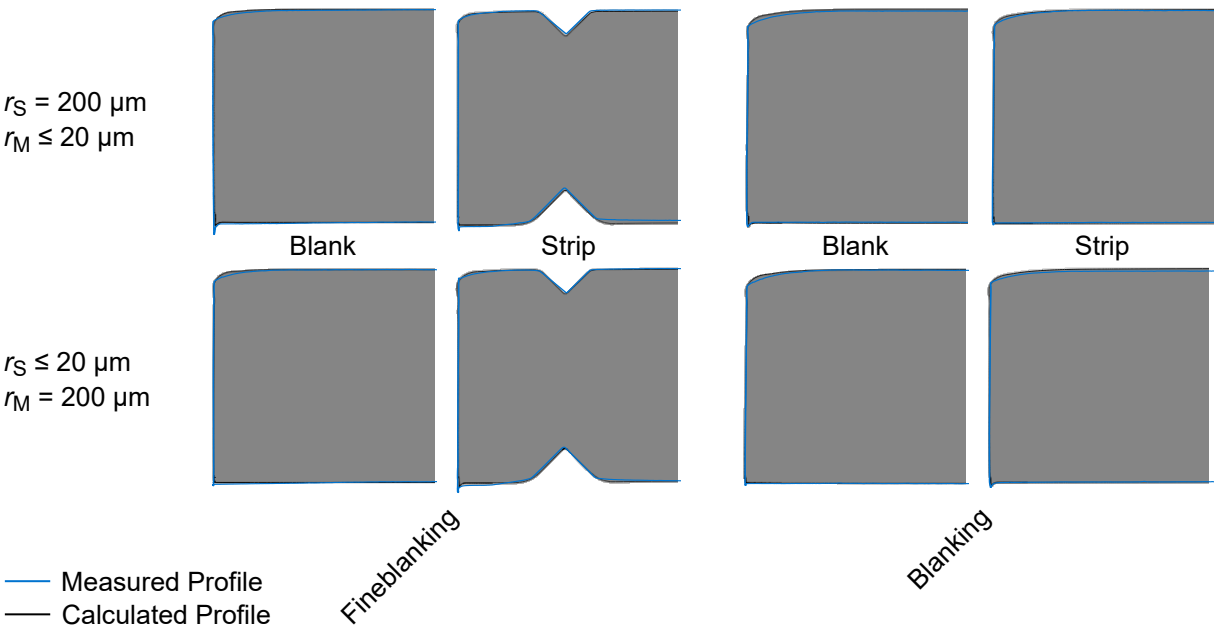

Figure 6.19: Comparison of representative measured cut-surface profiles (blue) and the calculated profiles (black).

7 Precision Shear Cutting Induced Residual Stresses

In this chapter, the parts manufactured by the different precision shear cutting processes are characterized regarding their residual stress state. Following, an explanation model for the development of the residual stress state is proposed. With this model, the influence of different tool setups and process parameter combinations are discussed regarding their effect on the process induced residual stresses.

7.1 Residual Stresses

7.1.1 Residual Stress Measurement

The residual stress measurements were carried out by the FZG on the X-ray diffractometer. Chromium-Kα radiation with 40 mA and 40 kV was used with a collimator hole diameter of 1 mm. The α-planes of ferrite were investigated on the $\{211\}$ plane.

Due to the restricted space in the X-ray diffractometer, the specimens were cut before measuring as illustrated in figure 7.1. If not mentioned otherwise, residual stresses were measured in the middle of the sheet thickness in axial (σ_{ax}) and tangential direction (σ_{tan}), which is illustrated in figure 7.1 as well. The tangential stress is also referred to as hoop stress. Here, the axial direction corresponds to the z direction and the tangential direction to the ϕ direction introduced in figure 6.15. Depth profiles were measured by etching an area of 7×3 mm with 5 % perchloric acid while sealing off the rest of the surface with tape. Following this, the depth was measured with a depth micrometer. If the desired depth was achieved, the residual stress state was measured on that surface. (Stahl, D. Müller, Tobie, et al., 2019)

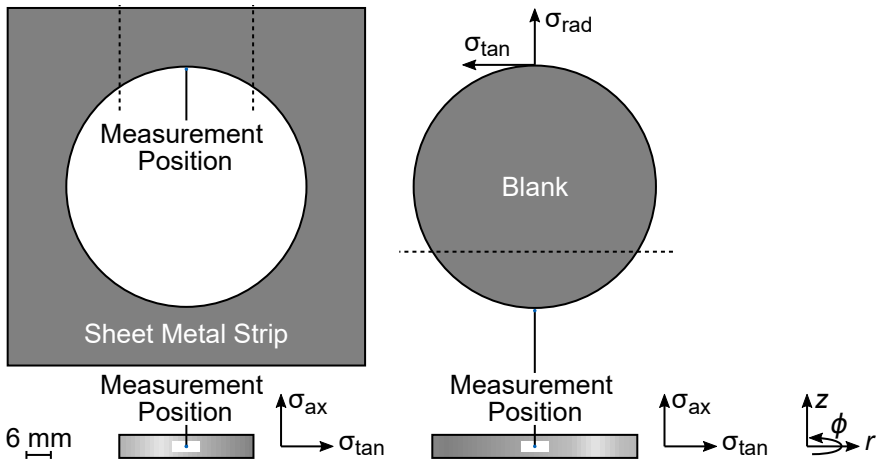

Figure 7.1: Specimen preparation and measurement position for the residual stress measurements according to Stahl, D. Müller, Tobie, et al., 2019.

7.1.2 Residual Stress State of the Blanks

The residual stresses in axial and tangential direction of the manufactured blanks are displayed in figure 7.2. As these will be discussed in detail, only a short overview is given. The tangential

stress ranges from -549 MPa for fineblanking with $u_{rel} = 0.5\,\%$, $r_S < 20\,\mu m$ and $r_M = 200\,\mu m$ to 574 MPa for precision blanking with $r_S = 200\,\mu m$ and $r_M < 20\mu m$. In both cases this stress is higher than the tensile strength measured in chapter 5.1. It should be noted that the residual stress measurement is also affected by the texture induced by shear cutting. This topic is a field of ongoing research addressed in the DFG priority program SPP 2013. Nevertheless, a qualitative comparison is possible as the parts show a similar hardness distribution which indicate similar strains at the surface.

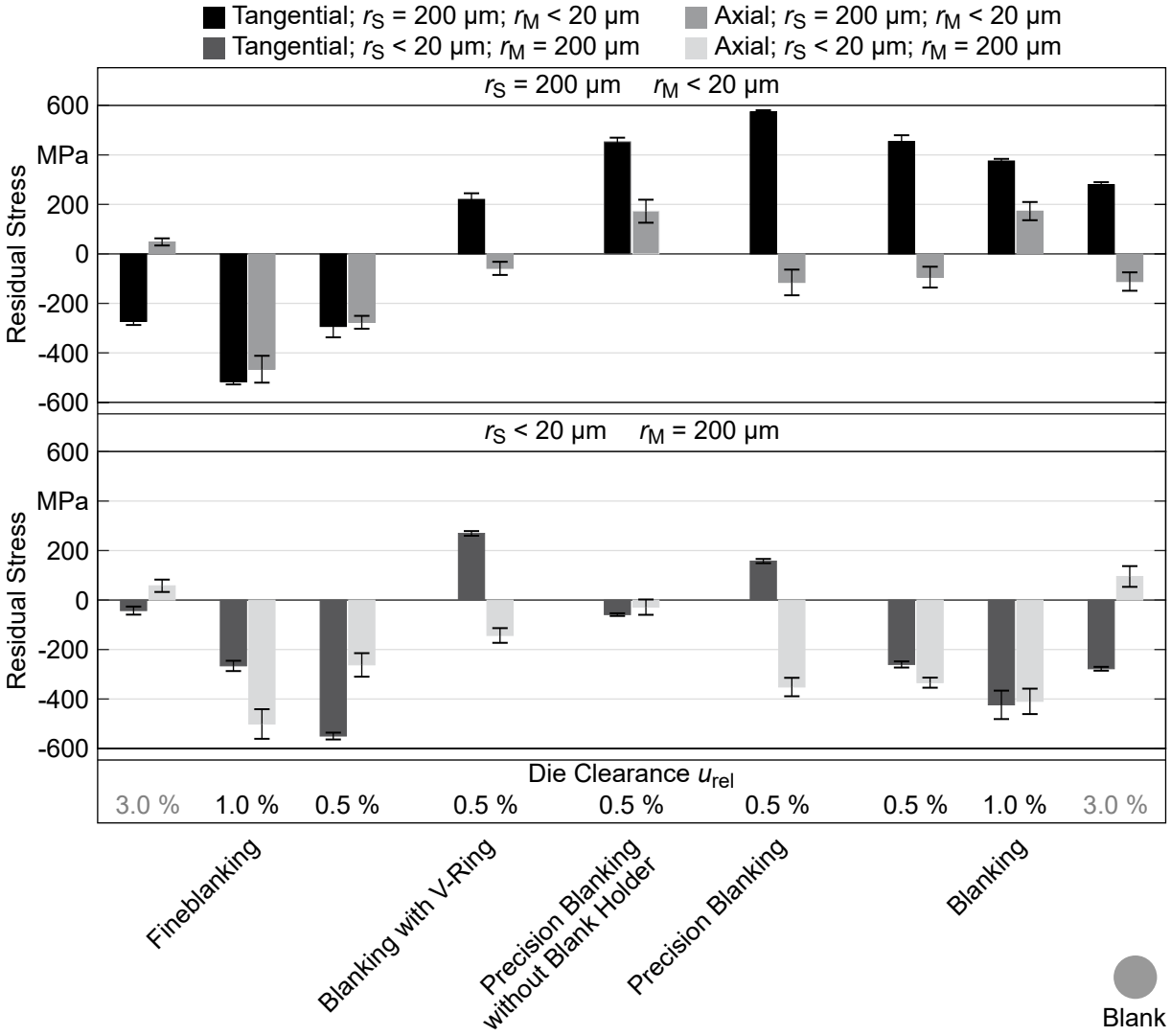

Figure 7.2: Surface residual stresses of the blanks in tangential and axial direction in the middle of the sheet thickness as published in Stahl, D. Müller, Tobie, et al., 2019 and Stahl, D. Müller, Nürnberger, et al., 2021.

For $r_S = 200\mu m$ and $r_M < 20\,\mu m$ tensile residual stresses in tangential direction are observed for all processes and die clearances except for fineblanking and precision blanking without blank holder. The variants with $r_S < 20\mu m$ and $r_M = 200\,\mu m$ show compressive tangential residual stresses for all processes and die clearances except for the blanks manufactured with precision blanking and blanking with v-ring.

The axial residual stresses range from -501 MPa for fineblanking with a die clearance of 1 %

with a rounded die edge to 173 MPa for normal blanking with a rounded punch edge and a die clearance of 1 %. A similar value was measured for precision blanking without blank holder with $r_S = 200\,\mu m$ and $r_M < 20\,\mu m$. It should be noted that this configuration shows a fracture zone in the middle of the sheet thickness. Therefore, additional measurements on the clean cut were carried out, which are displayed in figure 7.3 a).

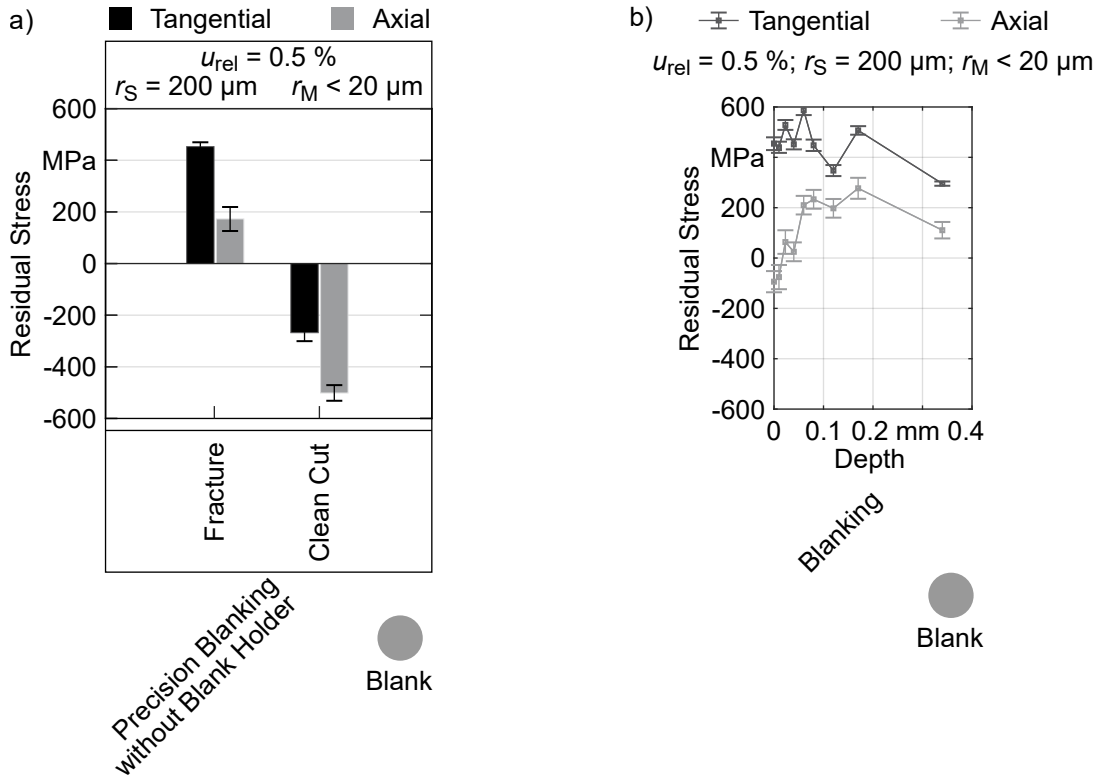

Figure 7.3: Surface residual stresses of the blank manufactured by precision blanking without blank holder in tangential and axial direction in the middle of the sheet thickness and on the clean cut (a) and depth distribution of the residual stresses for a blank manufactured by blanking with $u_{rel} = 0.5\,\%$, $r_S = 200\,\mu m$ and $r_M < 20\,\mu m$ (b) as published in Stahl, D. Müller, Tobie, et al., 2019.

While the fracture zone is subjected to tensile residual stresses both in axial and tangential direction, the clean-cut shows a compressive residual stress state. The residual stress depth distribution of a slug manufactured by blanking is shown in figure 7.3 b). From the surface to a depth of 0.08 mm the stress in tangential direction ranges between 440 and 587 MPa. A local minimum can be observed at a depth of 0.12 mm followed by a local maximum at 507 mm. Even at a depth of 0.34 mm, a tensile stress state was measured. In axial direction compressive stresses are measured up to a depth of 0.01 mm which change to tensile stresses afterwards.

7.1.3 Residual Stress State of the Sheet Metal Strips

The residual stresses in axial and tangential direction of the sheet metal strips are displayed in figure 7.4. Compared to the blanks the sheet metal strips show a compressive residual stress state in most cases. In axial direction only compressive stresses were measured. For the small

die clearance of 0.5 % tensile stresses in tangential direction were measured for the strips manufactured by precision blanking without blank holder for the variant with $r_S = 200\,\mu m$ and $r_M < 20\,\mu m$ and for the strips manufactured with blanking with v-ring with $r_S < 20\,\mu m$ and $r_M = 200\,\mu m$. Additionally, the strips manufactured with a die clearance of 3 % show tensile stresses for fineblanking with $r_S = 200\,\mu m$ and $r_M < 20\,\mu m$, and for blanking with both cutting edge variants.

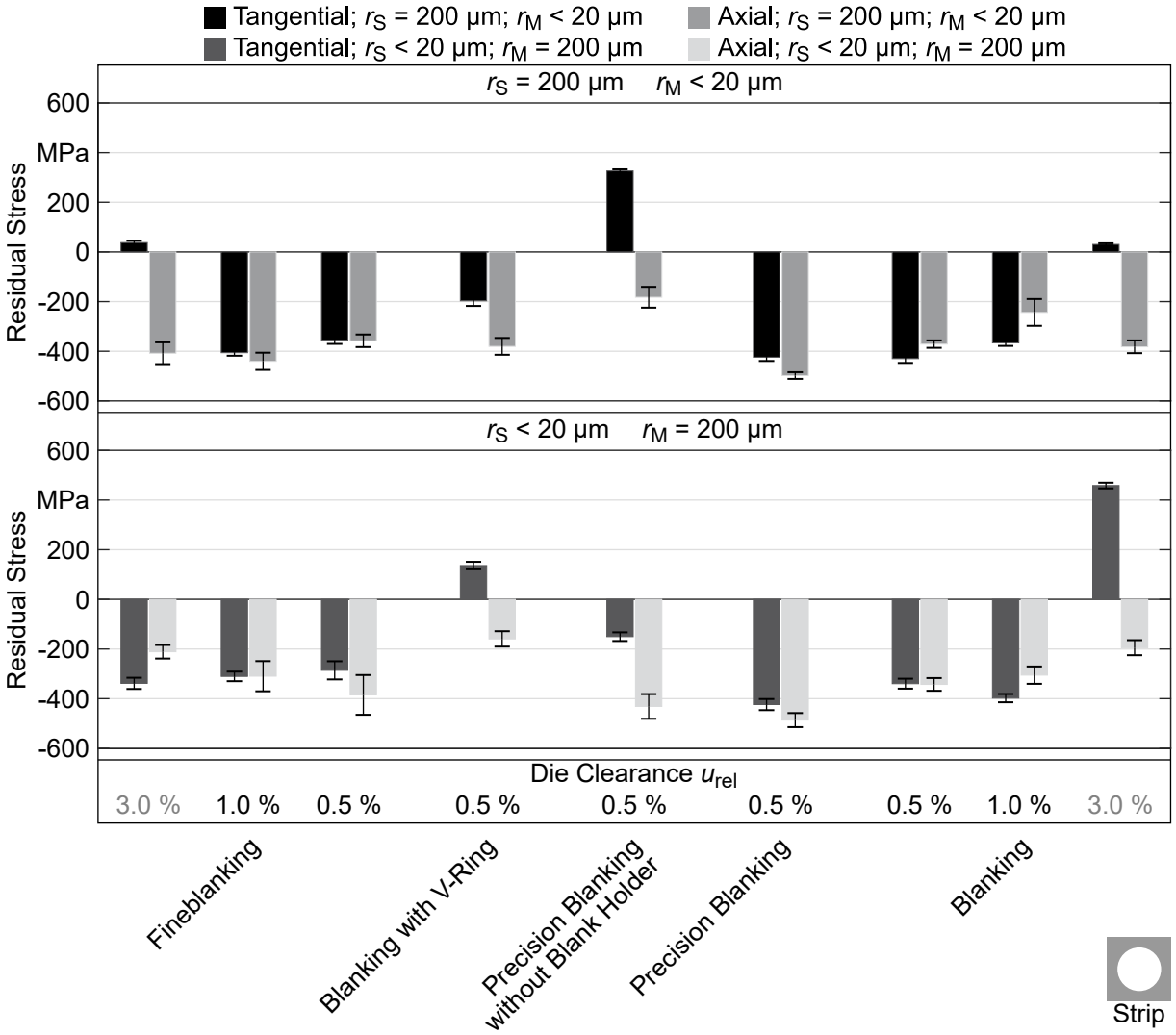

Figure 7.4: Surface residual stresses of the sheet metal strips in tangential and axial direction in the middle of the sheet thickness as published in Stahl, D. Müller, Tobie, et al., 2019, Stahl, D. Müller, Pätzold, et al., 2019 and D. Müller et al., 2021.

In both cases the strips manufactured with a die clearance of 3 % show a significant amount of fracture zone. Therefore, the residual stresses in the middle of the clean cut and the middle of the fracture zone were measured for the strips manufactured by blanking. These measurements are displayed in figure 7.5.

For both cutting edge variants a compressive residual stress state in tangential direction was measured in the middle of the clean cut. The variant manufactured with $r_S = 200\,\mu m$ shows a clean cut zone reaching over the middle of the sheet thickness. Here, tangential stresses close

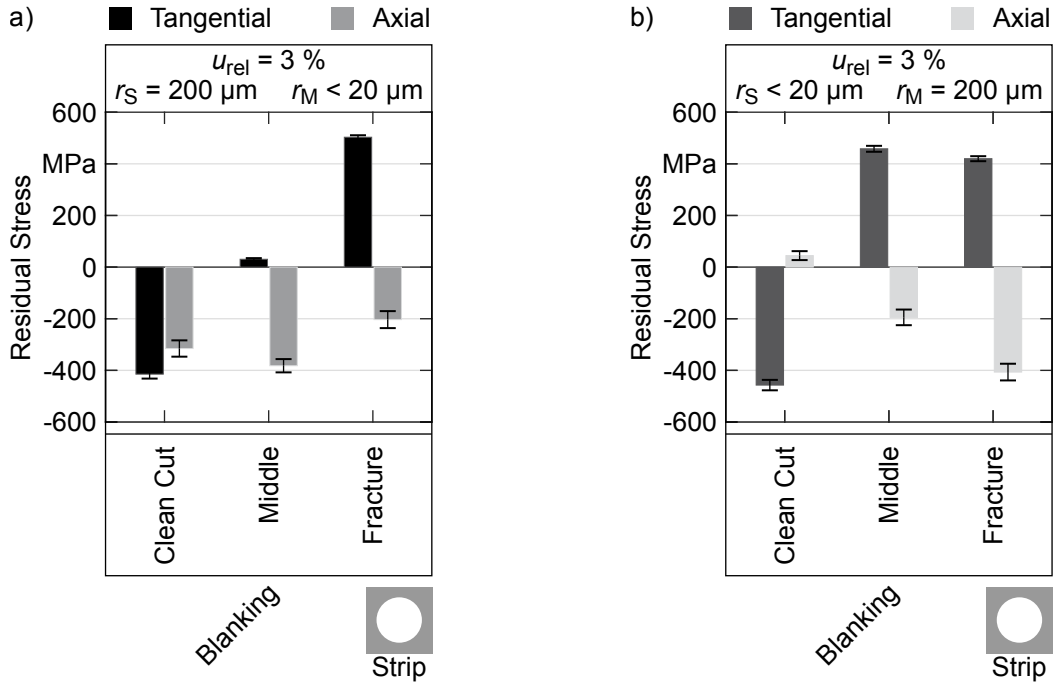

Figure 7.5: Surface residual stresses measured in the middle of the clean cut, the middle of the sheet thickness, and the middle of the fracture zone for sheet metal strips manufactured by blanking with a die clearance of 3 % as published in Stahl, D. Müller, Pätzold, et al., 2019 and D. Müller et al., 2021.

to zero were measured which change to a tensile stress of 503 MPa in the fracture zone. The strip manufactured with the sharp punch edge radius shows a fracture zone reaching close to the middle of the sheet thickness. Here and in the fracture zone high tensile stresses of 458 and 420 MPa can be observed. Compressive residual stresses were measured in axial direction for all positions and variants except for the clean cut of the variant with $r_S < 20\,\mu m$ which shows tensile stresses close to zero.

The residual stress depth distributions of the strips manufactured with a die clearance of 0.5 % and $r_S = 200\,\mu m$, measured in the middle of the sheet thickness, are shown in figure 7.6. In tangential direction, the strips by fineblanking and blanking with v-ring, show a compressive residual stress state at the surface which increases to a maximum with significant tensile stresses at a depth of approximately 0.1 mm. With increasing depth, the stresses are decreasing again. The stresses in axial also show an increase from the compressive stress state at the surface with local maxima at a depth around 0.1 mm. At a depth of more than 0.3 mm, a similar stress in axial and tangential direction was measured for both process variants.

The sheet metal strips manufactured by precision blanking and blanking show similarly increasing tangential residual stresses with increasing depth but with a maximum between 0.16 and 0.18 mm. The strip manufactured by precision blanking shows a similar axial and tangential stress profile. For blanking, the axial residual stress shows an additional minimum at a depth 0.16 mm. At a depth of 0.33 mm a similar stress in axial and tangential direction is measured. Precision blanking without blank holder is the only process that produces strips with signifi-

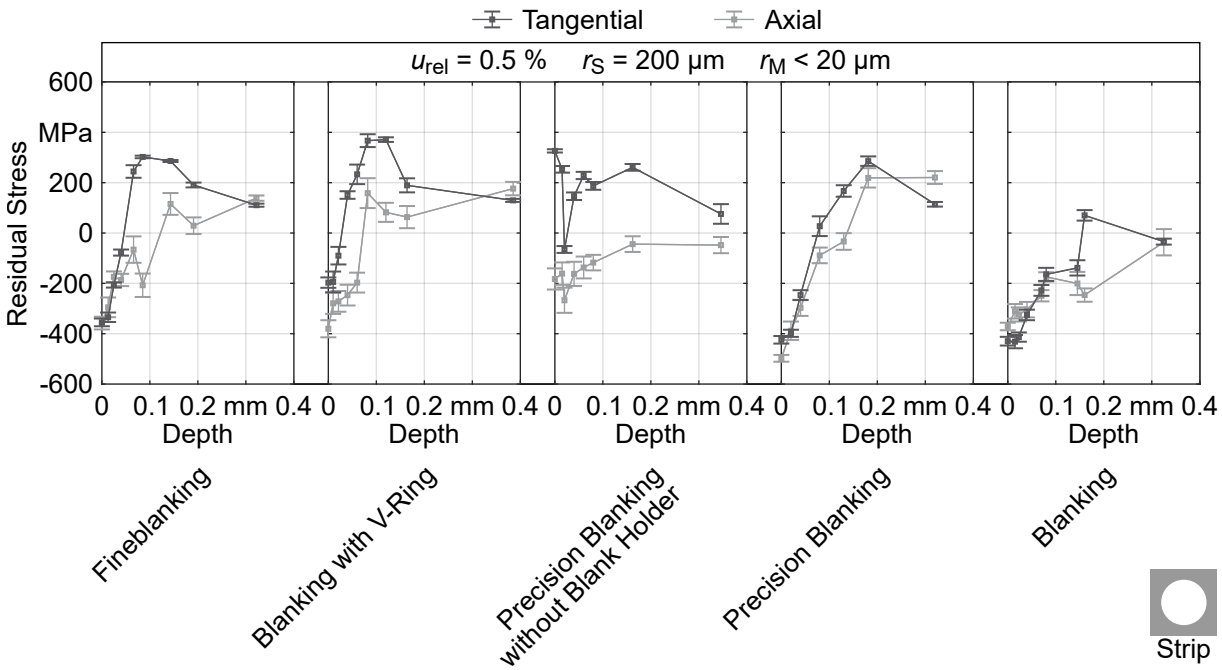

Figure 7.6: Residual stress depth distributions in tangential and axial direction of the sheet metal strips manufactured with a die clearance of 0.5 %, a punch edge radius of 200 µm, and a die edge radius smaller 20 µm as published in Stahl, D. Müller, Tobie, et al., 2019 and Stahl, D. Müller, Pätzold, et al., 2019.

cant tensile stresses in tangential direction at the specimen surface. This high tensile stress is decreasing and shows a minimum with compressive stresses at 0.02 mm. This minimum is followed by a sharp increase that results in tensile stresses over 146 MPa that decrease to 76 MPa at a depth of 0.35 mm. The axial stresses show a similar trend starting from a compressive stress state.

7.2 Discussion of Factors Influencing the Residual Stress State

The residual stress measurements clearly show that the residual stress state is significantly influenced by the chosen precision shear cutting process and its process parameters. These influences will be discussed in the following. At first an explanation model is proposed to understand the formation of the part's residual stress state. Afterwards, this model is used to understand the influence of tool and process parameter configurations. Finally, the results are summed up and evaluated regarding their ability to achieve a desired residual stress state.

7.2.1 Explanation Models

The explanation models are derived from macroscopic changes of the part geometry. Thus, it is assumed that a deviation from the perfect size and flatness is caused by an altered stress state during the shear cutting process which affects the part's springback. The available springback modes correspond to the available degrees of freedom. After the part is removed from the tool it can move in radial/tangential direction, i.e., perpendicular to the cutting line. Springback is also

possible in axial direction which means along the sheet metal thickness. Finally, the bending degree of freedom is available to alter the stress state. Of course not only macroscopic effects exist, i.e., effects on the scale of the whole part, but also effects on a smaller level. These effects are considered independently, as there is no macroscopic measure to evaluate them.

The mechanisms leading to the formation of tangential residual stresses can be categorized in radial springback and bending springback. In the following, the coupling between radial and tangential stresses should be kept in mind. The axial residual stress is also coupled to the tangential stress by the elastic constants.

Radial/Tangential Springback

While there are significant radial stresses on the clean cut during the shear cutting operation, these change to tangential stresses after springback, when there is no active element to counteract the radial stresses. At first, the mechanisms in radial direction are discussed without considering bending. These springback mechanisms are illustrated in figure 7.7.

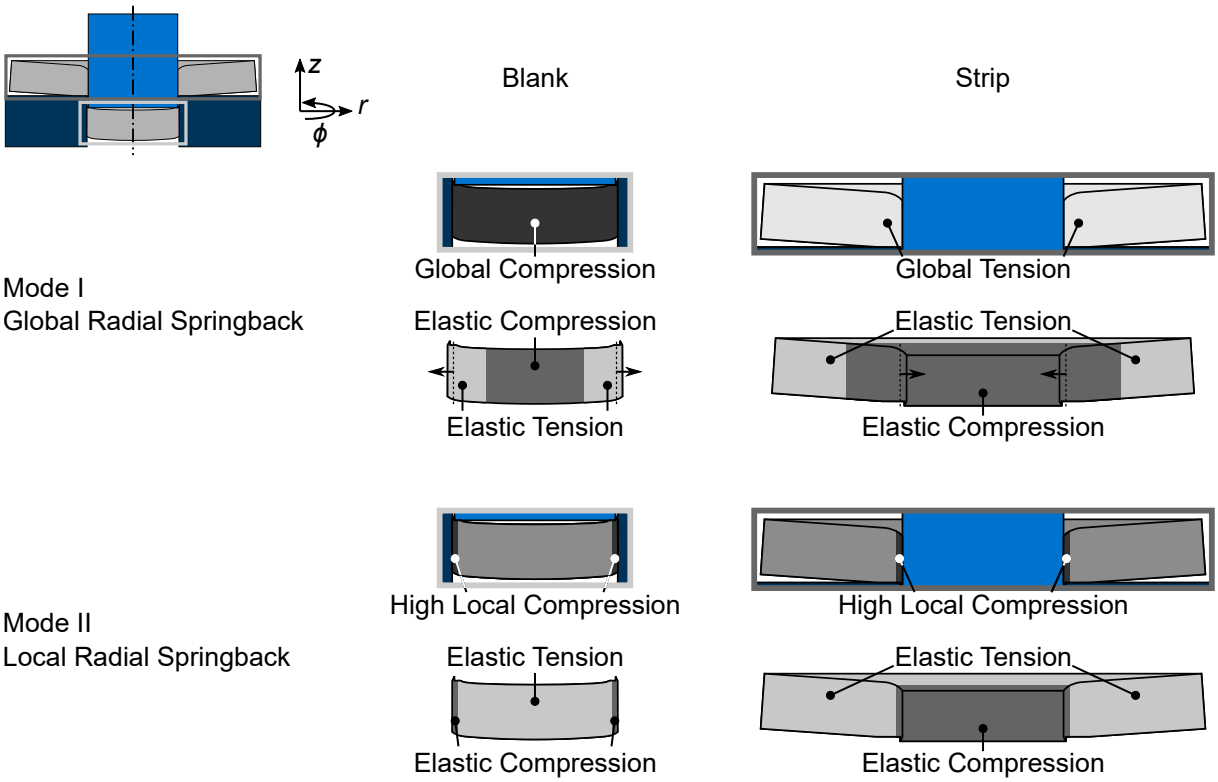

Figure 7.7: Global and local springback modes in radial direction of parts produced by a rotation-symmetric closed cut without the formation of a fracture zone.

The global radial springback mechanism is derived from the difference of the part geometry during the shear cutting process and afterwards, when the final part is removed from the tool. After the separation of the work piece during the shear cutting process, the blank is still stuck in the die channel while the sheet metal strip grips the punch. A force is necessary to push the blank through the die channel and to pull the punch out of the sheet metal strip, i.e., the

frictional force between the active elements and the parts has to be surpassed. The occurrence of these frictional forces means that the parts press against the active elements in radial direction. This also means that the blank is compressed in radial direction while the sheet metal strip is stretched by the punch.

As soon as the blank is removed from the die channel, this radial stress on the surface becomes zero. Due to the radial springback of the former compressive stress state, the blank gets slightly bigger, as observed in Volk, Kindsmüller, et al., 2018. According to Hook's law, the compressive radial surface stresses change to tensile tangential surface stresses. Inside the blank, this results in compressive stresses, as the part has to be in static equilibrium.

The sheet metal strip was initially stretched by the punch. Thus, the manufactured hole gets slightly smaller after the punch is pulled out. This results in compressive surface stresses in tangential direction and tensile stresses on the outer rim of the part. A similar effect can also be observed in other manufacturing techniques like in autofrettage. This hypothesis is supported by the observation that the sheet metal strips show compressive residual stresses in tangential direction on the clean cut in almost all cases (see figure 7.4). Tension stresses in tangential direction are measured on the blanks in many cases, especially when the blank was manufactured with a sharp die edge. Nevertheless, when a cut is carried out with a rounded die edge, this model is not able to explain the compressive stresses of the blanks in tangential direction.

The global springback mode is only an explanatory model considering the elastic and plastic deformation of the hole part or big areas of it. Nevertheless, on a smaller scale additional effects can be thought of which are caused by non-uniform plastic deformation. During shear cutting, high strain hardening and therefore high strains and stresses are observed in the shearing zone close to the clean-cut. Therefore, it seems obvious to look at the stresses close to the cutting edges. These local effects are illustrated in figure 7.7, as well. This time, the global springback modes are neglected, which means that stresses are only considered locally during the shear cutting process.

When a cut is carried out, significant compressive stresses are induced where the clean cut is formed. This means that the clean cut area is subjected to compressive stresses in radial and tangential direction. After the punch is removed, a static equilibrium has to be achieved. For the sheet metal strip, this means that this zone, pre-loaded with compressive stresses, has to get smaller, i.e., the hole diameter is getting smaller. As global stresses are considered zero during the shearing operation, the outer rim of the sheet metal strip is not pre-loaded. Now, as the punch is removed, the inner ring which was initially subjected to high compressive stresses is getting bigger, leading to tensile stresses on the outer rim. As the outer rim was not subjected to stresses initially, the inner ring can not fully springback and is still loaded with compressive stresses. As these mechanisms work in different directions, the size change of the final part due to the local springback can be expected to be comparably small.

This observation also means that for the sheet metal strip the local and global springback mode

in radial direction work in the same direction, i.e., they both favor compressive residual stresses after springback. For the blank, the global mode causes tensile stresses while the local mode favors compressive stresses. Therefore, the blank should be more sensitive to process parameter changes. This is accompanied by the different boundary conditions of sheet metal strip and blank. While the sheet metal strip can move freely, only restricted by friction in radial direction, the blank shows an axis of symmetry over which material flow is not possible. This makes global modes, i.e., plastification and springback of big areas of the sheet metal, much more likely for the sheet metal strip than for the blank.

The springback modes derive from theoretical models, but are also visible in the shear cutting simulations. This is shown for a sheet metal strip manufactured by blanking with $u_{rel} = 0.5\,\%$, $r_S = 200\,\mu m$, and $r_M < 20\,\mu m$ in figure 7.8. It is visible that significant tangential stresses dominate the hole sheet metal strip during the process (figure 7.8 a). This leads to a distinct field of pressure residual stresses in tangential direction after springback in the first third of the sheet metal strip beginning from the clean cut (figure 7.8 b). The outer rim on the other hand still shows tensile residual stresses. As this phenomenon affects the whole part, it shows the global springback mode. To look at the local springback, another scale has to be used to differentiate from the global mode. This is shown in figure 7.8 c) which shows the state after springback. It is visible that significant compressive residual stresses dominate the area close to the clean cut, followed by a band that shows smaller compressive residual stresses. This second band corresponds to the region where high tensile stresses are caused by the punch close to the clean cut during shear cutting. As this effect is only visible in the proximity of the punch's cutting edge, this effect is referred to as a local mode.

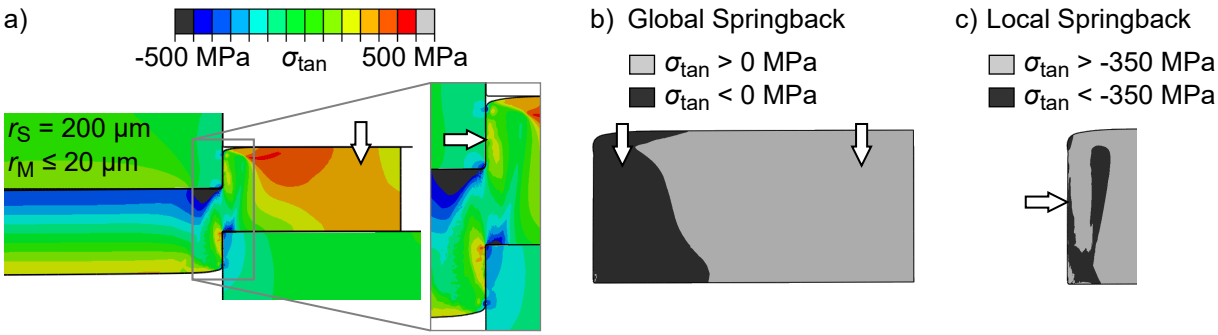

Figure 7.8: Global and local springback modes in radial direction of parts produced by a rotation-symmetric closed cut on the example of a sheet metal strip manufactured by blanking.

The significance of the global and local springback mode can be estimated as both influence the dimension of the manufactured blank or sheet metal strip. For the sheet metal strip the global and local springback mode work in the same direction: they make the shear-cut hole smaller than the punch for higher compressive residual stresses. This correlation is displayed in figure 7.9 for the four NNSBPs fineblanking (FB), blanking with v-ring (BV), precision blanking (PB) and standard blanking (B).

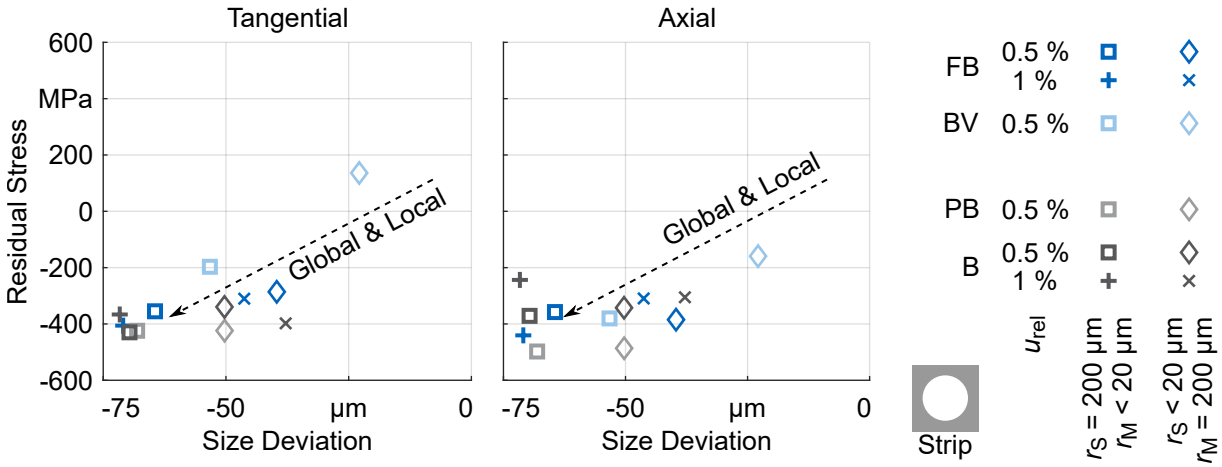

Figure 7.9: Correlation between the size deviation and the residual stresses in axial and tangential direction together with the expected trends from the global and local springback mode in tangential direction for the manufactured sheet metal strips.

As the residual stresses are challenging to interpret when the fracture zone is getting close to the measuring point, the variants manufactured with a die clearance of 3 % are not displayed here. Furthermore, the specimens manufactured by precision blanking without blank holder show a behavior that can rather be attributed to the part bending, they are also not displayed[18]. The trend in figure 7.9 shows that the dimensional accuracy is closely related to the residual stress state, both in tangential and in axial direction. Also, both springback modes, the global and local one in tangential direction, fit this observation. Furthermore, this shows that the tangential springback also influences the axial residual stresses as they are coupled to the tangential residual stresses by the elastic constants, as visible for the sheet metal strips manufactured by blanking with v-ring.

The same analysis can be carried out for the manufactured blanks. Here, a different behavior can be expected. When the blank gets smaller due to global springback, higher compressive residual stresses can be expected. The local mode on the other hand should show a different behavior. Higher local compressive stresses during the shear cutting process lead to higher compressive residual stresses after springback. The change of the part's dimension should not be significantly affected by the local mode. As the global mode still changes the part's dimension, higher compressive residual stresses caused by the local mode should be accompanied by a bigger diameter caused by the global mode. This correlation is displayed in figure 7.10. It can be observed that the local springback mode dominates the development of the residual stress state in tangential direction. This is reasonable as the blank is much stiffer in radial direction as the sheet metal strip. All variants follow the trend of the local mode expect for those manufactured by blanking with v-ring, which show high bending, and those manufactured by fineblanking with a die clearance of 1 %. Again, the axial residual stresses are also affected by the local springback in tangential direction.

[18]The complete figure can be found in the appendix.

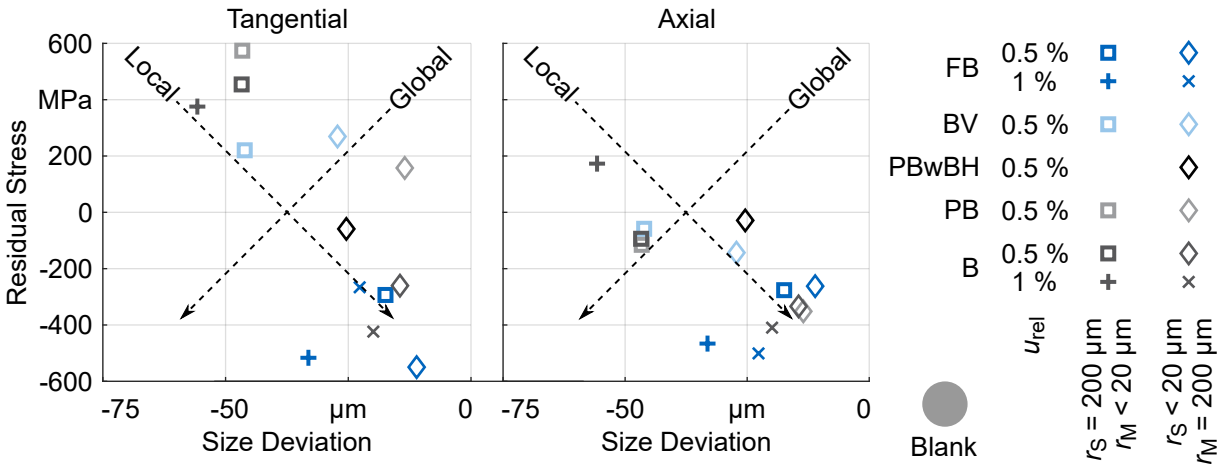

Figure 7.10: Correlation between the size deviation and the residual stresses in axial and tangential direction together with the expected trends from the global and local springback mode in tangential direction for the manufactured blanks.

Bending Springback

Another springback mode is derived from the observation of part bending during and after the shear cutting process. According to Romanowski, 1959 (see figure 2.5), two different torques are present for this bending: One caused by the resulting forces in punch movement direction and one caused by the radial forces. These torques cause the blank to lift of the lower surface of the punch and the sheet metal strip to lift of the upper surface of the die. After the punch is retracted from the strip and the slug is removed from the die, springback occurs in the different direction. This results in a bending stress profile across the sheet metal thickness as the stresses in radial direction change to stresses in tangential direction.

In the case of the blank, this causes tensile stresses in tangential direction on the burr side and compressive stresses on die roll side. The sheet metal strip on the other hand shows compressive stresses on the burr side, while the die roll side is subjected to a tensile stress state. The stress situation caused by these torques is illustrated in figure 7.11.

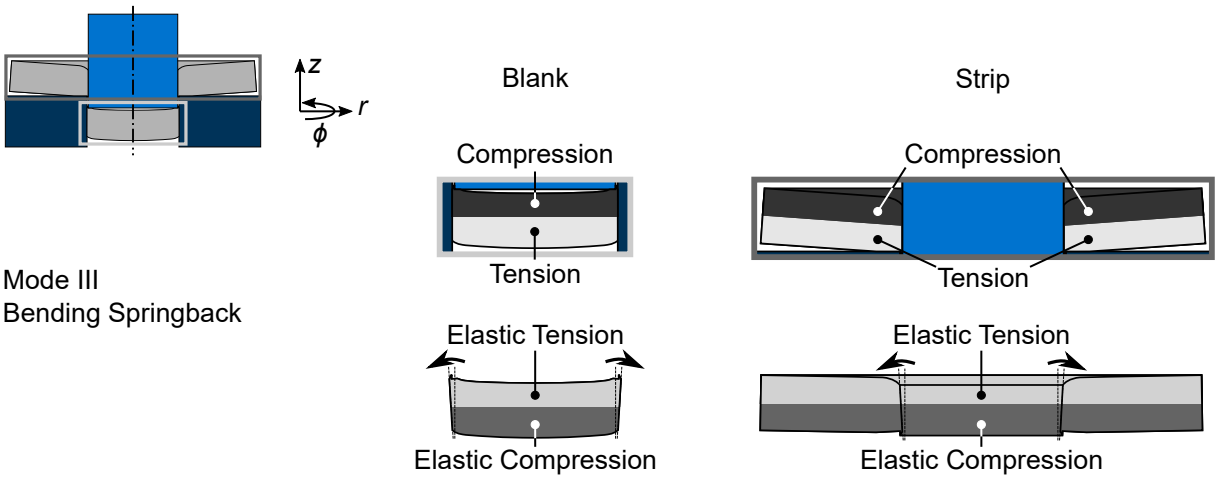

Figure 7.11: Bending springback mode of parts produced by a rotation-symmetric closed cut without the formation of a fracture zone.

After the punch is removed from the sheet metal strip, springback occurs and the part bends in the opposite direction. As investigated in many publications, this results in compressive stresses on the side initially subjected to tensile stresses[19]. The blank also bends during the shear cutting operation so that it lifts of the punch face which results in a springback after it is removed from the die channel. In this case, the bending springback causes compressive residual stresses on the die roll side and tensile stresses on the burr side. Again, these stresses are opposite to the stresses causing the bending during shear cutting.

Beside the bending coefficient, the bending springback mode can also be related to the clean cut angle. As the blank is still stuck in the die channel and the punch is in the hole in the sheet metal strip, the clean cut of blank and sheet metal strip is, within approximation, cylindrical. After springback, the clean cut gets conical, which is measured in a clean cut angle deviated from 90 °. Thus, the significance of the bending springback mode can be analyzed by the two measures for bending, the clean cut angle and the bending coefficient, which is shown in figure 7.12.

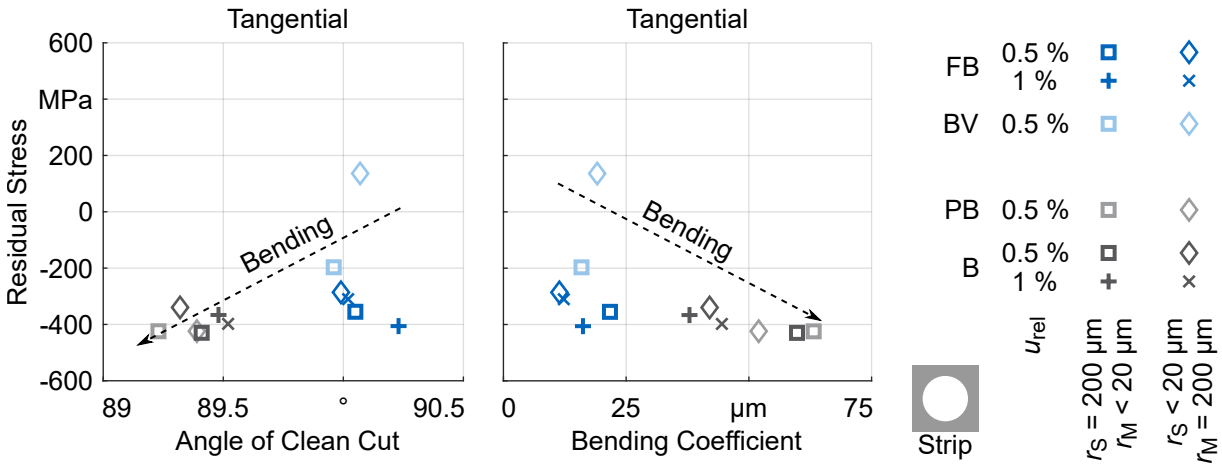

Figure 7.12: Correlation between the clean cut angle and the residual stress in tangential direction (left), and the bending coefficient and the tangential residual stress (right) together with the expected trend from the bending springback mode for the manufactured sheet metal strips.

Again, the results for precision blanking without blank holder and for a die clearance of 3 % are not displayed, as their interpretation is challenging. For both measures, two groups can be observed: One of those cut with a blank holder and one of those cut with a v-ring. Especially for the bending coefficient and the variants manufactured without a v-ring, a clear trend is visible where a bigger bending leads to higher compressive residual stresses in tangential direction. A clear trend can not be observed for the specimens manufactured by fineblanking and blanking with v-ring. To underline the importance of this springback mode for the specimen manufactured with a regular blank holder, i.e., blanking and precision blanking, it should be noted that the bending springback also causes a size deviation.

While a correlation between part bending and the tangential residual stresses was observed

[19] Here, only a simplified model considering half of the sheet metal thickness is illustrated.

for the sheet metal strips, this is not the case for the blanks. This correlation is displayed in figure 7.13. Again, the parts with the highest bending, in this case those manufactured by blanking with v-ring, are not displayed. That the results do not follow the expected trend shows that bending of the blanks is a minor factor regarding the residual stress formation, at least when bending is not severe.

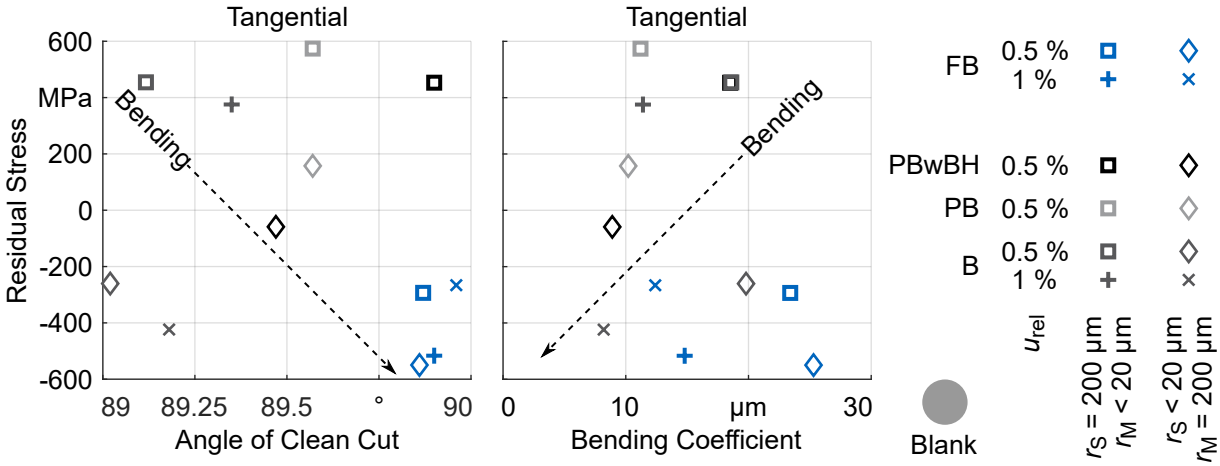

Figure 7.13: Correlation between the clean cut angle and the residual stress in tangential direction (left), and the bending coefficient and the tangential residual stress (right) together with the expected trend from the bending springback mode for the manufactured blanks.

Axial Springback

Springback is not only possible in radial, but also in axial direction. During the shear cutting process, the sheet metal material is deformed by punch and die. As the punch penetrates the work piece, it pushes material through the die channel and pulls material from the sheet metals upper surface, i.e., where the die roll is formed. The same observation can be made regarding the blank, where the die pulls material from the sheet metals lower surface. The pushing leads to high compressive stresses in axial direction between the cutting edges. These compressive stresses change to tensile stresses on the lateral surfaces of punch and die, i.e., where the clean cut of blank and sheet metal strip is formed. As this mechanism is only located in the shearing zone, it is purely locally and not a global phenomenon. Additionally, this phenomenon is most relevant in the middle of the clean cut, as the axial stress has to be zero on the die roll and burr side of the clean cut due to the free boundary. Therefore, a closer look at the stress situation is necessary, which is illustrated in figure 7.14.

The Hertzian contact stress is not the highest on the clean cut, but slightly below it in the sheet metal. Here, high axial stresses can be expected which are getting lower closer to the clean cut and to the non-plastified area of the sheet metal. After the shear cutting operation, this area which was subjected to high local tensile stresses, wants to get smaller. As the area subjected to the highest tensile stresses is getting smaller, it compresses the surrounding areas. After

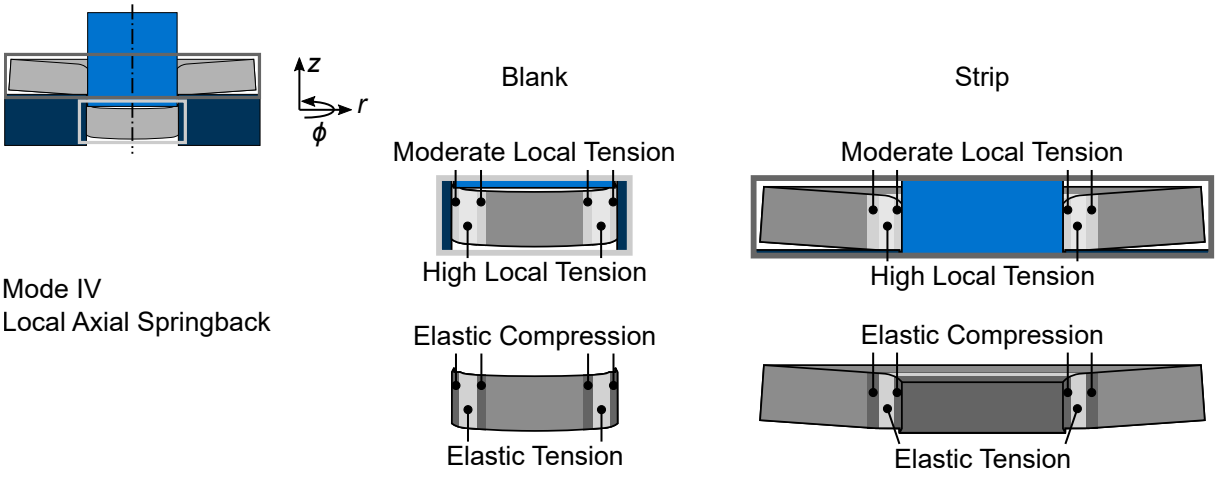

Figure 7.14: Springback mode in axial direction of parts produced by a rotation-symmetric closed cut without the formation of a fracture zone.

springback, it is still subjected to tensile stresses while the surroundings show compressive residual stresses. The rest of the sheet metal can be neglected in this case, as springback can occur freely due to the pure elastic deformation of the non-plastified areas. This mechanism is already happening during the shear cutting operation as the axial shear cutting force is lowering, but at the latest when fracture occurs. During shear cutting, they are still overlayed by frictional stresses. When the parts are removed from the tool the former tensile stresses during the shear cutting process lead to these compressive residual stresses in axial direction on the clean cut of sheet metal strip and blank. Again, tensile stresses inside the specimens are necessary to achieve a static equilibrium. This consideration is supported by the observation that nearly all investigated variants show compressive residual stresses in axial direction on the clean cut (see figure 7.2, 7.3, 7.4, and 7.5). Also, the local maxima of the stress profiles given in figure 7.6 hint that a local phenomenon contributes to the formation of the final residual stress state. Again, the axial stresses can also be expected to affect the tangential residual stress as they are coupled. The proposed springback modes are tested in the following regarding their ability to explain the residual stress state of the differently manufactured specimens.

7.2.2 Cutting Edge Preparation Influence

The cutting edge preparation influence on the part's residual stress state is shown on the example of blanking, as the comparably simple tool technology allows to single out important effects without excessive bending of sheet metal strip and blank. A comparison of the residual stresses on the clean cut for the two different cutting edge conditions is displayed in figure 7.15.

The blank shows higher compressive stresses in axial and tangential direction when it is cut with a sharp punch and a round die edge. The sheet metal strip on the other hand is not very sensitive compared to the blank. Here, the variant cut with a round punch edge and a sharp die shows slightly higher compressive residual stresses. To explain this behavior, the axial and tangential stresses during shear cutting were simulated. The tangential stresses are shown in

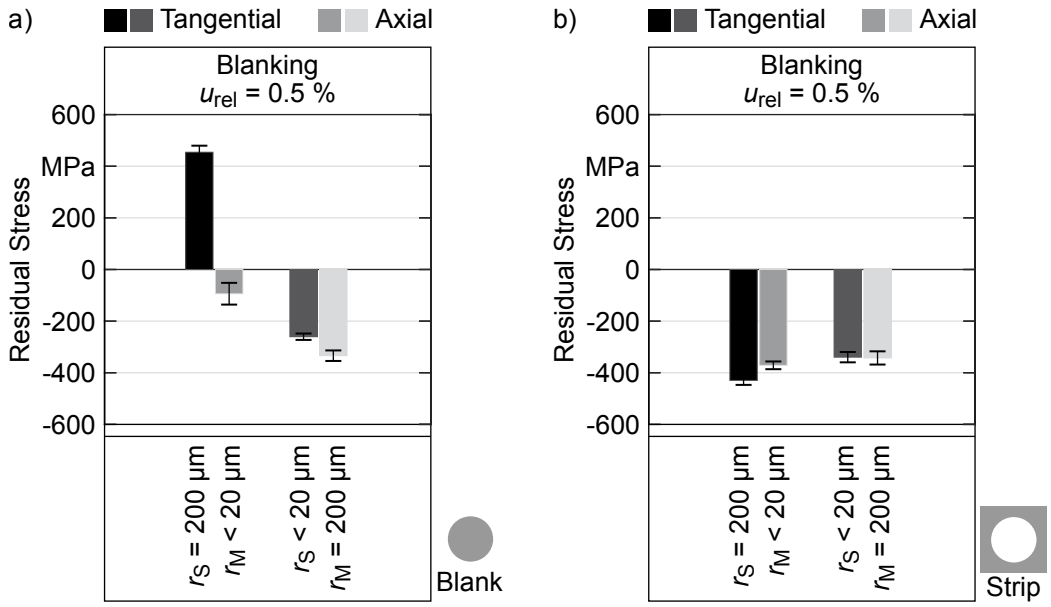

Figure 7.15: Comparison of the surface residual stresses of blank (a) and sheet metal strip (b) manufactured by blanking with two different cutting edge preparations.

figure 7.16.

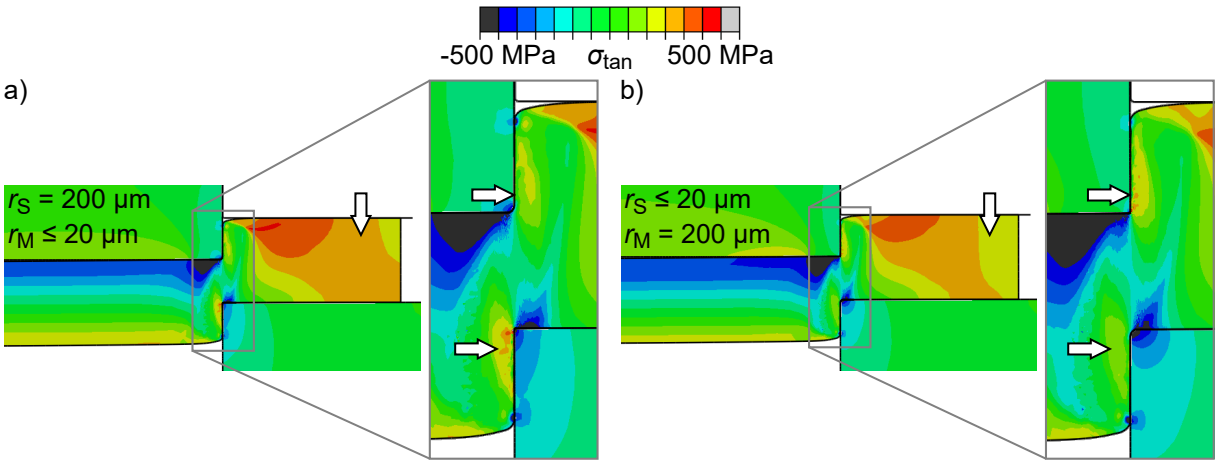

Figure 7.16: Tangential stresses in the sheet metal during blanking with a round punch edge and a sharp die edge (a), and with a sharp punch edge and a round die edge (b) for a die clearance of 0.5 %. Areas of interest are highlighted by arrows.

The first observation that can be made is that the outer rim of the sheet metal strip cut with a round punch edge and a sharp die edge shows higher tensile tangential stresses than the outer rim of the variant cut with a sharp punch edge and a round die edge, which is indicated by small arrows in figure 7.16. This means that a round punch edge pushes material towards the sheet metal strip which stretches the outer rim. After springback, this results in higher compressive residual stresses in tangential direction. Therefore, this corresponds to the global springback mode in radial direction. Moreover, the stresses close to the cutting edges are changed, which is also highlighted by small arrows in figure 7.16. On the clean cut of the sheet metal strip, lower tensile stresses are observed when a round punch edge is used. This means that the local

springback mode also shows lower tensile stresses after springback. In the case of the sheet metal strip, the local and global mechanisms work in the same direction, which means that the sheet metal strip is not as sensitive to process parameter changes. On the blank, this is the other way round. The global mode causes tensile stresses on the clean cut when the blank gets bigger in radial direction after springback. Here, the global stresses are not changed as much by a different cutting edge preparation, as visible in figure 7.16 in the blank. Locally, a round die edge induces compressive strains, especially close to the cutting edge. Also, the tensile stresses in the sheet metal are low compared to the variant with the sharp die edge. This means, that after springback, the variant with the round die edge still shows compressive residual stresses due to the local springback. For the blank cut with a sharp die edge, the global and the local mode favor tensile residual stresses after springback.

Of course this consideration can not only be made for the tangential stresses, but also for the radial stresses. The radial stress distribution is displayed in figure 7.17. Again, a round edge induces compressive stresses while sharp cutting edges causes tensile stresses. This also contributes to the formation of the residual stress state, especially for the compressive residual stresses of the blank cut with a round die edge.

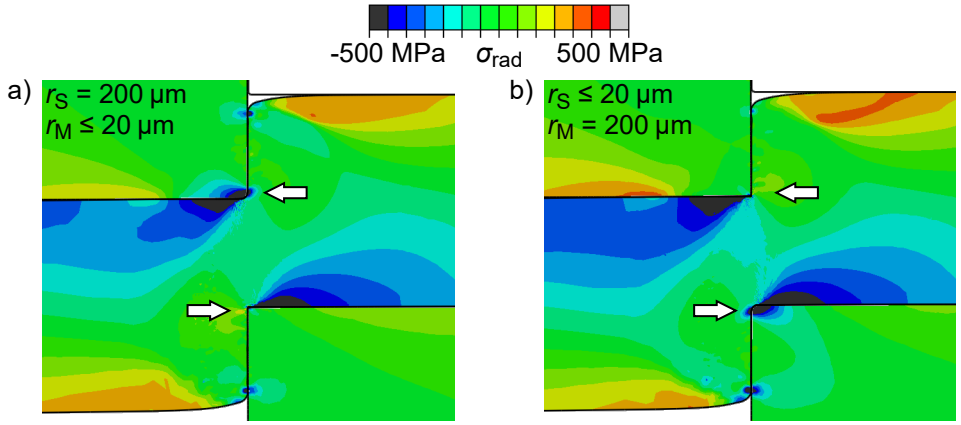

Figure 7.17: Radial stresses in the sheet metal during blanking with a round punch edge and a sharp die edge (a), and with a sharp punch edge and a round die edge (b) for a die clearance of 0.5 %. Areas of interest are highlighted by arrows.

In figure 7.18, the stress situation in axial direction is displayed. For both cutting edge variants, high tensile stresses beneath the surface are calculated. This corresponds to the Hertzian contact model. Also, higher tensile stresses are observed close to a sharp cutting edge. Nevertheless, the gradient is not as high, as there are also comparably high stresses on the sharp cutting edge. On a round cutting edge, this gradient is much bigger. This gradient is necessary for the formation of high compressive stresses, as proposed in the springback model, and leads to the higher compressive stresses measured in the experiments.

The above considerations were only carried out for blanking. A complete overview of the measured residual stresses for a die clearance of 0.5 % is given in figure 7.19 with the focus on the influence of the cutting edge preparation.

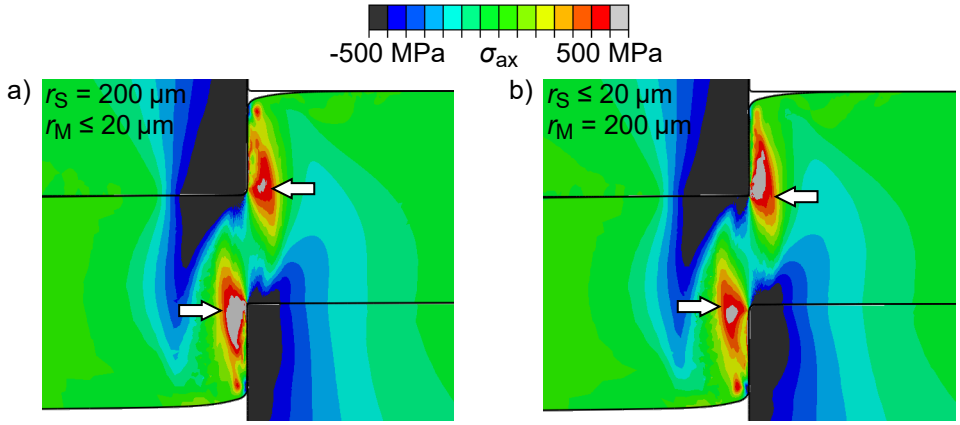

Figure 7.18: Axial stresses in the sheet metal during blanking with a round punch edge and a sharp die edge (a), and with a sharp punch edge and a round die edge (b) for a die clearance of 0.5 %. Areas of interest are highlighted by arrows.

It is visible that the tendencies explained for blanking are also valid for most variants. The residual stress in tangential direction decreases for all manufactured blanks when changing from a round punch and a sharp die edge to a sharp punch and a round die edge. Only for the blanks manufactured by blanking with v-ring, similar residual stresses were measured for both variants.

For the sheet metal strips it is the other way round. Here, a round punch edge and a sharp die edge favor compressive residual stresses. For precision blanking the cutting edge preparation does not affect the tangential residual stresses significantly. For precision blanking without blank holder a round punch edge and a sharp die edge cause tensile residual stresses. It can also be observed that the tangential stresses of the sheet metal strip are not as sensitive to a changed cutting edge preparation compared to the blanks.

In axial direction similar observations can be made. For the manufactured blanks, the variant with the round die edge favors higher compressive residual stresses. Only for fineblanking no significant difference can be observed. As for the tangential residual stresses, the axial residual stresses of the sheet metal strips are not very sensitive to the changed cutting edge preparation for fineblanking and precision blanking. For blanking with v-ring and blanking, the variant with the round punch edge causes higher compressive residual stresses. Again, precision blanking without blank holder stands out, where the sharp punch edge causes higher compressive residual stresses.

This shows that the considerations above are valid for most shear cutting processes. Especially for the blanks the interaction between the global and the local springback mode is shown. Here, the local compression caused by a round die edge causes significant compressive residual stresses, for example for blanking, while a sharp die edge leads to tensile stresses. Here, the global mode dominates in the variant with the sharp die edge while the global mode dominates in the variant with the round die edge. Also, the simulated stress gradient is more significant in the variants with the round die edges which finally leads to higher compressive stresses. The

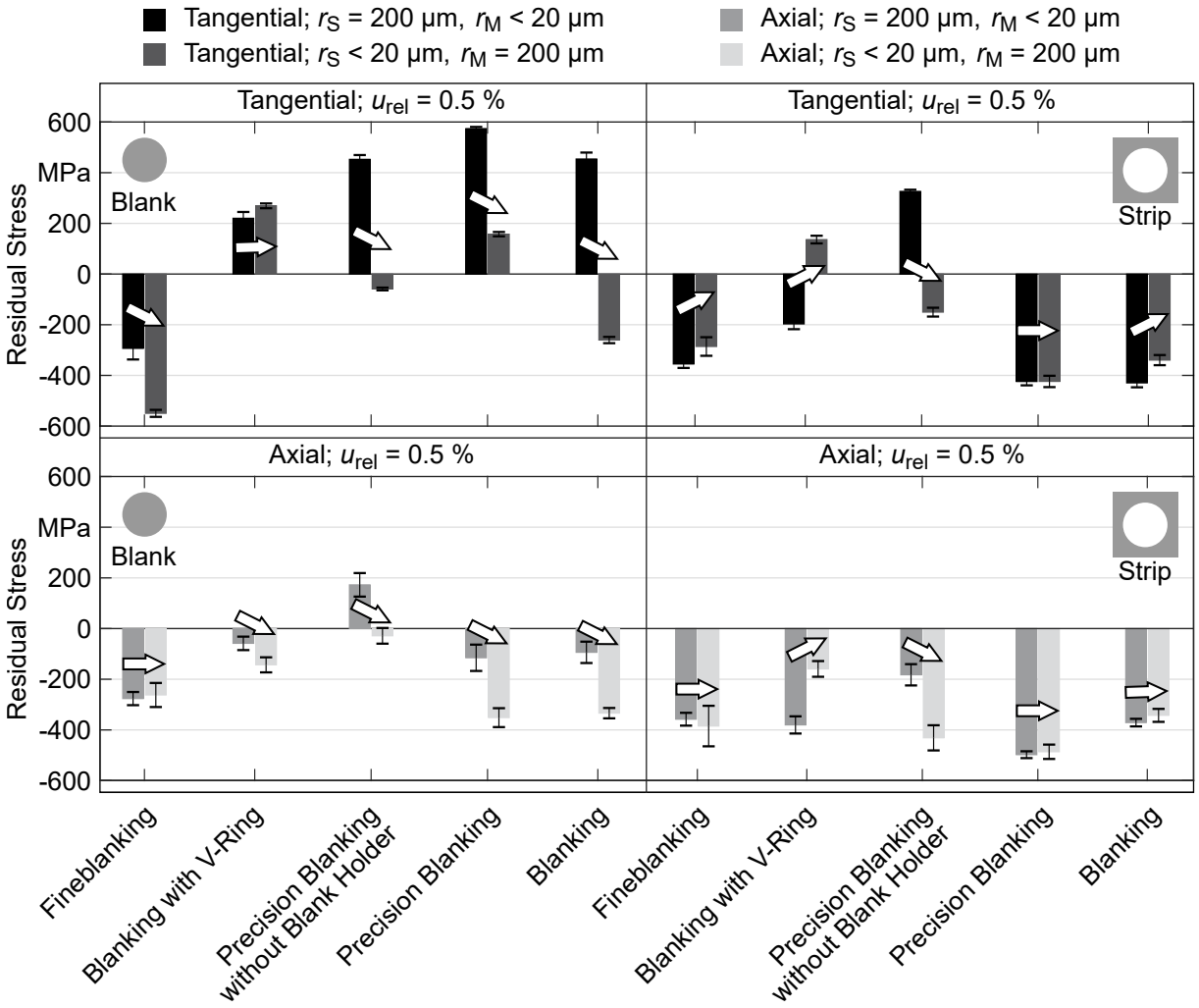

Figure 7.19: Comparison of the residual stresses in axial and tangential direction for the two cutting edge preparations measured in the middle of the sheet metal thickness for a die clearance of 0.5 %. Trends are indicated by arrows.

variants that do not follow these basic considerations, especially precision blanking without blank holder, will be discussed in detail in chapters 7.2.3 to 7.2.5.

7.2.3 Blank Holder Influence

The blank holder influence can be identified by comparing precision blanking to precision blanking without blank holder, as the only difference between these two processes is the missing blank holder in the second variant. It should be kept in mind that the blank produced by precision blanking without blank holder shows a significant fracture zone in the middle of the sheet thickness for $r_S = 200\,\mu m$ and $r_M < 20\,\mu m$. As this fracture affects the material flow, the variants with $r_S < 20\,\mu m$ and $r_M = 200\,\mu m$ are discussed in the following. A comparison of the residual stresses of these two is displayed in figure 7.20.

The blank manufactured by precision blanking without blank holder shows compressive residual stresses close to zero in tangential and axial direction while precision blanking leads to tensile stresses in tangential direction and significant compressive stresses in axial direction.

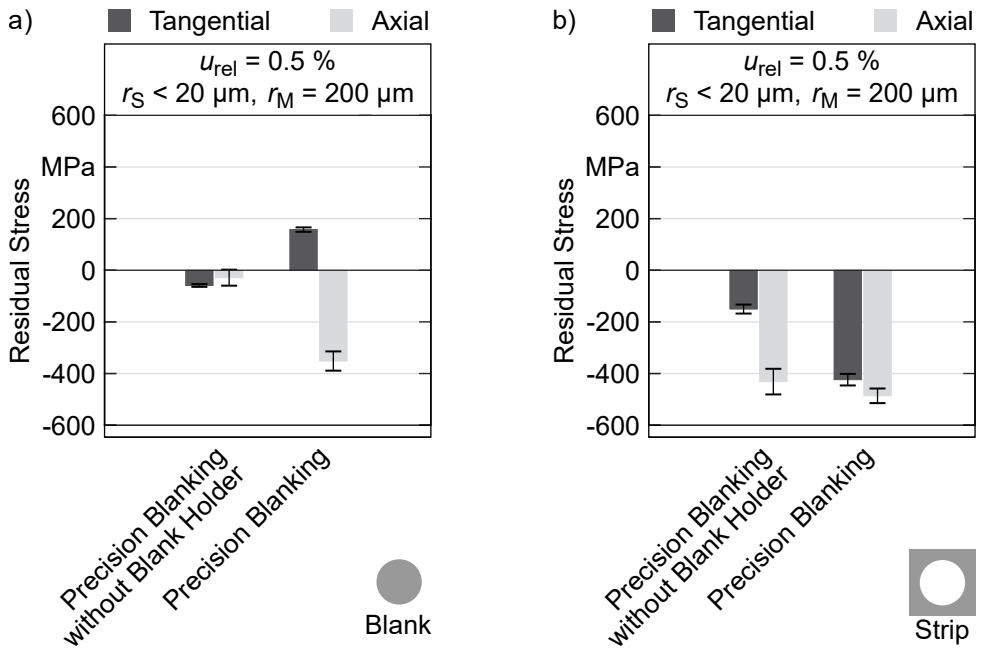

Figure 7.20: Comparison of the surface residual stresses of blank (a) and sheet metal strip (b) manufactured by precision blanking without blank holder and precision blanking for a die clearance of 0.5 %.

Although both processes show a counter punch, the blanks show a completely different residual stress state. This means that the blank holder significantly affects the material flow in the blank. A comparison of the stress situation in tangential direction is given in figure 7.21.

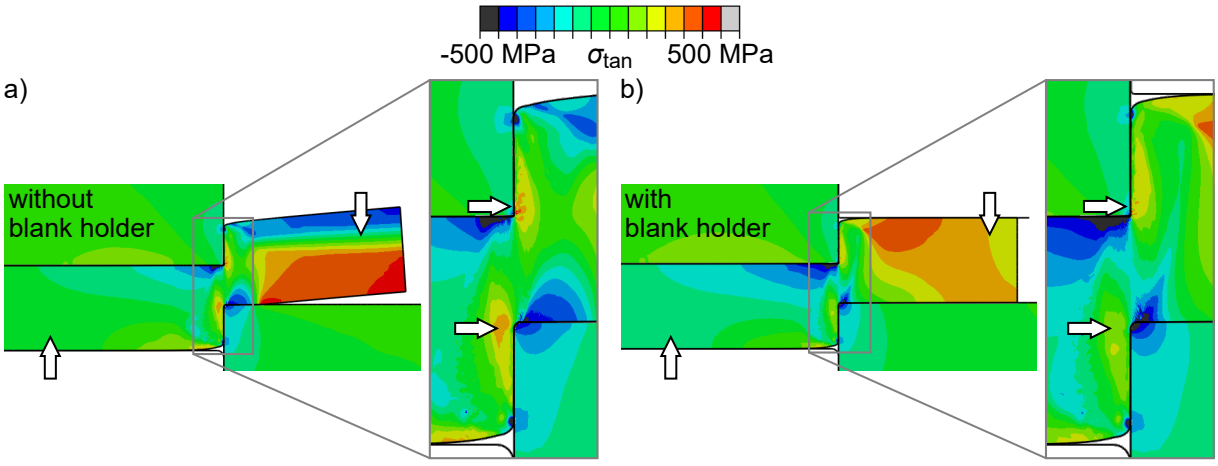

Figure 7.21: Tangential stresses in the sheet metal during precision blanking without blank holder (a) and precision blanking (b) for $r_S \leq 20\,\mu m$, $r_M = 200\,\mu m$, and a die clearance of 0.5 %. Areas of interest are highlighted by arrows.

By looking at the inner side of the blank close to the axis of symmetry, higher compressive stresses can be observed for precision blanking. As stated above, these correspond to the global springback and thus result in tensile stresses after springback. The blank manufactured by precision blanking without blank holder shows a much lower stress in this region. This also means that the missing blank holder favors material flow in the direction of the sheet metal strip. When looking at the local stresses, both variants show higher tensile stresses than the

blanks manufactured with blanking with a round die edge, as shown in figure 7.16 b). Directly at the die edge, both precision blanking without blank holder and precision blanking show comparably low stresses which change to tensile stresses inside the sheet metal. The low local stresses combined with the different stress states deep inside the blank lead to low tangential residual stresses at the surface of the blank produced by precision blanking without blank holder and to tensile surface stresses for precision blanking. At the outer rim of the sheet metal strip, the influence is more obvious. Here, precision blanking without blank holder causes the sheet metal to bend. Globally, this results in a bending springback which causes compressive residual stresses on the burr side and tensile stresses on the die roll side. For precision blanking this bending springback mode can be expected to be much smaller. Locally, the bending also causes higher tensile stresses close to the punch edge. The bending springback combined with these tensile stresses leads to the much lower tangential compressive residual stresses for the sheet metal strip manufactured by precision blanking without blank holder compared to precision blanking. Still, the global radial springback mode works the same way as for blanking which overlays the tensile stresses by compressive stresses.

Now that the sheet metal strip manufactured by precision blanking without blank holder for a sharp punch edge has been discussed, there is still the question of why the variant with round punch edge shows higher compressive tangential residual stresses. For this process, the bending springback mode is much more dominant than for the other shear cutting processes due to the missing blank holder. The clean cut angle can be taken as a measure for the bending springback, as a higher part bending also causes the clean cut to deviate from 90 °. Here, the sheet metal strip produced with a round punch edge shows a deviation of 6.95 ° while the variant with the sharp punch edge shows a deviation of 4.65 °. Thus, higher tensile stresses from the bending springback can be expected for the variant with the round punch edge. The early fracture of the blank for this variant alters the stress state which contributes to this behavior.

Regarding the axial residual stresses, the blanks are more sensitive to the missing blank holder than the sheet metal strips. The blanks produced by without a blank holder show small compressive residual stresses compared to the high compressive stresses of precision blanking. To investigate this, the axial stresses are displayed for these variants in figure 7.22.

Due to the missing blank holder, the blank produced by precision blanking without blank holder shows high tensile stresses at the die edge without a significant gradient. These stresses are much lower close to the die edge for precision blanking. Due to these different gradients, the blank produced by precision blanking shows a significant compressive axial residual stress compared to the low stress of precision blanking without blank holder. On the punch edge, both variants show similar gradients, only the shape of the stress field is slightly altered. Accordingly, similar axial residual stresses are measured here.

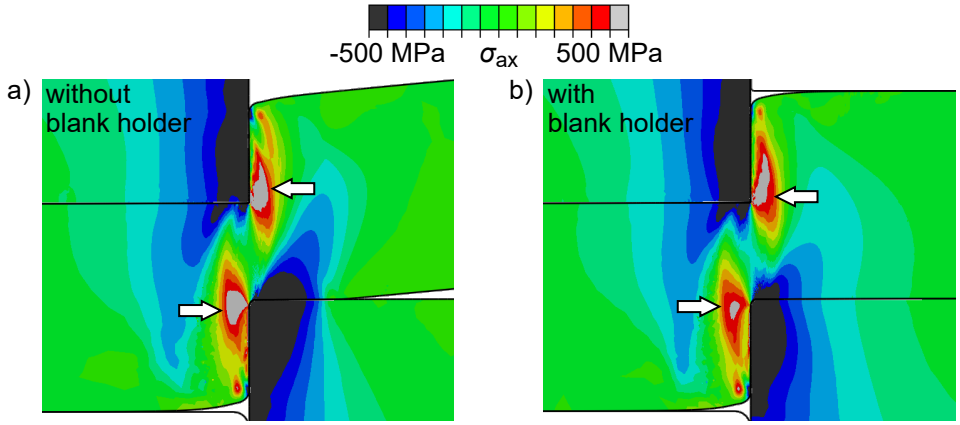

Figure 7.22: Axial stresses in the sheet metal during precision blanking without blank holder (a) and precision blanking (b) for $r_S \leq 20\,\mu m$, $r_M = 200\,\mu m$, and a die clearance of 0.5 %. Areas of interest are highlighted by arrows..

7.2.4 V-Ring Influence

For the discussion of the influence of the v-ring two shear cutting process variants are available: fineblanking and blanking with v-ring. Blanking with v-ring differs from blanking only by the use of a v-ring as does fineblanking from precision blanking. The second combination will be discussed first. A comparison is displayed in figure 7.23.

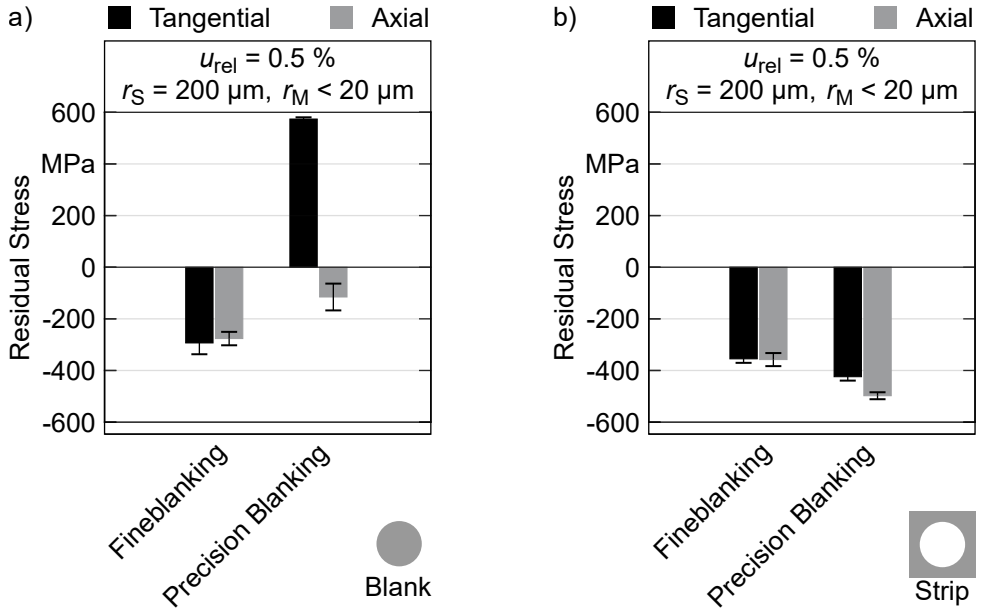

Figure 7.23: Comparison of the surface residual stresses of blank (a) and sheet metal strip (b) manufactured by fineblanking and precision blanking.

Especially for the blank, the v-ring has a significant influence. While the fineblanked blank shows high compressive stresses in tangential and axial direction, the blank manufactured by precision blanking shows high tensile stresses in tangential direction and small compressive stresses in axial direction. The sheet metal strips are not nearly as sensitive to the v-ring. Both fineblanking and precision blanking produce strips with high compressive residual stresses in tangential as well as in axial direction, although they are slightly higher for precision blanking in

both directions. To understand this behavior, the stress field in tangential direction is displayed in figure 7.24.

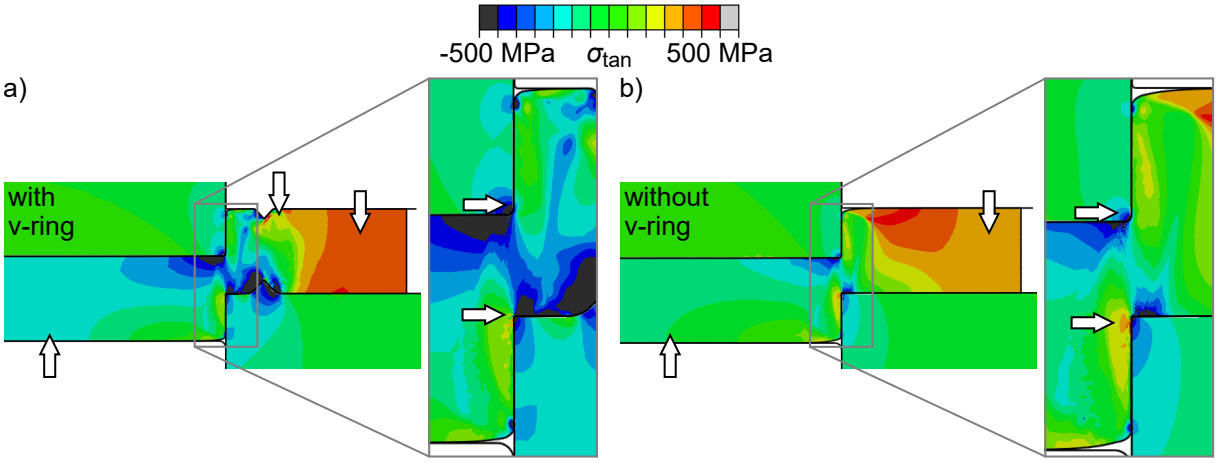

Figure 7.24: Tangential stresses in the sheet metal during fineblanking (a) and precision blanking (b) for $r_S = 200\,\mu m$, $r_M \leq 20\,\mu m$, and a die clearance of 0.5 %. Areas of interest are highlighted by arrows..

The first observation is that the v-ring causes high compressive stresses in the shearing zone and high tensile stresses on the outer rim of the sheet metal strip. Although the v-ring is located millimeters away from the blank, it causes compressive stresses even close at the axis of symmetry. This favors tensile stresses due to the global springback mode in radial direction. Nevertheless, the high compressive stresses in the shearing zone also reach around the sharp die edge. Tensile stresses are first observed at the die's lateral surface. Below the sheet metal surface only small tensile stresses can be observed despite the sharp die edge. When cutting without a v-ring, this region is subjected to high tensile strains. Thus, high compressive residual stresses can be expected from the global mode when cutting with a v-ring while the variant without a v-ring favors tensile surface stresses.

On the outer rim of the sheet metal strip, the v-ring causes high tensile stresses that change to stresses close to zero near the v-ring. Between v-ring and punch additional compressive stresses are caused. As the stresses on the outer rim are also high for precision blanking, similar tangential residual stresses are measured for both variants.

The v-ring does not only cause high compressive stresses in tangential, but also in radial direction, which is displayed in figure 7.25. Again, the biggest difference between the variant with and without a v-ring is visible in the shearing zone between the cutting edges. Here, the v-ring also induces high compressive stresses. Close to the cutting edges, similar observations as for the tangential stresses can be made. While the compressive stresses reach around the sharp die edge for fineblanking, they quickly change to tensile stresses for precision blanking. For both process variants the punch causes high compression stresses around the punch edge, which is also increased by the v-ring. Only on the outer rim of the sheet metal strip the effect of the v-ring is comparably small.

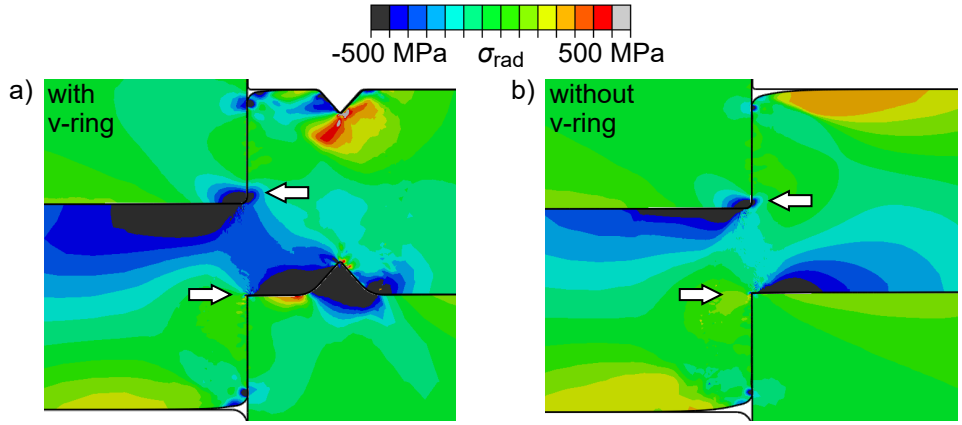

Figure 7.25: Radial stresses in the sheet metal during fineblanking (a) and precision blanking (b) for $r_S = 200\,\mu m$, $r_M \leq 20\,\mu m$, and a die clearance of 0.5 %. Areas of interest are highlighted by arrows.

As shown in figure 7.23, fineblanking produces high compressive residual stresses in axial direction on the blank while these are smaller for precision blanking. On the sheet metal strip it is the other way round: Here, precision blanking shows higher compressive residual stresses. The corresponding axial stress situation is displayed in figure 7.26. Again, fineblanking shows much higher compressive stresses in the shearing zone. In the blank, the variant with v-ring shows high tensile stresses with a high gradient towards the die edge. Without a v-ring, higher tensile stresses are observed which do not show such a high gradient. Thus, the axial springback causes higher compressive residual stresses in axial direction for the blank produced by fineblanking. In the sheet metal strip, much lower tensile stresses are observed for the variant with a v-ring. It should be kept in mind that the v-ring force is 250 kN higher than the blank holder force. Thus, the material is more compressed in axial direction just by the different process parameters. Still, fineblanking shows a distinct gradient with a lower maximum. The area subject to the high tensile stresses for precision blanking is bigger and shows higher tensile stresses while also showing a significant gradient. In combination, this leads to slightly higher axial compressive residual stresses after springback for the variant without a v-ring.

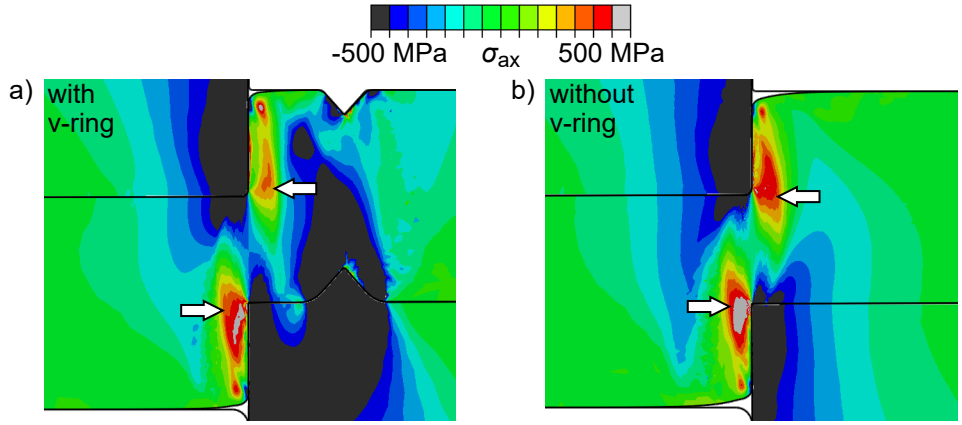

Figure 7.26: Axial stresses in the sheet metal during precision fineblanking (a) and precision blanking (b) for $r_S = 200\,\mu m$, $r_M \leq 20\,\mu m$, and a die clearance of 0.5 %. Areas of interest are highlighted by arrows..

The same tendencies can be observed when comparing the other variant combination with and without a v-ring. This comparison of blanking with v-ring and blanking is shown in figure 7.27. The tangential residual stress of the blank also changes to higher tensile stresses when no v-ring is used. On the sheet metal strip a v-ring causes lower compressive residual stresses. These are the same observations as for fineblanking and precision blanking. Regarding the axial stresses only small differences can be observed between blanking with v-ring and blanking. This leads to the conclusion that the v-ring does not significantly affect the axial residual stresses when no counter punch is used. The influence of the counter punch will be discussed in the following.

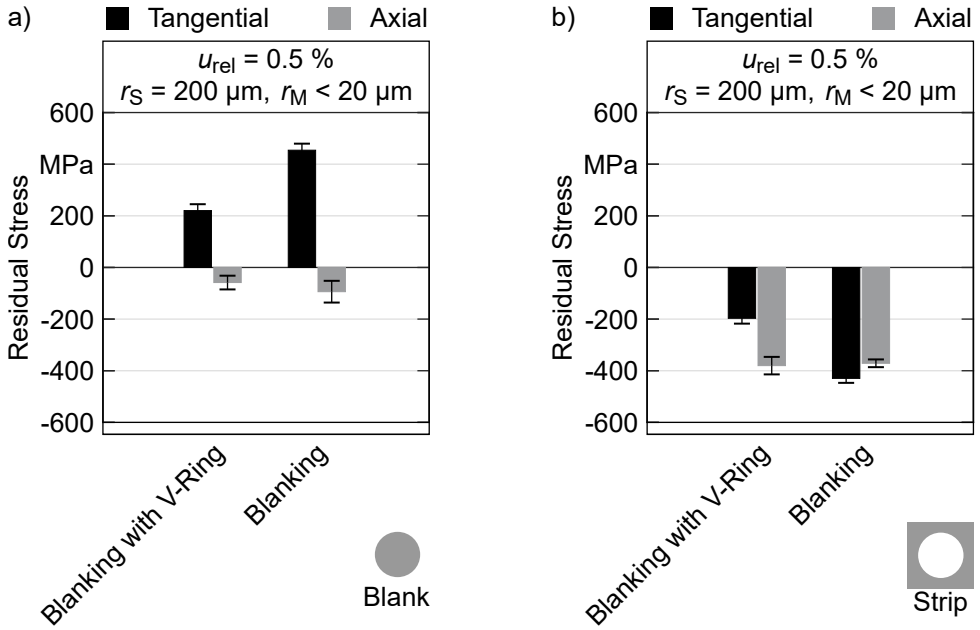

Figure 7.27: Comparison of the surface residual stresses of blank (a) and sheet metal strip (b) manufactured by blanking with v-ring and blanking.

7.2.5 Counter Punch Influence

To identify the influence of the counter punch, two variant combinations are available: fineblanking and blanking with v-ring, and precision blanking and blanking. A comparison of the measured surface residual stresses of the specimens manufactured by fineblanking and blanking with v-ring for the variant with the rounded die edge is shown in figure 7.28. The configuration with a sharp die edge shows similar tendencies, except for the axial residual stresses of the sheet metal strips, where no significant influence can be observed between the two processes.

Here, a clear tendency can be observed. Both in tangential and in axial direction the variant with a counter punch, i.e., fineblanking, shows higher compressive stresses. In tangential direction, tensile stresses are measured when no counter punch is used, i.e., for blanking with v-ring. To explain this behavior, the stress situation during the shear cutting is displayed in figure 7.29

Only small differences can be observed in the sheet metal strips close to the cutting edges. Between the punch edge and the v-ring on the other hand, fineblanking shows high compressive

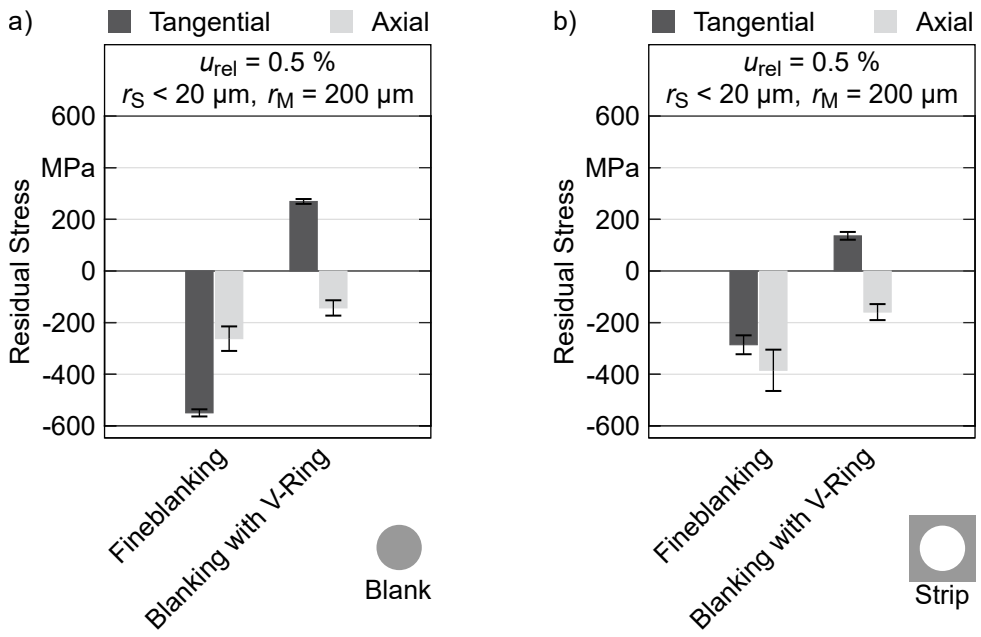

Figure 7.28: Comparison of the surface residual stresses of blank (a) and sheet metal strip (b) manufactured by fineblanking and blanking with v-ring.

tangential stresses while these are much smaller in the variant manufactured by blanking with v-ring. Thus, the local springback mode can be expected to result in much higher compressive residual stresses in the sheet metal strip manufactured by fineblanking. Accompanying, higher stresses can be observed on the outer rim of the fineblanked sheet metal strip, which favor compressive residual stresses caused by the global springback mode.

The significantly different stress situation can be explained by the use of a v-ring. The v-ring hinders material flow in the direction of the sheet metal strip. This causes the material to flow in the die channel when no counter punch is used. The high bending of the blanks manufactured by blanking with v-ring is a result of this additional material flow. This bending is visible by looking at the clean cut angle of the these blanks, which show the highest deviation from 90 ° of all investigated blanks (also see figure 6.9). In the simulated tangential stresses, this results in an inhomogeneous stress state close to the axis of symmetry. As the stresses are not significantly different close to the die edge, bending springback is most likely dominant for the blanks manufactured by blanking with v-ring. This springback mode finally results in the high tensile residual stresses in tangential direction.

By considering the blank bending, another effect can be explained. Blanking with v-ring produces blanks with tensile residual stresses in tangential direction for both cutting edge preparations. It is also the only variant where cutting with a round die edge results in slightly higher tensile residual stresses. This can be attributed to the higher bending of the blank which is again visible in the clean cut angle. The blank produced with a sharp die edge shows a deviation of 1.67 ° from 90 °, while a round die edge shows a deviation of 1.85 °. Thus, higher tensile stresses from bending springback can be expected.

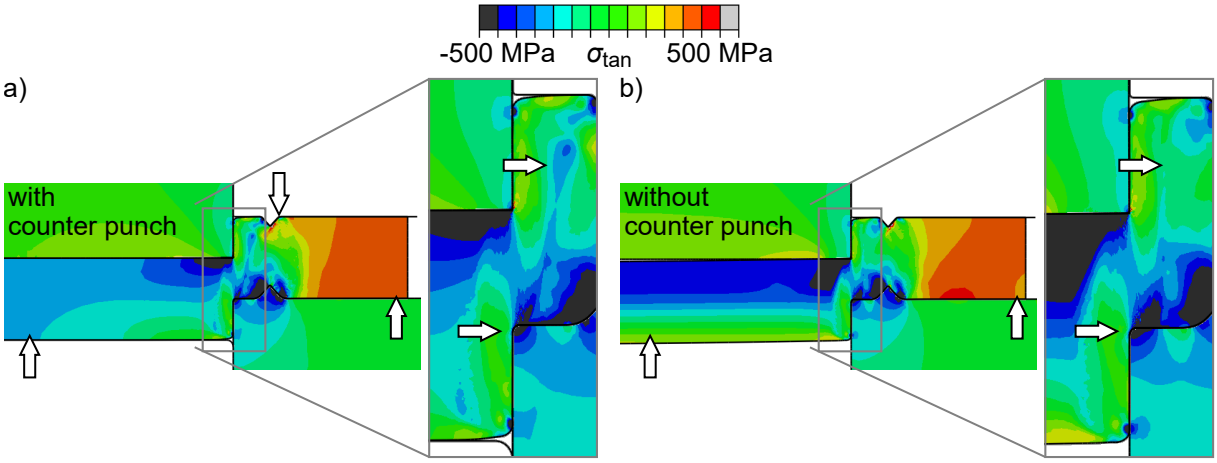

Figure 7.29: Tangential stresses in the sheet metal during fineblanking (a) and blanking with v-ring (b) for $r_S \leq 20\,\mu m$, $r_M = 200\,\mu m$, and a die clearance of 0.5 %. Areas of interest are highlighted by arrows.

The parts manufactured by blanking with v-ring also show smaller compressive residual stresses in axial direction than the fineblanked ones. A comparison of the stress situation during the shear cutting operation is displayed in figure 7.30.

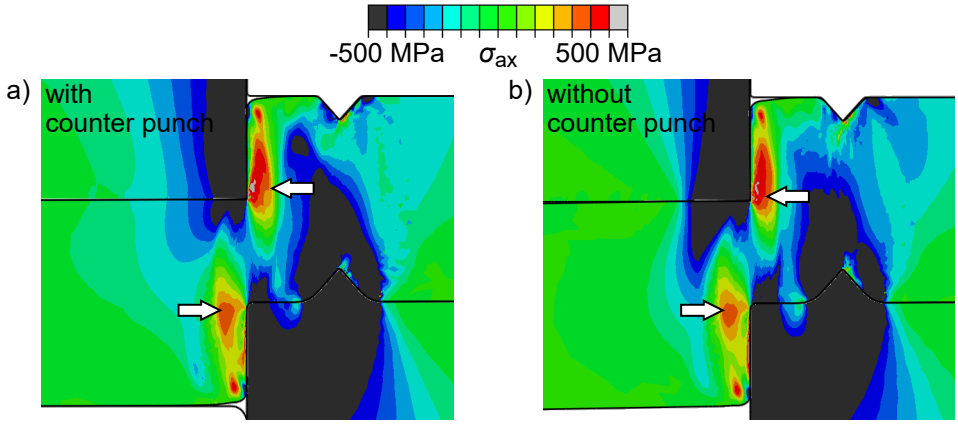

Figure 7.30: Axial stresses in the sheet metal during fineblanking (a) and blanking with v-ring (b) for $r_S \leq 20\,\mu m$, $r_M = 200\,\mu m$, and a die clearance of 0.5 %. Areas of interest are highlighted by arrows..

Only small differences are visible. The variant with a counter punch shows a slightly higher gradient close to the cutting edges. Again, a significantly different stress state can be observed in the sheet metal strip close to the v-ring, where the variant with the counter punch shows higher extended compressive stresses. The combination of the higher gradient close to the cutting edge and farther in the sheet metal are most likely responsible for the higher axial compressive residual stresses of the fineblanked part.

In axial direction, the same observation can be made for the comparison of precision blanking and blanking, the other process combination where the only difference is the utilization of a counter punch. This comparison is illustrated in figure 7.31. For both the blank and the strip, lower axial compressive residual stresses are observed when no counter punch is used.

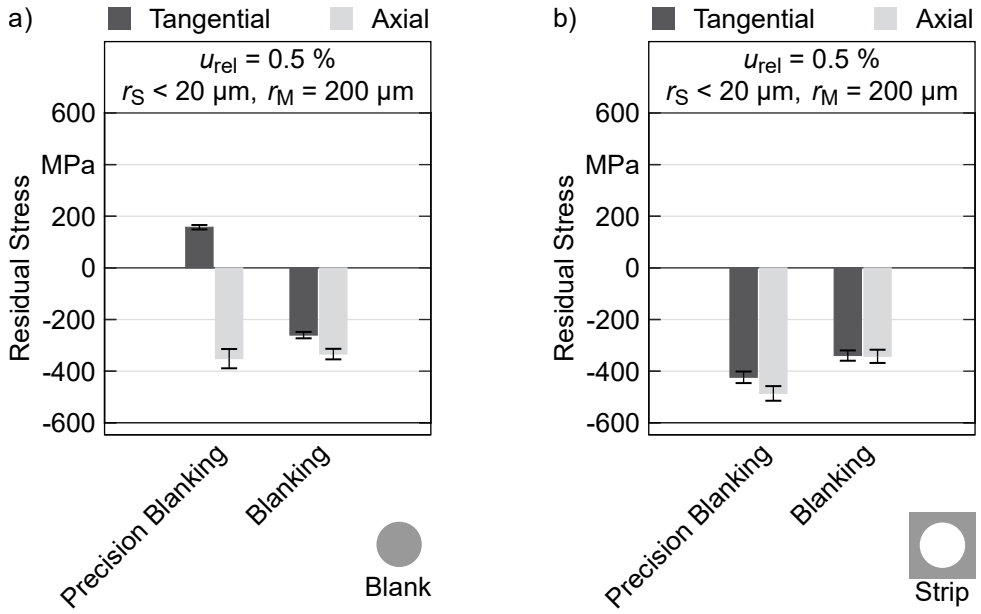

Figure 7.31: Comparison of the surface residual stresses of blank (a) and sheet metal strip (b) manufactured by precision blanking and blanking.

In tangential direction, a completely different behavior is observed for the blanks manufactured by precision blanking and blanking compared to fineblanking and blanking with v-ring. The use of a counter punch causes tensile residual stresses in the blanks manufactured by precision blanking. Due to the counter punch material flow in the die channel, i.e., towards the blank, is restricted. Additionally, precision blanking does not show a v-ring. This combination causes the material to flow towards the sheet metal strip as the flow towards the die channel is hindered by the counter punch. This causes the high tangential compressive stresses measured in the sheet metal strip, but is also responsible for the high tensile residual stresses of the blank.

7.2.6 Die Clearance Influence

The surface residual stresses for a changed die clearance, investigated for blanking and fineblanking, do not follow a strict trend as they are also affected by the different cutting edge preparations and the formation of a fracture zone. As visible in figures 7.3 and 7.5, the fracture zone shows significant tensile stresses. The variants manufactured with a die clearance of 3 % show a fracture zone so big that it is reaching the measurement position. Consequently, they are not further addressed as fracture is the dominant phenomenon for the formation of the residual stress state. The focus is on the highly relevant variants, i.e., the blanks manufactured with a sharp punch and a round die edge and the strips manufactured with a round punch edge and a sharp die edge. A comparison of these is displayed in figures 7.32 and 7.36. For the blanks manufactured by fineblanking, the bigger die clearance causes lower tangential residual stresses and higher axial residual stresses. For blanking, both residual stresses get bigger when the bigger die clearance is chosen. By looking at figure 7.10, the size deviation indicates that the local spring back mode is responsible for the lower tangential stress of the blanks manufactured by

fineblanking while the global mode causes the higher residual stresses in tangential direction for the blanks manufactured by blanking.

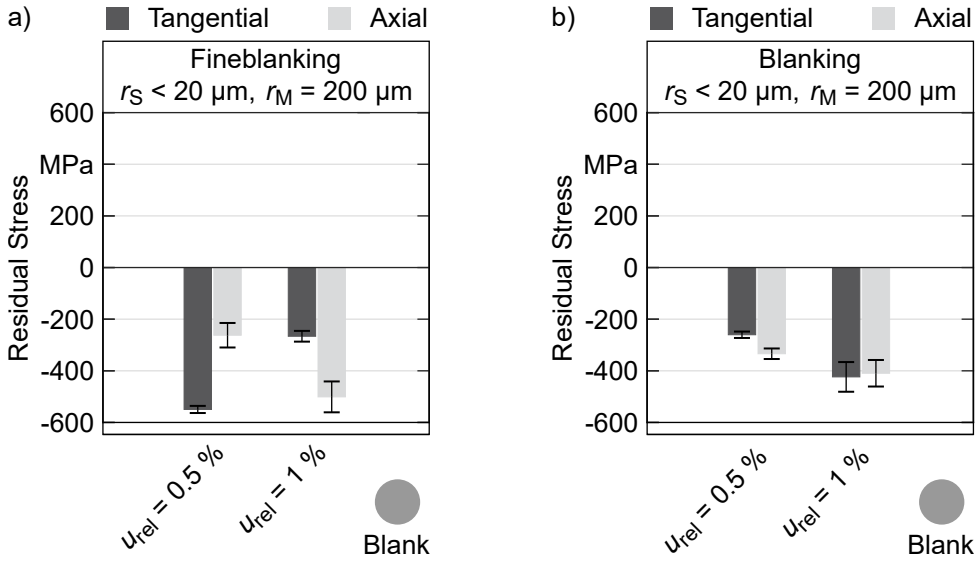

Figure 7.32: Comparison of the surface residual stresses of blanks manufactured by fineblanking (a) and by blanking (b) with a die clearance of 0.5 % and 1 %.

The stress fields obtained by the simulations for fineblanking are displayed in figure 7.33. Higher compressive stresses can be observed deep inside the blank and close to the die edge for the variant with a die clearance of 0.5 %. Again, this shows that the local springback mode is much more dominant for the blank, as the stress deep inside the blank would indicate higher compressive residual stresses in tangential direction for the blank manufactured with a die clearance of 0.5 %.

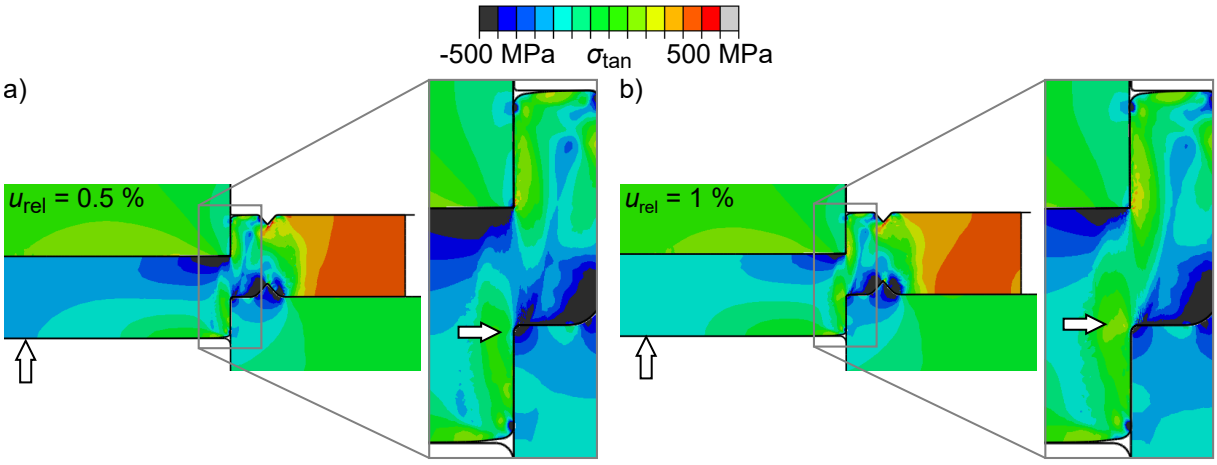

Figure 7.33: Tangential stresses in the sheet metal during fineblanking with a die clearance of 0.5 % (a) and 1 % (b) for $r_S \leq 20\,\mu m$ and $r_M = 200\,\mu m$. Areas of interest are highlighted by arrows.

The stress situation for blanking is shown in figure 7.34. Again, the variant with the die clearance of 0.5 % induces slightly higher pressure close to the die edge. However, directly at the edge the difference is comparably small. Deep inside the blank, the small die clearance causes

higher bending stresses, which finally lead to a higher part bending (see figure 6.9). As the stresses causing the local and the global springback mode are comparable, it can be assumed that this higher bending is responsible for the lower tangential residual stress of the variant manufactured with a die clearance of 0.5 %. Furthermore, higher bending at otherwise comparable stresses would be measured as a bigger blank diameter. This would be interpreted as a global springback mode when only the size deviation is considered.

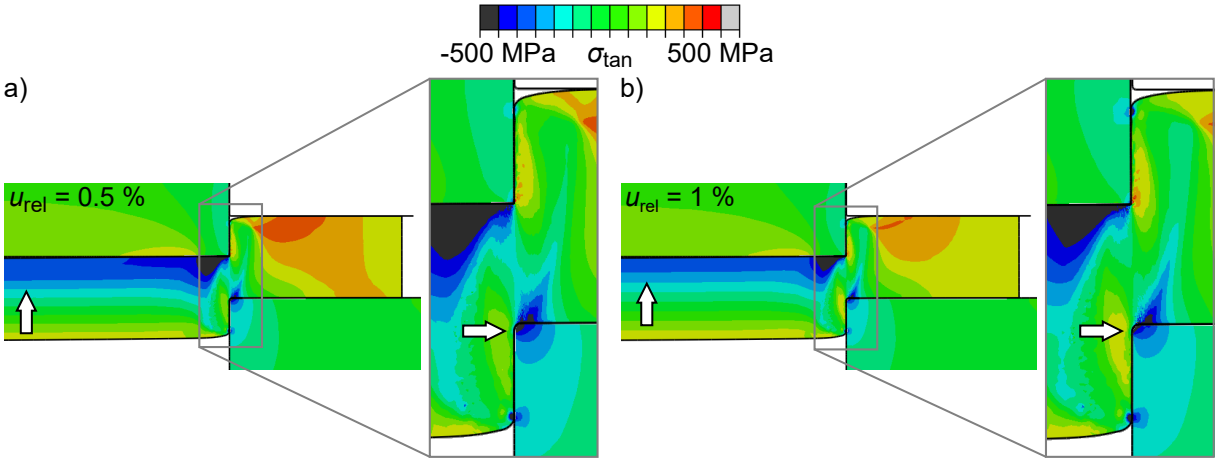

Figure 7.34: Tangential stresses in the sheet metal during blanking with a die clearance of 0.5 % (a) and 1 % (b) for $r_S \leq 20\,\mu m$ and $r_M = 200\,\mu m$. Areas of interest are highlighted by arrows.

In axial direction both the blanks manufactured by fineblanking and by blanking show higher compressive residual stresses in axial direction when the bigger die clearance is chosen. The corresponding stress fields for blanking are displayed in figure 7.35.

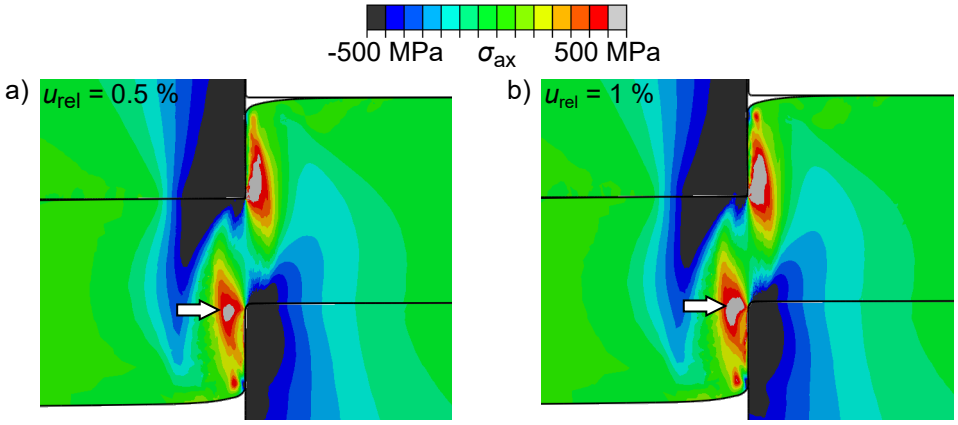

Figure 7.35: Axial stresses in the sheet metal during blanking with a die clearance of 0.5 % (a) and 1 % (b) for $r_S \leq 20\,\mu m$ and $r_M = 200\,\mu m$. Areas of interest are highlighted by arrows.

Both variants show significant tensile stresses close to the die edge. Nevertheless, the gradient is much higher when a die clearance of 1 % is used, which causes the higher compressive residual stresses in axial direction. A similar effect can be expected for the blanks manufactured by fineblanking.

In comparison to the blanks, the sheet metal strips show an opposite behavior regarding the influence of the die clearance on the tangential residual stresses. This is displayed in figure 7.36. For fineblanking, a bigger die clearance causes slightly higher compressive stresses and for blanking slightly lower stresses. The fineblanked holes correspond to the combined global and local mode regarding their size deviation (see figure 7.9). The blanked strips do not follow this behavior, but correspond very well with the bending springback (see figure 7.12).

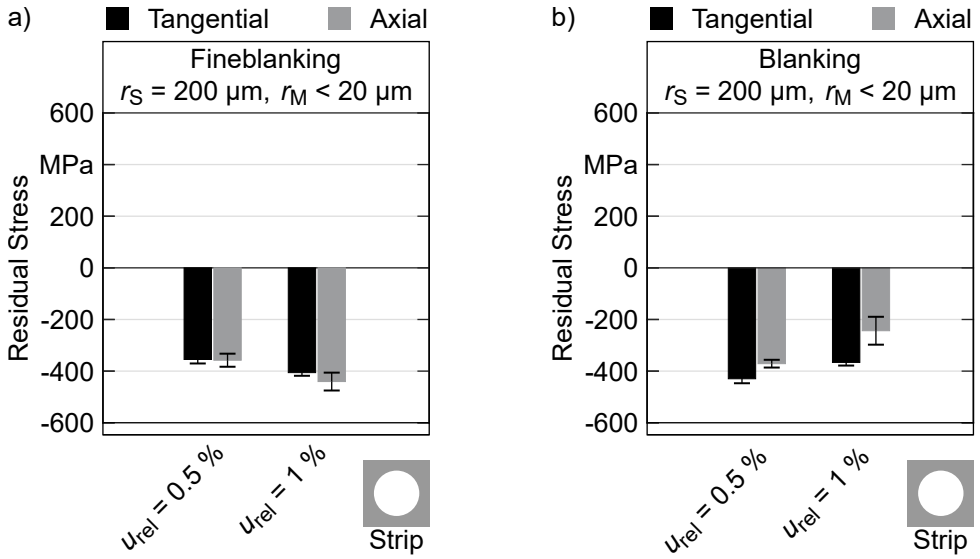

Figure 7.36: Comparison of the surface residual stresses of sheet metal strips manufactured by fineblanking (a) and by blanking (b) with a die clearance of 0.5 % and 1 %.

As the changes caused by the die clearance are so small and the correlation fits very well, no additional finite-element simulations are given.

In axial direction, only minor changes of the residual stresses are observed for fineblanking when a different die clearance is chosen[20]. For blanking on the other hand, slightly lower compressive stresses are measured. To investigate this, the stress field for blanking is given in figure 7.37.

Surprisingly, almost the same behavior residual stress behavior as for the blanks can be observed. This also means that the difference can not be fully explained by the axial springback mode, as the gradient close to the punch edge is much higher for the variant with the bigger die clearance of 1 %. Thus, other effects like the coupling of the elastic behavior in axial and tangential direction caused by the part bending seem to be responsible.

7.3 Conclusion

Not only are significant residual stresses induced by shear cutting, but they can also be adjusted to custom needs by choosing a suitable Near-Net-Shape Blanking process with suitable process

[20]This is not only observed for the variants cut with $r_S = 200\,\mu m$ and $r_M < 20\,\mu m$ but also for those with $r_S < 20\,\mu m$ and $r_M = 200\,\mu m$

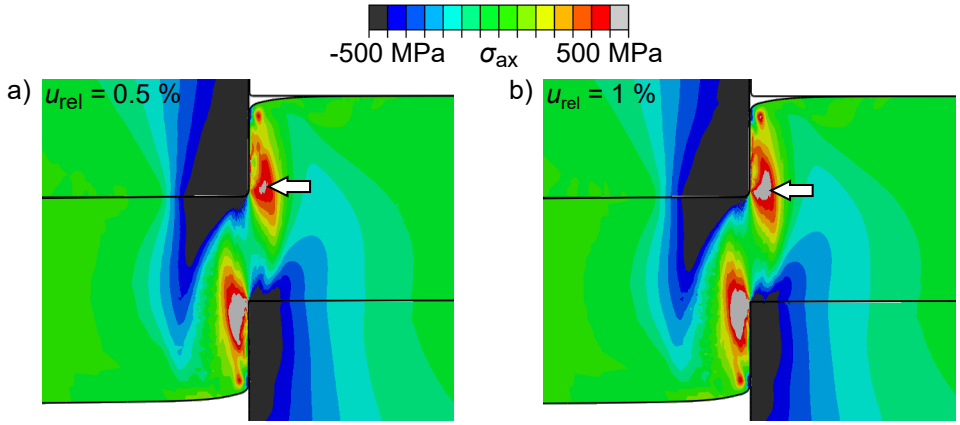

Figure 7.37: Axial stresses in the sheet metal during blanking with a die clearance of 0.5 % (a) and 1 % (b) for $r_S = 200\,\mu m$ and $r_M \leq 20\,\mu m$. Areas of interest are highlighted by arrows.

parameters. Here, blanks are much more sensitive to a changed tool setup or a change in process parameters.

A round cutting edge on the punch favors compressive stresses of manufactured holes while a round die edge has the same effect for blanks. In most cases, the residual stress state of the blanks is very sensitive to a changed cutting edge geometry while the changes are much smaller for the sheet metal strip. This can be attributed to the global and local springback modes in radial direction. For the blank the global and local mode counteract while they both favor compressive stresses for the sheet metal strip.

A blank holder should be used. Without blank holder the stress situation is significantly changed which can lead to the formation of a fracture zone. This can cause tensile residual stresses on both blank and sheet metal strip. As the bending leads to additional tensile residual stresses on the die roll side of the sheet metal strip, it is not reasonable to cut a hole without a blank holder.

When holes are manufactured, the use of a v-ring causes slightly smaller compressive residual stresses. For blanks on the other hand, it causes high compressive stresses as long as a counter punch is used. When no counter punch is used, the additional material flow towards the die channel caused by the v-ring leads to significant bending of the blank, which causes high tensile residual stresses.

This changed material flow caused by the counter punch also affects the residual stress state of the manufactured hole. When no counter punch is used, material is pushed towards the die channel, i.e., it is pulled from the sheet metal strip. This causes tensile residual stresses especially in tangential direction. This behavior may benefit the residual stress state of the blank but, again, can cause a significant part bending. Another way to control and use the effect of the part bending could be the use of a convex or concave counter punch together with a corresponding punch in order to form a desired bending of the whole part.

For holes manufactured by the precision shear cutting processes, the die clearance has a com-

parably small influence as long as no fracture zone reaches close to the measurement position. A fracture zone shows significant tensile stresses. However, this influence is much stronger for blanks.

The influence of the chosen process variant and its process parameters can be explained by their influence on the stress state during the shear cutting operation. Depending on this stress state, four basic springback modes lead to the development of the final residual stress state. These springback modes are the global and local springback in tangential/radial direction, bending springback and axial springback. The results presented above are summed up in table 7.1.

Table 7.1: Summary of the factors influencing the surface residual stresses together with their relevant effects.

	Relevant Effect			**Residual Stress**	
	Global	Local	Bending	σ_{tan}	σ_{ax}
Blank					
Use of a					
rounded die edge	++	+++	+	↘	↘
blank holder	++	++	+	↗	↘
v-ring	+++	+++	++	↘	→
counter punch[21]	++	+	+++	↘	↘
smaller die clearance	++	+++	+	-	-
Strip					
Use of a					
rounded die edge	++	+++	++	↘	→
blank holder	+	+	+++	↘	→
v-ring	+++	+++	+	↗	→
counter punch	++	+++	+	↘	↘
smaller die clearance	++	+++	+	-	-

[20] in combination with a v-ring Relevancy: + small ++ medium +++ high

The dimensional accuracy and the residual stress state strongly correlate. The smaller the manufactured hole compared to the used punch, the higher are the compressive residual stresses. For blanks, it is the other way around. A bigger blank size compared to the used die diameter causes higher compressive residual stresses. Not only the size of the manufactured part but also its bending is correlated to the residual stress state.

The proposed explanation model is able to explain the formation of final part's residual stress state, especially for a die clearance of 0.5 %. Thus, a detailed look at the stress situation during the shear cutting process allows drawing conclusions on the formation of the stress state after the process.

8 Fatigue Behavior of Parts Manufactured by Precision Shear Cutting

In this chapter, the fatigue strength of C-profiles is investigated with a special focus on the influence of the residual stress state. As given in chapter 2.3.1, the residual stress state is only one of many factors affecting the fatigue strength of a shear-cut edge. Thus, the part geometry is investigated more detailed than in the last chapter by giving the bending and the surface roughness of the manufactured specimens. Additionally, the stress situation in the fatigue testing rig is investigated. This is used to interpret the fatigue testing results regarding the different influencing factors. Finally, conclusions are drawn regarding the significance of residual stresses and the other influencing factors on the fatigue strength. A more phenomenological look is given on manufactured parts compared to the fundamental research in the last chapter. This means that global tendencies are analyzed and not each process variant and process parameter configuration are discussed in detail.

8.1 Fatigue Testing

8.1.1 Fatigue Testing Procedure

All fatigue experiments were performed at the FZG on the servo-hydraulic fatigue testing system. A tensile load with $R_S = 0$ and a sine form was chosen. Therefore, the upper load S_o or the upper force is used in the following. Two upper load levels of 16 and 19 kN were used for testing in the finite life fatigue region. The specimens were clamped with an offset to the applied force to induce a bending torque as illustrated in figure 8.1. A frequency of 50 Hz was set. A failure probability of 50 % calculated with equation 2.18, i.e., $N_{50\,\%}$, is shown in all diagrams. The k-factor is evaluated with equation 2.19.

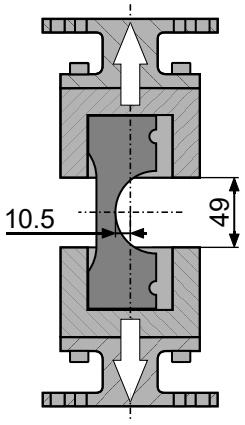

Figure 8.1: Fatigue testing setup as published in Stahl, D. Müller, Tobie, et al., 2019.

8.1.2 Numerical Analysis of the Fatigue Testing Procedure

The stress situation in the fatigue testing setup was investigated in Abaqus 2018 as well. The model is shown in figure 8.2. The symmetry of specimen and clamping on the x-y plane is used to reduce the computational effort. The rough surface of the clamping jaws is modeled with a

high friction coefficient of 0.3. All degrees of freedom are fixed for the right clamp except the translation in z direction. The left clamp is allowed to move in y and z direction. The rotational degree of freedom of both clamps around the y-axis is locked due to the high stiffness of the testing rig.

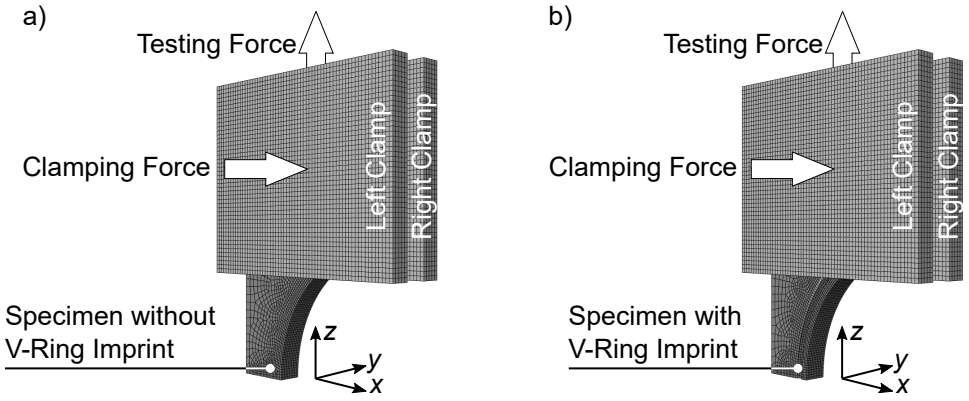

Figure 8.2: Model setup for investigating the stress situation in the fatigue testing system for an ideal specimen without v-ring imprint (a), and with v-ring imprint (b).

At first, the left clamp is subjected to a clamping force of 190 kN, which corresponds to the clamping force induced by a screw in the real setup. After the clamping step, the upper test force is applied to the clamps in z direction. Only elastic deformation of the specimen is considered.

Three kinds of specimen are investigated. The first has an ideal rectangular cut-surface without die roll, fracture zone and burr. The second ideal specimen shows an additional imprint of the v-ring. The third kind is modeled after the geometry measured in the experiments to investigate errors caused by the fatigue testing rig. All specimens are modeled using C3D8 elements without reduced integration.

8.1.3 Fatigue Strength

The fatigue testing results are displayed in figure 8.3. Here, the upper test loads and the upper nominal stresses are given which are calculated by dividing the upper test force by the nominal cross section area[22]. For the strips manufactured by fineblanking with a die clearance of 0.5 %, $r_S = 200\,\mu m$, and $r_M < 20\,\mu m$, a complete Wöhler curve was tested, which is displayed in figure 8.3 a). This line shows a slope of $k = 4.8$ in the finite lifetime range. At $2.4 \cdot 10^5$ cycles to failure the finite lifetime goes over to the endurance range below a test load of 10.9 kN.

Identifying a complete Wöhler curve is time-consuming as it requires to test many specimens. To reduce the experimental effort, only the finite lifetime range will be discussed in the following, as it still allows drawing conclusion on how the different part properties affect the fatigue behavior. This is shown for the configuration with a round punch edge in figure 8.3 b). For a die clearance of 0.5 %, $r_S = 200\,\mu m$ and $r_M < 20\,\mu m$, the strips manufactured by fineblanking show the highest number of cycles to failure for the high test load of 19 kN. These are followed

[22] A more detailed look at the stress situation is given in chapter 8.2.2

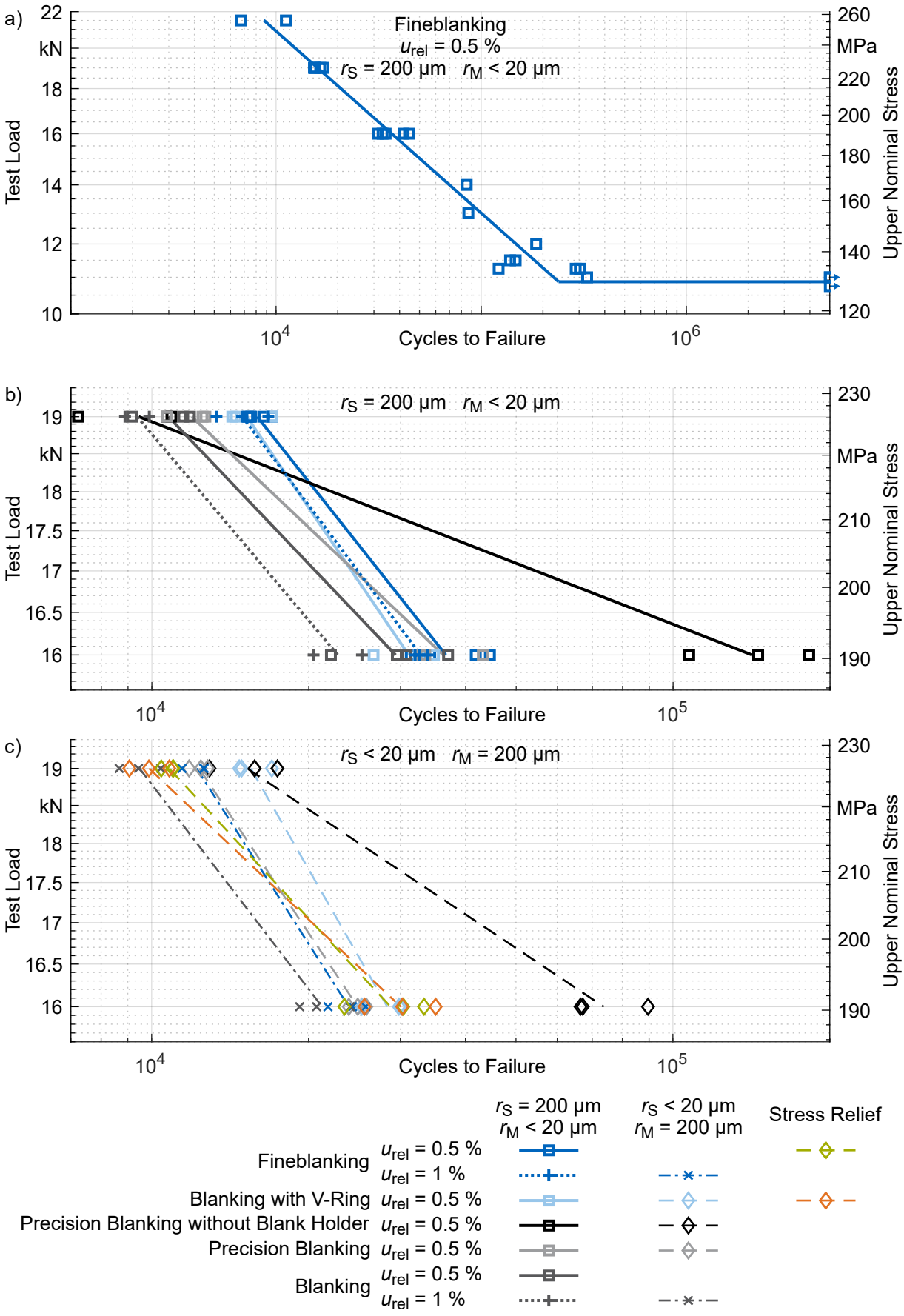

Figure 8.3: Fatigue strength of the manufactured parts as published in Stahl, D. Müller, Pätzold, et al., 2019 and D. Müller et al., 2021.

by the ones produced by blanking with v-ring ($k = 4.2$), precision blanking ($k = 6.5$), blanking ($k = 5.8$) and precision blanking without blank holder ($k = 15.8$). At the low test force of 16 kN, precision blanking without blank holder shows the highest number of cycles to failure, followed by fineblanking, precision blanking, blanking with v-ring and blanking. The variants produced with a die clearance of 1 % show a lower number of cycles to failure for both load levels compared the specimens manufactured with the small die clearance of 0.5 %.

The specimens produced with a die clearance of 0.5 %, a sharp punch edge of $r_S < 20\,\mu m$ and the round die edge $r_M = 200\,\mu m$ show a slightly different behavior, which is displayed in figure 8.3 c). For the high test load, blanking with v-ring ($k = 3.5$) shows the highest number of cycles to failure. This is followed by precision blanking without blank holder ($k = 9.2$), and precision blanking ($k = 4.1$). At the low test load, the highest number of cycles to failure was observed for precision blanking without blank holder, followed by blanking with v-ring, and precision blanking. The specimens subjected to a stress relief heat treatment (SR) after being cut, also with a die clearance of 0.5 %, show a similar number of cycles to failure and different slopes of $k = 5.7$ for fineblanking and $k = 6.5$ for blanking with v-ring compared to their non heat treated counterparts. Again, the variants produced with a bigger die clearance of 1 % show a lower number of cycles to failure. Here, the parts manufactured by fineblanking ($k = 3.9$) show a higher number of cycles to failure than those manufactured by blanking ($k = 4.7$). The crack origin could not be identified due to the plastic deformation of the specimens before complete failure.

8.2 Discussion of Factors Influencing the Fatigue Strength

In the following, the factors influencing the fatigue strength of the parts with shear-cut edges will be discussed. In the state of the art, several general influencing factors are listed. These are the hardness of the material, the surface roughness, the part geometry, and the residual stress state. An interpretation of these factors for common shear-cut edges is presented. Additionally, corrosion, initial defects, size effects, and the externally applied stress state and history affect the fatigue strength. Due to the identical conditions of all investigated parts, these factors are not considered.

8.2.1 Influence Factors

General factors influencing the fatigue strength are the chosen material, its hardness, the geometry of the part and the residual stress state. An overview over these adapted for shear-cut parts is given in figure 8.4. The chosen material shows a base hardness and a ductility. These properties are not influenced by the shear cutting process. Nevertheless, shear cutting causes strain hardening on the shear-cut edge. Thus, the materials strain hardening behavior can be expected to influence the hardness of the investigated edge.

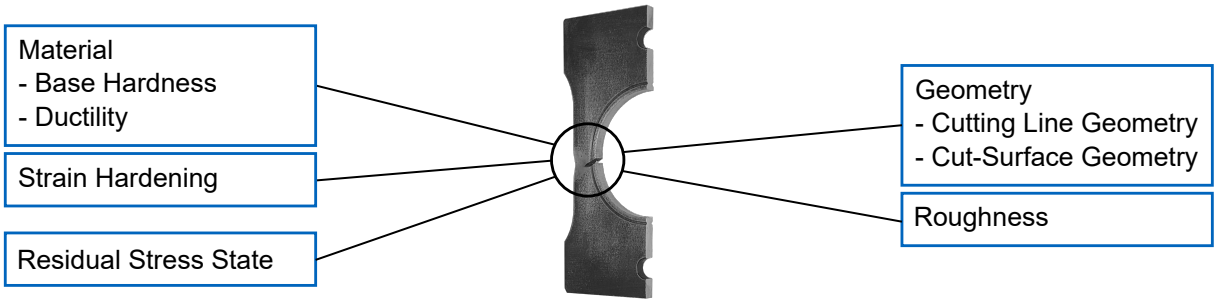

Figure 8.4: Factors influencing the fatigue strength of shear-cut parts.

As shown in chapter 7, the chosen shear cutting process and its process parameters significantly influence the part's residual stress state. The cutting line geometry is often fixed by the part's function. The part geometry is usually considered by notch factors, i.e., the stress concentration is calculated by this geometry. Nevertheless, shear cutting alters the edge geometry on two additional scales. At first, a cut surface is formed which shows a die roll, a clean cut with a clean cut angle, a fracture zone with a fracture zone angle, and a burr. Part bending can be observed as well. Second, the part roughness, i.e., the geometry on a micro scale, is altered. This is particularly clear by looking at the smooth clean cut compared to the rough fracture zone.

Except for the residual stress state, the influence of the shear cutting process on the part properties has been investigated by many authors, as shown in chapter 2.1.4. Thus, the influence of each of these relevant factors on the fatigue strength is discussed in the following to single out the influence of the residual stress state.

8.2.2 Part Geometry Influence

The part geometry influence on the fatigue strength is analyzed by investigating part properties beginning from the macro scale and then proceeding to smaller scales. At first, the influence of the v-ring is examined as it changes the geometry by several millimeters. This is followed by the influence of the part bending, which also affects the whole part. Finally, the cut-surface characteristics and the part roughness are investigated.

V-Ring Influence

To identify the influence of the v-ring on the fatigue strength, finite element simulations were carried out. Here, ideal specimens geometries which only differ by a v-ring were investigated. The von Mises stresses of the two variants and load levels are shown in figure 8.5.

For the configuration without a v-ring imprint an average stress in the notch root of 343 MPa was calculated for a testing force of 16 kN and 412 MPa for 19 kN. The specimens with v-ring imprint resulted in stresses of 349 MPa and 419 MPa for the two forces. For both load cases, the stress of the specimen with v-ring is only 1.8 % higher compared to the specimen without v-ring imprint. In average, the stress in the notch root for the variant without a v-ring is 1.81

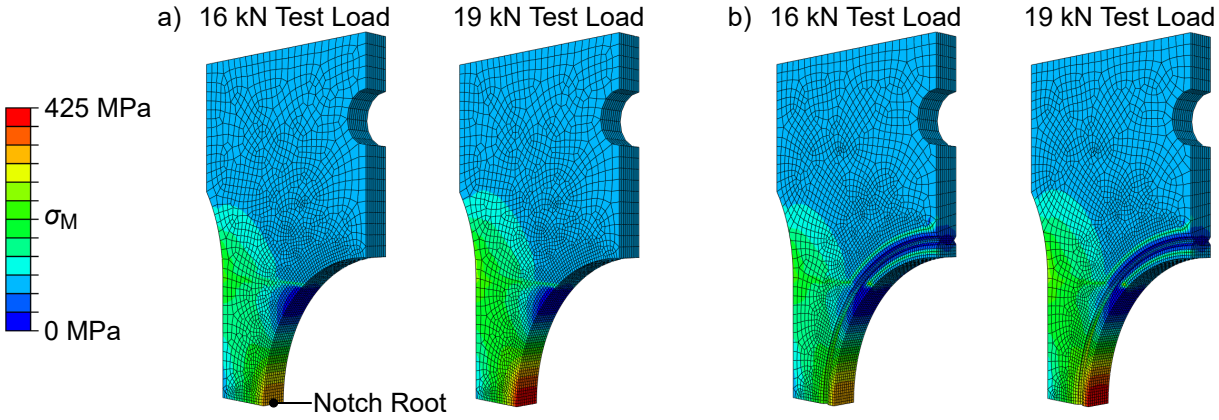

Figure 8.5: Comparison of the von Mises stresses for the different testing forces for the ideal cut-surface geometry without a v-ring imprint (a), and with a v-ring imprint (b).

times higher than the nominal stress calculated without bending and stress concentration. For the variant with v-ring, a 1.84 times higher stress is calculated. This higher stress in the notch root is one factor responsible for the lower *k*-factor of the variants with a v-ring.

Part Bending Influence

The influence of the strip bending is analyzed by correlating the number of cycles to failure with the measured bending coefficients. This is displayed in figure 8.6.

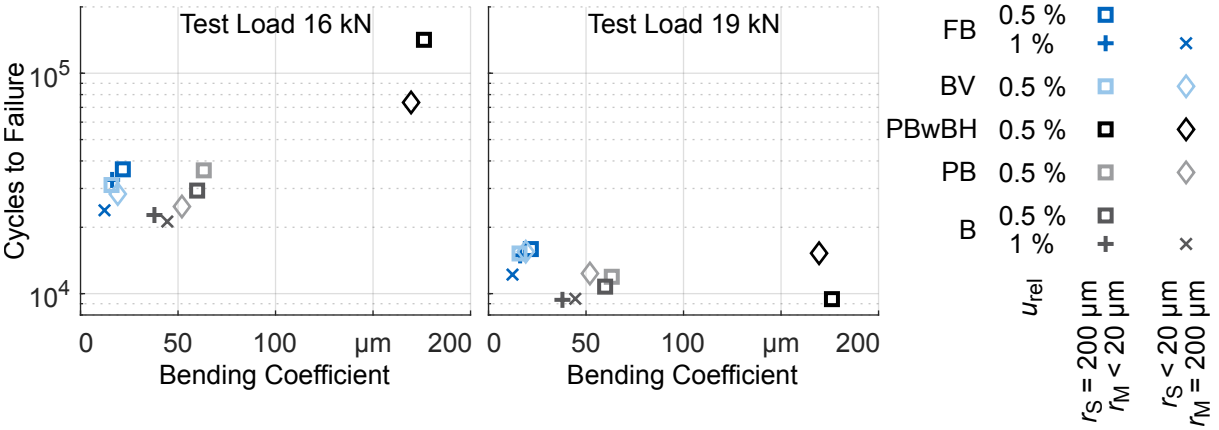

Figure 8.6: Correlation between the bending coefficient and the number of cycles to failure for the low (left) and the high test load (right).

For the low and the high test load, the variants with a v-ring, i.e., fineblanking and blanking with v-ring, show little differences in the part bending. Thus, a correlation between the bending and the number of cycles to failure can not be observed. The variants without a v-ring and with a v-ring on the other show a clear correlation between the bending coefficient and the number of cycles to failure. Here, parts that show a higher bending show a higher number of cycles to failure. The specimens manufactured by precision blanking without blank holder show the same behavior. For the high test load, no clear correlation can be observed.

To identify the influence of the part bending on the fatigue stress, the stress situation in the pulsating rig is analyzed by a finite element simulation. For this model, a cone was fitted to the surface measurement data, i.e., to the burr side surface of the sheet metal strip, for a specimen manufactured by blanking with $u_{rel} = 0.5\,\%$, $r_S = 200\,\mu m$ and $r_M < 20\,\mu m$. Otherwise, an ideal cut-surface is used. Only the clamping force was applied to identify the initial stress situation. The result is displayed in figure 8.7.

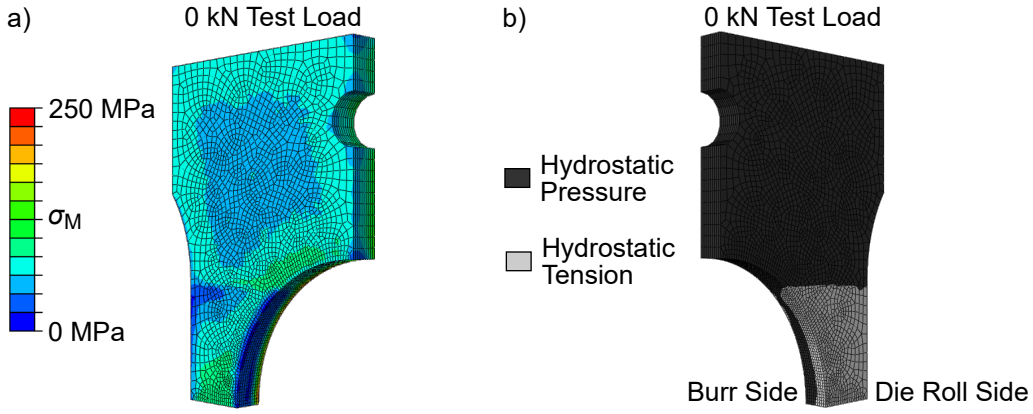

Figure 8.7: Influence of part bending on von Mises stress (a) and the hydrostatic stress (b).

As the clamps straighten out the initially bent part, especially the die roll side is stressed. Here, a tensile hydrostatic stress is observed. The burr side on the other hand is subjected to hydrostatic pressure. As published by (Lara, Picas, and Casellas, 2013), a crack usually originates close to the burr. Thus, hydrostatic pressure on the burr side can be expected to improve the fatigue behavior. As a higher part bending results in higher hydrostatic pressure, a higher part bending results in an increased number of cycles to failure. Nevertheless, if the stress in the specimen is too high, plastic deformation occurs. This explains why the correlation between the part bending and the number of cycles to failure is not as clear for the high test load. To ensure that mainly elastic behavior is investigated, only the low test load of 16 kN is considered in the following. Also, the results for the specimens manufactured by precision blanking without blank holder are only shown for completeness, as they can be expected to be mainly influenced by the part bending.

Cut-Surface Characteristics Influence

The cut-surface shows a die roll, a clean cut, a clean cut angle, a fracture zone and burr. Except for the clean cut, all the other cut surface characteristics cause a deterioration of the real geometry from an ideal geometry. The die roll directly reduces the amount of load bearing surface in the notch root. On the other hand, a high amount of clean cut can be expected to improve the fatigue behavior as it increases the load bearing surface. In absence of a fracture zone, a higher die roll reduces the clean cut height, thus these measures are not independent. To identify the influence of these measures, a correlation of the die roll height and the number of cycles to failure is shown together with the correlation for the clean cut height in figure 8.8.

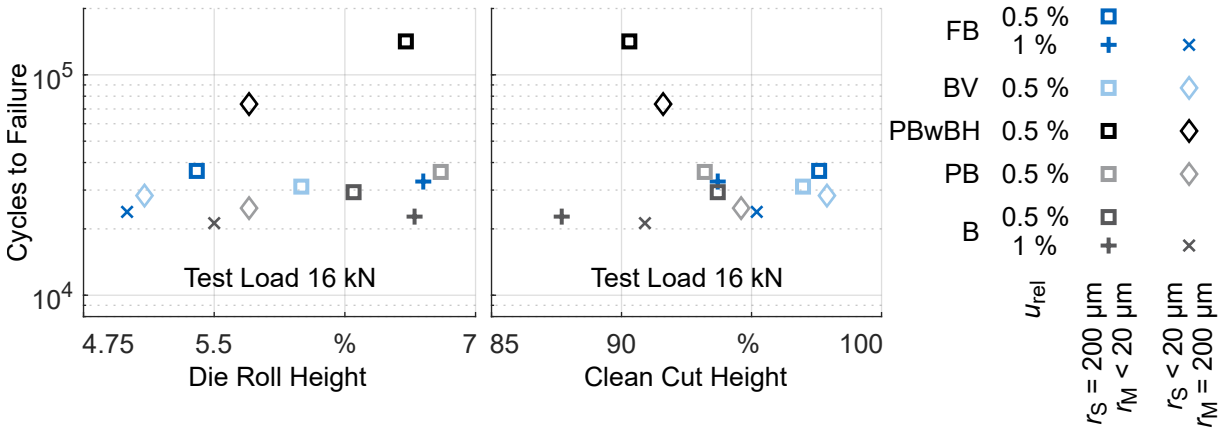

Figure 8.8: Correlation between the die roll height and the number of cycles to failure (left) and between the clean cut height and the number of cycles to failure (right).

Almost no correlation between the die roll height and the number of cycles to failure can be observed. Only for the variants manufactured without a v-ring, a slight trend is visible. This tendency indicates that an increased die roll height causes an increased number of cycles to failure, which is not reasonable as a bigger die roll decreases the available surface in the notch root. Thus, this effect is most likely caused by the part bending, which shows the same trend as the die roll height for the variants without a v-ring.

Similar observations can be made regarding the clean cut height. Again, the trend for the variants manufactured without a v-ring and with $u_{rel} = 0.5\,\%$ suggests that a higher amount of clean cut results in a reduced number of cycles to failure. As a higher amount of clean cut, i.e., a higher amount of load bearing surface, should increase the number of cycles to failure, this behavior is most likely caused by other effects. Not even for the specimens manufactured with the big die clearance of 1 % a clear trend can be observed.

As the specimens manufactured with a die clearance of 1 % show a fracture zone, looking at just the clean cut is not enough. The corresponding correlation is shown together with the one for the burr height in figure 8.9.

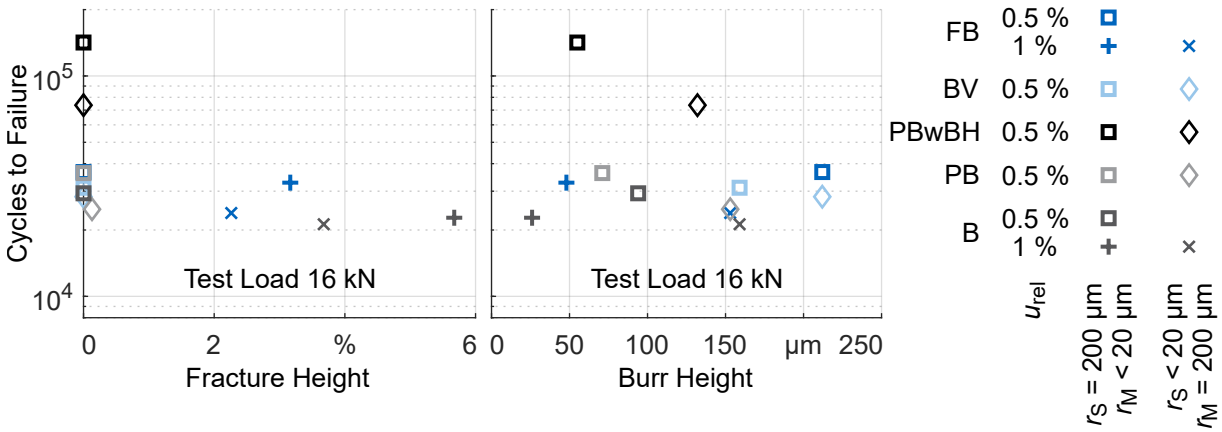

Figure 8.9: Correlation between the fracture height and the number of cycles to failure (left) and between the burr height and the number of cycles to failure (right).

As most of the manufactured specimens show no fracture zone at all, it is not a good measure to evaluate the fatigue strength. Not even for the specimens that show a fracture zone, the fracture zone height is the dominating factor.

The burr height also has little influence on the number of cycles to failure. The results are, except for precision blanking without blank holder, distributed in a horizontal band which shows almost no trend. As the clean cut angle and the part bending are highly correlated, as visible in figure 6.10, the influence of the clean cut angle is not separately addressed in this chapter.

Roughness Influence

Regarding the influence of the roughness on the fatigue strength two different measures have to be analyzed. At first, the roughness of the clean cut is of interest, especially for all variants that do not show a fracture zone. For the other specimens, the much higher roughness of the fracture zone has to be considered as well. This differentiation is carried out by using the maximal measured roughness, i.e., the clean cut roughness for variants that do not show a fracture zone and the fracture zone roughness for all others. As the fracture zone of the specimens manufactured with $u_{rel} = 1\,\%$ is too small to be measured, the mean roughness of the fracture zone for $u_{rel} = 3\,\%$ is used. The correlation between these two measures and the number of cycles to failure is displayed in figure 8.10.

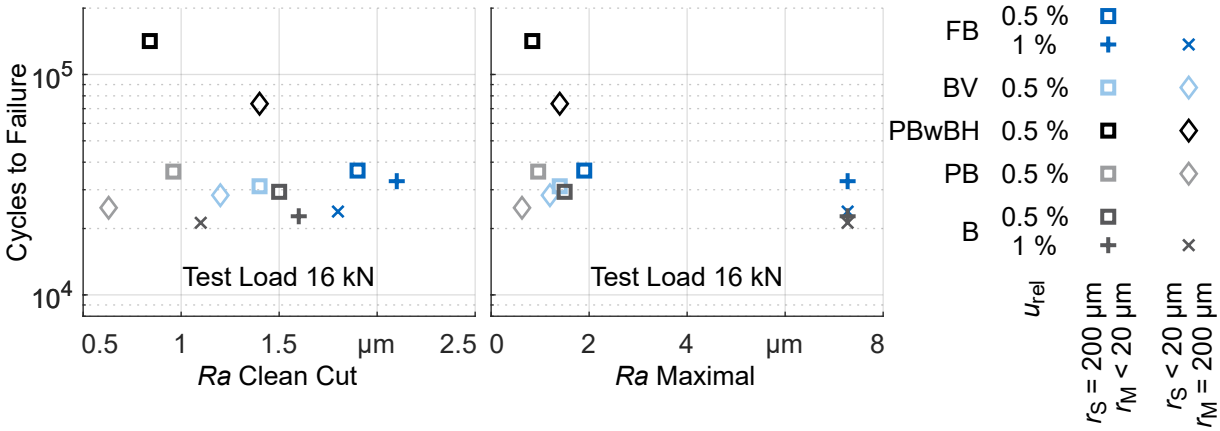

Figure 8.10: Correlation between the clean cut roughness and the number of cycles to failure (left) and between the maximal roughness and the number of cycles to failure (right).

It can be observed that the clean cut roughness does not significantly influence the number of cycles to failure, as all results are randomly distributed. Not even the maximal roughness shows a visible trend.

This low influence of the surface roughness is in agreement with the results published by Dittmann and Pätzold, 2018. As shown by McKelvey and Fatemi, 2012 for forged parts, ductile materials with a comparably low hardness are not as prone to an increased surface roughness as materials with a high hardness.

8.2.3 Part Hardness Influence

To identify the hardness influence two approaches can be thought of. As proposed in Pätzold et al., 2017, the maximum hardness can be investigated. On the other hand, it seems likely that a crack occurs on the location of the cut-surface with the minimal hardness. Thus, both measures are investigated here. The maximal hardness was analyzed by calculating the mean of three measurement points with the highest hardness. The same procedure, only for the three points with the lowest hardness, was used to identify the minimal hardness. As the hardness far away from the notch root is not as relevant, only hardness measurement at a distance smaller 0.35 mm from the clean cut were considered. The corresponding results are shown in figure 8.11.

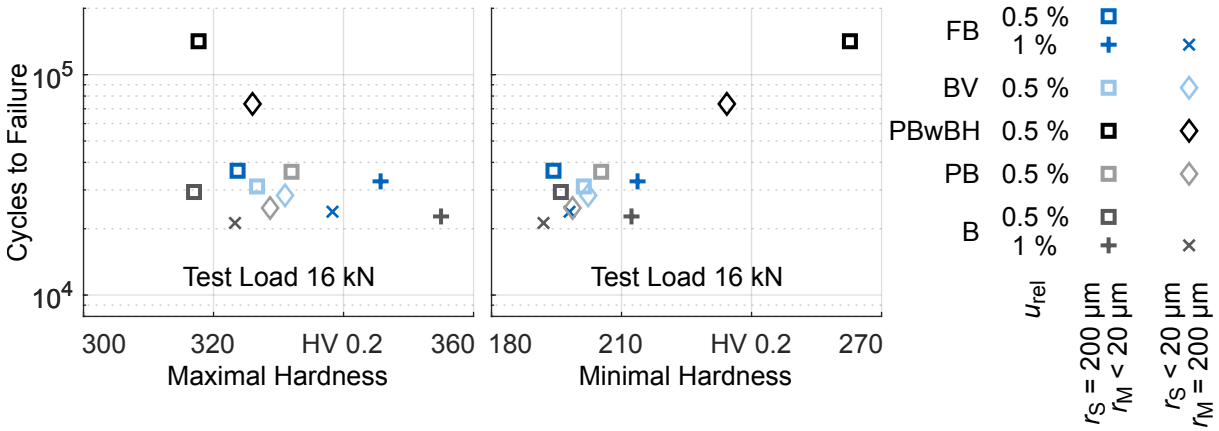

Figure 8.11: Correlation between the maximal hardness and the number of cycles to failure (left) and between the minimal hardness and the number of cycles to failure (right).

Regarding the maximal hardness no significant trend can be observed. The minimal hardness on the other hand shows a better correlation. Especially the results for the specimens manufactured without a v-ring and with $u_{rel} = 0.5\,\%$ show a clear trend, where a higher minimal hardness results in a higher number of cycles to failure. This is in good agreement with the observations made, for example by Casagrande, Cammarota, and Micele, 2011, where an overall higher hardness results in a higher fatigue strength. This behavior is another reason why the fatigue strength of the specimens manufactured by precision blanking without blank holder is high compared to the other variants. While this correlation can also be observed for the specimens manufactured with $u_{rel} = 1\,\%$, it is not applicable for the specimens manufactured with $u_{rel} = 0.5\,\%$ and a v-ring. This means that other effects are dominating their behavior.

8.2.4 Residual Stress State Influence on the Fatigue Strength

After discussing all other relevant factors that affect the part's fatigue strength, the influence of the residual stress state is analyzed. As part bending significantly alters the fatigue behavior, only variants that show a similar bending are compared in the following. Among these are all variants manufactured with a v-ring. The results for the part subjected to a stress relief heat treatment are given as they show a similar geometry and hardness but differ in the residual

stress state. Their stress state is assumed to be zero based on the initial investigations presented in chapter 5.1. Nevertheless, a complete overview is given in the appendix (see figure F.3). To investigate the die clearance influence, i.e., the residual stress state effect while a fracture zone is present, results for fineblanking with a die clearance of 1 % are given as well. It should be noted that the stress state in the middle of the sheet metal is considered as the fracture zone is too small to measure.

Regarding the variants without a v-ring, only the results for the parts manufactured by blanking and precision blanking with $r_S = 200\,\mu m$ and the sharp die edge are presented as they show a comparable bending. Additionally, the part manufactured by precision blanking with a sharp punch edge shows a very small fracture zone that might nevertheless affect the fatigue behavior. The correlations between the axial and tangential residual stresses and the number of cycles to failure are shown for the selected variants in figure 8.12.

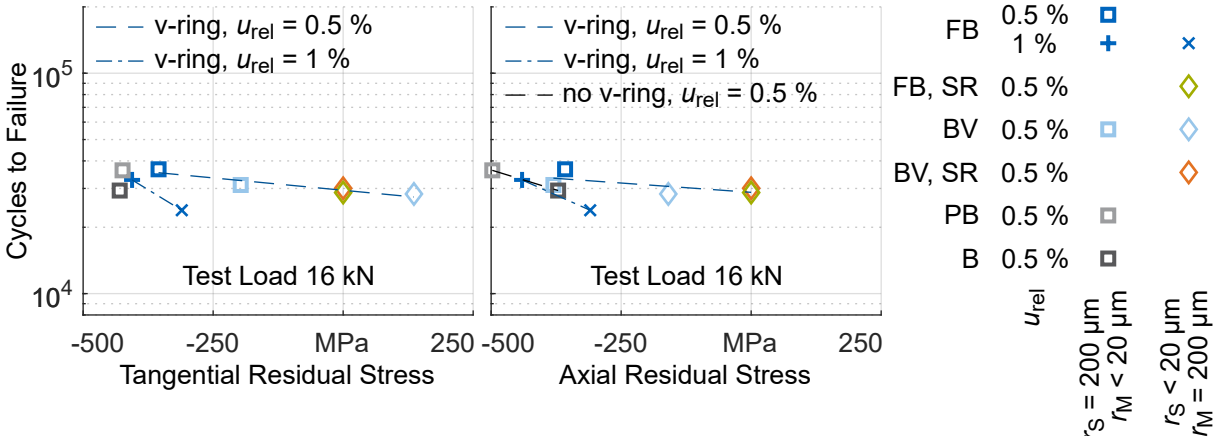

Figure 8.12: Overview of the correlation between the residual stress state on the number of cycles to failure with calculated trends (dashed lines) for similar groups.

The tangential residual stress state shows a clear correlation with the number of cycles to failure for the variants with a v-ring. Here, higher compressive stresses lead to a higher number of cycles to failure. This effect is stronger for parts manufactured with $u_{rel} = 1\,\%$. As the parts manufactured by precision blanking and blanking show no significantly different tangential residual stress, no correlation can be observed here.

Thus, the axial residual stress state has to be considered as well. In this direction, the variants manufactured without a v-ring show significantly different residual stresses. Accordingly, higher compressive stresses lead to a higher number of cycles to failure. The same trend, with an almost identical slope is observed for the specimens manufactured with a v-ring and $u_{rel} = 1\,\%$. A lower gradient is observed for the remaining variants. Again, a comparison is difficult as the specimens manufactured by fineblanking and blanking with v-ring show almost identical residual stresses in axial direction.

As both, the axial and the tangential residual stresses, influence the fatigue strength, two additional measures are investigated. At first, the mean surface residual stress is calculated. This is

based on the idea behind the Sines approach (see chapter 2.3.1), although the hydrostatic stress is not calculated directly.

The second measure assumes that the residual stress perpendicular to the loading direction has a smaller influence than those in loading direction. A constant that connects the elastic stresses in these directions is the Poisson's ratio ν. Thus, the residual stress in loading direction $\sigma_{R,\parallel}$, which is the tangential residual stress, and perpendicular to the loading direction $\sigma_{R,\perp}$, the axial residual stress, are weighted with the following formula, resulting in the elastic average residual stress $\sigma_{\nu AV}$:

$$\sigma_{\nu AV} = (1-\nu)\sigma_{R,\parallel} + \nu\sigma_{R,\perp} \tag{8.1}$$

The correlations between these two measures and the number of cycles to failure are displayed in figure 8.13.

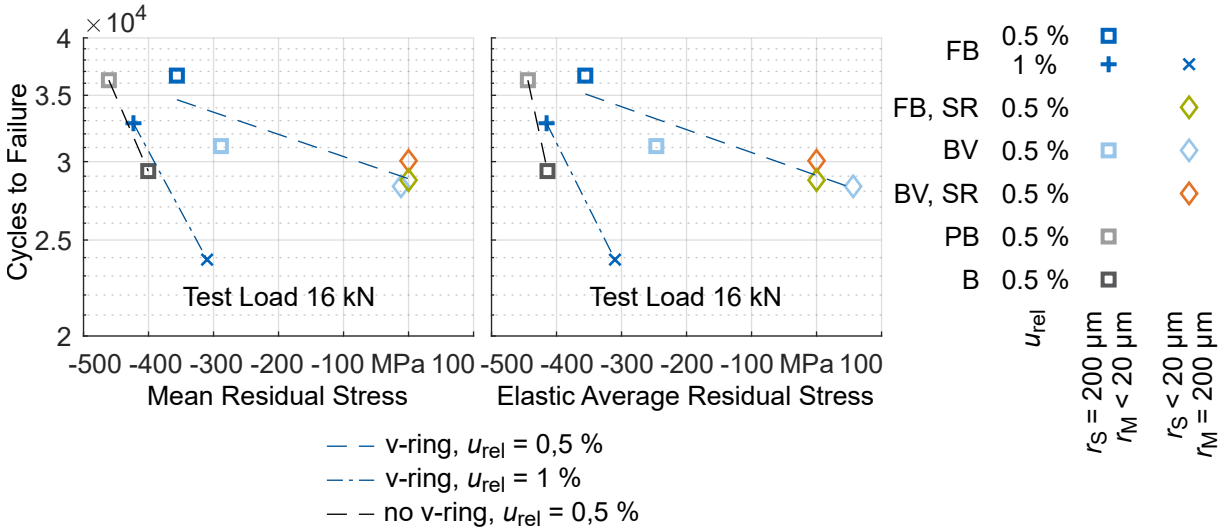

Figure 8.13: Detailed look at the correlation between the mean residual stress on the number of cycles to failure (left) together with the correlation between the elastic average residual stress and the number of cycles to failure (right).

It can be observed that the mean residual stress shows the expected trend for all three groups. Only the specimens manufactured by blanking with v-ring are not in agreement. They show a higher compressive mean residual stress but lower cycles to failure than the specimens subjected to the stress relief heat treatment. Regarding this behavior, the elastic average residual stress is a better measure. These results show that the residual stress state is a major factor influencing the fatigue strength. Furthermore, both the axial and the tangential residual stresses have to be considered.

8.3 Conclusion

The fatigue strength of shear cut edges is significantly influenced by the chosen shear cutting process and its process parameters. At the low load level, a difference between the lowest and the highest measured cycles to failure of more than factor 6.6 was observed. This big range is caused by several factors. The major influencing factors are:

- Fracture zone
- Part Bending
- Residual Stress State

The occurrence of a fracture zone has several disadvantages. It is rough compared to the clean cut, it reduces the available surface in the highly stressed notch root and it may show a tensile residual stress state. When a fracture zone is observed, the materials forming capacity was exhausted during shear cutting. Thus, it is also likely that initial cracks are present. Furthermore, a fracture zone leads to a comparably low hardness close to the burr which also reduces the fatigue strength.

As shown by the correlation analysis, presence and height of the fracture zone alone is not able to explain the fatigue behavior of the investigated specimens. The part bending shows a clear correlation, especially for specimens manufactured without a v-ring. Part bending causes compressive stresses on the critical burr side when the specimen is gripped in the fatigue testing setup. This increases the part lifetime. As many parts are also flattened in practice, for example by screws or weld spots during the assembly, this is not strictly an error but can be used in many applications. Additionally, a higher part bending is correlated with higher compressive stresses in many cases.

The residual stress state is the third significant influencing factor. This was shown by investigating parts subjected to an additional stress relief heat treatment after shear cutting. But also for specimens that otherwise show similar geometrical and mechanical properties a positive effect of higher compressive residual stresses was observed.

The minimal hardness in the highest stresses region seems to be an important factor as well. As this factor is also accompanied by severe bending or the occurrence of a fracture zone, additional research is necessary to confirm this.

Some factors that influence the fatigue strength for other materials and processes are not significant for edges manufactured by the investigated shear cutting processes and the process parameter range. The clean cut height and die roll height alone do not show a reasonable tendency. In accordance with other publications, the maximal hardness and the clean cut roughness do not significantly affect the fatigue strength.

To fully use the material's load bearing capacity, the residual stress state caused by shear cutting has to be considered, as it has the potential to increase the part's lifetime by more than 29 %. The proposed elastic averaged stress is an easy measure to consider the residual stresses in and perpendicular to the loading direction. Additionally, the part bending has to be examined in future investigations. Despite the fact that almost all shear cut parts are bent which significantly influences the stress situation in the test rig, this factor has not been investigated yet.

9 Residual Stress State Improvement and Transfer to Industrial Applications

9.1 Residual Stress State Improvement

In the previous chapter, it was shown that the shear cutting process induced residual stresses significantly influence the manufactured edge's fatigue strength. Nevertheless, only comparably coarse process parameter gradations were investigated, especially for the active element edge preparations. In the following, suitable shear cutting processes are selected for piercing and blanking for a further improvement of the residual stress state regarding an increased fatigue strength.

9.1.1 Piercing

Selection of a Suitable Process

At first, cutting of holes, i.e., piercing, is addressed. As shown in chapter 8, the cut-surface geometry significantly influences the fatigue strength. Therefore, a variant without a fracture zone is desired which was achieved with a die clearance of 0.5 %. Additionally, a high compressive residual stress state is beneficial to delay the growth of cracks. Regarding an industrial application, a low sensitivity to the chosen active element edge preparation is desirable, as the edges may change due to wear. Precision blanking fulfills all of these requirements. It does not only show the highest compressive residual stresses in axial direction for the sheet metal strip regardless of the cutting edge preparation, but also shows very little changes when the cutting edge preparation is changed. In tangential direction, precision blanking with a round punch edge 200 µm and a die edge smaller 20 µm shows the highest compressive residual stresses of all investigated blanking processes. For the round punch edge, only blanking shows slightly higher compressive stresses. Precision blanking also shows a comparably high share of clean cut without using a v-ring. As the use of a v-ring is often not possible, for example when holes are close to each other or when a flat surface is required, this is beneficial. Finally, regarding an industrial application a small burr height is often required, for example to reduce the risk of injury, which requires the burr to be removed by additional manufacturing steps. For precision blanking, the burr is significantly smaller for the variant with the sharp die edge. Due to these requirements, precision blanking with a die clearance of 0.5 % and a cutting edge preparation with a punch edge radius of 200 µm and a sharp die edge is chosen as a starting point for further investigations.

At first, a further improvement by varying the punch edge radius is carried out. Due to the robustness of this shear cutting process only small changes of the residual stress state can be expected. Therefore, a comparably big range is chosen with additional radii of $r_S = 50\,\mu m$ and $r_S = 260\,\mu m$. Although it was shown that part roughness does not significantly affect the

fatigue strength, a smooth surface is often required. This can be achieved by polished and coated active elements. To determine the influence of the active element coating, additional strips were manufactured with a punch that was coated with Balinit Alcrona Pro (see chapter 5.3) after polishing.

Results

The resulting residual stress state for the additional punch edge radii is shown in figure 9.1. As expected, the punch edge has a comparably small influence on the residual stress state, which shows that parts can be produced robustly even for significant tool wear. A bigger punch edge radius slightly increases the compressive residual stresses in axial direction. Nevertheless, the punch edge radius also affects the cut-surface characteristics. For the big punch edge radius of 260 µm, the clean cut is reduced by a bigger die roll height and the formation of a fracture zone. A very small fracture zone also reduces the clean cut height of the variant with $r_S = 50\,\mu m$.

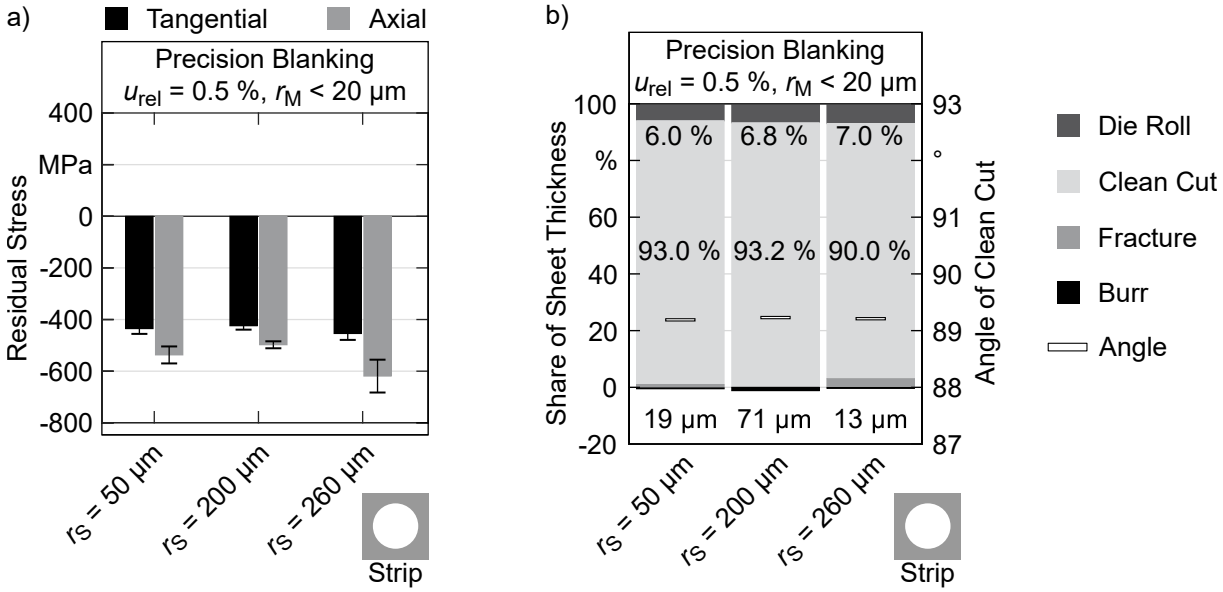

Figure 9.1: Punch edge radius influence on the residual stress state of sheet metal strips manufactured by precision blanking (a) together with the corresponding cut-surface characteristics (b) as published in Stahl, D. Müller, Nürnberger, et al., 2021.

The residual stress state for parts manufactured with a coated punch is compared to that of the uncoated reference in figure 9.2. Again, only small changes of the residual stress state are visible. Only in axial direction slightly smaller compressive residual stresses were measured. The cut-surface characteristics are also not significantly affected. The coated parts show a slightly smaller die roll and clean cut height, but also a small fracture zone. The roughness of the clean-cut on the other hand was reduced from $Ra = 0.96 \pm 0.17\,\mu m$ to $Ra = 0.38 \pm 0.16\,\mu m$.

Discussion

The results show that the residual stress state is comparably robust regarding a changed punch edge radius, i.e., a worn punch is not critical for the stress state of punched holes. The influence

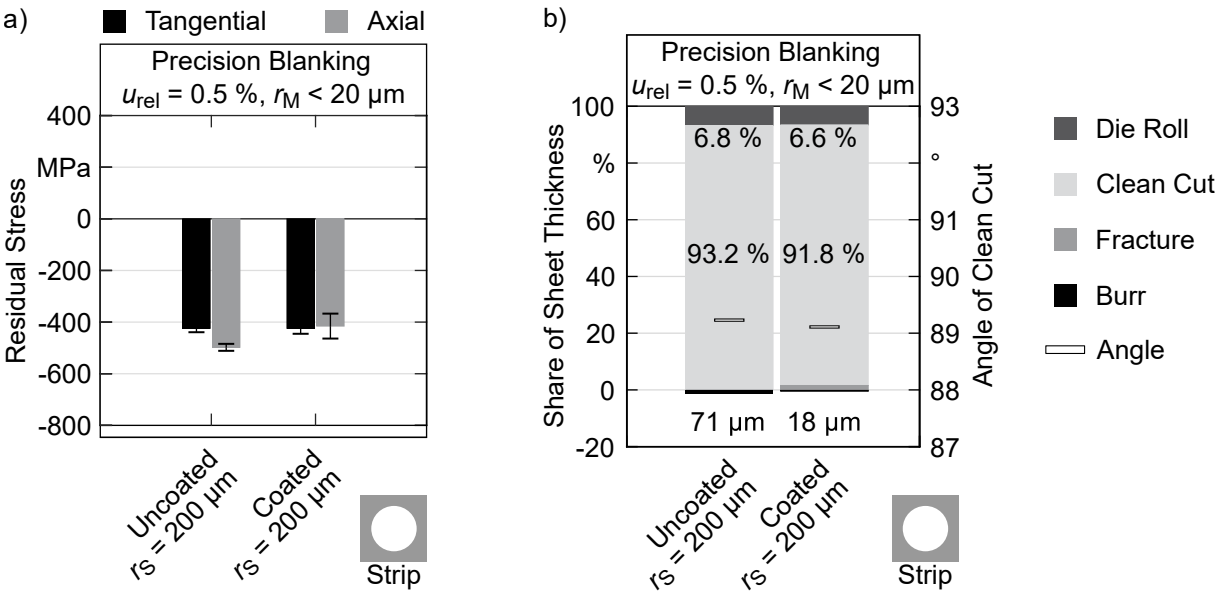

Figure 9.2: Active element coating influence on the residual stress state of sheet metal strips manufactured by precision blanking (a) together with the corresponding cut-surface characteristics (b) as published in Stahl, D. Müller, Nürnberger, et al., 2021.

of the punch radius on the residual stress state also confirms the proposed explanation model, as the bigger punch edge radius of 260 µm results in higher compressive stresses compared to the 200 µm radius. A bigger punch edge radius stretches the material and induces higher stresses. Thus, it favors both the local and the global springback mode. Nevertheless, the initial variant with $r_S = 200$ µm not only offers a cut-surface without a fracture zone but also high compressive residual stresses and should therefore be favored.

The active element coating does not significantly affect the residual stress state of a shear-cut hole. The slightly lower stress in axial direction is most likely caused by the lower friction. Again, the small fracture zone might be problematic for edges subjected to a cyclic loading.

9.1.2 Blanking

Selection of a Suitable Process

The same part requirements as for piercing are also valid for blanking. Again, high compressive residual stresses are desired to increase the part's fatigue strength. Additionally, the residual stresses should be robust regarding process parameter changes. Blanks produced by fineblanking were the only ones that showed compressive residual stresses in axial and tangential direction for both cutting edge preparations which means that the robustness is given. Furthermore, the blank produced by fineblanking with $r_M = 200$ µm showed the highest tangential compressive residual stresses of all investigated variants. Regarding an industrial application, a high amount of clean cut and a small burr height are desired as well. The small burr height can be achieved by using a sharp punch edge. Once more, an edge without a fracture zone can only be

achieved with the small die clearance of 0.5 %. For this reason, fineblanking with a die clearance of 0.5 %, a sharp punch edge radius of $r_S < 20\,\mu m$ and a round die edge $r_M = 200\,\mu m$ is chosen as the basis for further investigations. To cover a broader range, two additional die edge radii of $r_M = 50\,\mu m$ and $r_M = 260\,\mu m$ are chosen.

Results

The influence of the die edge radius on the residual stress state and the cut-surface characteristics is displayed in figure 9.3. Regarding the residual stresses, a clear tendency is visible: higher compressive residual stresses in axial and tangential direction are achieved by using a bigger die edge radius. The cut-surface characteristics on the other hand vary only in a comparably small range. All three variants do not show a fracture zone and achieve a clean cut share of over 95.1 %.

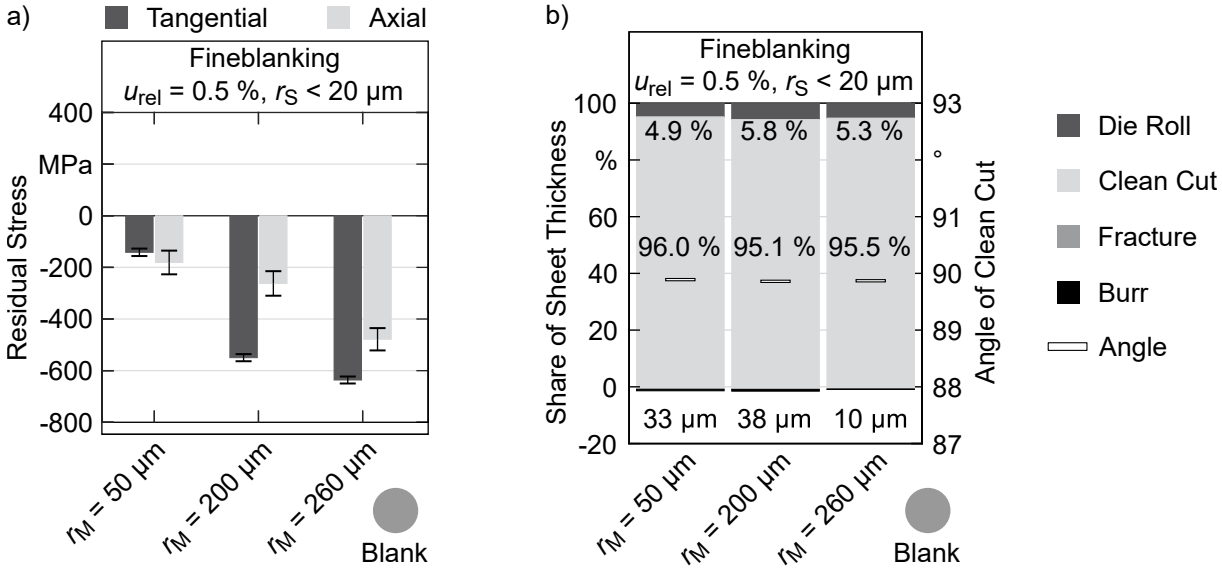

Figure 9.3: Influence of the die edge radius on the residual stress state of blanks manufactured by fineblanking (a) together with corresponding cut-surface characteristics (b) as published in Stahl, D. Müller, Nürnberger, et al., 2021.

Discussion

A bigger die edge radius results in higher surface residual stresses of the manufactured blanks. This can easily be manufactured when high compressive residual stresses are desired. Additionally, this means that a die edge radius increased by tool wear improves the part quality when a high fatigue strength is of interest. While the residual stresses vary in this comparably big range, the cut-surface characteristics are only slightly affected. Due to this combination of high compressive residual stresses, a high portion of load bearing surface, and a small burr height, choosing the big die edge radius is advisable.

9.2 Transfer to a Convex-Concave Geometry

Specimen Geometry and Preparation

Previously, only circular geometries have been investigated. Of course, in most cases the cutting line is not circular but shows convex and concave parts. Therefore, a convex-concave blank is examined in this chapter. The specimen preparation is similar to those of the circular geometries. It is displayed, together with the specimen geometry, in figure 9.4.

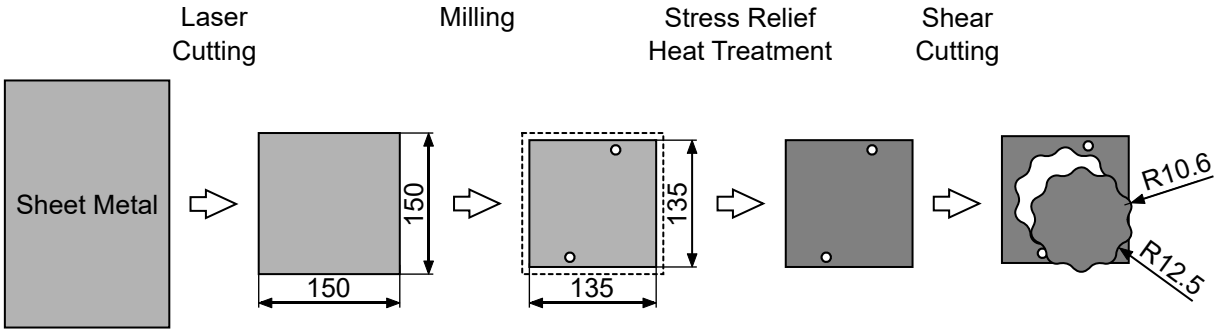

Figure 9.4: Preparation and geometry of the convex-concave specimens.

The geometry follows a shortened epicycloidal geometry that can be approximated with a radius of 10.6 mm on the convex edge and a radius of 12.5 mm on the concave position. Measurements were carried out on the maximum and minimum distance of the cutting line to the part's center.

Fineblanking with a die clearance of 0.5 %, a sharp punch edge radius of $r_S < 20\,\mu m$ and a round die edge $r_M = 200\,\mu m$ is chosen as this process shows the best results for manufacturing blanks when a high compressive residual stresses are desired. The same force per v-ring length, and the same counter punch pressure were chosen as for the circular geometry. This results in the forces listed in table 9.1.

Table 9.1: Forces set for the convex-concave cutting line geometry.

Precision Shear Cutting Process	Blank Holder Force	Counter Punch Force
Fineblanking	791 kN	554 kN

Results

The resulting residual stresses are shown together with the cut-surface characteristics in figure 9.5. The residual stresses in axial direction are significantly affected for both the concave and the convex geometry. In both cases, much higher compressive stresses are measured, especially on the convex edge (R10.6). In tangential direction much smaller changes are observed. Here, the concave edge (R12.5) shows a residual stress state comparable to the circular geometry (D60). The concave geometry (R10.6) on the other hand shows much higher compressive stresses. The cut-surface characteristics also show comparably big changes. A much bigger die roll height is measured on the convex edge (R10.6) compared to the circular geometry while the die roll height is much smaller on the concave edge (R12.5). As the cut-surfaces of all

three geometries do not show a fracture zone, this changed die roll height is directly reducing the clean cut height. Thus, the convex edge shows a smaller clean cut height compared to the circular reference while the concave edge shows a bigger clean cut height.

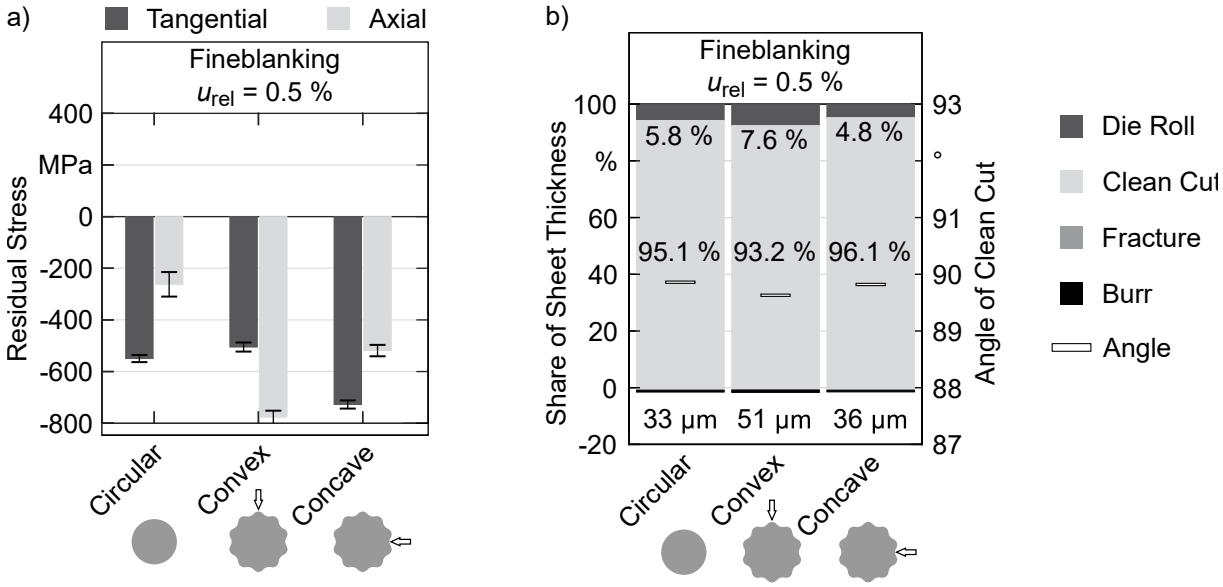

Figure 9.5: Influence of the cutting line geometry on the residual stress state of blanks manufactured by fineblanking with $u_{rel} = 0.5\,\%$, $r_S < 20\,\mu m$ and $r_M = 200\,\mu m$ (a) together with the corresponding cut-surface characteristics (b) as published in Stahl, D. Müller, Nürnberger, et al., 2021.

Discussion

Although a direct transfer of the residual stress state from the circular to the convex-concave geometry is not possible, the multiaxial material flow caused by the non-circular cutting line, increases the compressive residual stresses in axial direction. As the tangential residual stresses either show a comparably high or a higher compressive residual stress, parts manufactured with such a convex-concave cutting line can be expected to show a similar or better fatigue strength than a circular geometry.

9.3 Cycloidal Gear Application

On the basis of the presented results, the stability of residual stresses of parts manufactured by precision shear cutting processes are tested in a real gear application. The cycloidal convex-concave geometry is adjusted, inserted in a cycloidal drive and tested on the gear lifetime test bench described in chapter 4.13.

9.3.1 Specimen Preparation and Test Setup

The designed cycloidal gear is displayed in figure 9.6. Its main parts are a drive shaft with two eccentric cylinders, the shear-cut disks, pins in the housing, and an output shaft. On the eccentric cylinders of the drive shaft, the two cyloidal gears are mounted by needle bearings.

Two gear disks were chosen to reduce the dynamic imbalance caused by the eccentric assembly. The disks transmit the torque over hardened pins (steel 1.2067) in the housing to the output shaft. Copper-Zinc bearings are located between the gear and the output shaft. Both the drive shaft and the output shaft are mounted by ball bearings to reduce friction. To be able to measure the temperature inside the housing, a hole for a thermocouple was manufactured. The whole cycloidal drive can be mounted on the gear lifetime test bench.

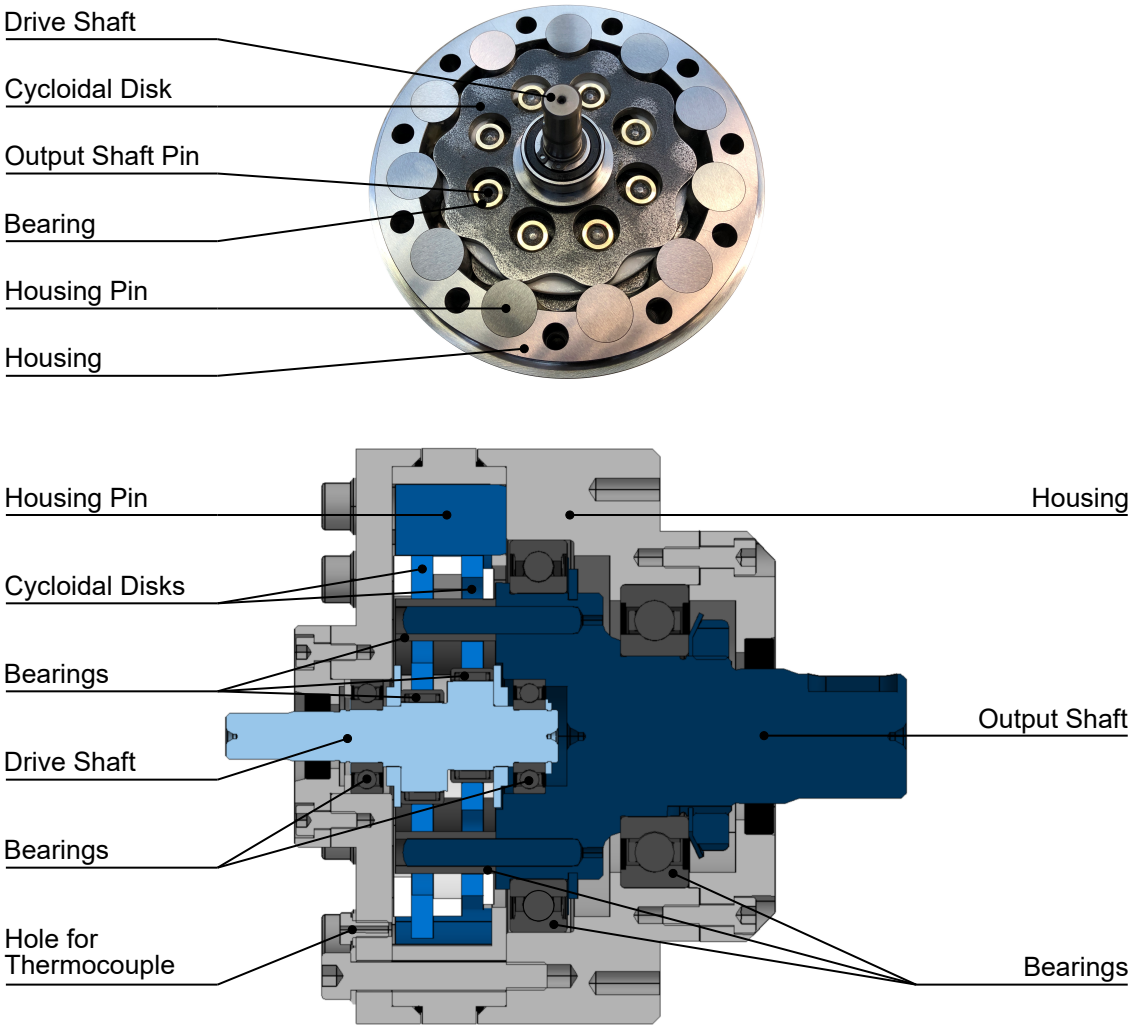

Figure 9.6: Cycloidal drive used for the endurance investigations with an open lid (top) and in a sectional view (bottom).

To manufacture the cyloidal gear, an epicyloid outer contour, holes for the output shaft, and an additional hole for the drive shaft are necessary. The specimen preparation is illustrated in figure 9.7. At first, the outer contour of the specimen is milled and the specimen is subjected to the stress relief heat treatment. Afterwards, two positioning holes and the center hole for the drive shaft are manufactured by milling. Following, the holes for the output shaft are cut by blanking with a die clearance of 0.5 %, a punch edge radius of 200 µm and a sharp die edge radius smaller 20 µm. This shear cutting process with these process parameters offers a good fatigue strength while no counter punch is needed. A counter punch is challenging, as it may damage the positioning holes when multiple holes are cut. To minimize the influence of the

holes on each other, a pattern as displayed in figure 9.7 was chosen, which is realized by four positioning pins on the die.

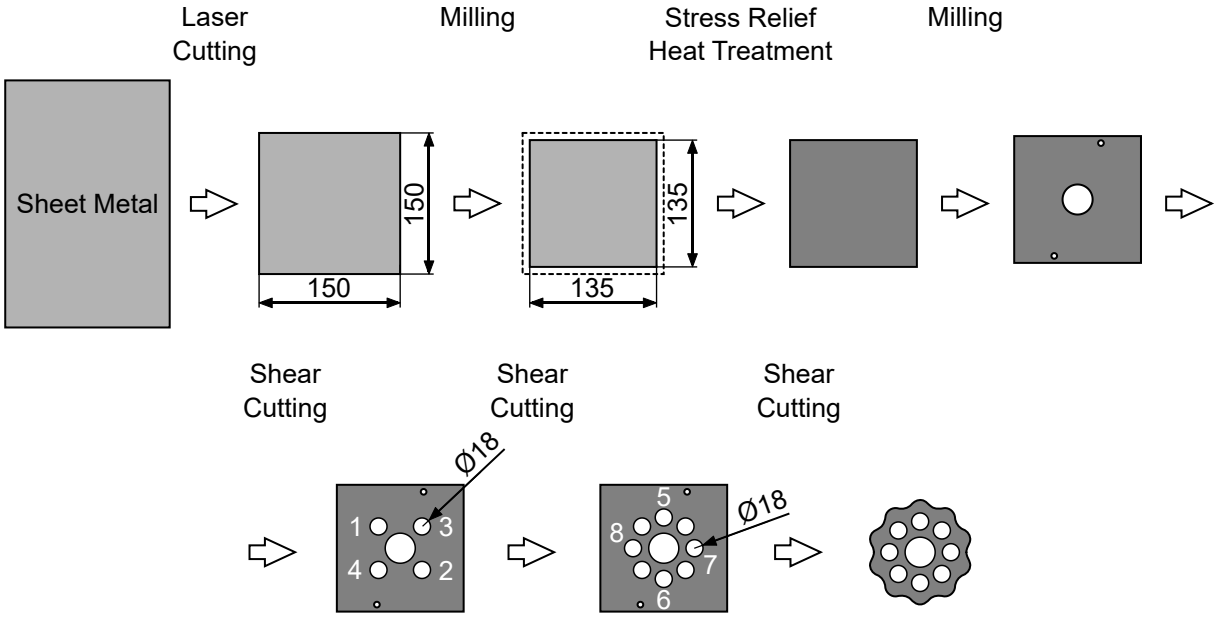

Figure 9.7: Preparation of the cycloidal gears with hole pattern.

Subsequently, the outer contour was manufactured by fineblanking with a die clearance of 0.5 %, a sharp punch edge radius smaller 20 µm and a die edge radius of 200 µm. Again, this process with these process parameters is chosen due to its favorable residual stress and fatigue properties. It also allows to include the findings of chapter 9.2. This final cut is carried out on the same side as for the holes, to imitate the conditions in an industrial tool, i.e., the burrs of the holes and the outer contour are on different sides.

Due to the eight holes with a diameter of 18 mm, the surface of the sheet metal is reduced compared to the one without holes shown in chapter 9.2. To achieve the same counter punch pressure, a smaller force was set. The same v-ring force as for the convex-concave geometry was chosen. For cutting the holes, the lowest possible blank holder force of the press was set. These forces are listed in table 9.2. Finally, the burr was removed by grinding with a 1200 grade sand paper, as a chipped-off burr may destroy the bearings.

Table 9.2: Forces set for the convex-concave cutting line geometry.

Precision Shear Cutting Process	Blank Holder Force	Counter Punch Force
Fineblanking	791 kN	363 kN
Blanking	140 kN	-

9.3.2 Experimental Procedure

The shear cut disks were put in the gearbox and lubricated with a grease recommended by Klüber Lubrication München SE & Co. KG, München (Germany). Afterwards, the complete cycloidal drive was connected to the gear lifetime test bench. Following, the torque was in-

creased after a defined number of load cycles, i.e., after a certain number of drive shaft revolutions, while maintaining the input rotational speed at 600 min^{-1}. The temperature in the housing and the torque of the output shaft were measured. The vibration signal is used together with these to detect eventual failure.

After a run well within the endurance range, the disks were removed and the residual stress state was measured. Here, the Sentenso X-ray measurement device (see chapter 4.12) was used. Due to its flexibility there is no need to cut out small pieces of the disks to be able to measure the residual stresses. Nevertheless, it is not capable of measuring axial residual stresses with a high accuracy why only the highly relevant tangential residual stresses were considered. As the cutting of the holes may affect the residual stresses on the outer contour, measurement positions as shown in figure 9.8 were chosen to capture this effect. Finally, this residual stress state was compared the one of new disks to investigate the stability of the residual stresses under industrial conditions.

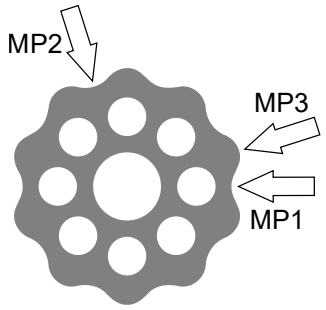

Figure 9.8: Measurement positions (MPs) on the cycloidal disk.

The output torque was increased beginning from 20 Nm to 59 Nm. At first, steps of approximately 500.000 load cycles were chosen which were increased to approximately 1.000.000 load cycles at 50 Nm and finally the test was stopped after approximately 4.600.000 load cycles, i.e., well within the endurance range, at the maximum torque of 59 Nm. In total more than 7.200.000 load cycles were applied.

9.3.3 Results

The torque course is displayed in figure 9.9 a). Here, the lower peaks indicate a maintenance interval at which the sensors and the lubrication condition were checked. During the last phase a mean temperature of 57.6 °C was measured inside the housing with values ranging from 49.1 to 62.1 °C. The mean room temperature during the test was 28.2 °C. The residual stresses in tangential direction are displayed in figure 9.9 b). At measurement position 1 and 2 negligible differences can be observed. Only at measurement position 3 a significantly altered residual stress state is measured.

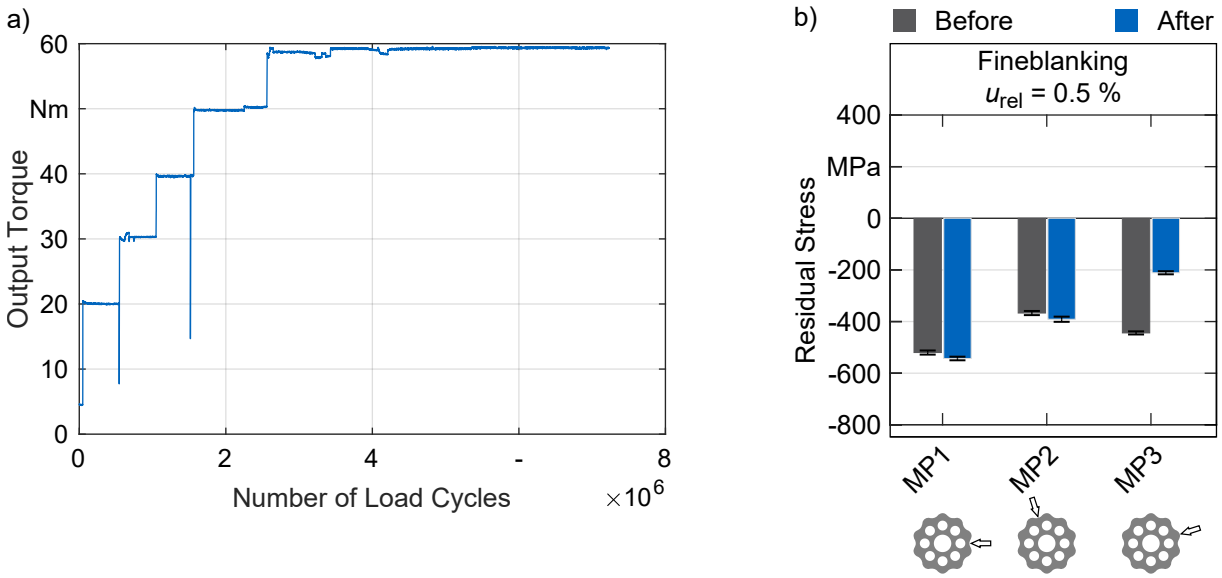

Figure 9.9: Output torque during the test (a) and a comparison of the residual stresses in tangential direction before and after the run (b).

9.3.4 Discussion

The small changes of the residual stress state on measurement positions 1 and 2 lead to the conclusion that the residual stresses are stable at typical operational temperatures and loads, i.e., they can be used to increase the fatigue strength. Nevertheless, a lower stress is measured on measurement position 3, the tooth which is in direct contact with the hardened pins. To interpret this behavior, a picture of a disk before and after the gear test are shown in figure 9.10.

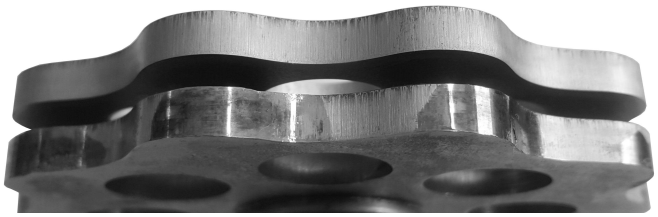

Figure 9.10: Surface of cycloidal disks before (top) and after the endurance test (bottom).

It is visible that plastic deformation and abrasive wear occurred in the region of direct contact, which are most likely responsible for the altered stress state. A high contact temperature might contribute to this. Still, a significant compressive residual stress is available. The local plastic deformation also shows that structural steels are more tolerant than hardened steels as they are able to withstand a deformation without fracture. It should be noted that figures 9.9 and 9.5 show slightly different values due to the different measurement devices, different measurement spot sizes, and a possibly altered material flow due to the initially cut holes inside the disk.

Thus, the following conclusions can be derived from the experiment:

- The designed gear is able to transmit high torques within the endurance region.
- Residual stresses are stable under typical operation temperature and loads.

- High local pressure which leads to abrasive wear, high temperatures, and plastic deformation leads to reduced compressive residual stresses.
- The used structural steel has enough forming capability left that local plastic deformation is possible without fracture, i.e., the designed gear is much more tolerant to high local pressure than a hardened steel.

9.4 Shear Cutting Induced Residual Stresses in Part Design and Production

This subchapter gives an outlook on how the residual stresses can be considered in part design on the one hand, and directly in the production. Thus, results and discussion are not strictly divided.

9.4.1 Consideration of Residual Stresses in Part Design

The developed material model and simulation setup can not only be used to explain the material behavior during the shear cutting process, but also to calculate the part's final residual stress state. To accomplish this, an implicit springback step has to be added after the shear cutting operation. Here, the same procedure was used as for the determination of the cut-surfaces after springback.

A comparison of a measured and a calculated residual stress distribution is shown in figure 9.11. Due to the scatter of the simulated stress distribution, the mean over a height of 4 mm located in the middle of the sheet metal thickness was calculated. Only the axial residual stresses are considered as they are not as much affected by the specimen preparation, i.e., the cutting of the sheet metal strip before the measurements. It can be observed that the simulation and experiment show the same trends with a good prediction at the surface and a comparably high error below the surface. Errors in the simulation might be attributed to the neglected temperature dependency, the challenging material testing at high strains and strain rates, time dependent material effects, and load history dependent material behavior. Additionally, small pieces of the specimens were cut out before measuring which is not considered in the simulations. This results in a free boundary in tangential direction which should also lead to lowered residual stresses in axial direction due to the elastic coupling. Nevertheless, the residual stress state can be calculated with sufficient accuracy, especially at the surface where it is of the highest interest. Hence, the model can be used for a relative comparison of different process parameter combinations but is not capable of delivering the measured residual stress state due to the different boundary conditions.

This surface residual stress state can be used together with the results shown in figure 8.13, where the influence of the residual stress state on the resulting fatigue strength were shown. By using the elastic average residual stress obtained from the simulations, the fatigue strength of the edge under bending loads can be estimated within the tested process parameter range. As shear cutting simulation still is a highly challenging task due to the high material deforma-

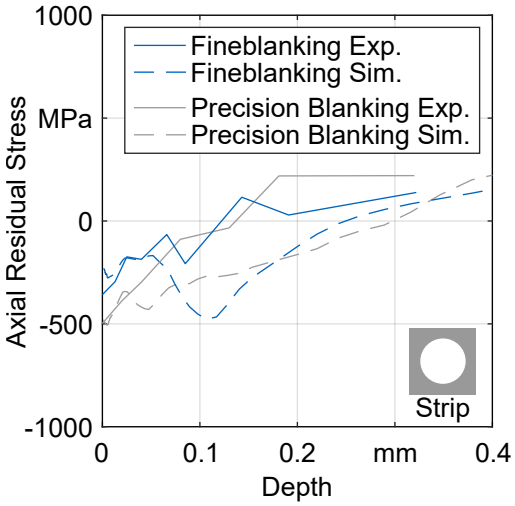

Figure 9.11: Comparison of the measured and simulated residual stress depth distributions for sheet metal strips manufactured with $r_S = 200\,\mu m$, $r_M \leq 20\,\mu m$, and $u_{rel} = 0.5\,\%$.

tion, high temperatures, and strain rates combined with computational challenges, i.e., the very high calculation time and unstable elements during fracture, experimental approaches are more suitable to get a quick estimation of the residual stress state.

9.4.2 Process Monitoring of Residual Stresses

The sheet metal strip grips the punch after cutting. Thus, the punch has to be pulled out of the sheet metal. As explained in chapter 7.2.1, this leads to a radial/tangential springback and is therefore connected with the part's final residual stress state. Consequently, the retraction force which is necessary to pull the punch out of the sheet metal, denoted F_{R2} in chapter 2.1.2, should be correlated with the tangential residual stresses. To be more precise, a higher retraction force should favor the global springback mode in radial/tangential direction and should result in higher tangential residual stresses. This correlation is shown in figure 9.12 exemplary for fineblanking, precision blanking without blank holder, and blanking.

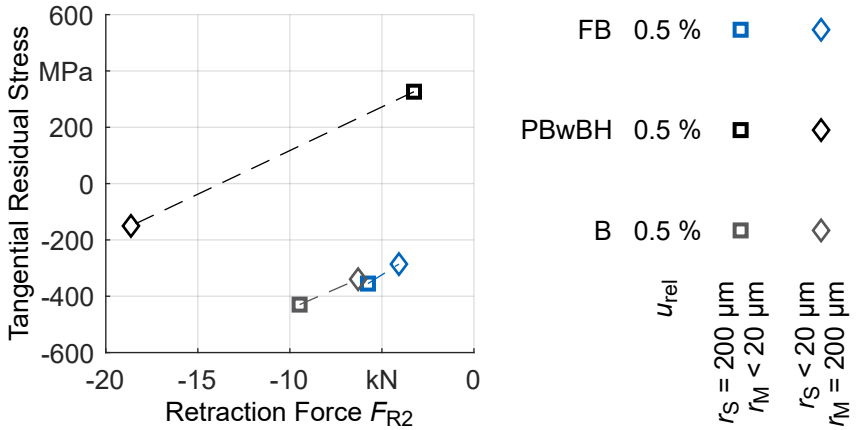

Figure 9.12: Correlation between the retraction force and the tangential residual stress of the manufactured holes.

It can be observed that the measured values follow that consideration. For all three variants higher compressive residual stresses correlate with a higher absolute retraction force. Also, the slopes are similar for the three investigated processes. This means that the strip's tangential residual stresses can be monitored by measuring the retraction force. To accomplish this, comparably cheap measurement equipment consisting of strain gauges or load cells is sufficient and no expensive residual stress measurement devices are needed. An additional benefit is that those force measurement techniques are fast enough to use them inline to detect parts with an unsuitable residual stress state.

10 Conclusion and Outlook

Although it is long known that residual stresses influence the fatigue strength, this effect has not been addressed in detail for the highly economic precision shear cutting processes. As parts manufactured by these processes are widely used, for example in automobile drivetrains or in gears, this offers the possibility to increase the part lifetime. Alternatively, parts with a similar lifetime but a lower weight can be produced by using the higher fatigue strength. Thus, manufacturing cost and/or energy consumption can be reduced wherever shear-cut edges are subject to cyclic loads.

This thesis closes that gap by generating a fundamental understanding of how residual stresses are induced by the investigated precision shear cutting processes, how they can be adjusted and to which extent they are able to increase the part lifetime.

Precision Shear Cutting Induced Residual Stresses

The five investigated processes are fineblanking, blanking with v-ring, precision blanking without blank holder, precision blanking, and blanking. By manufacturing and characterizing blanks and sheet metal strips, the influence of different tool setups on the residual stress state was singled out. Additionally, it was investigated how the process parameters cutting edge preparation and die clearance influence the residual stresses.

For the investigated process variants and cutting edge preparations, it was found that the formation of the final part's residual stress state can be traced back to different springback modes, each of them acting on a different scale and in a different direction. Furthermore, these springback modes could be correlated to changes in the part dimensions. The relevant dimensional changes are the diameter of the manufactured holes and disks and the part bending. During the process, the basis for the springback modes is formed by the stress field induced by the tool. It was found that it is possible to adjust the surface residual stresses of blanks and sheet metal strips in the range of two times the sheet metal's tensile strength. Thus, either compressive or tensile residual stresses at the part surface can be achieved.

While the manufactured holes show compressive residual stresses in most cases, the produced blanks are much more sensitive to a changed process setup or changed process parameters. The tool setup severely influences the residual stress state of the final part. The active element edge preparation has a smaller effect, which is still bigger than that of the die clearance in most cases, at least when no fracture zone is formed.

Regarding the active element edge preparation it was found that a round die edge combined with a sharp punch edge favor compressive residual stresses on the blank's surface while a round punch edge and a sharp die edge favor compressive residual stresses on the sheet metal strip's surface. Additionally, a small die clearance should be chosen when high compressive surface residual stresses are desired, as a fracture zone may show significant tensile stresses.

Fatigue Strength of Edges Manufactured by Precision Shear Cutting

Fatigue tests were performed in the endurance range and in the finite lifetime range. Here, the shear-cut specimens were subject to a bending load. To single out how the residual stress state influences the shear-cut edges' fatigue strength, the effect of the part geometry and hardness were investigated at first.

It was found that the part geometry on a large scale, i.e., flatness of the whole part, significantly influences the resulting fatigue strength. This measure has not been investigated in other publications and should be considered in the future. It should be noted that a higher strip bending, i.e., a reduced flatness, can also cause higher compressive stresses that delay failure.

A higher hardness of the sheet metal strip's cut surface has a positive effect on the part lifetime. Here, the minimal hardness in the highest stressed region was found to be a suitable measure. A v-ring on the other hand has a comparably small effect. The presence of a fracture zone has a negative effect on multiple levels as it is comparably rough, reduces the amount of load bearing surface and may be subject to significant tensile residual stresses. Apart from the rough fracture zone, the roughness has a negligible influence. By comparing the lifetime of specimens that show a comparable geometry and hardness, it was found that a suitable residual stress state can increase the part lifetime by more than 29 %. The flow chart illustrated in figure 10.1 helps to choose a suitable piercing process when a high fatigue strength in the lower load range of the limited lifetime region is desired.

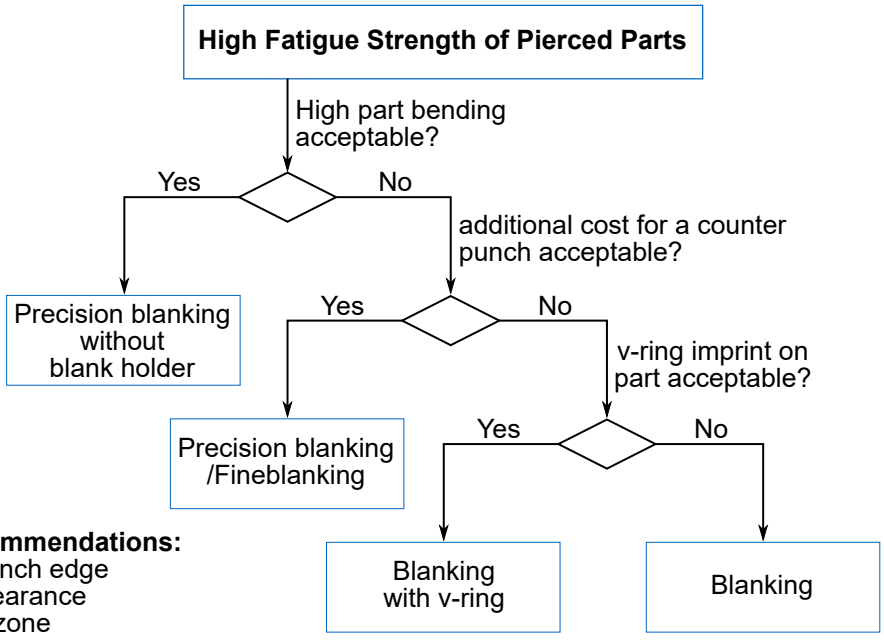

Figure 10.1: Flow chart to achieve a high fatigue strength in the lower load range of the limited lifetime region for piercing.

Industrial Applications

Additional active element edge preparations were investigated to research the robustness of the residual stress state regarding active element wear. It was found that the sheet metal strip is not significantly affected by a changed punch edge radius while a bigger die edge radius causes higher compressive stresses in blanks. Thus, wear is acceptable when compressive residual stresses are desired. The active element roughness also does not significantly influence the residual stress state. A complex geometry was investigated to transfer the results to arbitrary geometries. Especially in axial direction, higher compressive residual stresses were measured on this complex geometry compared to a circular disk.

To use the positive effect of the residual stress state on the fatigue strength, the stresses have to be stable under operational conditions. This was checked by testing convex-concave disks in a specially designed cycloidal gear. It was found that even at high applied torques and typical operation temperatures the residual stress state is stable. Only in regions where significant plastic deformation was observed, smaller residual stresses were measured after the test.

To consider the results in an early design phase, it was shown that process induced residual stresses can be simulated with a sufficient accuracy by using the finite element method. As these simulations are challenging even for comparably simple, axisymmetric geometries and residual stress measurement usually requires expensive testing equipment, an alternative way to get a relative measure for tangential residual stresses was proposed. This approach showed that the punch retraction force and the tangential residual stresses correlate for sheet metal strips. Thus, this force can be used for an estimation of tangential residual stresses or to monitor residual stresses during production.

Outlook

Future works should extend the findings of this thesis to further improve the fatigue behavior. Part bending, which is usually considered an error, can be used as it induces compressive residual stresses on the critical burr side. This can be further improved by a suitable assembly, which flattens the part and thus increases the compressive stresses. This effect could also be used if the part would be bend for example by a convex counter punch or blank holder.

The results should be tested for materials with a higher tensile strength as they usually show a higher fatigue strength. Additionally, harder materials reduce local plastification in regions of direct contact. Thus, the stability of the residual stress state can be improved.

The convex-concave blank geometry showed promising results when a compressive residual stress state is desired on complex geometries. Nevertheless, a different material flow can be expected for small cutting line radii, as they are common in involute gears. These small radii also cause a high amount of die roll as shown in the state of the art. This challenge can be faced by using suitable process parameters. To show the potential of cutting with improved process

parameters, an involute gear has been manufactured, which is shown in figure 10.2.

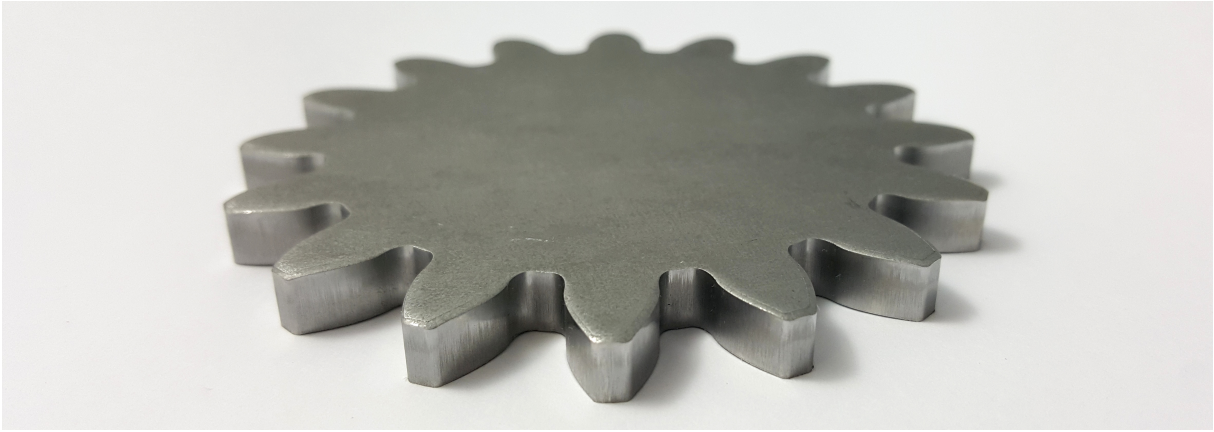

Figure 10.2: Fineblanked involute gear wheel with a small die roll due to improved process parameters.

Almost no die roll is visible, especially in the tooth root. This shows that it is possible to manufacture gear wheels with a very high precision. Nevertheless, calculation guidelines have to be developed for the relevant forming steels to predict the gear wheel lifetime.

For shear-cut gear wheels, a clean cut angle deviation from 90 ° could be useful when two wheels are joined so that their burr sides are meeting. Thus, a crowning, a desired convexity of the contact surfaces, can be achieved as in milled gears.

Finally, cycloidal gears with blanked disks should be further investigated, as the shortened epicyloid geometry is very suitable for blanking compared to the involute geometry. Due to the comparably big radii, a much lower active element wear can be expected. That cycloidal gears with disks made of fine grain structural steel are able to submit high torques was shown in this thesis. By simply adding two additional disks the transmissible torque of the designed drive can be increased to over 100 Nm on the output shaft. This application shows that the benefits of the manufacturing process on the part performance can be combined with the requirements of manufacturing on the part design.

A List of Figures

B List of Tables

C Bibliography

ABRAMS PREMIUM STEEL (2019). *Premium 1.2379*. Data Sheet. URL: http://www.premium-steel.co.uk/images/filedownloads/datasheets/BD2.pdf (visited on 01/11/2019).

ARAVIND, U., U. CHAKKINGAL, P. VENUGOPAL (2019). Investigation of a Modified Fine Piercing Process on Extra Deep Drawing Grade Steel. In: *Journal of Materials Engineering and Performance*, 1–15. DOI: 10.1007/s11665-019-04509-x.

BAER, O., A. FEUERHACK, H. VOIGTS, T. BERGS (2019). Investigation of the Mechanical Punch Loads during Fine Blanking of High-Strength Steels with Cemented Carbide. In: *Procedia Manufacturing* **34**. 47th SME North American Manufacturing Research Conference, NAMRC 47, Pennsylvania, USA., 90–100. ISSN: 2351-9789. DOI: https://doi.org/10.1016/j.promfg.2019.06.125.

BATES, C. (2001). Squeezing out a better stamping. In: *American Machinist*. URL: http://www.ebway.com/wp-content/themes/ebway/pdf/american-machinist-article-2007-09-18.pdf.

BAUMÜLLER NÜRNBERG GMBH (2005). *Drehstrom-Synchronmotoren - DSD 45-100..540 V - DS 45-100..540 V*. Technical data sheet.

BEHRENS, B.-A., T. PIELKA (2011). *Einfluss der Presseneigenschaften auf den Werkzeugverschleiß und die Schnittflächenqualität: Ergebnisse eines Vorhabens der Industriellen Gemeinschaftsforschung (IGF)*. EFB-Forschungsbericht. EFB. ISBN: 9783867763752.

BENKERT, T. (2019). "Blechradkörper für Leichtbauzahnräder - Eine Machbarkeitsstudie zur Herstellung von tiefgezogenen und feingeschnittenen Innenteilen mehrteiliger Zahnräder". Dissertation. München: Technische Universität München.

BERGMANN, W. (2013). *Werkstofftechnik 1: Struktureller Aufbau von Werkstoffen - Metallische Werkstoffe - Polymerwerkstoffe - Nichtmetallisch-anorganische Werkstoffe*. Carl Hanser Verlag GmbH & Company KG. ISBN: 9783446435810.

BLACK, J.T., R.A. KOHSER (2011). *DeGarmo's Materials and Processes in Manufacturing*. Wiley. ISBN: 9780470924679.

BOHDAL, Ł., A. KUŁAKOWSKA, R. PATYK, M. KULAKOWSKI (2016). Numerical Investigations of the Effect of Process Parameters on Residual Stresses, Strains and Quality of Final Product in Blanking Using SPH Method. In: *Materials Science Forum* **862**, 238–245. DOI: 10.4028/www.scientific.net/MSF.862.238.

BOLOTIN, V.V. (1999). *Mechanics of Fatigue*. Mechanical and Aerospace Engineering Series. Taylor & Francis. ISBN: 9780849396632.

BUCHMANN, K. (1962). *Beitrag zur Verschleißbeurteilung beim Schneiden von Stahlfeinblechen*. Forschungsberichte des Landes Nordrhein-Westfalen. Springer Fachmedien Wiesbaden. ISBN: 9783663071266.

CAMMANN, J.H. (1986). "Untersuchungen zur Verschleißminderung an Scherschneidwerkzeugen der Blechbearbeitung durch Einsatz geeigneter Werkzeugstoffe und Beschichtungen". Dissertation. Technische Hochschule Darmstadt.

CASAGRANDE, A., G.P. CAMMAROTA, L. MICELE (2011). Relationship between fatigue limit and Vickers hardness in steels. In: *Materials Science and Engineering: A* **528**.9, 3468–

3473. ISSN: 0921-5093. DOI: https://doi.org/10.1016/j.msea.2011.01.040. URL: http://www.sciencedirect.com/science/article/pii/S0921509311000487.

ČESNIK, D., V. BRATUŠ, B. KOSEC, M. BIZJAK (2012). Distortion of ring type parts during fine-blanking. In: *Metalurgija* **51**, 157–160.

CUBBERLY, W.H., R. BAKERJIAN (1989). *Tool and Manufacturing Engineers Handbook Desk Edition*. Desk Edition. Society of Manufacturing Engineers, 33–9. ISBN: 9780872633513.

DASSAULT SYSTEMES SE (2020[a]). *Axisymmetric solid element library*. Documentation. URL: https://abaqus-docs.mit.edu/2017/English/SIMACAEELMRefMap/simaelm-r-axisymelem.htm (visited on 11/10/2020).

— (2020[b]). *Simulia - Abaqus Unified FEA*. Technical data sheet. URL: https://www.3ds.com/fileadmin/PRODUCTS/SIMULIA/PDF/brochures/simulia-abaqus-unified-fea-brochure.pdf (visited on 01/16/2020).

DEHMANI, H., C. BRUGGER, T. PALIN-LUC, C. MAREAU, S. KOECHLIN (2016). Experimental study of the impact of punching operations on the high cycle fatigue strength of Fe–Si thin sheets. In: *International Journal of Fatigue* **82**, 721–729. ISSN: 0142-1123. DOI: https://doi.org/10.1016/j.ijfatigue.2015.09.030. URL: http://www.sciencedirect.com/science/article/pii/S0142112315003230.

DEMMEL, P. (2014). "In-situ Temperaturmessung beim Scherschneiden". Dissertation. München: Technische Universität München.

DEMMEL, P., R. GOLLE, H. HOFFMANN, R. PETRY (2015). "Schneiden". In: *Blechumformung: Verfahren, Werkzeuge und Maschinen*. Ed. by K. SIEGERT. Berlin, Heidelberg: Springer Berlin Heidelberg, 223–240. ISBN: 978-3-540-68418-3. DOI: 10.1007/978-3-540-68418-3_6. URL: https://doi.org/10.1007/978-3-540-68418-3_6.

DIN 50125 (2016). *Testing of metallic materials - Tensile test pieces*.

DIN 6507 (2018). *Metallic materials - Vickers hardness test - Part 1: Test method*.

DIN 6930-2 (2011). *Stamped steel parts – Part 2: General tolerances*.

DIN 8580 (2016). *Manufacturing processes - Terms and definitions, division*.

DIN 8588 (2013). *Manufacturing processes severing - Classification, subdivision, terms and definitions*.

DIN EN 10149-2 (2013). *Hot rolled flat products made of high yield strength steels for cold forming – Part 2: Technical delivery conditions for thermomechanically rolled steels*.

DIN EN ISO 4287 (2010). *Geometrical Product Specifications (GPS) - Surface texture: Profile method - Terms, definitions and surface texture parameters*.

DIN EN ISO 4957 (2018). *Tool steels (ISO 4957:2018)*.

DIN EN ISO 6892-1 (2009). *Metallic materials - Tensile testing - Part 1: Method of test at room temperature*.

DITTMANN, F., I. PÄTZOLD (2018). *Einfluss der Kantenbearbeitung auf die Festigkeitseigenschaften von Stahl-Feinblechen unter quasistatischer und schwingender Beanspruchung*. Tech. rep. 306. Forschungsvereinigung Automobiltechnik e.V.

DOEGE, E., B.-A. BEHRENS (2010). "Blechumformung". In: *Handbuch Umformtechnik: Grundlagen, Technologien, Maschinen*. Berlin, Heidelberg: Springer Berlin Heidelberg, 259–468.

ISBN: 978-3-642-04249-2. DOI: 10.1007/978-3-642-04249-2_3. URL: https://doi.org/10.1007/978-3-642-04249-2_3.

DOEGE, E., B. FUGGER (1983). Untersuchung der Verschleißmechanismen beim Scherschneiden. In: *Oberflächenbehandlung · Bearbeitungsverfahren*. Ed. by Wolfgang BUNK, Jörn HANSEN, Manfred GEYER. Berlin, Heidelberg: Springer Berlin Heidelberg, 273–310. ISBN: 978-3-642-82059-5.

DOEGE, E., H.-J. KÜHNE (1990). Einfluß des Schneidvorganges und innerer Materialspannungen auf die Maßhaltigkeit beim Scherschneiden von Elektroblechen. In: *Präzisionsumformtechnik*. Ed. by K. LANGE, H. G. DOHMEN. Berlin, Heidelberg: Springer Berlin Heidelberg, 25–26. ISBN: 978-3-642-95606-5.

FEINTOOL INTERNATIONAL HOLDING AG (2002). *Betriebsanleitung für ölhydraulische Feinschneidautomaten, Fabrik-Nr.: 7.8038*. Technical data sheet.

FEISTLE, M., W. VOLK (2015). *Bestimmung der werkstoffspezifischen prozessbeeinflussenden Parameter und Optimierung der Prozessparameter für das Durchsetzen hochfester Stähle: IGF-Nr. 17103 N*. Forschung für die Praxis. Verlag und Vertriebsgesellschaft mbH. ISBN: 978-3-942-54160-2.

FRITSCH, C. (2002). "Einfluss der Prozessparameter auf das Feinschneiden von Aluminiumlegierungen". Dissertation. München: Technische Universität München.

FRITSCH, R. (1983). *Untersuchung zum Einfluß unterschiedlicher Bearbeitungsverfahren auf die Dauerfestigkeit*. Technologiearbeitskreis WZL RWTH Aachen.

FUCHS WISURA GMBH (2018). *WISURA FMO 5001 (ZO 3180) - Feinschneid- und Umformschmierstoff*. Technical data sheet.

GASSNER, E., H. LOWAK (1978). Bedeutung der Unregelmäßigkeit Gauß'scher Zufallsfolgen für die Betriebsfestigkeit. In: *Materialwissenschaft und Werkstofftechnik* **9**.7, 246–256. DOI: 10.1002/mawe.19780090706. eprint: https://onlinelibrary.wiley.com/doi/pdf/10.1002/mawe.19780090706. URL: https://onlinelibrary.wiley.com/doi/abs/10.1002/mawe.19780090706.

GESELLSCHAFT FÜR OPTISCHE MESSTECHNIK (2008). *Industrieller High-End 3D-Digitalisierer*. Technical data sheet.

GEY, M.H. (2008). "Atomspektroskopie". In: *Instrumentelle Analytik und Bioanalytik: Biosubstanzen, Trennmethoden, Strukturanalytik, Applikationen*. Berlin, Heidelberg: Springer Berlin Heidelberg, 291–308. ISBN: 978-3-540-73804-6. DOI: 10.1007/978-3-540-73804-6_7. URL: https://doi.org/10.1007/978-3-540-73804-6_7.

GUPTA, K., N.K. JAIN, R. LAUBSCHER (2017). Chapter 4 - Advances in Gear Manufacturing. In: *Advanced Gear Manufacturing and Finishing*. Ed. by K. GUPTA, N.K. JAIN, R. LAUBSCHER. Academic Press, 67–125. ISBN: 978-0-12-804460-5. DOI: https://doi.org/10.1016/B978-0-12-804460-5.00004-3. URL: http://www.sciencedirect.com/science/article/pii/B9780128044605000043.

HABSCHIED, M., B. de GRAAFF, A. KLUMPP, V. SCHULZE (2015). Fertigung und Eigenspannungen. In: *HTM Journal of Heat Treatment and Materials* **70**.3, 111–121.

HÄFELE, P., L. ISSLER, H. RUOSS (2003a). "Grundlagen der Schwingfestigkeit". In: *Festigkeitslehre — Grundlagen*. Berlin, Heidelberg: Springer Berlin Heidelberg, 327–444. ISBN:

978-3-540-73485-7. DOI: 10.1007/978-3-540-73485-7_11. URL: https://doi.org/10.1007/978-3-540-73485-7_11.

HÄFELE, P., L. ISSLER, H. RUOSS (2003b). "Überelastische Beanspruchung". In: *Festigkeitslehre — Grundlagen*. Berlin, Heidelberg: Springer Berlin Heidelberg, 231–295. ISBN: 978-3-540-73485-7. DOI: 10.1007/978-3-540-73485-7_9. URL: https://doi.org/10.1007/978-3-540-73485-7_9.

HAIBACH, E. (2006). *Betriebsfestigkeit - Verfahren und Daten zur Bauteilberechnung*. 3. korr. u. erg. Aufl. 2006. Berlin Heidelberg: Springer Science & Business Media. ISBN: 978-3-540-29363-7.

HARTMANN, C., H.A. WEISS, P. LECHNER, W. VOLK, S. NEUMAYER, J.H. FITSCHEN, G. STEIDL (2021). Measurement of strain, strain rate and crack evolution in shear cutting. In: *Journal of Materials Processing Technology* **288**, 116872. ISSN: 0924-0136. DOI: https://doi.org/10.1016/j.jmatprotec.2020.116872. URL: http://www.sciencedirect.com/science/article/pii/S0924013620302867.

HAUK, V., H.-J. NIKOLIN (1988). The Evaluation of the Distribution of Residual Stresses of the I. Kind (RS I) and of the II. Kind (RS II) in Textured Materials. In: *Textures and Microstructures* **8**, 693–716. ISSN: 0730-3300. DOI: 10.1155/TSM.8-9.693.

HEYN, E. (1913). "Eigenspannungen, insbesondere Reckspannungen und die dadurch bedingten Krankheitserscheinungen in Konstruktionsteilen". In: *Jahrbuch der Schiffbautechnischen Gesellschaft: Vierzehnter Band*. Berlin, Heidelberg: Springer Berlin Heidelberg, 510–533. ISBN: 978-3-642-92038-7. DOI: 10.1007/978-3-642-92038-7_17. URL: https://doi.org/10.1007/978-3-642-92038-7_17.

— (1921). Über Eigenspannungen in Metallen, ihre Ursachen und Folgen. In: *Naturwissenschaften* **9**.18, 321–325. ISSN: 1432-1904. DOI: 10.1007/BF01487886. URL: https://doi.org/10.1007/BF01487886.

HOFFMANN, H., F. HÖRMANN (2007). Improving the Cut Edge by Counter-Shaving. In: *Sheet Metal 2007*. **344**. Key Engineering Materials. Trans Tech Publications Ltd, 217–224. DOI: 10.4028/www.scientific.net/KEM.344.217.

HOFFMANN, H., R. NEUGEBAUER, G. SPUR (2012). *Handbuch Umformen*. Carl Hanser Verlag GmbH & Company KG. ISBN: 9783446430044.

HOOGEN, M. (1999). "Einfluß der Werkzeuggeometrie auf das Scherschneiden und Reißen von Aluminiumfeinblechen". Dissertation. München: Technische Universität München.

HÖRMANN, F. (2008). "Einfluss der Prozessparameter auf einstufige Scherschneidverfahren zum Ausschneiden mit endkonturnaher Form". Dissertation. München: Technische Universität München.

HYDREL AG (2020). Verzahnungen - Grenzen und Möglichkeiten. URL: https://www.schaeffler.com/remotemedien/media/_shared_media/08_media_library/01_publications/schaeffler_2/brochure/downloads_1/hydrel_faq_verzahnungen_ch_de.pdf (visited on 05/14/2020).

INSTRON (2020). *8872 SERVOHYDRAULIC FATIGUE TESTING SYSTEM - 25 kN*. Technical data sheet. URL: https://www.instron.co.uk/-/media/literature-library/products/2012/10/8872-servohydraulic-fatigue-testing-system.pdf?la=en-GB (visited on 01/16/2020).

JOHNSON, G.R., W.H. COOK (1985). Fracture characteristics of three metals subjected to various strains, strain rates, temperatures and pressures. In: *Engineering Fracture Mechanics* **21**.1, 31–48. ISSN: 0013-7944. DOI: https://doi.org/10.1016/0013-7944(85)90052-9. URL: http://www.sciencedirect.com/science/article/pii/0013794485900529.

KAHLOW, K.J., B. AVITZUR (1974). Void Behavior as Influenced by Pressure and Plastic Deformation. In: *Journal of Engineering for Industry* **96**.3, 901–911. ISSN: 0022-1817. DOI: 10.1115/1.3438459.

KANIT, T., S. FOREST, I. GALLIET, V. MOUNOURY, D. JEULIN (2003). Determination of the size of the representative volume element for random composites: statistical and numerical approach. In: *International Journal of Solids and Structures* **40**.13, 3647–3679. ISSN: 0020-7683. DOI: https://doi.org/10.1016/S0020-7683(03)00143-4. URL: http://www.sciencedirect.com/science/article/pii/S0020768303001434.

KASPARBAUER, M. (1999). *Optimierte Bestimmung der Prozeßkräfte beim Feinschneiden*. München.

KEYENCE CORPORATION (2015). *Konfokales 3D Laserscanning-Mikroskop - VK-X250/ X150/ X120*. Technical data sheet.

KIENZLE, O. (1956). Der Vorgang des Schneidens. In: *MICROTECNIC* **10**.6, 261–264.

— (1963). *Verfahren zur Erzielung glatter Schnittflächen beim vollkantigen Schneiden von Blech*. Forschungsberichte des Landes Nordrhein-Westfalen. Springer Fachmedien Wiesbaden. ISBN: 9783663051503.

KIENZLE, O., F.W. TIMMERBEIL (1955). Die Erzielung sauberer Blech-Schnittflächen durch Schaben. In: *Mitteilungen der Forschungsgesellschaft Blechverarbeitung*, 37–42.

KIM, J., I. WEIDLICH (2017). Identification of Individual District Heating Network Conditions using Equivalent Full Load Cycles. In: *Energy Procedia* **116**, 343–350. DOI: 10.1016/j.egypro.2017.05.081.

KIM, J.D., H. K. KIM, Y. M. HEO, S.H. CHANG (2012). A Study on the Effect of V-Ring Position on the Die Roll Height in Fine Blanking for Special Automobile Seat Recliner Gear. In: *Manufacturing Science and Technology, ICMST2011*. **383**. Advanced Materials Research. Trans Tech Publications Ltd, 7122–7127. DOI: 10.4028/www.scientific.net/AMR.383-390.7122.

KLEEMANN, U., H. ZENNER (2006). Bauteiloberfläche und Schwingfestigkeit – Untersuchungen zum Einfluss der Randschicht auf die Dauerschwingfestigkeit von Bauteilen aus Stahl. In: *Materialwissenschaft und Werkstofftechnik* **37**.5, 349–373. DOI: 10.1002/mawe.200600995. eprint: https://onlinelibrary.wiley.com/doi/pdf/10.1002/mawe.200600995. URL: https://onlinelibrary.wiley.com/doi/abs/10.1002/mawe.200600995.

KLOCKE, F. (2013). "Sheet Metal Separation". In: *Manufacturing Processes 4: Forming*. Berlin, Heidelberg: Springer Berlin Heidelberg, 407–456. ISBN: 978-3-642-36772-4. DOI: 10.1007/978-3-642-36772-4_5. URL: https://doi.org/10.1007/978-3-642-36772-4_5.

KLOCKE, F., C. BRECHER (2016). *Zahnrad- und Getriebetechnik: Auslegung - Herstellung - Untersuchung - Simulation*. Carl Hanser Verlag GmbH & Company KG. ISBN: 9783446431409.

KLOOS, K. H. (1979). Eigenspannungen, Definition und Entstehungsursachen. In: *Materialwissenschaft und Werkstofftechnik* **10**.9, 293–302. DOI: 10.1002/mawe.19790100906. eprint:

https://onlinelibrary.wiley.com/doi/pdf/10.1002/mawe.19790100906. URL: https://onlinelibrary.wiley.com/doi/abs/10.1002/mawe.19790100906.

KOBELEV, V. (2018). "Fatigue of Spring Materials". In: *Durability of Springs*. Cham: Springer International Publishing, 174. ISBN: 978-3-319-58478-2. DOI: 10.1007/978-3-319-58478-2_8. URL: https://doi.org/10.1007/978-3-319-58478-2_8.

KOHTZ, D. (2013). *Wärmebehandlung metallischer Werkstoffe: Grundlagen und Verfahren*. VDI-Buch. Springer Berlin Heidelberg. ISBN: 9783642468353.

KOLBE, M., W. HELLWIG (2015). "Grundlagen des Schneidens". In: *Spanlose Fertigung Stanzen: Präzisionsstanzteile, Hochleistungswerkzeuge, Hochgeschwindigkeitspressen*. Wiesbaden: Springer Fachmedien Wiesbaden, 21–45. ISBN: 978-3-658-09948-0. DOI: 10.1007/978-3-658-09948-0_4. URL: https://doi.org/10.1007/978-3-658-09948-0_4.

KOLLMORGEN EUROPE GMBH (2005). *Synchron-Servomotoren AKM*. Technical data sheet.

KONDO, K., K. MAEDA (1972). "Development of a New Precision Shearing Process: Opposed Dies Shearing Process". In: *Proceedings of the Twelfth International Machine Tool Design and Research Conference*. Ed. by F. KOENIGSBERGER, S. A. TOBIAS. London: Macmillan Education UK, 61–68. ISBN: 978-1-349-01397-5. DOI: 10.1007/978-1-349-01397-5_9. URL: https://doi.org/10.1007/978-1-349-01397-5_9.

KÖNIG, W., F. ROTTER (1982). *Stanzen von Löchern hoher Formtreue und Oberflächengüte in dickwandigen Bauteilen aus Stahl durch Anwendung der Feinschneidtechnologie*. Kernforschungszentrum Karlsruhe GmbH.

KOPP, T.M. (2017). "Einfluss der Werkzeugsteifigkeit auf Scherschneidprozess und Werkzeugverschleiß beim offenen Schnitt". Dissertation. Mün-chen: Technische Universität München.

KOPP, T.M., J. STAHL, P. DEMMEL, P. TRÖBER, R. GOLLE, H. HOFFMANN, W. VOLK (2016). Experimental investigation of the lateral forces during shear cutting with an open cutting line. In: *Journal of Materials Processing Technology* **238**, 49–54. ISSN: 0924-0136. DOI: https://doi.org/10.1016/j.jmatprotec.2016.07.003. URL: http://www.sciencedirect.com/science/article/pii/S0924013616302205.

KRÄMER, W. (1975). Schneiden. In: *Lehrbuch der Umformtechnik - Band 3: Blechumformung*. Ed. by K. LANGE. Springer Berlin Heidelberg. ISBN: 978-3-662-22090-0. DOI: 10.1007/978-3-662-22089-4.

KRINNINGER, M. (2019). "Ansätze zur Reduzierung der prozessbedingten Flitterbildung beim Scherschneiden von Aluminiumblechen im offenen Schnitt". Dissertation. München: Technische Universität München.

KÜHLEWEIN, R. (2003). "Einfluss der Prozessparameter auf das Nachschneiden schergeschnittener Konturen". Dissertation. München: Technische Universität München.

LANGE, K. (2002). *Umformtechnik: Grundlagen*. Engineering online library. Springer Berlin Heidelberg. ISBN: 9783540436867.

LARA, A., I. PICAS, D. CASELLAS (2013). Effect of the cutting process on the fatigue behaviour of press hardened and high strength dual phase steels. In: *Journal of Materials Processing Technology* **213**.11, 1908–1919. ISSN: 0924-0136. DOI: https://doi.org/10.1016/j.jmatprotec.2013.05.003. URL: http://www.sciencedirect.com/science/article/pii/S0924013613001519.

LECHNER, P., G. FUCHS, C. HARTMANN, F. STEINLEHNER, F. ETTEMEYER, W. VOLK (2020). Acoustical and Optical Determination of Mechanical Properties of Inorganically-Bound Foundry Core Materials. In: *Materials* **13**.11. DOI: 10.3390/ma13112531.

LECO CORPORATION (2005). *AMH43 Automatic Micro/Macro-indentation Hardness Testing System*. Instruction Manual.

LEHMANN, M. (1976). "Berechnung und Messung der Kräfte in einem Zykloiden-Kurvenscheiben-Getriebe". Dissertation. Technische Universität München.

— (1981). "Die Beschreibung der Zykloide, ihrer Äquidistanten und Hüllkurven unter besonderer Berücksichtigung der Planeten-Getriebe mit Zykloiden-Kurvenscheiben". Habilitation. Technische Universität München.

LIEBING, H. (1979). "Erzeugung gratfreier Schnittflächen durch Aufteilen des Schneidvorgangs (Konterschneiden)". Dissertation. Stuttgart: Universität Stuttgart.

LINKE, H. (2010). "Fertigung von Stirnradverzahnungen". In: *Stirnradverzahnung*. Hanser, 630–730. ISBN: 9783446414648.

LOIBL, D. (2003). "Standzeit und Teilequalität beim Lochen von Feinblechen mit keramischen Schneidstempeln". Dissertation. München: Technische Universität München. ISBN: 978-3-8979-1328-8.

LUDWIK, P. (1909). *Elemente der Technologischen Mechanik*. Springer Berlin Heidelberg. ISBN: 9783662402931.

MACHERAUCH, E., H. WOHLFAHRT, U. WOLFSTIEG (1973). Zur zweckmäßigen Definition von Eigenspannugen. In: *HTM Härtereitechnische Mitteilungen* **28**.3, 201–211.

MACKENSEN, A., M. GOLLE, R. GOLLE, H. HOFFMANN (2010). Experimental investigation of the cutting force reduction during the blanking operation of AHSS sheet materials. In: *CIRP Annals* **59**.1, 283–286. ISSN: 0007-8506. DOI: https://doi.org/10.1016/j.cirp.2010.03.110. URL: http://www.sciencedirect.com/science/article/pii/S0007850610001113.

MAHR GMBH (2005). *Technische Daten - Konturenvorschubgerät PCV*. Technical data sheet.

— (2007a). *Tastarm-Datenblatt PCV 350 / 59*. Technical data sheet.

— (2007b). *Tastarm-Datenblatt PCV 350-M ± 9*. Technical data sheet.

MANOPULO, N. (2011). "An ALE based FE formulation for the 3D simulation of the fineblanking process". en. PhD thesis. ETH Zurich. ISBN: 978-3-909386-23-9. DOI: 10.3929/ethz-a-006929254.

MARONNE, E., A. GALTIER, J.-L. ROBERT, T. ISHIKAWA (2003). Cutting process influence on fatigue steel sheets properties. In: *WIT Transactions on Engineering Sciences* **40**.

MARTINS, J., L. CARDOSO, J. FRAYMANN, S. BUTTON (2006). Analyses of residual stresses on stamped valves by X-ray diffraction and finite elements method. In: *Journal of Materials Processing Technology* **179**, 30–35. DOI: 10.1016/j.jmatprotec.2006.03.072.

MCKELVEY, S.A., A. FATEMI (2012). Surface finish effect on fatigue behavior of forged steel. In: *International Journal of Fatigue* **36**.1, 130–145. ISSN: 0142-1123. DOI: https://doi.org/10.1016/j.ijfatigue.2011.08.008. URL: http://www.sciencedirect.com/science/article/pii/S0142112311002180.

MEURLING, F., A. MELANDER, J. LINDER, M. LARSSON (2001). The influence of mechanical and laser cutting on the fatigue strengths of carbon and stainless sheet steels. In: *Scandinavian journal of metallurgy* **30**.5, 309–319.

MILELLA, P.P. (2012). *Fatigue and Corrosion in Metals*. Springer Milan. ISBN: 9788847023352.

MOENCH, J., D. CETTIER (2006). *Exzentergetriebe mit Zykloiden-Triebstock-Verzahnung*. Patent.

MOESDIJK, R.D. van de, H.H. WISSELINK, A.H. van den BOOGAARD, J. HUÉTINK, P.J. BOLT, W.H. SILLEKENS (1998). Blanking by means of the finite element method. In: *Fourth World Congress on Computational Mechanics IACM, Buenos Aires, June*. **29**. Citeseer.

MÜLLER, C., M. WÄCHTER, R.r MASENDORF, A. ESDERTS (2017). Distribution functions for the linear region of the SN curve. In: *Materials Testing* **59**.7-8, 625–629.

MÜLLER, D., J. STAHL, I. PÄTZOLD, R. GOLLE, T. TOBIE, W. VOLK, K. STAHL (2021). Influence of Shear Cutting Process Parameters on the Residual Stress State and the Fatigue Strength of Gears. In: *Forming the Future - Proceedings of the 13th International Conference on the Technology of Plasticity*, 2331–2344. DOI: 10.1007/978-3-030-75381-8_195.

MÜLLER-BOLLENHAGEN, C. (2011). "Verformungsinduzierte Martensitbildung bei mehrstufiger Umformung und deren Nutzung zur Optimierung der HCF-und VHCF-Eigenschaf-ten von austenitischem Edelstahlblech". Dissertation. Universität Siegen.

MURAKAMI, S. (2012). *Continuum Damage Mechanics: A Continuum Mechanics Approach to the Analysis of Damage and Fracture*. Solid Mechanics and Its Applications. Springer Netherlands. ISBN: 9789400726666.

NABERTHERM GMBH (1988). *Mod. N 250 / A*. Type label.

NEUGEBAUER, R., M. PUTZ, H. BRÄUNLICH, V. KRÄUSEL (2004). Schneiden und Lochen– ein entwicklungsorientierter Bereich der Blechbearbeitung. In: *Tagungsband zur Internationalen Konferenz „Neuere Entwicklungen in der Blechumformung ". Fellbach*. **11**, 12.

NIEMANN, G., H. WINTER (2003). "Zahnradherstellung". In: *Maschinenelemente: Band 2: Getriebe allgemein, Zahnradgetriebe - Grundlagen, Stirnradgetriebe*. Springer Berlin Heidelberg, 230–242. ISBN: 978-3-662-11873-3.

OERLIKON BALZERS COATING GERMANY GMBH (2019). *BALINIT ADVANCED Series: Good times for round edges*. Technical data sheet. (Visited on 05/09/2019).

PÄTZOLD, I., F. DITTMANN, M. FEISTLE, R. GOLLE, P. HÄFELE, H. HOFFMANN, W. VOLK (2017). Influence of shear cutting parameters on the fatigue behavior of a dual-phase steel. In: *Journal of Physics: Conference Series* **896**.1, 012107. URL: http://stacks.iop.org/1742-6596/896/i=1/a=012107.

PURWO, K. (2014). "Improvement of Strength and Quality of Sheared Edge in Punching of High Strength Steel Sheets". Dissertation. Toyohashi: Toyohashi University of Technology.

RADAJ, D. (2003). "Weitere Einflußgrößen zur Schwingfestigkeit". In: *Ermüdungsfestigkeit: Grundlagen für Leichtbau, Maschinen- und Stahlbau*. Berlin, Heidelberg: Springer Berlin Heidelberg, 53–112. ISBN: 978-3-662-07107-6. DOI: 10.1007/978-3-662-07107-6_3. URL: https://doi.org/10.1007/978-3-662-07107-6_3.

REIHLE, M.M. (2015). "Entstehung und Ausprägung von Eigenspannungen in Verbundgussteilen". Dissertation. München: Technische Universität München.

RICE, J.R., D.M. TRACEY (1969). On the ductile enlargement of voids in triaxial stress fields. In: *Journal of the Mechanics and Physics of Solids* **17**.3, 201–217.

RICHTER, F. (2020). *The Physical Properties of Steels*. Data Sheet. URL: https://www.tugraz.at/fileadmin/user_upload/Institute/IEP/Thermophysics_Group/Files/Staehle-Richter.pdf (visited on 01/22/2020).

ROMANOWSKI, W.P. (1959). *Handbuch der Stanzereitechnik*. Berlin: VEB Verlag Technik.

ROSAKIS, A., J. MASON, G. RAVICHANDRAN (1993). The Conversion of Plastic Work to Heat Around a Dynamically Propagating Crack in Metals. In: *Journal of the Mechanical Behavior of Materials* **4**, 12. DOI: 10.1515/JMBM.1993.4.4.375.

SALZGITTER FLACHSTAHL GMBH (2011). *S355MC - High-strength steels for cold-forming, thermomechanically-rolled*. Data Sheet. URL: https://www.salzgitter-flachstahl.de/fileadmin/mediadb/szfg/informationsmaterial/produktinformationen/warmgewalzte_produkte/eng/S355MC.pdf (visited on 01/11/2019).

SCHAJER, G.S. (1988). Measurement of non-uniform residual stresses using the hole-drilling method. Part I—Stress calculation procedures. In: *Journal of Engineering Materials and Technology* **110**.

SCHMIDT, R.A., M. HELLMANN, R. BURKHARD, P. RADEMACHER, P. HÖFEL, F. BIRZER, H. HOFFMANN (2007). *Cold forming and Fineblanking*. 2nd ed. München Wien: Carl Hanser Verlag. ISBN: 978-3446413504.

SCHULER GMBH (1996). "Blechumformung und Schneiden". In: *Handbuch der Umformtechnik*. Berlin, Heidelberg: Springer Berlin Heidelberg, 123–404. ISBN: 978-3-662-07703-0. DOI: 10.1007/978-3-662-07703-0_4.

SCHUMANN, H. (1975). Verformungsinduzierte Martensitbildung in metastabilen austenitischen Stählen. In: *Kristall und Technik* **10**.4, 401–411. DOI: 10.1002/crat.19750100409. URL: https://onlinelibrary.wiley.com/doi/abs/10.1002/crat.19750100409.

SENN, S., M. LIEWALD (2018). Numerical investigation of a new sheet metal shear cutting tool design to increase the part quality by superposed compression stress. In: *Journal of Physics: Conference Series* **1063**, 012181. DOI: 10.1088/1742-6596/1063/1/012181.

— (2019). Investigation of a new sheet metal shear cutting tool design to increase the part quality by superposed compression stress. In: *IOP Conference Series: Materials Science and Engineering* **651**, 012088. DOI: 10.1088/1757-899X/651/1/012088.

SHIRASAWA, H. (1994). Concurrent Influence of an Increase in Tensile Strength and Thickness Reduction on Fatigue Strength of Hot Rolled Steel. In: *Isij International - ISIJ INT* **34**, 285–289. DOI: 10.2355/isijinternational.34.285.

SINT TECHNOLOGY S.R.L. (2015). *Restan - system for measuring residual stress by the hole-drilling method*. Manual.

SONSINO, C.M. (2005). Dauerfestigkeit–Eine Fiktion. In: *Konstruktion* **57**.4, 87–92.

SPIESS, L., G. TEICHERT, R. SCHWARZER, H. BEHNKEN, C. GENZEL (2009). "Röntgenographische Spannungsanalyse". In: *Moderne Röntgenbeugung: Röntgendiffraktometrie für Materialwissenschaftler, Physiker und Chemiker*. Wiesbaden: Vieweg + Teubner, 305–382. ISBN: 978-3-8349-9434-9. DOI: 10.1007/978-3-8349-9434-9_10. URL: https://doi.org/10.1007/978-3-8349-9434-9_10.

STAHL, J. (2015). “Aufbau, Durchführung und Validierung einer thermomechanisch gekoppelten Scherschneidsimulation unter Berücksichtigung der Temperaturabhängigkeit von Materialmodell und Bruchkriterium”. MA thesis. Technische Universität München.

STAHL, J., D. MÜLLER, A. NÜRNBERGER, T. GRESS, P. LECHNER, T. TOBIE, K. STAHL, W. VOLK (2021). On the Formation of Residual Stresses in Blanks Manufactured by Near-Net-Shape-Blanking Processes. In: *Journal of Materials Processing Technology*. Status: under review.

STAHL, J., D. MÜLLER, I. PÄTZOLD, R. GOLLE, T. TOBIE, W. VOLK, K. STAHL (2019). The Influence of Residual Stresses Induced by Near-Net-Shape Blanking Processes on the Fatigue Behavior under Bending Loads. In: *IOP Conference Series: Materials Science and Engineering* **651**, 012086. DOI: 10.1088/1757-899x/651/1/012086.

STAHL, J., D. MÜLLER, T. TOBIE, R. GOLLE, W. VOLK, K. STAHL (2019). Residual stresses in parts manufactured by near-net-shape-blanking. In: *Production Engineering* **13**.2, 181–188.

STAHL, J., I. PÄTZOLD, R. GOLLE, C. SUNDERKÖTTER, H. SIEURIN, W. VOLK (2020). Effect of One-and Two-Stage Shear Cutting on the Fatigue Strength of Truck Frame Parts. In: *Journal of Manufacturing and Materials Processing* **4**.2, 52.

STENICO, A. (2007). “Werkstoffmechanische Untersuchungen zur Zahnfußtragfähigkeit einsatzgehärteter Zahnräder”. Dissertation. München: Technische Universität München.

STROMBERGER, C., T. THOMSEN (1965). Glatte Lochwände beim Lochen. In: *Werkstatt und Betrieb* **98**, 739–747.

SU, C.J., X.H. DONG, S.M. GUO, Q.L. LI, T.T. LI (2014). Research on parameters optimization of bilateral ring gear blank-holder in thick-plate fine blanking. In: *Frattura ed Integrita Strutturale* **30**, 502–514. DOI: 10.3221/IGF-ESIS.30.61.

SUBRAMONIAN, S., T. ALTAN, C. CAMPBELL, B. CIOCIRLAN (2013). Determination of forces in high speed blanking using FEM and experiments. In: *Journal of Materials Processing Technology* **213**.12, 2184–2190. ISSN: 0924-0136. DOI: https://doi.org/10.1016/j.jmatprotec.2013.06.014. URL: http://www.sciencedirect.com/science/article/pii/S0924013613002057.

TEKKAYA, A.E., P.-O. BOUCHARD, S. BRUSCHI, C.C. TASAN (2020). Damage in metal forming. In: *CIRP Annals* **69**.2, 600–623. ISSN: 0007-8506. DOI: https://doi.org/10.1016/j.cirp.2020.05.005. URL: http://www.sciencedirect.com/science/article/pii/S0007850620301384.

THEIMERT, P.-H. (1975). *Kräfte und Werkstoffverhalten beim Lochen von Grobblechen: die Fragwürdigkeit der Formulierung von Schnittkraft-und Rückzugkraftgesetzen*. Hanser.

THOMAS, D.J., M.T. WHITTAKER, G.W. BRIGHT, Y. GAO (2011). The influence of mechanical and CO2 laser cut-edge characteristics on the fatigue life performance of high strength automotive steels. In: *Journal of Materials Processing Technology* **211**.2, 263–274. ISSN: 0924-0136. DOI: https://doi.org/10.1016/j.jmatprotec.2010.09.018. URL: http://www.sciencedirect.com/science/article/pii/S0924013610003006.

TIMMERBEIL, F.W. (1957). Untersuchung des Schneidvorganges bei Blech, insbesondere beim geschlossenen Schnitt - Erster Teil: Der Schneidvorgang bei scharfen Werkzeugkanten - Die Schneidkräfte. In: *Werkstattstechnik und Maschinenbau* **47**.7.

TOTTEN, G.E., M.A.H. HOWES, T. INOUE (2002). *Handbook of residual stress and deformation of steel*. Materials Park Ohio: ASM International. ISBN: 0871707292.

TRÖBER, P., R. GOLLE, W. VOLK (2015). Influence of lubrication on the measured thermoelectric volt-age and temperature in the forming zone when embossing S355MC. In: *Dry Metal Forming Open Access Journal*.

VDI 2906-1 (1994). *Quality of cut faces of (sheet) metal parts after cutting, blanking, trimming or piercing - General introduction, characteristic values, materials*.

VDI 2906-2 (1994). *Quality of cut faces of (sheet) metal parts after cutting, blanking, trimming or piercing - Shearing, form of sheared edge and characteristic values*.

VDI 2906-5 (1994). *Quality of cut faces of (sheet) metal parts after cutting, blanking, trimming or piercing - Fine blanking*.

VDI 2906-6 (1994). *Quality of cut faces of (sheet) metal parts after cutting, blanking, trimming or piercing - Counter shearing*.

VDI 3345 (1980). *Fine blanking*.

VITZTHUM, S., M. EDER, C. HARTMANN, W. VOLK (2018). Investigation on strain dependent elastic behavior for accurate springback analysis. In: *Journal of Physics: Conference Series* **1063**, 012118. DOI: 10.1088/1742-6596/1063/1/012118. URL: https://doi.org/10.1088%2F1742-6596%2F1063%2F1%2F012118.

VOCE, E. (1948). The relationship between stress and strain for homogeneous deformation. In: *Journal of the Institute of Metals* **74**, 537–562.

VOLK, W., P. GROCHE, A. BROSIUS, A. GHIOTTI, B.L. KINSEY, M. LIEWALD, L. MADEJ, J. MIN, J. YANAGIMOTO (2019). Models and modelling for process limits in metal forming. In: *CIRP Annals* **68**.2, 775–798. ISSN: 0007-8506. DOI: https://doi.org/10.1016/j.cirp.2019.05.007. URL: http://www.sciencedirect.com/science/article/pii/S0007850619301647.

VOLK, W., A. KINDSMÜLLER, I. PÄTZOLD, J. STAHL (2018). *Ursache und Vorhersage von hochkommenden Stanzbutzen*. 1. Aufl. Hannover: Europäische Forschungsgesellschaft für Blechverarbeitung e.V. (EFB). ISBN: 978-3-867-76547-3.

VOLK, W., J. STAHL (2015). Shear Cutting. In: *CIRP Encyclopedia of Production Engineering*. SpringerLink. DOI: 10.1007/978-3-642-35950-7_16,823-1.

— (2020). *Machbarkeits- und Geometrievorhersage von Blechbauteilen mit Durchsetzungen aus hoch- und höchstfesten Stählen*. iGF Forschungsbericht. ISBN: 978-3-946885-26-9.

WALKER, T. (1997). Print Tolerances Available Out of the Die. In: *American Machinist*. URL: http://www.ebway.com/wp-content/themes/ebway/pdf/gripflow-metal-forming-magazine.pdf.

WEISS, H.A. (2019). "Fertigung effizienter Elektromotoren". Dissertation. München: Technische Universität München.

WEISS, H.A., N. LEUNING, S. STEENTJES, K. HAMEYER, T. ANDORFER, S. JENNER, W. VOLK (2017). Influence of shear cutting parameters on the electromagnetic properties of non-oriented electrical steel sheets. en. In: *Journal of Magnetism and Magnetic Materials* **421**, 250–259. DOI: 10.1016/j.jmmm.2016.08.002.

WEISSBACH, W., M. DAHMS (2007). *Werkstoffkunde: Strukturen, Eigenschaften, Prüfung*. Viewegs Fachbücher der Technik. Vieweg+Teubner Verlag. ISBN: 9783834802958.

WENZEL PRÄZISION GMBH (2012). *3D-Koordinatenmessgerät (KMG) LH 87*. Technical data sheet.

WESNER, T. (2017). "Virtuelle und experimentelle Methoden zur Voraussage des Prozessfensters beim Feinschneiden". de. PhD thesis. Zürich: ETH Zurich. ISBN: 978-3-906327-67-9. DOI: 10.3929/ethz-a-010866486.

WITHERS, P., H.K.D.H. BHADESHIA (2001a). Residual stress Part 1 - Measurement techniques. In: *Materials Science and Technology* **17**, 355–365.

— (2001b). Residual stress Part 2 – Nature and origins. In: *Materials Science and Technology* **17**, 366–375.

YASUTOMI, T., S. YONEMURA, T. YOSHIDA, M. MIZUMURA, S. HIWATASHI (2017). Blanking Method with Aid of Scrap to Reduce Tensile Residual Stress on Sheared Edge. In: *Journal of Physics: Conference Series* **896**.1, 012098. URL: http://stacks.iop.org/1742-6596/896/i=1/a=012098.

ZAIZEN, Y., T. OMURA, M. FUKUMURA, K. SENDA, H. TODA (2016). Evaluation of stress distribution due to shearing in non-oriented electrical steel by using synchrotron radiation. In: *AIP Advances* **6**.5, 055926. DOI: 10.1063/1.4944342.

ZHAO, P.J., Z.H. CHEN, C.F. DONG (2016). Experimental and numerical analysis of micromechanical damage for DP600 steel in fine-blanking process. In: *Journal of Materials Processing Technology* **236**, 16–25. ISSN: 0924-0136. DOI: https://doi.org/10.1016/j.jmatprotec.2016.05.002. URL: http://www.sciencedirect.com/science/article/pii/S0924013616301327.

ZHENG, P.F., L.C. CHAN, T.C. LEE (2005). Numerical analysis of the sheet metal extrusion process. In: *Finite Elements in Analysis and Design* **42**.3, 189–207. ISSN: 0168-874X. DOI: https://doi.org/10.1016/j.finel.2005.06.002. URL: http://www.sciencedirect.com/science/article/pii/S0168874X0500079X.

ZIMMERMANN, M., F. KLOCKE, F. SCHONGEN, B. FELDHAUS (2011). Fine blanking of helical gears - Finite element simulations and first experimental results. In: *Special Edition: 10th International Conference on Technology of Plasticity, ICTP 2011*, 581–585.

ZWICKROELL GMBH (1998). *Betriebsanleitung Material Prüfmaschine*. Instruction Manual.

D Publications

Die nachfolgend aufgeführten Zeitschriftenaufsätze, Konferenzbeiträge und Präsentationen entstanden während meiner Zeit als wissenschaftlicher Mitarbeiter an der Technischen Universität München. Wesentliche Teile dieser Dissertation wurden unter meiner Autoren- und Koautorenschaft bereits vorab als Zeitrschriftenaufsätze, Konferenzbeiträge und Präsentationen veröffentlicht. Alle relevanten Vorveröffentlichungen ($*$) sind entsprechend der gültigen Promotionsordnung ordnungsgemäß gemeldet. Sie sind deshalb nicht zwangsläufig im Detail einzeln referenziert. Vielmehr wurde bei der Referenzierung eigener Vorveröffentlichungen Wert auf Verständlichkeit und inhaltlichen Bezug gelegt.

The following journal papers, conference proceedings, and presentations arose during my time as a research associate at the Technical University of Munich. Several parts of this thesis were published under my author and co-authorship beforehand in journal papers, conference proceedings, and presentations. All relevant prior printed publications ($*$) are registered according to the valid doctoral regulations. However, not all of them are quoted explicitly everywhere as they are part of this present work being official documents. Whether these personal prior printed publications were referenced depended on maintaining comprehensibility and providing all necessary context.

FEISTLE, M., M. KRINNINGER, I. PAETZOLD, J. STAHL, R. GOLLE, W. VOLK (2017). Design and conceptualization of a cutting tool to investigate the influence of the shear cutting-process on edge crack sensitivity. In: *Journal of Physics: Conference Series* **896**, 012106. DOI: 10.1088/1742-6596/896/1/012106.

$*$ FRANCESCHI, A., J. STAHL, C. KOCK, R. SELBMANN, S. ORTMANN-ISHKINA, A. JOBST, M. MERKLEIN, B. KUHFUSS, M. BERGMANN, B.-A. BEHRENS, W. VOLK, P. GROCHE (2021). Strategies for residual stress adjustment in bulk metal forming. In: *Archive of Applied Mechanics* **91**, 3557-3577. ISSN: 1432-0681. DOI: 10.1007/s00419-021-01903-7. URL: https://link.springer.com/article/10.1007/s00419-021-01903-7.

GREß, T., M. GRUBER, J. STAHL, S. WITTMANN, F. STEINLEHNER, V. GLÜCK NARDI, B. TONN, W. VOLK (2020). Experimental and numerical investigations into the deformation and fracture behavior of intermetallics and base materials in as-cast Al-Cu compounds. In: *Materials Today Communications* **25**, 101278. ISSN: 2352-4928. DOI: 10.1016/j.mtcomm.2020.101278. URL: http://www.sciencedirect.com/science/article/pii/S2352492820322893.

GREß, T., T. MITTLER, H. CHEN, J. STAHL, S. SCHMID, N. BEN KHALIFA, W. VOLK (2020). Production of aluminum AA7075/6060 compounds by die casting and hot extrusion. In: *Journal of Materials Processing Technology* **280**, 116594. ISSN: 0924-0136. DOI: 10.1016/j.jmatprotec.2020.116594. URL: http://www.sciencedirect.com/science/article/pii/S0924013620300078.

GREß, T., J. STAHL, T. MITTLER, L. SPANO, H. CHEN, N. BEN KHALIFA, W. VOLK (2019). Mechanical characterization of as-cast AA7075/6060 and CuSn6/Cu99.5 compounds using an experimental and numerical push-out test. In: *Materials Science and Engineering: A* **751**, 214–225. ISSN: 0921-5093. DOI: 10.1016/j.msea.2019.02.080. URL: http://www.sciencedirect.com/science/article/pii/S0921509319302540.

KOPP, T.M., J. STAHL, P DEMMEL, P. TRÖBER, R. GOLLE, H. HOFFMANN, W. VOLK (2016). Experimental investigation of the lateral forces during shear cutting with an open cutting line. In: *Journal of Materials Processing Technology* **238**, 49–54. ISSN: 0924-0136. DOI: 10.1016/j.jmatprotec.2016.07.003. URL: http://www.sciencedirect.com/science/article/pii/S09

24013616302205.

LECHNER, P., J. STAHL, F. ETTEMEYER, B. HIMMEL, B. TANANAU-BLUMENSCHEIN, W. VOLK (2018). Fracture Statistics for Inorganically-Bound Core Materials. In: *Materials* **11**.11. ISSN: 1996-1944. DOI: 10.3390/ma11112306. URL: https://www.mdpi.com/1996-1944/11/11/2306.

∗ MÜLLER, D., J. STAHL, I. NÜRNBERGER, R. GOLLE, T. TOBIE, W. VOLK, K. STAHL (2021). Shear Cutting Induced Residual Stresses in Involute Gears and Resulting Tooth Root Bending Strength of a Fineblanked Gear. In: *Archive of Applied Mechanics* **91**, 3679-3692. ISSN: 1432-0681. DOI: 10.1007/s00419-021-01915-3. URL: https://link.springer.com/article/10.1007/s00419-021-01903-7.

∗ MÜLLER, D., J. STAHL, I. PÄTZOLD, R. GOLLE, T. TOBIE, W. VOLK, K. STAHL (2021). Influence of Shear Cutting Process Parameters on the Residual Stress State and the Fatigue Strength of Gears In: *Forming the Future – Proceedings of the 13th International Conference on the Technology of Plasticity*. 2331-2344, DOI: 10.1007/978-3-030-75381-8_195.

∗ STAHL, J., D. MÜLLER, A. NÜRNBERGER, T. GREß, P. LECHNER, T. TOBIE, K. STAHL, W. VOLK (2021). On the Formation of Residual Stresses in Blanks Manufactured by Near-Net-Shape-Blanking Processes. In: *Journal of Materials Processing Technology*. Status: in review process.

∗ STAHL, J., D. MÜLLER, I. PÄTZOLD, R. GOLLE, T. TOBIE, W. VOLK, K. STAHL (2019). The Influence of Residual Stresses Induced by Near-Net-Shape Blanking Processes on the Fatigue Behavior under Bending Loads. In: *IOP Conference Series: Materials Science and Engineering* **651**, 012086. DOI: 10.1088/1757-899x/651/1/012086.

∗ STAHL, J., D. MÜLLER, T. TOBIE, R. GOLLE, W. VOLK, K. STAHL (2019). Residual stresses in parts manufactured by near-net-shape-blanking. In: *Production Engineering* **13**.2, 181–188. DOI: 10.1007/s11740-018-0865-5.

∗ STAHL, J., I. PÄTZOLD, R. GOLLE, C. SUNDERKÖTTER, H. SIEURIN, W. VOLK (2020). Effect of One-and Two-Stage Shear Cutting on the Fatigue Strength of Truck Frame Parts. In: *Journal of Manufacturing and Materials Processing* **4**.2, 52. DOI: 10.3390/jmmp4020052

∗ STAHL, J., I. PÄTZOLD, L. VAN DEN BOSCH, A. KINDSMÜLLER, R. GOLLE, W. VOLK (2021). The frictional force between slug and die in shear cutting after material separation. In: *Key Engineering Materials* **883**, 285-293. DOI: 10.4028/www.scientific.net/KEM.883.285. URL: https://www.scientific.net/KEM.883.285.

∗ STAHL, J., P. TRÖBER, M. FEISTLE, R. GOLLE, W. VOLK (2017). An inverse approach for the geometry prediction of sheet-metal parts with embossings made of high- and ultra-high strength steels. In: *Journal of Physics: Conference Series* **896**, 012097. DOI: 10.1088/1742-6596/896/1/012097.

VOLK, W., A. KINDSMÜLLER, I. PÄTZOLD, J. STAHL (2018). Ursache und Vorhersage von hochkommenden Stanzbutzen. 1. Aufl. Hannover: Europäische Forschungsgesellschaft für Blechverarbeitung e.V. (EFB). ISBN: 978-3-867-76547-3.

VOLK, W., M. KRINNINGER, J. STAHL (2018). Inverse Calibration of a Shear Cutting Simulation and Investigation of Various Shear Cutting Parameters. In: *Forming Technology Forum 2018*.

VOLK, W., J. STAHL (2015). Shear Cutting. In: *CIRP Encyclopedia of Production Engineering*. SpringerLink. DOI: 10.1007/978-3-642-35950-7_16823-1

VOLK, W., J. STAHL (2020): Machbarkeits- und Geometrievorhersage von Blechbauteilen mit Durchsetzungen aus hoch- und höchstfesten Stählen. iGF Forschungsbericht. ISBN: 978-3-946885-26-9.

VOLK, W., S. VOGT, J. STAHL, S. PRAUSER (2019). Introduction to residual stresses in production technology. In: *Production Engineering* **13**.2, 119–121. DOI: 10.1007/s11740-019-00881-8.

E Student Theses

The student theses listed below were carried out in the context of the present dissertation at the Chair of Metal Forming and Casting at the Technical University of Munich. The task and processing as well as the evaluation, interpretation and presentation of results were carried out under the scientific supervision of Jens Stahl. Some of the results obtained have been incorporated into this work.

Nürnberger, A.: Experimentelle und simulationsgestützte Untersuchung feingeschnittener Verzahnungen

Nürnberger, A.: Konstruktion eines Cyclo-Getriebes mit feingeschnittenen Kurvenscheiben

Sanal, U.: Verbesserung der Robustheit der Finite-Elemente Simulation von Near-Net-Shape-Blanking-Prozessen und Analyse des entstehenden Eigenspannungsverlaufs

Sommer, K.: Analyse und Bewertung der Eigenspannungsmessung mittels Nanoindentation

F Appendix

F.1 Calculation of Process Forces

The maximum cutting force F_{Smax} is calculated according to Schmidt et al., 2007 by considering the sheet metal material's tensile strength R_m (see table 5.2), the sheet thickness s, the length of the cutting line l_S, and a correction factor of 0.9:

$$F_{Smax} = 0.9\, R_m\, s\, l_S = 0.9\, R_m\, s\, \pi\, d_{ActiveElement} = 498.8\,\text{kN} \tag{F.1}$$

The blank holder force should be 30 % of the maximum cutting according to Loibl, 2003. As a comparably small sheet metal strip is investigated in this thesis, a higher blank holder force of 35 % is chosen an rounded up:

$$F_{NH} = 0.35\, F_{Smax} = 174.6\,\text{kN} \approx 200\,\text{kN} \tag{F.2}$$

V-ring force can be calculated according to Schmidt et al., 2007 by using the material's tensile strength R_m, the height of the v-ring h_{RZ}, the length of the v-ring l_{RZ}, and a correction factor of approximately 4:

$$F_{RZ} = 4\, R_m\, l_{RZ}\, h_{RZ} = 406.4\,\text{kN} \approx 450\,\text{kN} \tag{F.3}$$

Counter punch force according to Schmidt et al., 2007 should apply a pressure of 20 to 70 MPa. Thus, it can be calculated by:

$$F_{GH} = 70\,\text{MPa}\, \pi\, (0.5\, d_{ActiveElement})^2 = 197.8\,\text{kN} \approx 200\,\text{kN} \tag{F.4}$$

F.2 Cut-Surface Characteristics

Table F.1: Cut-surface characteristics of the blanks manufactured by the five different precision shear cutting processes.

Precision Shear Cutting Process	u_{rel}	Die Roll	Clean Cut	Burr	Angle
r_S = 200 µm, r_M < 20 µm					
FB	0.5 %	5.0 ± 0.2 %	95.5 ± 0.3 %	319 ± 95 µm	89.9 ± 0.1 °
FB	1.0 %	4.5 ± 0.4 %	94.7 ± 1.6 %	214 ± 35 µm	89.9 ± 0.1 °
FB	3.0 %	5.0 ± 0.6 %	50.0 ± 6.2 %	177 ± 44 µm	90.5 ± 0.1 °
BV	0.5 %	4.9 ± 0.2 %	94.9 ± 0.6 %	305 ± 40 µm	88.3 ± 0.1 °
PBwBH	0.5 %	8.6 ± 0.4 %	39.7 ± 2.5 %	171 ± 59 µm	89.0 ± 0.2 °
PB	0.5 %	7.4 ± 0.2 %	92.7 ± 0.4 %	175 ± 36 µm	89.6 ± 0.1 °
B	0.5 %	6.9 ± 0.3 %	93.2 ± 0.6 %	200 ± 44 µm	89.1 ± 0.1 °
B	1.0 %	7.3 ± 0.3 %	90.1 ± 1.5 %	221 ± 27 µm	89.4 ± 0.2 °
B	3.0 %	8.1 ± 0.4 %	41.9 ± 11.5 %	176 ± 38 µm	89.8 ± 0.1 °
r_S < 20 µm, r_M = 200 µm					
FB	0.5 %	5.8 ± 1.4 %	95.1 ± 0.4 %	38 ± 32 µm	89.9 ± 0.1 °
FB	1.0 %	6.3 ± 0.3 %	92.0 ± 3.5 %	21 ± 20 µm	90.0 ± 0.1 °
FB	3.0 %	7.2 ± 0.4 %	47.9 ± 9.0 %	18 ± 18 µm	90.3 ± 0.2 °
BV	0.5 %	5.3 ± 0.2 %	94.6 ± 0.7 %	59 ± 61 µm	88.2 ± 0.2 °
PBwBH	0.5 %	9.8 ± 0.3 %	90.2 ± 0.6 %	68 ± 39 µm	89.5 ± 0.1 °
PB	0.5 %	8.0 ± 0.3 %	92.3 ± 0.3 %	61 ± 29 µm	89.6 ± 0.1 °
B	0.5 %	7.7 ± 0.3 %	92.3 ± 0.6 %	113 ± 56 µm	89.0 ± 0.1 °
B	1.0 %	7.8 ± 0.3 %	89.3 ± 1.7 %	9 ± 13 µm	89.2 ± 0.1 °
B	3.0 %	9.0 ± 0.3 %	53.5 ± 10.3 %	15 ± 10 µm	89.4 ± 0.2 °

Table F.2: Cut-surface characteristics of the strips manufactured by the five different precision shear cutting processes.

Precision Shear Cutting Process	u_{rel}	**Die Roll**	**Clean Cut**	**Burr**	**Angle**
r_S = 200 µm, r_M < 20 µm					
FB	0.5 %	5.4 ± 0.4 %	97.6 ± 0.4 %	212 ± 84 µm	90.1 ± 0.1 °
FB	1.0 %	6.7 ± 0.3 %	93.7 ± 3.0 %	48 ± 45 µm	90.2 ± 0.2 °
FB	3.0 %	6.7 ± 0.7 %	81.3 ± 4.9 %	46 ± 34 µm	90.2 ± 0.1 °
BV	0.5 %	6.0 ± 0.4 %	97.0 ± 0.5 %	159 ± 34 µm	90.0 ± 0.1 °
PBwBH	0.5 %	6.6 ± 0.3 %	90.3 ± 0.6 %	55 ± 29 µm	83.1 ± 0.3 °
PB	0.5 %	6.8 ± 0.3 %	93.2 ± 0.5 %	71 ± 44 µm	89.2 ± 0.1 °
B	0.5 %	6.3 ± 0.2 %	93.7 ± 0.6 %	94 ± 66 µm	89.4 ± 0.1 °
B	1.0 %	6.6 ± 0.2 %	87.7 ± 2.0 %	26 ± 18 µm	89.5 ± 0.1 °
B	3.0 %	7.0 ± 0.1 %	63.8 ± 7.2 %	33 ± 15 µm	89.8 ± 0.4 °
r_S < 20 µm, r_M = 200 µm					
FB	0.5 %	4.9 ± 0.4 %	97.5 ± 0.5 %	212 ± 62 µm	90.0 ± 0.1 °
FB	1.0 %	5.0 ± 0.2 %	95.2 ± 3.9 %	153 ± 42 µm	90.0 ± 0.1 °
FB	3.0 %	5.0 ± 0.3 %	67.6 ± 18.1 %	195 ± 62 µm	90.2 ± 0.4 °
BV	0.5 %	5.1 ± 0.2 %	97.9 ± 0.3 %	212 ± 34 µm	90.1 ± 0.1 °
PBwBH	0.5 %	5.7 ± 0.2 %	91.6 ± 0.3 %	132 ± 30 µm	85.4 ± 0.2 °
PB	0.5 %	5.7 ± 0.2 %	94.6 ± 0.4 %	153 ± 33 µm	89.4 ± 0.2 °
B	0.5 %	5.4 ± 0.2 %	94.2 ± 1.0 %	156 ± 24 µm	89.3 ± 0.1 °
B	1.0 %	5.5 ± 0.2 %	90.9 ± 1.6 %	159 ± 42 µm	89.52 ± 0.2 °
B	3.0 %	5.8 ± 0.2 %	51.9 ± 9.8 %	169 ± 69 µm	90.1 ± 0.2 °

F.3 Comparison of the Surface Roughness of Blanks and Strips

Table F.3: Surface roughness Ra of the blanks and sheet metal strips manufactured by the five different precision shear cutting processes in the middle of the clean cut with the roughness of the fracture zone in braces.

Precision Shear Cutting Process	u_{rel}	r_S = 200 µm, r_M < 20 µm	r_S < 20 µm, r_M = 200 µm
Blank			
Fineblanking	0.5 %	2.1 ± 0.50 µm	1.0 ± 0.17 µm
Fineblanking	1.0 %	1.5 ± 0.21 µm	1.2 ± 0.21 µm
Fineblanking	3.0 %	1.3 ± 0.29 µm	1.0 ± 0.24 µm
		(4.1 ± 0.54 µm)	(5.5 ±1.4 µm)
Blanking with v-ring	0.5 %	2.0 ± 0.28 µm	2.5 ± 0.18 µm
Precision blanking without blank holder	0.5 %	0.93 ± 0.27 µm	2.2 ± 0.29 µm
Precision blanking	0.5 %	1.4 ± 0.25 µm	2.1 ± 0.43 µm
Blanking	0.5 %	1.5 ± 0.73 µm	2.4 ± 0.62 µm
Blanking	1.0 %	1.0 ± 0.25 µm	2.2 ± 0.17 µm
Blanking	3.0 %	0.89 ± 0.15 µm	1.9 ± 0.39 µm
		(4.2 ± 1.0 µm)	(5.3 ± 0.31 µm)
Sheet Metal Strip			
Fineblanking	0.5 %	1.9 ± 0.21 µm	0.94 ± 0.18 µm
Fineblanking	1.0 %	2.1 ± 0.18 µm	1.8 ± 0.43 µm
Fineblanking	3.0 %	1.5 ± 0.24 µm	1.1 ± 0.14 µm
		(6.3±3.1 µm)	(7.6±3.4 µm)
Blanking with v-ring	0.5 %	1.4 ± 0.29 µm	1.2 ± 0.15 µm
Precision blanking without blank holder	0.5 %	0.84 ± 0.24 µm	1.4 ± 0.19 µm
Precision blanking	0.5 %	0.96 ± 0.17 µm	0.63 ± 0.04 µm
Blanking	0.5 %	1.5 ± 0.26 µm	0.61 ± 0.08 µm
Blanking	1.0 %	1.6 ± 0.10 µm	1.1 ± 0.26 µm
Blanking	3.0 %	1.3 ± 0.19 µm	0.91 ± 0.06 µm
		(6.5±1.5 µm)	(8.7±6.6 µm)

F.4 Hardness of the Blanks

The HV 0.2 hardness distribution of blanks manufactured by the five precision shear cutting processes is displayed together with representative cut-surface profiles in figure F.1.

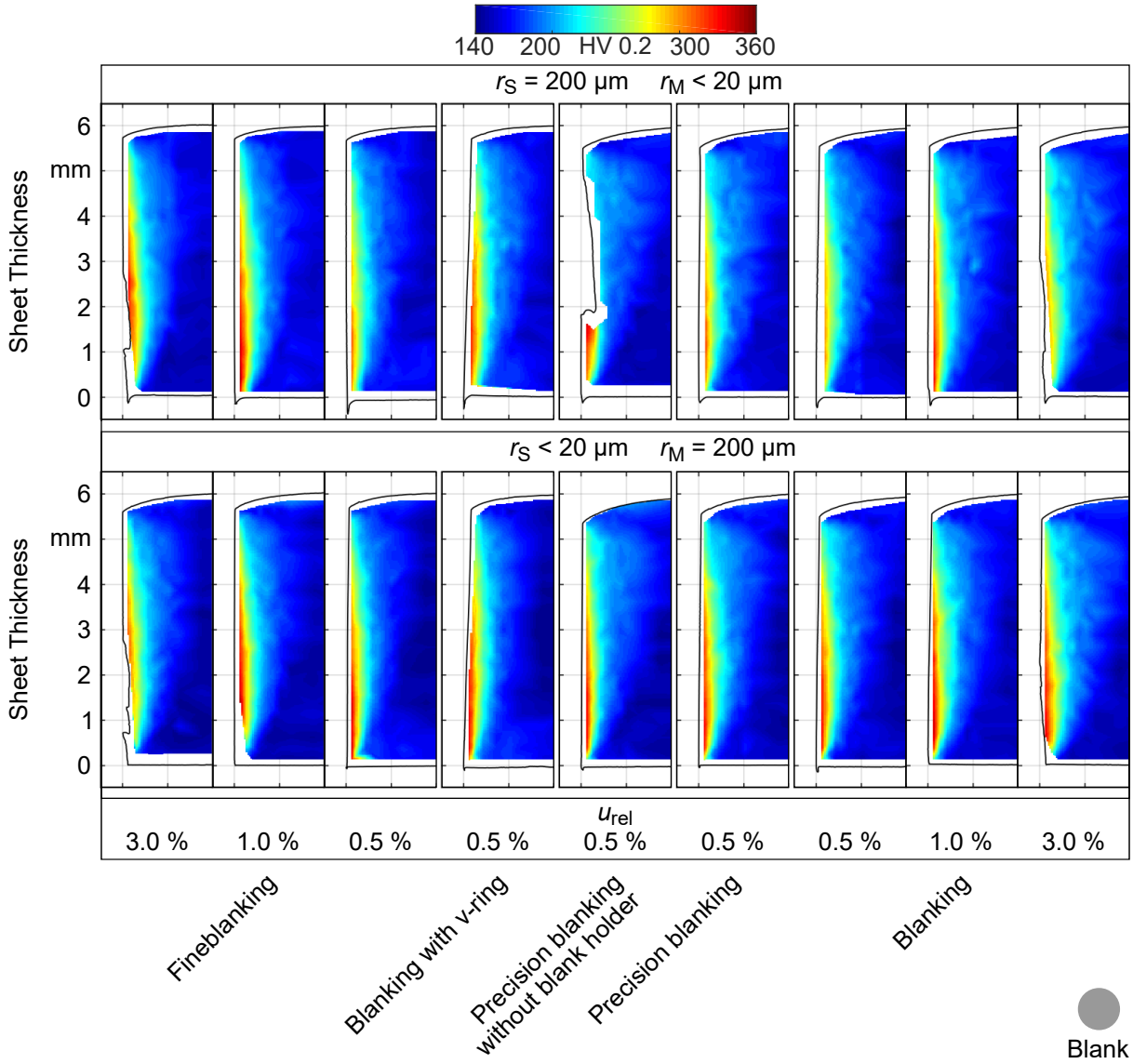

Figure F.1: HV 0.2 hardness distribution of the blanks manufactured by the five precision shear cutting processes together with exemplary cut-surface profiles as partially published in Stahl, D. Müller, Tobie, et al., 2019.

F.5 Complete Overview of the Correlation between Size Deviation and Residual Stresses

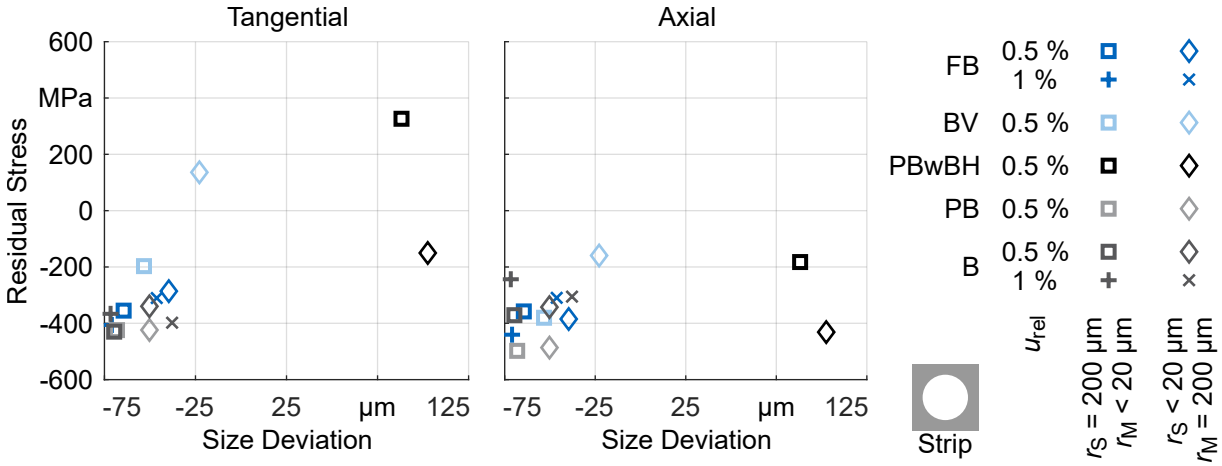

Figure F.2: Complete overview over the correlation between the size deviation and the residual stresses in axial and tangential direction for the manufactured sheet metal strips.

F.6 Complete Overview of the Influence of the Residual Stress State on the Fatigue Strength

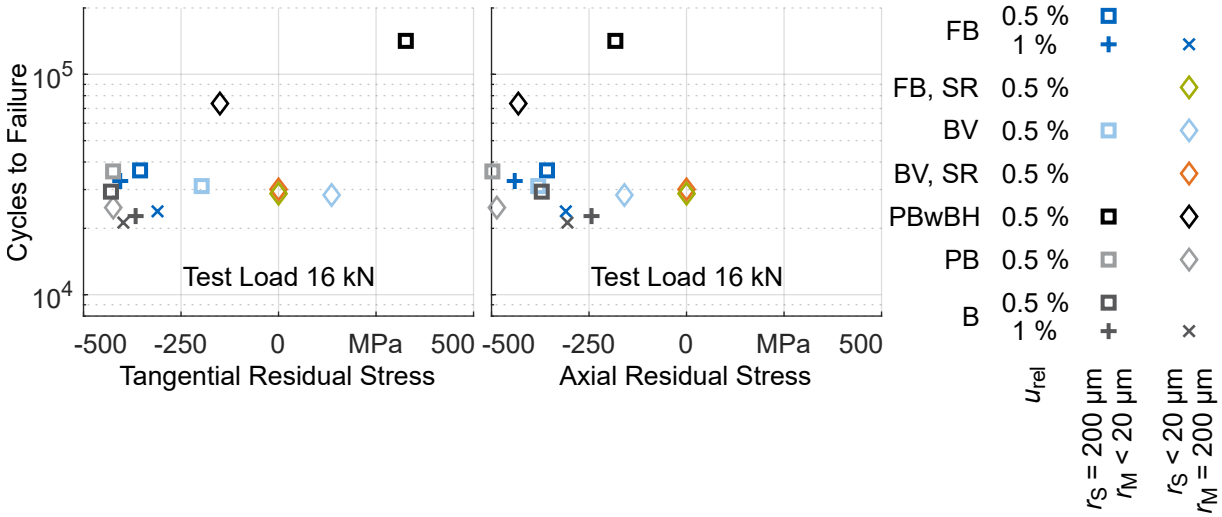

Figure F.3: A complete overview over the influence of the residual stress state on the fatigue strength together with the specimens subjected to a stress relief heat treatment (SR).